SELECTIVE REMOVAL OF INORGANIC FINE SOLIDS, HEAVY METALS AND SULFUR FROM BITUMEN/HEAVY OILS

Xiangyang Zou

2003

SELECTIVE REMOVAL OF INORGANIC FINE SOLIDS, HEAVY METALS AND SULFUR FROM BITUMEN/HEAVY OILS

BY

Xiangyang Zou

A thesis submitted in conformity with the requirements
for the degree of Doctor of Philosophy
Graduate Department of Chemical Engineering and Applied chemistry
University of Toronto

Selective Removal of Inorganic Fine Solids, Heavy Metals and Sulfur from Bitumen/Heavy Oils

Doctor of Philosophy, 2003

Xiangyang Zou

Department of Chemical Engineering and Applied chemistry

University of Toronto

ABSTRACT

This study focuses on understanding the impact of phase behavior, particularly solid phase behavior, on heavy oil partitioning processes in upgrading operations. Multiphase behaviors for the model systems Athabasca Bitumen Vacuum Bottoms (ABVB), a 525+ °C fraction containing 32 wt % asphaltenes, + pentane, heptane and dodecane are investigated using a variable volume X-ray view-cell. The mixtures exhibit complex fluid phase behaviors with asphaltene solidification. Two three-phase LLV zones, L1L2V and L2L3V, were found for ABVB + pentane mixtures. The L1L2V zone is expected since it is close to the vapour pressure curve of pure alkane, a typical characteristic of asymmetric mixtures. However the L2L3V zone, found at temperatures T >230 °C for 40~45 wt % ABVB + pentane mixtures and T = 20~340 °C for 50 wt % ABVB + pentane mixtures, was unexpected. The pressure range of the L2L3V region was very narrow and this zone has great potential for developing selective separation processes. Existing processes such as Residuum Oil Supercritical Extraction processes are currently operating in L1L2V zone. Solids when present can be completely dispersed, completely settled, or remain partially dispersed and partially settled. In addition, adherent deposits, including liquids, are observed at T < 200 °C over a broad range of conditions.

Composition analysis for specific phases revealed that mineral matter is easily and quantitatively separated from ABVB by adding sufficient amounts of an alkane solvent to create a second liquid phase, while selective removal of nickel, vanadium, sulfur and nitrogen from ABVB + pentane mixtures is not realized. Chemical reactions coupled with multiphase behavior are required to selectively remove heavy metals. Saturate-Aromatics-Resins-Asphaltenes (SARA) analysis indicates that the rejected phases contain saturates, aromatics and resins while the extracted phases contain asphaltenes, suggesting aromatics, resins and asphaltenes constitute a compositional continuum with respect to both molar mass and polarity.

The X-ray view-cell technology was also enhanced during this study. Detection of precipitated phase/phases and apparent phase density measurements were improved. A new phase density calibration method using a beryllium insert as an internal standard was developed and automated. Software was prepared to process experimental data.

ACKNOWLEDGEMENTS

I am deeply grateful to all people whose assistance and support have contributed to success of this project. My thesis supervisor, professor John M. Shaw, brought me into the fascinating field of phase diagrams and gave me thoughtful supervision and endless encouragement and support throughout the entire project. Constructive criticism and valuable suggestions from professors Charles A. Mims and M. Kawaji made a big difference.

I am always in debt to my master thesis supervisor, professor Tian-Min Guo, who taught me fluid phase equilibrium. Helpful discussions with Dr. Julian Zuo and Dr. James Du at Oilphase DBR, Schlumberger, and Dr. Huanquan Pan at Stanford University are greatly appreciated.

I thank all colleagues in our research group, Haiyong, Viema, Dan, Martin, Iva, Xiaohui and Elham. Without your help and cooperation, this undertaking would not have been as much fun.

I gratefully acknowledge the Scholarship Programs at the University of Toronto: Mary H. Beatty Fellowship, Open Fellowship and Ontario Graduate Scholarship, and research funds from Imperial Oil and NSERC.

I thank Jacqueline for her kindness and seemingly inexhaustive help to me. I also thank Julie, Gorette, Leticia, Joan, Dan, Terry and Paul for their generosity with their time. They have all been very nice whenever they were needed.

Companionship and encouragement from my close friends, Frank and Weiyang of this department have been invaluable to me during the course of my study as a student.

No words could describe my debt to my parents, my dad Deke Zou and my mom Zhonglian Li, and my siblings for their sacrifices and for giving me the opportunity to pursue higher education. None of this work would be possible without their encouragement and moral support.

Love to my wife, Bei Lu and my daughter, Xuanxuan, whose company, tolerance and inspiration were most important to me during the completion of this thesis. I dedicate this thesis to my wife and my daughter.

Table of Contents

List of Figures

List of Table

List of Symbols

A	The light component in a binary mixture
ABVB	Athabasca Bitumen Vacuum Bottoms
B	The heavy component in a binary mixture
C	1. Number of components, 2. Carbon element
°C	Celsius, temperature unit
E	Energy of incident beam, keV
EOS	Equation of State (PR EOS: Peng-Robinson Equation of State)
F	Degrees of freedom
H	Hydrogen element
I_0	Intensity of the incidental beam
$I_0^c(\lambda_j)$	Intensity of incidental X-ray at wavelength λ_j (through the calibrant)
$I_0^s(\lambda_j)$	Intensity of incidental X-ray at wavelength λ_j (through the sample)
I	Intensity of the transmitted beam
$I^c(\lambda_j)$	Intensity of transmitted X-ray at wavelength λ_j (through the calibrant)
$I^s(\lambda_j)$	Intensity of transmitted X-ray at wavelength λ_j (through the sample)
k	1. Number of critical phase, 2. A constant for calibration equation (Eq. 3-18)
K point	1. Point where L_1 and V become critical in the presence of L_2 2. Kelvin, temperature unit
L point	Point where L_1 and L_2 become critical in the presence of V
L	Liquid phase
L_1	Light liquid phase
L_2	Heavy liquid phase
LCST	Lower critical solution temperature (see definition in Table 2-3a)
LCEP	Lower critical end point (see definition in Table 2-3a)
MCR	Microcarbon Residue
m	A intermediate constant used for deriving calibration Eq. (Eq. 3-16 and Eq. 3-17)

N	Nitrogen element
Ni	Nickel element
n-C5	Normal pentane
n-C7	Normal heptane
n-C12	Normal dodecane
P	Pressure
P_c	Critical pressure
P_r	Reduced pressure, P/P_c
PR	Peng - Robinson Equation of State
Q point	Point at which four phases are in equilibrium (see definition in Table 2-3a).
ROSE	Residuum Oil Supercritical Extraction
S	1. Solid phase, 2. Sulfur element
SANS	Small Angle Neutron Scattering
SARA	Saturates – Aromatics – Resin – Asphaltene
SAXS	Small Angle X-rays Scattering
SCF	Supercritical Fluid
SCFE	Supercritical Fluid Extraction
T	Temperature
T_c	Critical temperature
TCP	Tricritical point (see definition in Table 2-3a)
T_r	Reduced temperature, T/T_c
UCST	Upper critical solution temperature (see definition in Table 2-3a)
UCEP	Upper critical end point (see definition in Table 2-3a)
V	1. Vapour phase, 2. Vanadium element
W_i	Mass fraction of component i
w_i^c	Mass fraction of element i in the calibrant;
x_i	Mole fraction of component i
Δx	Thickness of sample penetrated by X-rays

Greek Letters

π	Number of phases
ρ	Density
ρ_c	Density of the calibrant
ρ_s	Density of the sample
λ	Wavelength of X-ray beam
λ_e	Effective wavelength of polychromatic X-ray beam
λ_e^c	Equivalent wavelength for X-rays passing through the calibrant
λ_e^s	Equivalent wavelength for X-rays passing through the sample
μ	1. Chemical potential 2. Mass absorption coefficient
μ_i	1. Chemical potential of component i 2. Mass absorption coefficient of component i for a monochromatic x-ray beam at wavelength λ.
μ_{ij}	Mass absorption coefficient of component i for a polychromatic x-ray beam at a wavelength of λ_j.
$\mu_i^{\lambda_e^c}$	Mass absorption coefficient of element i at wavelength λ_e^c
$\mu_i^{\lambda_e^s}$	Mass absorption coefficient of element i at wavelength λ_e^s

Chapter 1 Introduction

1.1 Introduction

1.1.1 Heavy Oils/Bitumen—Our Future Energy Resource

As the world's resources of light and sweet crude oil become depleted, the stocks of heavy oil and bitumen are becoming more and more important as a component in supplying the demand for fuels and petrochemical feeds. Particularly in Canada, a major part of liquid hydrocarbons are currently produced from bitumen: there are 1.7 trillion barrels of bitumen (one-third of the world's known petroleum reserves) in Alberta, which could meet Canada's energy needs for the next two centuries. For example, about 70% of Imperial Oil's synthetic *crude oils* are currently recovered from bitumen and this percentage is expected to increase significantly over the next five years. Consequently, over the past two decades, the average quality of petroleum delivered to refineries has diminished by approximately two points on the API Scale, accompanied by increases in the contents of inorganic solids, heavy metals and heteroatoms (Speight, 1999). Meanwhile the market for heavier fuels is decreasing while that for middle distillates is increasing at a rapid rate, so ideally heavy oils and bitumen recovered in the upstream oil fields, along with residues produced in the downstream refineries, should be upgraded as much as possible into middle distillates.

1.1.2 Characteristics of Heavy Oils/Bitumen

Heavy oils/bitumens include atmosphere residues (AR) and vacuum residues (VR), topped crude oils, coal oil extracts, crude oils extracted from tar sands, etc. (Gray, 1994).

The characteristics of heavy oils/bitumen are quite different from those of conventional crude oils. They generally have a high specific gravity (>0.95), a low hydrogen-to-carbon ratio (~1.5), and contain large amounts of asphaltenes (>5 wt %), heavy metals (such as vanadium and nickel), heteroatoms (such as sulfur, nitrogen and oxygen) and inorganic fine solids. Inorganic fine solids, heavy metals and heteroatoms all appear throughout the entire boiling range of the crude oil but tend to concentrate in the heaviest fractions, such as resins and asphaltenes (Reynolds, 1994 & 1999; Chung et al., 1997; Boduszynski, 1987). These characteristics also bring the petroleum industry a host of new challenges in heavy oil/bitumen recovery, transportation and upgrading processes.

1.1.3 New Challenges in Heavy Oil/Bitumen Production

The first challenge in heavy oil/bitumen production is solids drop out, which results from high asphaltene and fine solid content in heavy oil/bitumen. One of the most notorious traits of asphaltenes is their pronounced tendency to form aggregates in hydrocarbon solutions and under unfavourable solvent conditions, asphaltene aggregates are prone to further aggregation into clusters and precipitate from solution (The research groups of Speight, Yen, Firoozabadi, Overfield, Mansoori, Sheu and others). Inorganic fine solids are generally associated with asphaltenes, so precipitated asphaltenes often contain high concentration of inorganic fine solids. The solids drop out phenomena poses a host of severe problems during heavy oil/bitumen recovery (formation damage and well plugging), transportation (line plugging) and processing (reactor and line coking and catalyst deactivation) (The research groups of Speight, Yen, Wiehe, Storm, Gray, Mansoori, Watkinson and others).

Other challenges in heavy oil/bitumen production can be traced to their high content of heavy metals and heteroatoms, mainly sulfur, nitrogen, oxygen. Although the concentration of these elements may be quite small, their impact is significant. For example, the deposition of trace heavy metals (vanadium and nickel) and/or chemisorption of nitrogen-containing compounds on the catalysts are the main reasons for catalyst passivation and/or poisoning in catalytic operations, and thus necessitate frequent regeneration of the catalyst or its replacement. The presence of trace heteroatoms may also be responsible for objectionable characteristics in finished products causing environmental concerns (Reynolds, 1994 & 1999; Gray, 1994; Speight 1999; Yen, 1975), so the levels of heteroatoms in finished products have to be reduced following more and more stringent environmental regulations.

These new problems are related. For example, solids drop out problems are expected for heavy oil with high contents of fine solids, heteroatoms and heavy metals. On the other hand, solid precipitates contain very high concentrations of these heteroatoms. Therefore, part of fine solids, heavy metals and heteroatoms can be removed along with asphaltenes from bulk phases as precipitates (Cartlidge et al., 1996; Kotlay, et al., 1999; Savastano, 1991; Reynolds, 1994&1999; Chung et al., 1997; Boduszynski, 1987; Yen, 1975). This is the basis of solvent deasphalting technologies, which are discussed in section 2.3.3 in more detail.

1.1.4 Technologies to Meet These Challenges

The oil industry needs new technologies to maximize middle distillate yield and minimize waste with a minimum capital investment and operating cost, and thus, to ensure flexibility and profitability. One of the goals of the CONRAD Upgrading

Technical Program Group is to develop simple inexpensive processes suitable for field use which produce a product, with a yield of ~ 90 %, that can be fed to a conventional refinery. The following technologies are currently applied to solve the above challenging problems.

Generally, solids drop out problems in recovery and transportation in oil fields are avoided by identifying operating limits in temperature-pressure-composition zones (boundaries in multiphase diagrams, such as solid-liquid-gas (SLV), solid-liquid-liquid-gas (SLLV)) to be avoided/exploited. Under these conditions (Temperature < 200 °C), solids drop out due to chemical reaction is negligible. Thus, it can be considered as a phase equilibrium problem. In processing operations, solids may also precipitate as a result of composition changes due to chemical reactions (Gray, 1994; Wiehe, 1993 & 1994; Speight, 1999; Abedi, 1999; Watkinson, 1999; Asomaning et al., 1999; Sanaie, N.; et al., 1999; Takatsuka et al; 1989; Lemke, 1998). Therefore, it should be described by a combination of phase equilibrium and chemical reaction kinetic theories. The main limitation to making predictions is the complexity of both the solids and the liquid solutions (Speight, 1999). In addition to using phase diagram, solids drop out problems in processing operations are also alleviated or solved by preprocessing feedstocks, such as the selective removal, from bulk feedstocks, of those constituents with high solid-forming propensity. By far, it is well established that solids drop out (except wax precipitation) problems are related to the asphaltene constituents. Untangling asphaltene precipitation is the starting point to solve these problems.

Challenges due to high heavy metal and heteroatom content are met downstream. These problems can also be alleviated or solved by preprocessing of feedstocks, such as

by selective removal of part of the high heteroatom-containing constituents from the bulk feedstock through phase separation, and thus, can be referred to as physical technologies. Typical industrial processes falling in this category includes solvent deasphalting and Residuum Oil Supercritical Extraction (ROSE), which often operate at temperatures between 150 ~250 °C. Alternatively, these constituents can be converted to other constituents through chemical reactions and then separated from feedstocks in down stream processes specially designed for heteroatom removal (Gray, 1994; Reynolds, 1994 & 1999; Speight, 1999; Savastano, 1991). These processes can be catalytic or non-catalytic and with or without hydrogen, but generally operate at temperatures T>350 °C and are often referred to as chemical technologies. When the heavy metal or heteroatom content exceeds the operating limit of these processes, physical technology is used to preprocess the feedstock. Since physical and chemical technologies work at quite different temperature conditions, they are generally treated separately. Currently, there are no technologies operating between 250~350 °C.

Fortunately the constituents with high solid-forming propensity are generally the very constituents with high content of heavy metals and heteroatoms; they are asphaltenic. Therefore, selective removal of those asphaltenes with high solid-forming propensity and high contents of heavy metals and heteroatoms from heavy oils, can not only alleviate or solve solids drop out problems, but can also simultaneously solve problems from high heavy metal and heteroatom content, or at least alleviate the burden of heavy metal and heteroatom removal processes downstream. The coincident reduction in feed stock viscosity is also desirable. Conventional deasphalting processes, such as the ROSE process, now widely employed in industry, were developed on the basis of this

principle (Savastano et al., 1991; Northup, et al., 1996; Chung et al. 1997; Stegeman et al., 1992).

1.1.5 Solvent Deasphalting Process

In the Residuum Oil Supercritical Extraction (ROSE) process, a heavy feedstock is split into two fluid phases in the presence of a near critical/supercritical solvent. Asphaltenes and fine solids are concentrated in one phase and lighter fractions in the other. However, this industrial process is not sufficiently selective for use with heavy oils and bitumen because up to 50 % of the heavy oil/bitumen reports to the “reject stream” (Shaw, 1999; Savastano, 1991). The product losses are unacceptable considering even 35~60 wt% asphaltenes can be upgraded to middle distillates. An ideal process capable of selective separation of the inorganic fine solids, heavy metals and heteroatom constituents while precipitating only a minor amount of asphaltenes is desirable. Obviously, its development needs a more extensive and accurate knowledge of asphaltenes, heavy metals and heteroatoms and of their characteristics, particularly the multiphase behaviour of heavy oil mixtures and partitions of these objectionable constituents among phases in the equilibrium. This is the focus of this research.

1.1.6 Recent Progress Related to Deasphalting Processes

Motivated by the industrial need for a more selective process discussed above, research areas related to asphaltenes are very active and some important progress has been achieved. Experimental data (Kotlyar, et al., 1999; Cartlidge et al., 1996; Dukhedin Lalla, 1996) show that separation of only a fraction of asphaltenes from feedstocks can selectively remove inorganic fine solids and heteroatom constituents from heavy oils. For

example, preliminary experiments performed at the University of Toronto with Athabasca Bitumen Vacuum Bottoms (ABVB, 40 wt% asphaltenes) + dodecane + hydrogen mixtures (Cartlidge et al., 1996) are listed in Table 1-1. It is also well known that other heavy metals, sulfur and inorganic solids also concentrate in asphaltenic deposits.

Table 1-1 Preliminary vanadium separation results for ABVB + dodecane + hydrogen mixtures

wt% ABVB in the feed	ppm Vanadium in the feed	%ABVB reporting to liquid product phase	ppm vanadium in the liquid product phase	% vanadium reporting to the solid phase
33	122	77	44	67
50	183	88	26	87
100	366	70	76	86

The above experimental results suggest the possibility for such a process that is capable of selective separation of the inorganic fine solids and heteroatom constituents (up to 90 %) while only precipitating a minor part of the asphaltene content (less than 15%).

1.1.7 A Conceptual Design for a Prospective Deasphalting Process

On the basis of these new findings, Shaw (1999) proposed a conceptual design for a new deasphalting process (Figure 1-1).

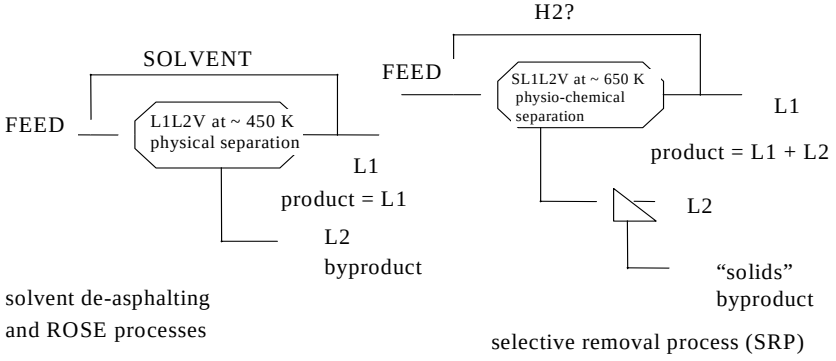

Figure 1-1 Schematics for conventional deasphalting processes and the proposed selective removal process.

As shown above, the proposed process consists of two stages. In the first stage, the feedstock is partitioned initially into two phases. The denser phase containing the bulk of heavy metals and inorganic solids is then fed into the second stage and partitioned at even more extreme conditions. The liquid products from the first and second stages, which contain much less objectionable constituents and are less viscous, could then be combined to produce a readily upgradeable final product. The solid effluent could be "coked" at low temperatures to avoid oxidation of the sulfur and to recover residual organic constituents or land filled if such secondary processing is proven to be uneconomic. At present, there are no data on which to base the selection of process equipment or operating conditions for such a process. More investigation is needed to identify conditions leading to a selective separation, and in particular to achieve such a separation with minimum amounts of solvent. The experimental results of Abedi et al. (1998) provide some guidance to look for the operating conditions for this new process concept.

1.1.8 Possible Operating Conditions for This Deasphalting Process

Abedi et al. (1998) observed L_1L_2V phase behavior in a model heavy oil system at elevated temperatures. They also observed that a solid phase separated from the heavy liquid phase L_2 irreversibly at temperatures greater than ~ 650 K. This solid phase did not separate from the light liquid phase L_1 even at temperatures up to 700 K(Figure 1-2). These important results not only show that asphaltenic solids can be concentrated in a small fraction of heavy feedstocks, but also identify operating conditions meriting detailed investigation.

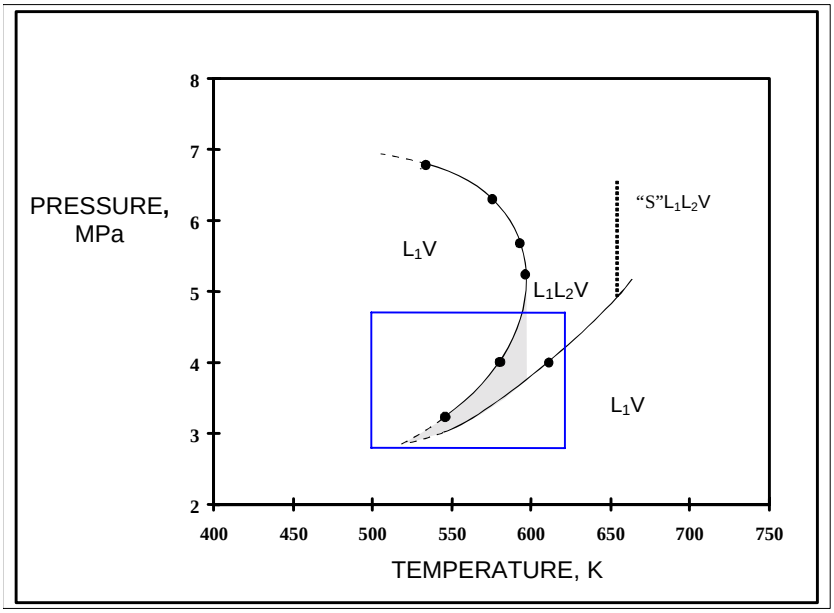

Figure 1-2 Partial phase diagram for the model heavy oil ABVB 25 wt % + dodecane 73 wt % + hydrogen 2 wt %.

1.2 Objectives

As discussed above, the first and most important step in developing such a new separation process is understanding the phase equilibrium of asphaltene-containing heavy oil mixtures, and particularly conditions under which high heteroatom-containing asphaltenes separate selectively from readily upgradeable constituents (reversibly or irreversibly). A key aim of this thesis is to extend the capability of the unique X-ray and beryllium view cell technology, and to improve the understanding of the reversible and irreversible multi-phase behavior of heavy oils, particularly solid-liquid-liquid-vapor, liquid-liquid-vapor and solid-liquid-vapor phase behaviors. The principal objectives are:

1. To explore the multiphase behaviour of the model heavy oil mixture, alkanes + Athabasca Bitumen Vacuum Bottoms (ABVB).

2. To investigate the effects of hydrogen addition on the LLV phase behavior of the model heavy oil mixture, alkanes + ABVB. Hydrogenation is an important upgrading technology in the petroleum industry. Phase separation is often suspected to play a key role on heavy oil upgrading processes.
3. To examine partitioning of inorganic fine solids, heteroatoms, heavy metals among phases in equilibrium.
4. To improve the precision and accuracy of density measurements and extend denser phase detection capability of the current X-ray + beryllium view cell equipment.
5. To automate phase boundary and density detection by developing computer software to analyze voluminous images cropped in experiment.

1.3 Thesis Outline

Chapter 2 covers the background materials for this thesis, including relevant literature review and X-ray absorption physics. Chapter 3 describes the X-ray view cell technology (principle and calibration), equipment modification and experimental method verification. The conventional Results and Discussion section is divided into Chapter 4 and Chapter 5 for clarity. The multiphase behavior of ABVB + alkane mixtures are presented in Chapter 4. Industrial implications based on the multiphase behavior and sample analysis, such as selectivity of inorganic fine solids, heavy metals and sulfur removal, and solids precipitation and dispersion, are discussed in Chapter 5. Conclusions are drawn in Chapter 6. Finally the thesis is wrapped up with recommendations in Chapter 7.

Chapter 2 Background

2.1 Introduction

For a thorough understanding of complex phase behavior of asphaltene containing heavy oil mixtures, a grounding in the fundamentals of phase diagrams, Gibbs phase rule and phase behavior characteristics of binary and ternary mixtures is indispensable. These topics are addressed in section 2.2. The characteristics of heavy oils/bitumens, asphaltene solution behavior and distribution of fine inorganic solids, heavy metals and sulfur in heavy oils/bitumen fractions are covered in section 2.3. The unique experimental technology used in this research has been developed on the basis of de-convolution of transmitted polychromatic X-ray images, so this chapter closes with an overview of X-ray absorption physics.

2.2 Understanding phase diagrams

2.2.1 Basic concepts

2.2.1.1 System

In thermodynamics, a system generally refers to a specific and isolated portion of material subjected to limited ranges of conditions. The quantity of material within a system is always assumed to be sufficient to ensure the applicability of thermodynamic laws concerning large ensembles of particles. The conditions, also called independent variables, include temperature (T), pressure (P), magnetic field, etc., and they determine the state of a system.

The system referred to in this research is only a special case of the above thermodynamic system. It can be characterized by a combination of chemical species known as components (i, i=1,2…), and their concentration (x_i). The system is subjected only to variations of temperature (T) and pressure (P). A system is heterogeneous if the material inside the system, at a fixed T and P, is present in different aggregate states and/or structures. In contrast, the system is homogeneous if the material is present in only one aggregate state or structure.

2.2.1.2 Definition of a phase

A phase means a homogeneous, physically distinct and mechanically separable portion of material present inside a system. According to the definition above, each particle of a homogeneous solid or each droplet of a homogeneous liquid can be treated as a phase as long as it is separated from the rest of the system by an interface. Such a strict definition may be justified thermodynamically, but usually only portions of a system differing in structure or composition are considered phases. Phases are separable parts of a system but they need not form a continuous body. For example, there are only two phases when one liquid is dispersed in another.

In asphaltene containing mixtures, asphaltenes often form quite stable aggregates, and the number, structure and size distribution of these aggregates depend on the interactions between asphaltenes and their surrounding medium. It is still a debate whether these aggregates form a separate phase/phases. Obviously it depends on the scale which asphaltene containing mixtures is investigated. This study focuses on the bulk phase behavior of asphaltene containing heavy oil mixtures rather than the size and structure of asphaltenes.

2.2.1.3 Phase equilibria and phase diagrams

For a multiphase system subjected to fixed conditions, the coexisting phases are in equilibrium when there is no net energy and mass transfer between any two phases within the system and between the system and its environment. Phase equilibrium is an ideal state, so theoretically a real system can approximate infinitely to but can never reach a perfect phase equilibrium state. A real system is often treated to be at phase equilibrium if we believe it is close enough to its equilibrium state. Obviously the degree of such approximation may vary from one specific situation to another. As the system conditions such as T and P change, the aggregate state and/or structure of the material within the system may change. The coexisting phases are no longer in equilibrium. Consequently, the number of phases, and the mass and the physiochemical properties of each phase change with the conditions until the system reaches a new phase equilibrium state; this process is called a phase transition. The set of phase transitions for a system arising from variations of T, P and x is referred to as system phase behavior. Phase behavior can be represented by tables, but more effectively and intuitively by graphs called phase diagrams. All combinations of independent system variables can be used as axes for phase diagrams. Given the large number of variables for multicomponent systems, description of phase behavior is challenging. For instance, how does one choose axis variables? How are these variables related? Fortunately the discovery of the phase rule by Gibbs in 1875 brought a measure of order by providing a framework for the interpretation and classification of phase diagrams.

2.2.1.4 Gibbs phase rule

The number of variables which can be altered independently and arbitrarily without causing the disappearance of a phase or the formation of a new phase or a change in another variable is called the number of degrees of freedom of a system. Gibbs phase rule relates the number of degrees of freedom with the number of components, the number of equilibrium phases and other constraints within a multiphase system. For a system with C components distributed over π phases, Gibbs phase rule is presented in Table 2-1.

Table 2-1 Derivation of the Gibbs phase rule

Independent Variables	Independent Equations (constraints)
π (C-1) (mole or mass fraction) ($\sum_{i=1}^{C} x_i^n = 1$, i=1,…, C; n=1,…, π)	(π-1)C (the equality of chemical potential of components in different phases at equilibrium) $\mu_i^1 = \mu_i^2 = \cdots = \mu_i^\pi$
2 (Temperature, Pressure)	2k (k=the number of critical-with each other-phases) 2 constraints for each pair of critical phases
	R (Chemical Reaction Equilibria)
	Q (Other constraints, such as magnetic field)
Total independent variables: π (C-1)+2	Total independent equations: (π-1)C+R+2k+Q
Degrees of Freedom: f=C+2-π-2k-R-Q	
Degrees of Freedom: f=C+2-π-2k (No reaction, No other constraints)	

The application of Gibbs phase rule imposes constraints on the number of degrees of freedom for a multiphase system at equilibrium, and consequently, imposes additional geometrical constraints on the resulting phase diagrams. The constraints are very useful for grasping key features of phase diagrams summarized in Table 2-2. For example, if

f=0, the number of phases is invariant and represented by a unique point or points; if f=1, the system is monovariant and represented by a single curve or a series of curves.

Table 2-2 Application of Gibbs phase rule: f=C+2-π-2k

C	π	k	f	Geometrical Features	Example	Presentation style in phase diagrams
Unary system						
1	3	0	0	Points	SLV triple	Empty triangle Δ
1	2	0	1	Lines	SL, LV, SV	Solid thick line (—)
1	1	0	2	Surfaces	S, L, V	
1	1	1	0	Points	L=V, L1=L2	Dark circle •
Binary System						
2	4	0	0	Points	S_1S_2LV, SL_1L_2V	Filled rectangular ■
2	3	0	1	Lines	SLV, S_1S_2L, L_1L_2V	Dash thick line (---)
2	2	0	2	Surfaces	LV, SV, SL, LL	
2	1	0	3	Volumes	S, L, V	
2	2	1	0	Points	UCEP (K): $L_2+L_1=V$ LCEP (L): $L_2=L_1+V$	Filled triangle ▲
2	1	1	1	Lines	L=V, L1=L_2	Solid thin line (—)
Ternary System						
3	5	0	0	Points	$S_1S_2L_1L_2V$	
3	4	0	1	Lines	S_1S_2LV, SL_1L_2V	
3	3	0	2	Surfaces	SLV, S_1S_2L, L_1L_2V	
3	2	0	3	Volumes	LV, SV, SL, LL, etc.	
3	1	0	4	4-dimensions	S, L, V	
3	3	1	0	Points	$S+L_2+L_1=V$, $S+L_2=L_1+V$	
3	2	1	1	Lines	$L_2+L_1=V$, $L_1=L_2+V$	
3	1	1	2	Surfaces	L=V, L1=L_2	

2.2.1.5 Field variables and density variables

The variables describing a multiphase system at equilibrium can be classified into two categories: field variables and generalized density variables. The field variables, sometimes referred to as state variables, are defined to be those that are identical in all phases at equilibrium, such as T, P and chemical potential of each component (μ_i); generalized density variables are those that differ from phase to phase, such as density, composition, internal energy, etc. The criteria for phase equilibrium are the equality of all corresponding field variables in each of coexisting phases.

Using field variables as axes imposes additional geometrical constraints on phase diagrams making them more concise. For example, an SLLV quadruple point for a binary system is represented by a set of four points in the PTx space but by only one point in the PTμ space. The most widely used and convenient axes for phase diagrams are field variables T and P because they are common engineering variables and easy to understand when compared with the chemical potential of component i, which seems quite abstract. Using T and P as axes also makes phase diagrams readily applicable in guiding industrial processes. Composition x_i is also often used as an axis variable in case people want to know how the equilibria phases differ from each other. The above geometrical constraints are used as guides in the following discussion of phase diagrams for unary, binary and multicomponent systems.

2.2.2 Phase diagrams for unary systems

Phase diagrams for unary systems are the simplest because there is only one component in the systems. The maximum number of degrees of freedom is 2, so two-dimensional phase diagrams are sufficient. To facilitate the illustration of typical

characteristics of phase diagrams for a unary system, a schematic partial phase diagram of water using P-T as axes is shown in Figure 2-1.

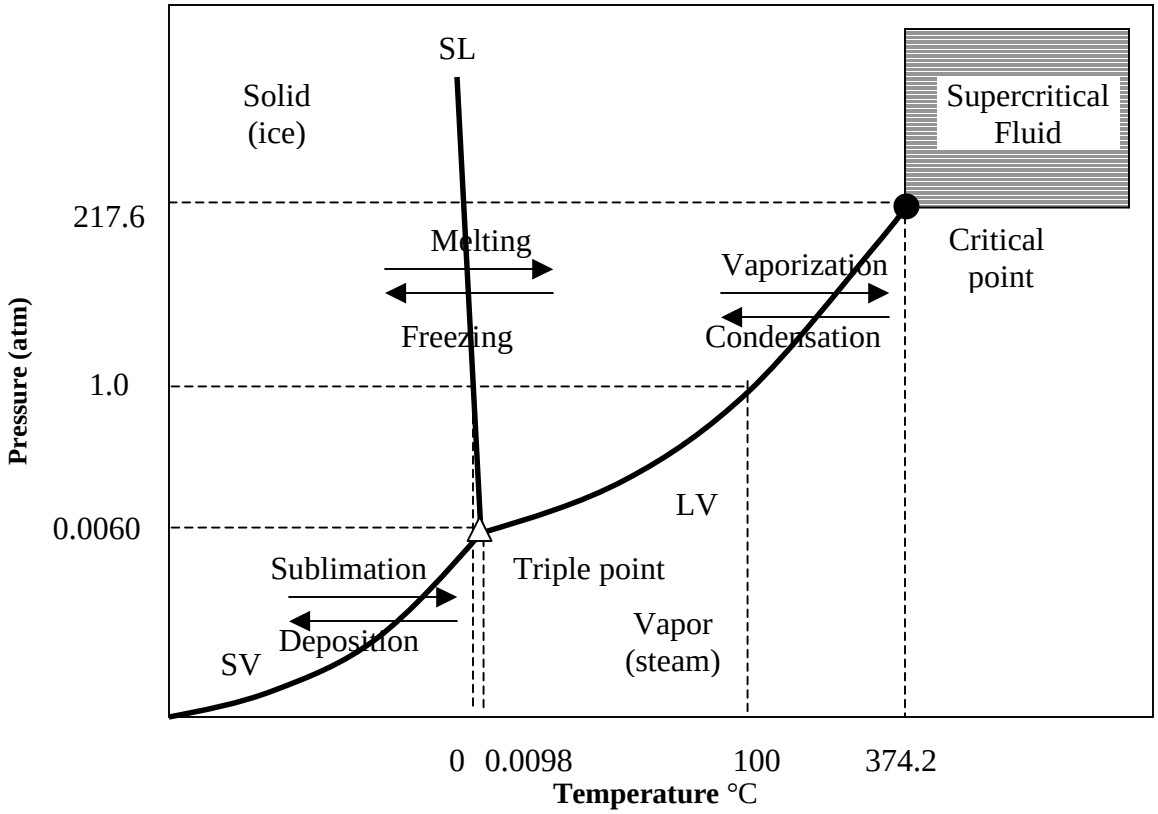

Figure 2-1 Schematic partial phase diagram of water for explanation of symbols (Table 2-2)

According to Gibbs phase rule, f=3-p-2k (Table 2-2). If the system is in one-phase, two-phase or three phase equilibrium, the system has zero, one or two degrees of freedom, and thus is represented on the P-T phase diagram by points, curves or regions, respectively. The three curves (SV, LV and SL) in the diagram have one degree of freedom, and represent solid⇔vapor, liquid⇔vapor, and solid⇔liquid equilibrium respectively. Regions not on a curve represent one-phase zones and have two degrees of freedom, i.e., P and T may be varied independently without changing the number or nature of phases present. There are two special points on this diagram with zero degrees of freedom. One is the "triple point" (T=0.0098 °C and P=0.0060 atm) at the intersection

of the LV, SL and SV curves where all three phase are at equilibrium. The other is the vapor–liquid critical point (T_c =374.2 °C and P_c =217.6 atm) at which the vapor phase and the liquid phases become identical. Above the critical temperature T_c, the fluid cannot be liquefied by increasing pressure and nor can it be vaporized by increasing temperature. The shadowed region ($T>T_c$ and $P>P_c$) is often referred to as the supercritical region, and the fluid is referred to as a supercritical fluid (SCF). Supercritical fluids possess both gas-like and liquid-like properties, but are neither liquids nor gases. Supercritical fluid extraction (SCFE) processes take advantage of some unique characteristics of supercritical fluids. These characteristics are discussed further in section 2.2.6.

2.2.3 Phase diagrams for binary systems

2.2.3.1 Phase transitions definitions and presentation convention of binary phase behavior

Phase diagrams for binary systems are more complicated than those of unary systems since the number of degrees of freedom increases by one with the addition of a second component. The maximum number of degrees of freedom is 3, so a three-dimensional phase diagram is required to depict a binary system (Figure 2-2 a). However, three-dimensional diagrams are often hard to construct and read, so instead, mainly two-dimensional diagrams are used in practice. The most widely used two-dimensional diagrams are projections of invariant points and monovariant curves on PT plane and sections of the PTx-space keeping one of these variables constant. Before a detailed discussion about binary phase diagrams, it is helpful to review some definitions of typical phase transitions and conventions for their presentation that are followed by many

research groups (Street, 1980; Th.W. de Loos, 1993; C. J. Peters et al; 1993 and Shaw, 1999). These are summarized in Table 2-3 a & b.

Table 2-3 a Definitions of phase transitions

Abbreviation	Transition	Description
LCST	Lower critical solution temperature	Temperature at which two phases, become critical as the system temperature is lowered. LCST at different compositions forms a curve in the PT plane.
UCST	Upper critical solution temperature	Temperature at which two phases become critical as the system temperature is raised. UCST at different compositions form a curve in the PT plane.
LCEP	Lower critical end point	The point at which a LCST line intersects with a three phase line, usually at a low pressure. LCEP corresponds to a point in the PT plane.
UCEP	Upper critical end point	The point at which an UCST line intersects with a three phase line, usually at a low pressure. UCEP corresponds to a point in PT plane.
K point		The point at which a liquid and a vapor phase become critical in the presence of a second liquid phase. (L_2+L_1=V)
L point		The point at which two liquid phases become critical in the presence of a vapor phase. (L_2=L_1+V)
Q point		The point at which four phases, such as SSLV and SLLV, are in equilibrium. Q point corresponds to a point in PT plane.
TCP point	Tricritical point	The point where the L_1L_2V curve converges to a point and the L-point and the K-point on this branch coincide.

Table 2-3b Conventions for phase diagram presentation for binary systems

Symbols	Meaning
A	the light component
B	the heavy component
X	the composition (mole fraction or mass fraction) of the heavy component
L_1	the component A rich low density liquid phase
L_2	the component B rich high density liquid phase
S	solid phase

The phase transitions in Table 2-3a are key features in phase diagrams since they determine what kind of multiphase behavior are possible in the neighborhood of these transitions. The locations of these phase transition are very important both in theoretical research and industrial production. However it is quite challenging to determine the location of these transitions since sometimes they are only points in PTx space as listed in Table 2-2. A brief discussion about how to locate a K point is provided in the Results and Discussion section of this thesis. An exhaustive review of the phase behavior of binary systems is beyond the scope of this thesis. These definitions and conventions are exemplified using a single case (Figure 2-2).

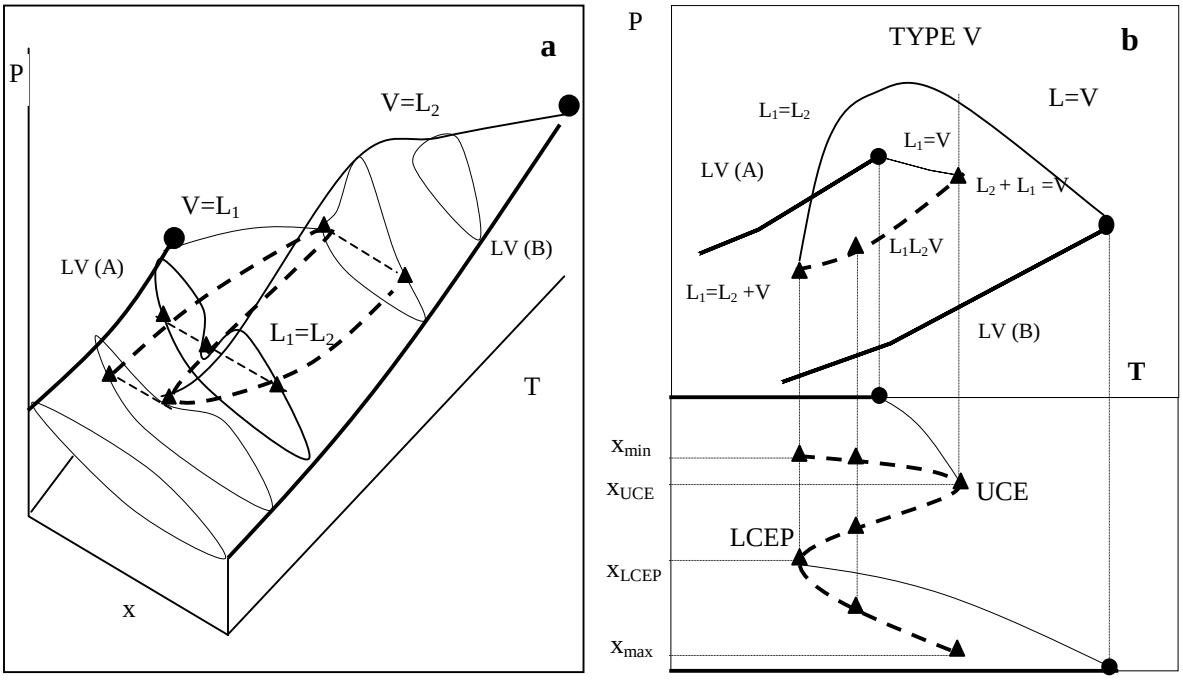

Figure 2-2 A typical set of schematics for the phase behavior of a binary system
a: PTx three-dimensional; b: PT and Tx projections of the PTx three-dimensional

Figure 2-2 shows a set of schematics for the phase behavior of a binary system including a PTx three-dimensional (Figure 2-2a) and its PT and Tx projections (Figure 2-2b). The pure component vapor-pressure curves (thick solid line LV(A) and LV(B)) and critical

points (•) are shown along with two branches of the binary critical (thin solid line) locus; the critical locus starting from the critical point of A ends at the UCEP (▲) and the locus starting from the critical point of B ends at the LCEP (▲).The UCEP and LCEP are single points in the PT projection but two points in the Tx projection. Similarly the three-phase equilibria represented by three curves in the three-dimensional diagram and the Tx projection, are represented by only one curve in the PT projection. This is because P and T are field variables and x is a density variable: at one temperature, equilibrium phases have different compositions but the same pressure.

PT projections are much more concise, as clearly only unique points, critical curves and three-phase curves are projected. PTx sections keeping one variable constant are often used to supplement PT projections for multicomponent equilibria. Figure 2-3 illustrates Tx, Px and PT sections in the three-dimensional PTx phase diagram of Figure 2-2.

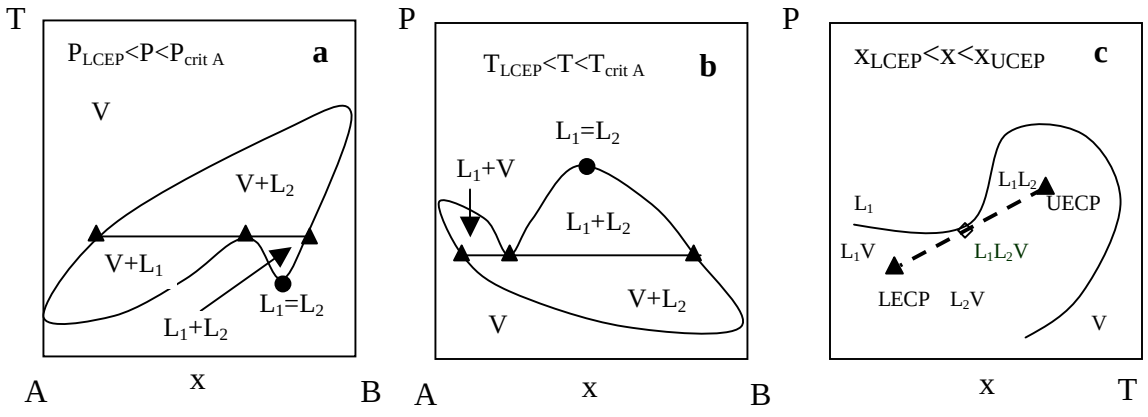

Figure 2-3 Schematic phase diagram sections: a: P,x-section (constant T); b: T,x-section (constant P); c: P,T-section (constant x)

In Figure 2-3a, a Tx section shows schematically how the composition of L_1, L_2 and V change with temperature at a fixed pressure. In Figure 2-3b, a Px section shows schematically how the composition of L_1, L_2 and V change with pressure at a fixed

temperature. Also shown in the two diagrams are L_1=L_2 critical points. For a binary system, one phase and two-phase equilibria are regions in the Tx and Px sections but three-phase L_1L_2V equilibria is a line. Any line connecting two phases at equilibrium is a "tie line". The mass in each coexisting phase is governed by the Lever Rule pivoted at the point of total composition. The Lever Rule can be readily derived from mass balances. In Figure 2-3c a PT section (isopleth) shows phase boundaries at a specific total composition. Understanding the PT section is very important since in daily phase behaviour experiments, the sample compositions are often fixed and phase diagrams obtained are isopleths. Further discussion of PT sections is given in section 3.2.5. Projections and sections of PTx space are two kinds of complementary diagrams to present phase behavior of binary systems. The projections are more concise while sections can show additional information, such as compositions of phases in equilibrium. They are often combined to describe complex phase behavior.

2.2.3.2 Binary phase behavior classification by van Konynenburg and Scott

Due to the possible number of binary systems available, their phase behavior can appear chaotic even when presented as PT projections. Fortunately van Konynenburg and Scott (1980) analyzed phase diagrams of binary systems systematically and classified them into six types (type I through type VI) based on their PT projections. The illustrative example, figure 2-2, belongs to type V. Their complete classification scheme is outlined in Figure 2-4 where the key curves and points in the various PT projections are presented. The key boundary curves include: (1) pure component vapor pressure curves (solid thick curves), (2) critical curves (solid thin curve), and (3) three phase curves (dash curves). The key points include: (1) pure component critical points (dark circle), (2) critical end points (dark

triangle), formed by the intersection of an LL critical curve and an LLV three phase curve. In type I, II and VI, the vapor-liquid critical curve is continuous; it starts from the critical point of the light component A and ends at the critical point of the heavy component B. In type I, there is no LL immiscible region; In type II, there is an LL immiscible region, with a single LL critical curve bonded at low pressures by an upper critical end point $L_2=L_1+V$, where it intersects the LLV three-phase curve; In type VI, one or two LL critical curves are bounded at low pressure by upper and lower critical end points. In type III, IV and V, the vapor-liquid critical curve is not continuous with two branches originating from the critical point of the light component A and the critical point of the heavy component B, respectively. The branch of the critical curve starting from the critical point of the light component A finishes at an UCEP [$L_2 + L_1 =V$], the temperature of which is higher than critical temperature of the light component A. In type IV and V, the branch of vapor-liquid critical curve originating from the heavy component B goes to lower temperatures via a pressure maximum and ends in a lower critical end point ($L_2=L_1+V$). In type IV, there is a second LL immiscible region at lower temperatures, with a second LL critical curve ending at a second upper critical end point. Finally in type III, the branch of the critical curve starting from the critical point of the heavy component B goes to very high pressure, sometimes after passing through a maxima and minima in pressure and/or a minima in temperature. All of these phase behavior types are predicted using simple cubic equation of state (EOS).

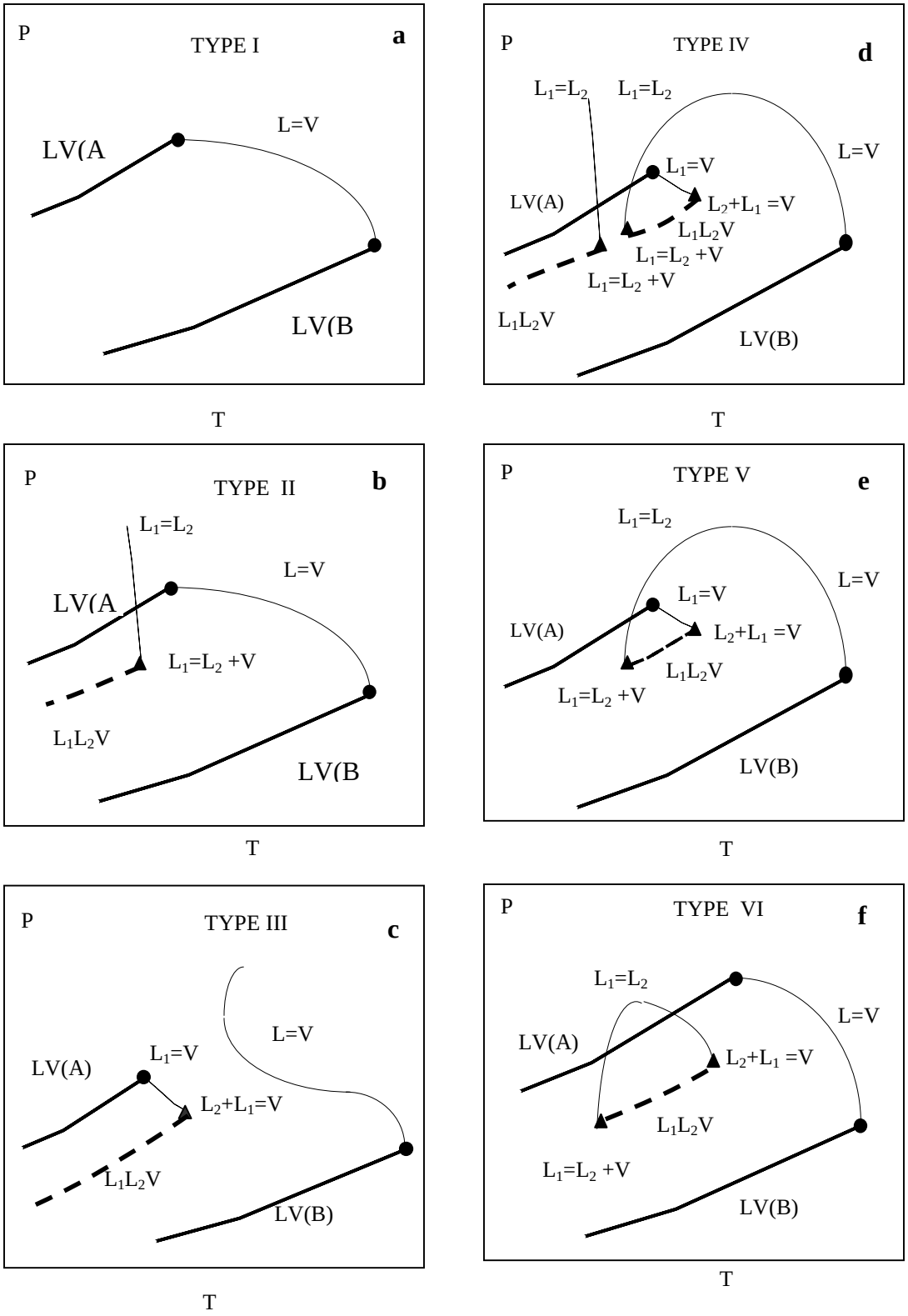

Figure 2-4 Binary phase behavior projections (van Konynenburg and Scott, 1980).

2.2.3.3 System asymmetry and phase behaviour type transitions in pseudo binary mixtures

The above classification scheme is found to relate to the degree of system asymmetry that measures the difference in the size, polarity and structure among components in a system. Raeissi, Gauter and Peters (1998) highlight the role of the degree of asymmetry on the nature of the phase behaviour exhibited by quasi binary mixtures of light gases (e.g., carbon dioxide, methane, propane) and members of various homologous series (alkyl-benzenes, n-alkanes, n-alcohols). The mixtures of light gases and the smallest members of homologous series have a minimum degree of asymmetry. Many such binaries are completely miscible and exhibit type I phase behavior. As the sizes of the homologous members increase, the mixtures become only partially miscible at low temperatures but remain miscible at elevated temperatures (type II phase behavior).

As the sizes of homologous members increase further, the mixtures become partially miscible at low temperatures and also near the critical region of the light component but remain completely miscible at intermediate temperatures (type IV phase behavior). If the degree of asymmetry is increased still further, the mixtures become only partially miscible (type III). Since the degree of asymmetry of these quasi binary system increases with size of the homologous members, the order of the degrees of asymmetry of these quasi binary mixtures is type I < type II < type IV < type III. The phase behavior transition from type II to type IV occurs at a tricritical point (TCP), where the high temperature branch of L_1L_2V curve in type IV converges to a point and the L-point and the K-point on this branch coincide. The phase behavior transition from type IV to type

III occurs at a double critical endpoint, DCEP, where the L-points of the two L_1L_2V equilibria curves join.

Minicucci et al. (2002) simulated such phase behavior transitions for anthracene and n-alkane mixtures (dash lines in Figure 2-5). The pseudo binary mixtures exhibit type III, type IV, and type II phase behavior for the carbon number range of 4.3~5.7, 5.7~6.1 and 6.1~6.2, respectively.

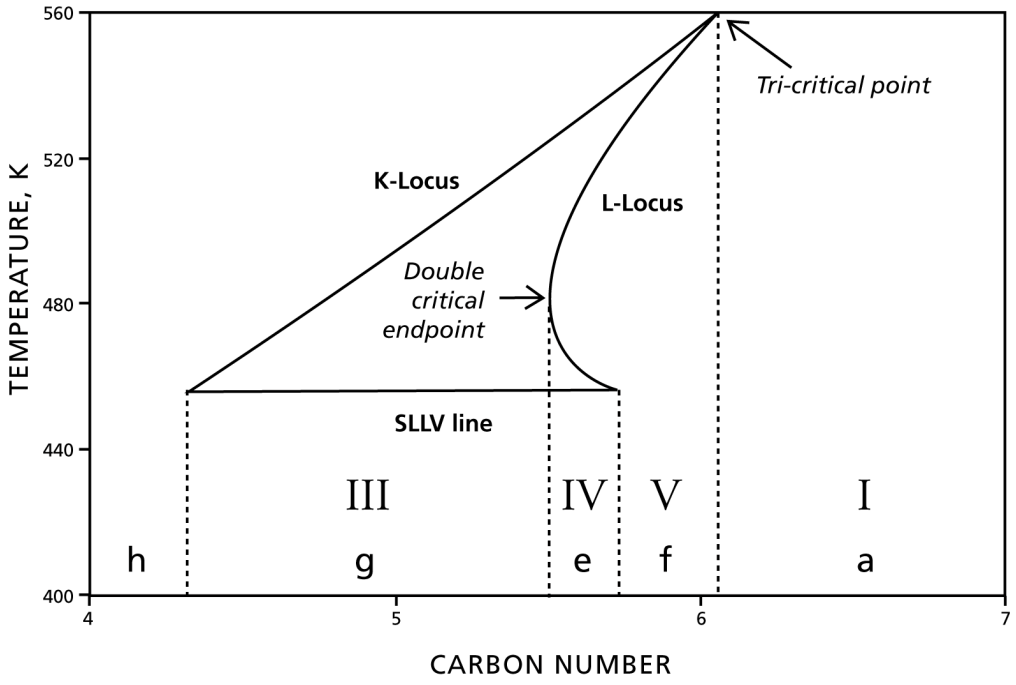

Figure 2-5 Simulated phase behavior types for anthracene + n-alkane mixtures (Minicucci et al., 2001).

This is an important concept and sets the stage for the exposition of multicomponent system phase behavior where abrupt changes in the nature of phase behavior, with composition, can be anticipated. One might also add that phase behavior type transitions complicate and hinder modeling efforts for such systems.

2.2.3.4 Solid interference

Industrial processes, such as supercritical extraction, often involve highly asymmetric systems, i.e., the critical temperatures of components involved are far apart. In many such systems, the critical temperature of the lighter component A lies below the triple point of the heavier component B, i.e., there is no common temperature range in which the two pure components are liquid. Consequently, these systems may exhibit SLLV and SLV multiphase behavior instead of LLV multiphase behavior as discussed in above. Using a binary type III mixture as an example, Figure 2-6 illustrates how the SLV multiphase behavior evolves from a typical LLV multiphase behavior in PT projections. In Figure 2-6a, the melting temperature of the heavier component is relatively low; the SL_2V curve stemming from the triple point of the heavier component intersects the L_1L_2V curve to form a SL_1L_2V four-phase point or Q-point (■). In Figure 2-6b, the melting temperature of the heavier component is relatively high. The SLV curve stemming from the triple point of the heavier component passes above the upper extreme of the L_1L_2V curve; SL_1L_2V phase behaviour is suppressed.

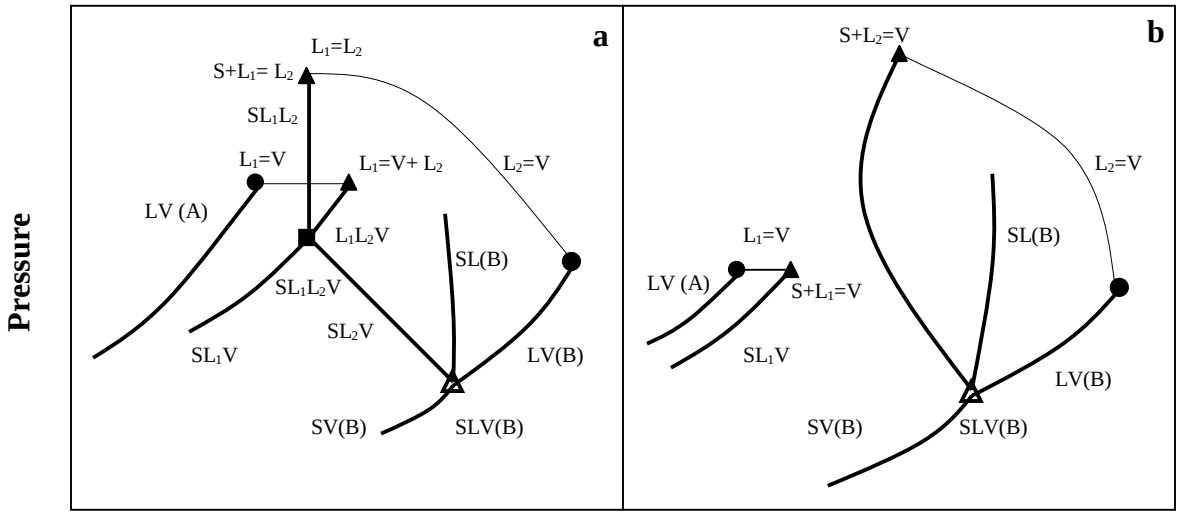

Figure 2-6 type III phase projection with solidification of the heavy component.

Binary fluids such as propane + phenanthrene or fluorine exhibit this type of phase behavior (Peters, et al., 1989). At the SLLV Q point, the vapour phase is essentially "pure" A (the light component), and the solid phase is essentially "pure" B (the heavy component).

2.2.4 Phase diagrams for multicomponent systems

Real systems, such as heavy oils, comprise many components and possess many more degrees of freedom. Phase diagrams for multicomponent systems are at least 4-dimensional. In practice, construction and interpretation of phase diagrams of multicomponent systems are similar to and based on those of binary systems. For instance, specific heavy oil mixtures are often interpreted using one type of phase behavior in the six-type classification proposed by van Koynenburg and Scott but allowing for the greater number of degrees of freedom. Illustrative examples are given below.

2.2.4.1 Phase behavior for multicomponent systems expanded from binary systems

Gregorowicz et al. (1992 & 1993) and Shaw et al. (1993 & 1997) reported detailed discussions on how to expand phase diagrams of binary systems to present phase behavior of ternary and higher order systems. Figure 2-7 illustrates their ideas using, as an example, a phase diagram with solid interference shown in Figure 2-6. Figure 2-7a shows the behavior of the binary mixture for a low heavy component mole fraction case, and Figure 2-7b for a high heavy component mole fraction case. Addition of a third component to this binary mixture increases the number of degrees of freedom by one, and thus expands the three-phase phase behaviors from curves to regions in the PT section as

shown in Figure 2-7c (for 2-7a) and 2-7d (for 2-7b), respectively. The Q point expands to a curve for ternary systems and a region for quaternary or more complex systems.

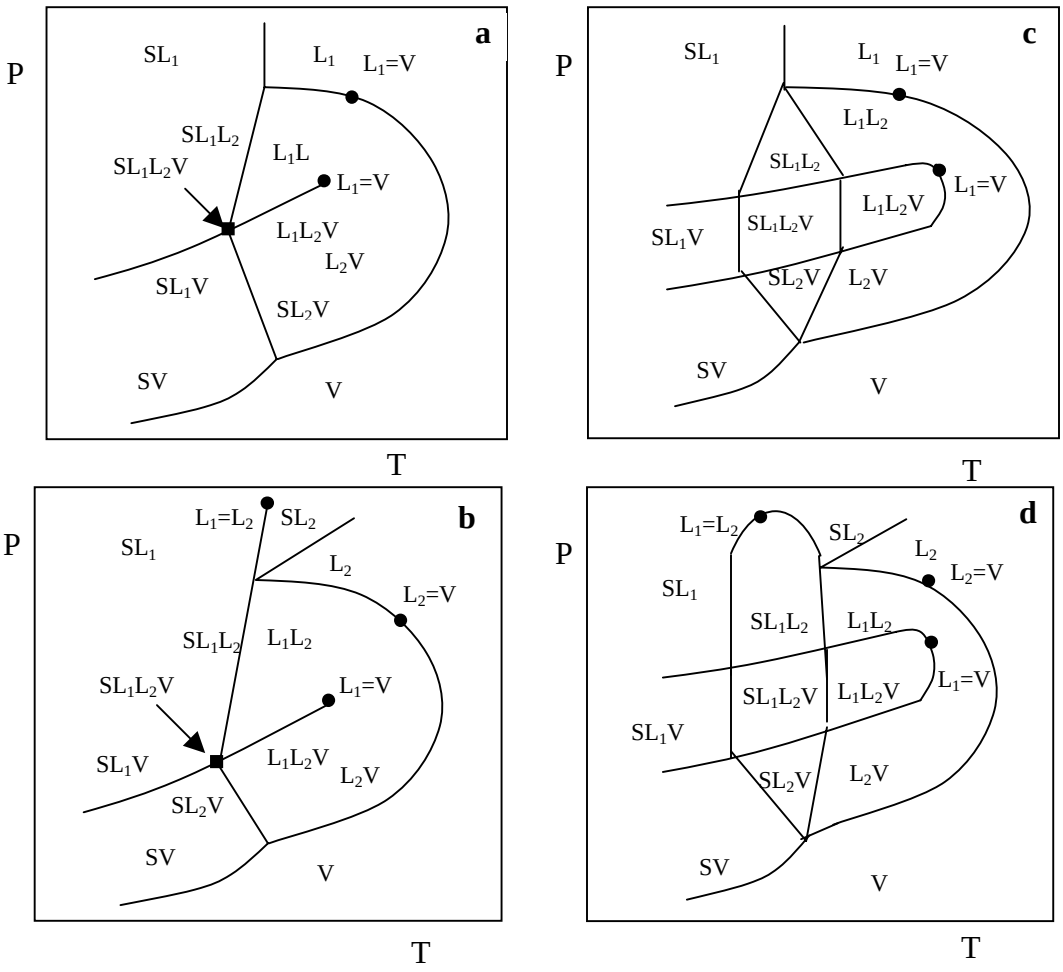

Figure 2-7 Expansion of P-T diagrams from binary mixtures to quaternary mixtures (Shaw et al., 1997).

The nature and amount of the third component also have impact on the location and size of multiphase regions. For a mixture exhibiting the phase behavior shown in Figure 2-2, if the third component is miscible with both components of the binary system, the three-phase region is shifted to higher temperatures and pressures. Furthermore, as the amount of the third component in the mixture increases, the L_2L_1V region shrinks. Eventually, the LCEP and the UCEP coincide at a tricritical point and a transition to type I phase

behavior arises. If the third component is immiscible with both components of the binary system, the three-phase region is shifted to lower temperatures but higher pressures and the L_1L_2V region is expanded—Figure 2-8. Simulation by Minicucci et al. (2001) shows that hydrogen shifts the three-phase regions of anthrancene + alkanes mixtures vertically to high pressures.

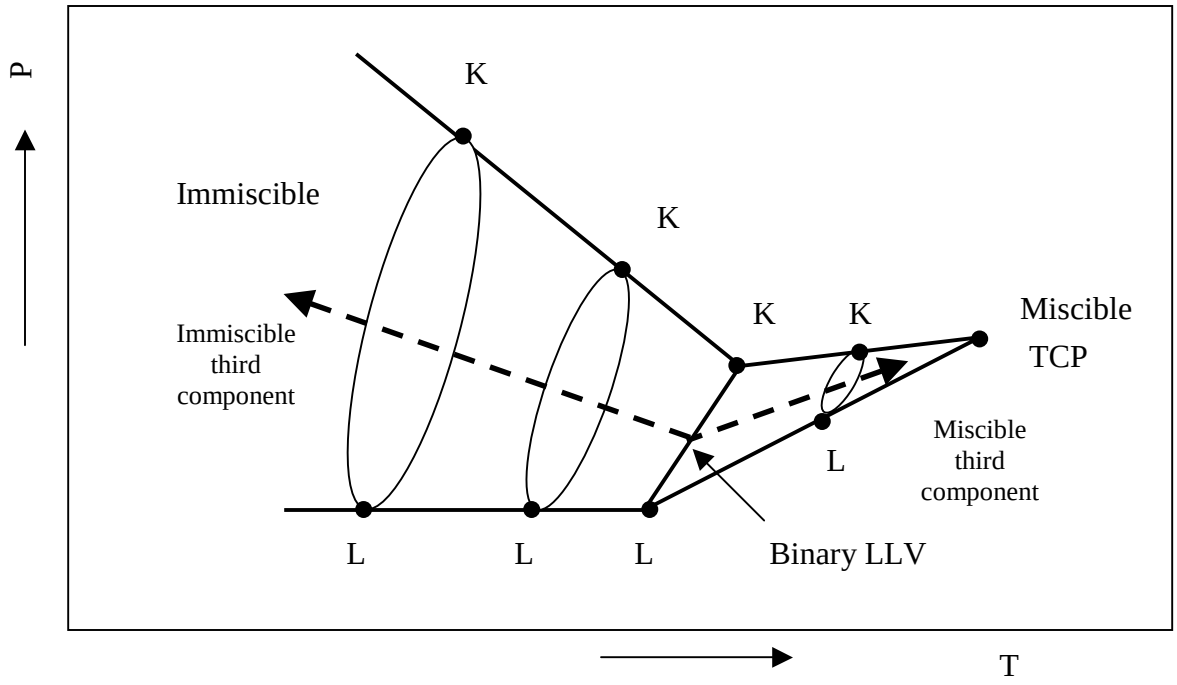

Figure 2.8 Schematic of three-phase region shift with addition of a third component to a binary mixture

These cartoons illustrate how multiphase regions can be controlled in the PT space through the addition of an appropriate third component. If the third component is a light gas (Shaw et al., 1993), the LLV region is shifted to dramatically higher pressures but slightly lower temperatures. Figure 2-7 also illustrates retrograde condensation phenomena around the L_1L_2V three-phase region where at fixed composition one observes, as pressure is increased at fixed temperature, sequences such as $V \rightarrow L_1 + V \rightarrow L_1 + L_2 + V \rightarrow L_1 + V \rightarrow V$ (D.B. Robinson, 1989) and $V \rightarrow L_1 + V \rightarrow L_1 + L_2 + V \rightarrow L_1 + V$

$\rightarrow L_1$ (Abedi et al., 1999). These findings among others are of great significance in solving industrial problems and in developing new industrial processes.

2.2.4.2 Equilateral triangle composition diagrams for ternary systems

The phase behavior of ternary mixtures can also be depicted as sections of PTx_1x_2-space keeping one or more variables constant. A widely used section for ternary systems is an equilateral triangle composition diagram at a fixed pressure and temperature (Figure 2-9).

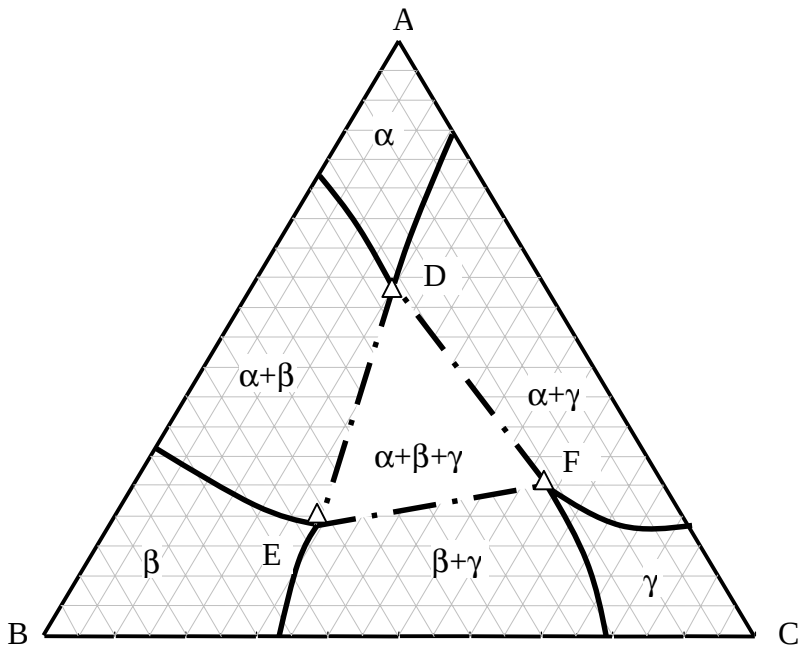

Figure 2-9 An example of equilateral triangle composition diagram for ternary mixtures at Fixed pressure and temperature. (The region enclosed by triangle DEF represents a three-phase zone)

In the above Figure, three vertexes (A, B and C) represent the three pure components, respectively; a point on a side (AB, BC or AC) represents a binary (A+B, B+C or A+C) mixture; a point within the triangle represents a ternary mixture (A+B+C). Since the compositions are in mole or mass fraction ($x_1+x_2+ x_3=1$), only two compositions are needed to locate a point in the diagram. At fixed temperature and pressure, the number of degrees of freedom for one-phase (α,β,γ), two-phase ($\alpha+\beta,\gamma+\alpha,\beta+\gamma$) and three-phase

(α+β+γ) behaviors are 2, 1 and 0, respectively; consequently, they are depicted in the triangle as regions (α,β,γ), curves (solid thick curves) and points (D, E, F), respectively. The region enclosed by triangle DEF (dash dot line) represents a three-phase zone. Points within the zone represent compositions of heterogeneous mixtures of three phases (α+β+γ); the compositions of these three phases are fixed and represented by D, E and F, respectively. The relative amount of each coexisting phase is determined from the mass balances. Shaw (2002) constructs equilateral triangle composition diagrams to describe the multiphase behavior of asphaltene containing heavy oil mixtures.

2.2.4.3 Three dimensional prism and pyramid phase diagrams

Prisms and pyramids, Figure 2-10 and 2-11, are also used to describe complex phase behavior.

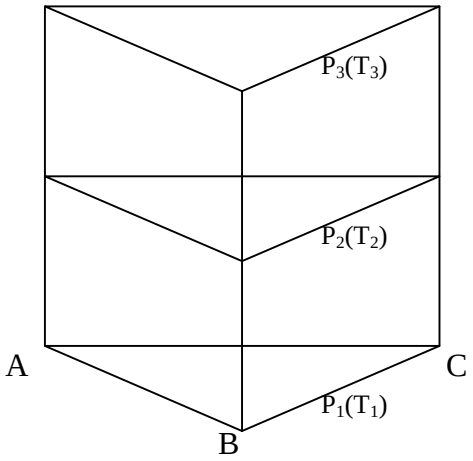

Figure 2-10 Prism schematic for a ternary mixture at fixed temperature (pressure).

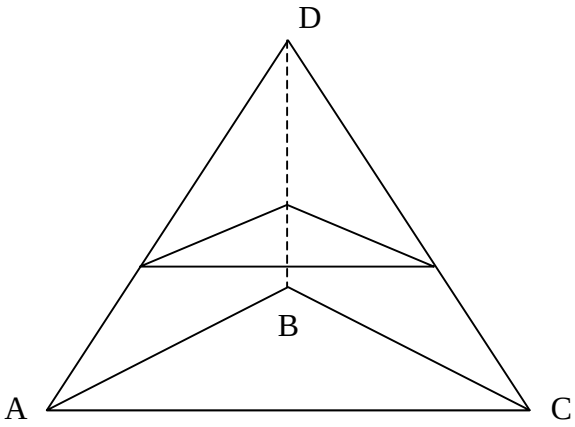

Figure 2-11 Pyramid schematic for a quaternary system at fixed pressure and fixed temperature.

Prisms are used to show the effect of pressure or temperature on the phase behavior of ternary systems. Pyramids are used to describe the phase behavior of quaternary systems at fixed temperature and pressure, and correspond to the triangle diagrams used for ternary systems. Figure 2-11 shows an example of a pyramid diagram: four vertexes

(A, B, C and D) represent the four pure components, respectively; a point on a side represents a binary mixture; a point on a triangle surface represents a ternary mixture; a point within the pyramid represents a quaternary mixture. Since the compositions are in mole or mass fractions, only three compositions are needed to fix a point in the pyramid. For a quaternary system at fixed temperature and pressure, one-phase, two-phase, three-phase and four phase behavior are depicted in the pyramid as three-dimensional spaces, regions, curves and points, respectively. Recently Shaw (2002) discussed the necessities of using pyramid diagrams to describe the complex behavior of asphaltene containing heavy oil mixtures.

2.2.5 Characteristics of SCF and SCFE processes

The most important characteristics of SCF are dramatic changes of its properties, such as density, viscosity, diffusion coefficient and solubility of solutes, with temperature and pressure near its critical point. Figure 2-12 shows PR EOS simulation results for the reduced density of pentane as a function of reduced temperature and reduced pressure. In the region close to the pentane critical point in Figure 2-12, small changes in pressure and temperature result in significant changes in fluid density. Since the solubility of a low volatile solute in a gas increases with the density of the gas, naturally dramatic changes of the solute solubility with pressure and temperature are expected in the supercritical region of the solvent. Figure 2-13 shows the solubility of naphthalene in compressed ethylene versus pressure at four different temperatures (Kurnick and Reid 1981).

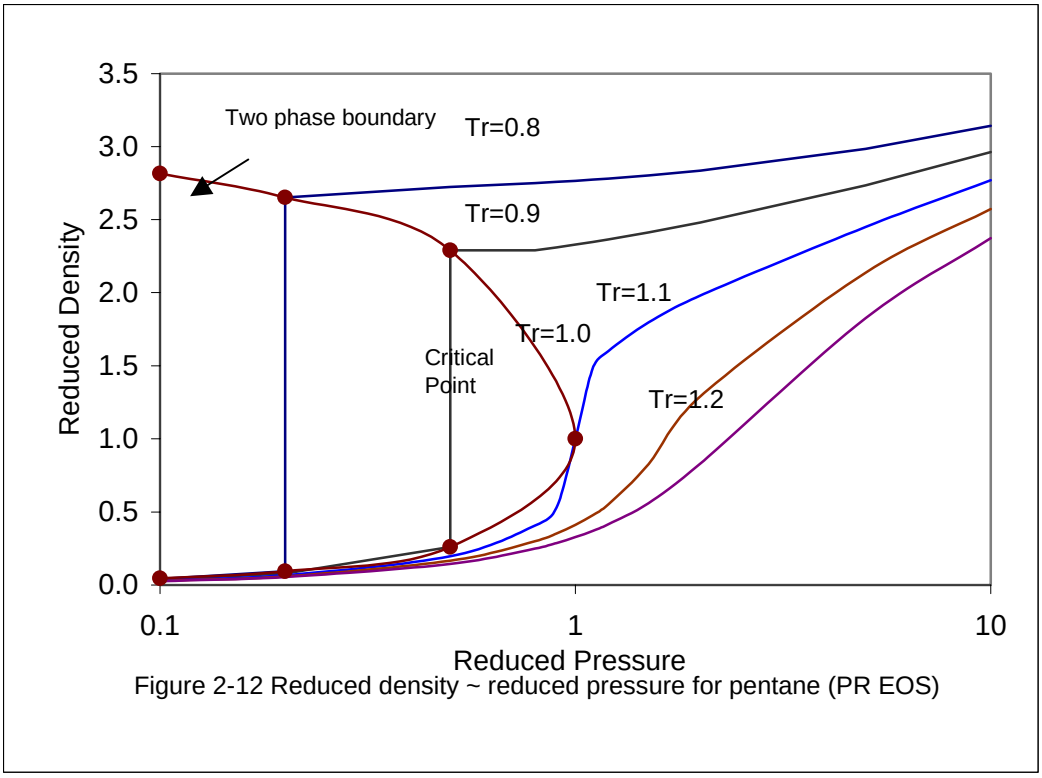

Figure 2-12 Reduced density ~ reduced pressure for pentane (PR EOS)

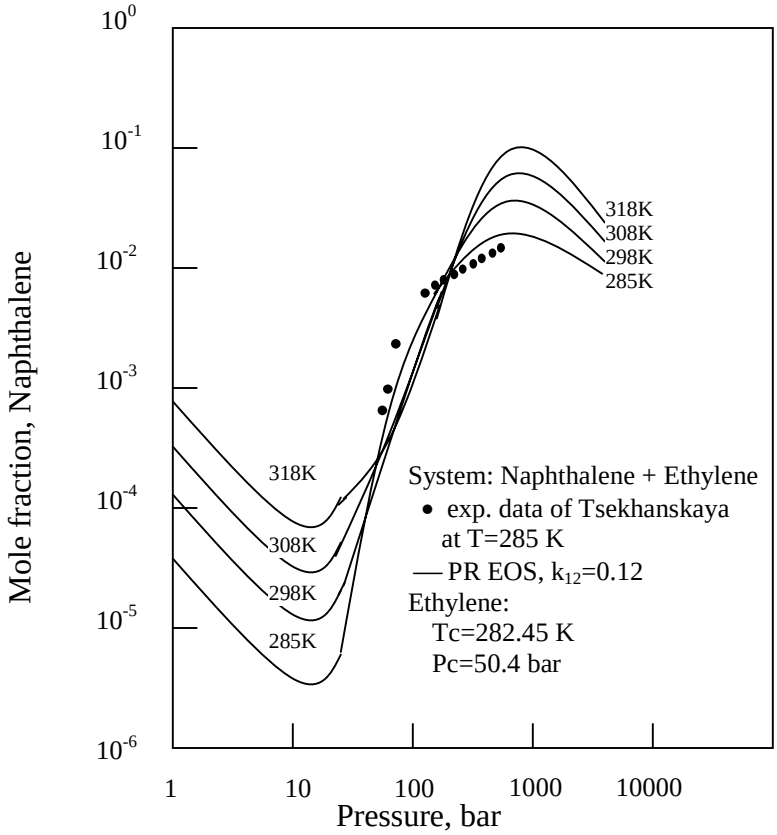

Figure 2-13 Solubility minima and maxima for naphthalene in compressed ethylene (Kurnick and Reid 1981).

The four isotherms in Figure 2-13 have a similar trend: a maxima and a minima. For each isotherm, at very low pressures, the vapour phase behaves like an ideal gas mixture and the solubility is governed by the vapour pressure of pure naphthalene, which is constant at a fixed temperature. Therefore the mole fraction in the gas phase decreases as the pressure increases at low pressures. As the pressure increases further, the density of the vapour phase increases and the naphthalene becomes more soluble. The cancellation of these two trends at an intermediate pressure results in solubility minima. As the pressure increases still further and approaches the critical pressure of ethylene, the solubility increases rapidly because of the dramatic density increase of the vapour phase to that of liquid. Further increases in pressure increase the repulsive force between ethylene and naphthalene, which "squeezes out" naphthalene from the vapour phase, so a maximum is observed at high pressure.

Viscosity and diffusion coefficients of SCFs demonstrate similar dramatic changes with pressure and temperature as that of density. SCFs have both gas-like and liquid-like properties; these are compared in Table 2-4. The gas-like viscosities and diffusion coefficients of SCFs help reduce resistance to mass transfer.

Table 2-4 Typical physical properties for gases, liquids and SCFs (Taylor, 1996)

	Density (g/ml)	Dynamic viscosity (g/cm-s)	Diffusion Coefficient (cm^2/s)
Gas (ambient)	0.0006~0.002	0.0001~0.003	0.1~0.4
SCF (T_c, P_c)	0.2~0.5	0.0001~0.003	0.0007
Liquid (ambient)	0.6~1.6	0.002~0.03	0.000002~0.00002

The above unique characteristics of SCFs have been exploited to develop new extraction processes—SCFE processes. SCFE processes have the following advantages:

(1) Liquid-like solvating power, but gas-like viscosities, diffusion coefficients and surface tension, which means a low solvent to feed ratio, fast separation and high energy efficiency;

(2) Dramatic change of solubility of solutes with pressure and temperature, which requires low pressure and/or temperature drop for separation, and this leads to fast and easy separation and recycle;

(3) Safe, cheap and environment friendly solvents (CO_2, C_2H_4, C_3H_8, etc.).

(4) Low operating temperature, low energy cost, good for separation of temperature sensitive materials:

(5) High selectivity, which can be adjusted by adding a co-solvent.

The successful application of SCFE processes depends on accurate phase behavior data within operating conditions, but the data are very hard to measure. Consequently, the potential of this new promising technique has not been fully demonstrated. Currently, a typical application of SCFE technology in the petroleum industry is residuum oil supercritical extraction (ROSE) processes discussed further in section 2.3.3.

2.3 Heavy oil/bitumen and production technology

2.3.1 Heavy oil/bitumen properties and characterization

2.3.1.1 definitions of heavy oil and bitumen

Heavy oils include atmospheric residues (AR) and vacuum residues (VR), topped crude oils, coal oil extracts, crude oils extracted from tar sands, etc. Bitumen is defined as “Any natural mixture of solid and semi-solid hydrocarbons”. These definitions are only

qualitative. UNITAR classifies heavy oils and bitumen on the basis of viscosity and density—Table 2-5.

Table 2-5 UNITAR definitions of heavy oils and bitumen (M. R. Gray, 1994).

	Viscosity mPa.s	Density G/cm^3	API Gravity
Heavy Oil	10^2~10^5	0.934~1.0	20~10
Bitumen	$>10^5$	>1.0	<10

Heavy oils/bitumen generally have a high specific gravity, low hydrogen-to-carbon ratio, and contain large amounts of asphaltenes and fine solids (Table 2-6).

Table 2-6 Comparison of light crude and heavy oils/bitumen.

	Athabasca Bitumen Vacuum Bottoms 525 °C +	Cold Lake Residue 424 °C +	Arabian E. Light Crude
Density, g/cm^3	1.045	0.994	0.832
H/C molar ratio	1.40	1.40	1.85
SARA analysis			
Saturates (wt%)	6.80	12.3	NA
Aromatics (wt%)	41.99	6.7	NA
Resins (wt%)	19.04	58.1	NA
Asphaltenes (wt%)	32.18	22.9	NA
Elemental composition			
Sulfur, wt%	6.87	5.1	1.10
Nitrogen, wt%	0.65	0.45	0.03
Ni, ppm	137	200	1
V, ppm	344	490	2
Data source	This study	Gray, 1994	Gray, 1994

2.3.1.2 SARA

One of the most widely used techniques in characterizing heavy oils is SARA analysis (ASTM D-2006, ASTM D-2007 and ASTM D-4124), in which heavy oils are fractionated, by selective precipitation (for the asphaltenes) and/or chromatographic techniques, into four classes of compounds: Saturates, Aromatics, Resins, and Asphaltenes (Figure 2-14).

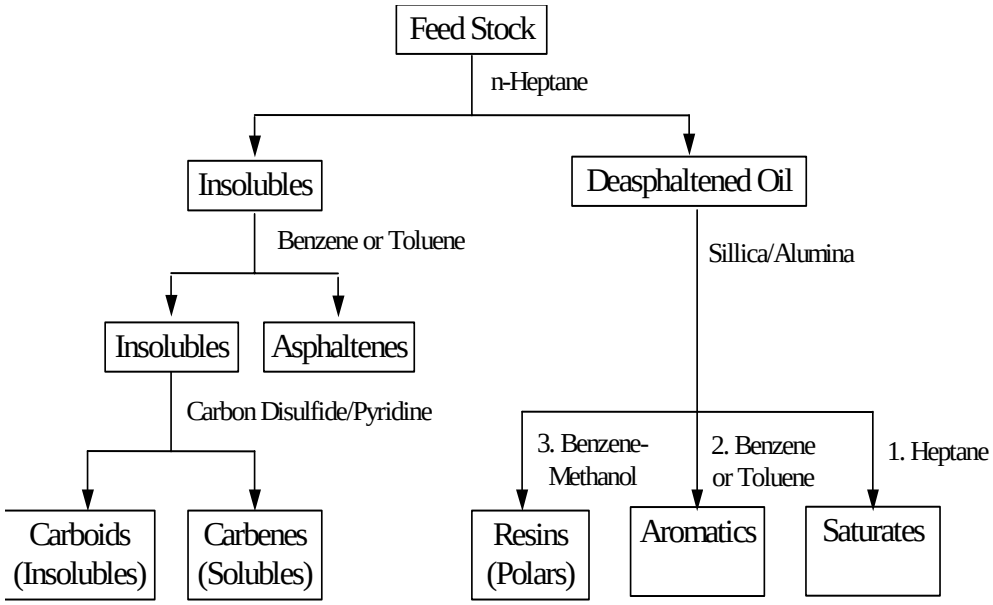

Figure 2-14 Petroleum fractionation (Speight et al, 1999)

Of the four classes of compounds identified, only saturates are distinguishable from the rest of the components in the mixture on the basis of objective criteria. The absence of π-bonds in the constituents of this class allows them to be easily differentiated. The remainder of the heavy oil is composed of aromatic and heteroatomic compounds of varying degrees of condensation, alky substitution, and functionalization. The resins are higher in heteroatoms and have a higher concentration of aromatic carbon, while the asphaltenes are the highest molar mass fractions and contain most of the polar

compounds. The mixture constitutes a compositional continuum with respect to both molar mass and polarity. Therefore, distinctions between the aromatic, resin and asphaltene fractions are inherently arbitrary and must be made in the light of the conditions employed to effect their separation. This issue is discussed further in section 2.3.2.

2.3.1.3 Composition maps

Alternatively, oil mixtures are characterized by composition maps. As we noted above, the composition of petroleum consists of two distributions: one of molar mass and the other of molecular type. Long and Speight (1999) developed compositional maps using the molar mass distribution and the molecular type distribution as axes. At first, the solubility parameter was chosen to represent molecular type. However, since measuring the overall solubility parameter of a petroleum fraction is very time-consuming, attempts have been made to find another characteristic parameter, which is easy to measure and can correlate with the solubility parameter and thus give an alternative continuum in molecular type. The hydrogen-to-carbon atomic ratio H/C of petroleum fractions was found to correlate well with the solubility parameter and was thus used to replace the solubility parameter in some composition maps (Long & Speight, 1999; Wiehe, 1992 & 1993). Such composition maps, once developed, can be used to describe chemical and physical properties of heavy oil and provide insights into many separation and conversion processes in petroleum refining (Speight & Long, 1999).

2.3.2 Asphaltenes and their solution behavior

2.3.2.1 What are asphaltenes?

Asphaltenes are identified by SARA analysis as a solubility class which is distinguishable from the de-asphalted oil because it is insoluble in the precipiting solvent under the operating conditions employed. They may be composed of molecules that differ significantly in their chemical characteristics (e.g. molar mass, aromaticity, heteroatom and metal content etc.). It has been widely accepted that asphaltenes are aromatic polycyclic clusters variably substituted with alkyl chains that may be quite long (up to C10-C12) and connected by alkyl and heteroatom bridges (Yen, 1984 & 1994; Strausz et al., 1992). The degree of condensation of each aromatic cluster may be more or less elevated, but generally does not exceed 5-6 rings. Their physical dimensions fall in the range of 1-100 nm (Overfield et al., 1989; Storm et al., 1994; Sheu et. al, 1992, 1994 & 1995, Mullins et a., 1995, Yen et al., 1992).

Being identified as a solubility class, the yield and chemical composition of asphaltenes naturally depend on many variables including choice of alkane solvent (Figure 2-15 a & b), time of mixing (Figure 2-15 c), diluting ratio (Figure 2-15 d), temperature and pressure conditions, the pore size of filter (Szewczyk et al., 1999), as well as carbonaceous fuel sources. ASTM has set up a series of standard procedures to guarantee consistent experimental results for the same sample separated by different researchers.

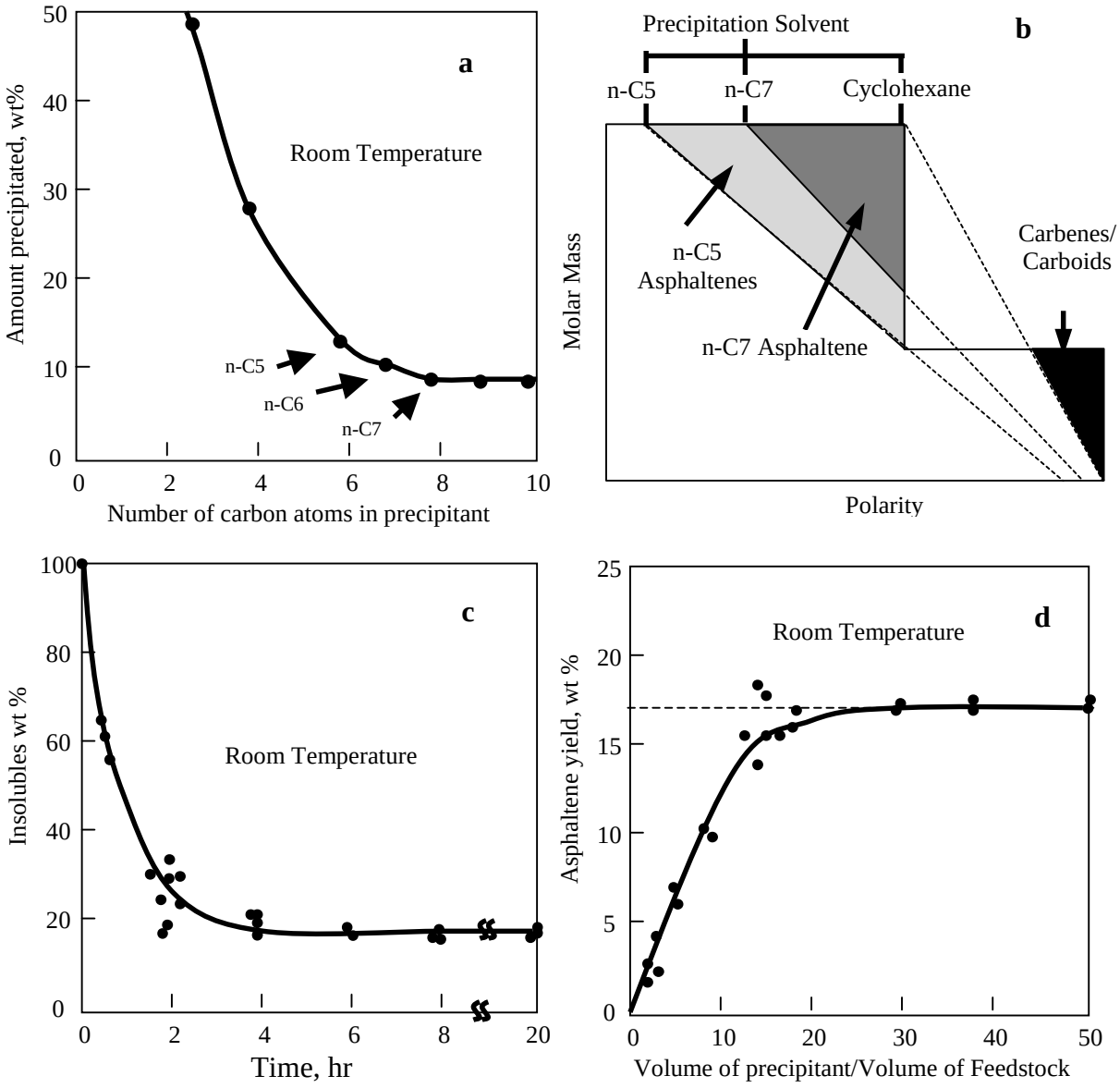

Figure 2-15 Effects on asphaltene precipitation (Speight et al., 1999). a: carbon number of solvent; b: solvent type; c: contact time; d: dilution ratio

Although having a wide distribution in molar size and molecular type, asphaltenes still have the following common characteristics. They generally (1) concentrate in end fractions of heavy oils and are primarily non-distillable materials; (2) contain most of fine

inorganic solids, heteroatoms and heavy metals; and (3) have a high coking tendency. These properties are consistent with properties of polar and heteroatomic materials separated from crude oils. But the most characteristic trait of asphaltenes is their solution behavior; i.e.; their pronounced tendency to form aggregates in hydrocarbon solutions (Overfield et al., 1989; Sheu et al. 1992 & 1995; Yudin et al., 1998).

2.3.2.2 Asphaltenes solution behavior

In solution, asphaltenes are partly dissolved and partly dispersed as aggregates. Asphaltene aggregates are commonly referred to as micelles in literature, based on an analogy drawn early on the behavior of surfactant molecules in solutions. The generally accepted picture of the physical behavior of asphaltenes in hydrocarbon media is illustrated schematically in Figure 2-16.

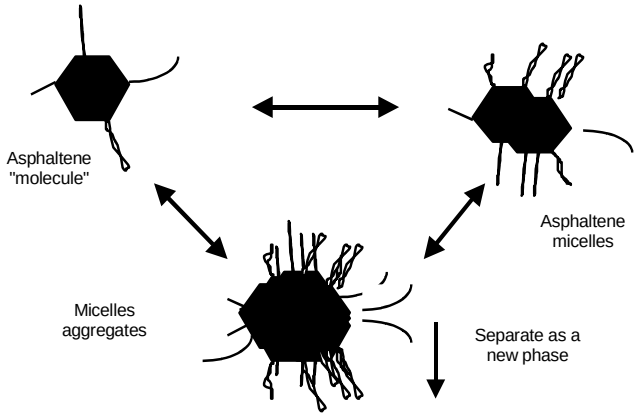

Figure 2-16 Schematic diagram of asphaltene aggregation process

SAXS and SANS studies (Overfield et al., 1989; Sheu et. al 1995) on asphaltenes dissolved in hydrocarbon solvents have shown that the dimensions of micelles also depend strongly on the nature of the solvent, asphaltene concentration, and system temperature and pressure. Under unfavorable solvent conditions, asphaltene micelles are prone to further aggregate into clusters that are unstable with respect to precipitation. On

the other hand, if dissolved in good organic solvents, asphaltenes appear to display the same qualitative behavior as in petroleum fractions.

2.3.2.3 Multiphase behaviour of asphaltene containing heavy oil mixtures

Asphaltene containing heavy oil mixtures, including reservoir fluids and bitumen + diluent mixtures, possess heavy and light fractions, from asphaltenes and resins to pentane. Typically, heavy fractions that contain asphaltenes are often present in significant mass fractions; but the light fractions dominate on a molar basis. From a phase behavior perspective, such fluids are referred to as asymmetric mixtures, and complex phase behaviors such as SLLV and LLV are expected. Construction of phase diagrams for asphaltene containing heavy oil mixtures is proven to be challenging (Shaw, 2002).

Model and actual reservoir fluids have both been shown to exhibit multiphase equilibria in and of themselves (Robinson, 1989; Gregorowicz et al., 1992; Jangkamolkulchai et al., 1998; Shaw et al., 1993; Estrera and Luks, 1987; Werner et al., 1996) or on addition of other fluids (Fall and Luks, 1986; Robinson et al., 1990; Shelton and Yarborough, 1976; Turek et al., 1988, Larson et al., 1989). In particular, the addition of carbon dioxide, nitrogen, and light hydrocarbon gases to reservoir fluids as envisaged in a number of secondary recovery process schemes is known to induce or enhance such complex phase behaviour over the range of pressures and temperatures encountered in hydrocarbon reservoirs. For example, Shelton and Yarborough (1976) found that the addition of carbon dioxide or a more or less equimolar mixture of methane, ethane and propane to a condensate rich reservoir fluid yielded four organic phase zones (solid-liquid-liquid-vapour) at intermediate pressures as well as large three phase (solid-liquid-

liquid and solid-liquid-vapour) zones. Solids drop out can also occur during normal reservoir depletion (Burke et al., 1990).

In the upgrading section, asphlatene containing hydrocarbon mixtures, such as bitumen + diluent mixtures, have also been found to exhibit multiphase equilibria (Minicucci et al., 2002; Abedi et al., 1998; Cartlidge et al., 1996a: Cartlidge et al., 1996b). Besides, asphaltene related phase behavior probably plays a key role in other phenomena, such as instability and incompatibility of the petroleum fluids (Mushrush and Speight, 1998), coking and fouling (Wiehe, 1993 &1994, Watkinson, 1999; Al-Atar et al., 1999).

Asphaltene related multiphase behavior, such as asphaltene deposition, poses problems in petroleum recovery and upgrading processes. Valuable hydrocarbons distributed among these various condensed phases or trapped by solid plugs is difficult to recover and consequently the utility of processes, based for example, on the injection of driving gases, is limited when complex phase equilibria arise. Thus there are incentives to have accurate phase diagrams and to be able to predict or interpolate phase behaviour. The appearance, prediction and properties of liquid-liquid-vapour and solid-liquid-liquid-vapour regions in model reservoir fluids have been addressed previously (Gregorowicz et al., 1992; Shaw et al., 1993, Peters et al., 1989; Shaw et al., 1997; Shaw and Behar, 1999).

The phase diagrams for these asymmetric fluids are characterized by lenses of four-phase behavior surrounded by three-phase and two-phase regions in both P-x at constant T, and P-T at constant x diagrams (Shaw, 2002). The most complex zones such as SLLV and LLV arise near the bubble pressure of the mixture, while SLL and LL phase behaviors extend from the bubble pressure to higher pressure. In most cases, these phase behaviors arise over narrow ranges of composition.

Many attempts have been made to understand the multiphase behavior of asphaltene containing heavy oils. Only limited success has been achieved due to the complexity of the mixture and lack of experimental techniques. Particularly multiphase behavior in the downstream section has not been investigated as intensively and extensively as in the upstream section. Multiphase behavior data of asphaltene containing mixtures under high pressure and high temperature conditions are of great practical and theoretical significance but seldom reported in the literature. Besides, some key topics, such as the reversibility of phase behavior of some components, particularly asphaltenes, are still debated (section 2.3.2.5).

2.3.2.4 Phase behaviour models for asphaltene containing heavy oil mixtures

Development of thermodynamic models for asphaltene containing heavy oil mixtures follow two distinct approaches. (1) thermodynamic molecular approach, and (2) thermodynamic colloidal approach. In the first approach, asphaltene "molecules" are assumed to be dissolved in oil in a true liquid state; thus, asphaltene precipitation is considered to be thermodynamically reversible. Phase equilibria models of this approach are developed on the basis of the classical Flory-Huggins polymer solution theory coupled with Hildebrand regular-solution theory (Hirschberg et al., 1984; Burke et al., 1990; Kokal et al., 1992, Andersen, 1994; Andersen et al., 1996, Kamath et al. 1994; Kawanaka et al., 1991; Macmillan et al., 1995; Cimino et al., 1995; Speight, 1991; and Yang et al., 1998; Lindeloff et al., 1998). The resin fraction is not considered explicitly in this approach, but is treated as an undifferentiated part of the solvent medium. The different asphaltene equilibria models that emerge within this thermodynamic molecular approach type can be classified further into two categories based on the treatment of

asphaltenes as: (i) monodispersed (homogeneous or single component) polymeric molecules and, (ii) polydispersed (heterogeneous or multicomponents) polymeric molecules. Polydispersity with respect to molar mass or solubility parameter (but not both) is used in model development. Generally, the polydispersed models give better results than monodispersed models. In order to simplify the mathematics, “molecular” models assume that the precipitated phase is solvent-free and solid asphaltenes. However, this assumption puts the asphaltene molecular model into direct conflict with the useful treatment of polymer solutions, from which they were inspired. Several groups have employed “molecular” models for interpolating experimental data, but none of these “molecular” models can be applied to predicting phase behavior. Furthermore, “molecular” models cannot explain two main factors in asphaltene precipitation: (1) the chemical association between asphaltene molecules, (2) the peptizing effect of resin molecules. Thermodynamic colloidal models, however, have overcome the two limitations satisfactorily.

In the thermodynamic colloidal approach (Leontaritis and Mansoori, 1987; Pan and Firoozabadi, 1997), the formation of asphaltene aggregates in hydrocarbon solvents and crude oil has been likened to the micellization of surfactants, and correspondingly asphaltene micelles have been likened to colloidals. These colloidal models can also be classified further: lyphobic colloidal models and lyphilic colloidal models. The lyphobic colloidal models treat asphaltenes in residue as lyphobic colloidals; i.e. two phase systems and inherently unstable with respect to flocculation. They assume that asphaltenes exist in the oil as solid particles in suspension and stabilized by resins (peptizing agents) adsorbed on their surface. The intermolecular repulsive forces between

resin molecules adsorbed on the asphaltene particles prevent them from flocculating. When the concentration of resins falls below a critical value, asphaltene particles may aggregate due to neutralization of their weak repulsive forces by mechanical or electrical means (Leontaritis and Mansoori, 1987; Kawanaka et al., 1991; Park and Mansoori, 1988, Mansoori, 1997). On the other hand, the lyphilic colloidal models treat the asphaltenes in residue as lyphilic colloidals solvated by the surrounding medium; i.e. a one-phase system. It implies that the asphaltene monomers and micelles are in thermodynamic equilibrium where the degree of association is determined by the relative energies of solvation of monomers and the micelles, and the entropy and enthalpy changes associated with the self-association of asphaltene monomers. According to this type of model, the stabilization of the asphaltene micelles by the resin fraction derives from the contribution of the latter to the solvent power (polarity and aromaticity) of the medium. Analogously, destabilization of the asphaltene micelles leading to their phase separation occurs when the solvating power of the medium towards asphaltene monomers and micelles is reduced to the point where they are no longer fully soluble (Pan and Firoozabadi, 1997, 1998 & 1999, Wu and Prausnitz, 1998). However, colloidal models, which contain even more parameters to be regressed from experimental data and are more complicated than molecular models, are also hard to apply for predicting asphaltene phase behavior and have been limited thus far to the explanation and interpolation of experimental data. Some of the underlying physical assumptions for all of these models have not been verified experimentally.

The successful development and verification of models always depend on the availability of sufficient amount of high quality experimental data. Unavailability of such

data accounts for the limitation of current thermodynamic models for asphaltene containing heavy oil mixtures. Therefore, the bottleneck here can only be broken by developing of novel experimental technique and accumulating more high quality data.

2.3.2.5 Hotly debated topics related to asphaltenes

Although asphaltenes and their solution behavior have been investigated intensively during the past five decades, some important aspects of this area are only partially understood. Many questions are still debated. Even the difference between asphaltenes and asphalts, and the difference between bitumen, pitch, residue, asphalt and heavy oil, are sometimes confused. Reversibility of phase boundaries with P, T and x are debated. Several relevant questions are discussed below.

1. Molar mass of asphaltene and resin

The accurate measurement of the molar mass of asphaltene is difficult due to their complex composition and self-association. Association of asphaltene and resin molecules provides further complications. As a result, a wide range of molar masses has been reported (500-50,000 Amu) (Wiehe, 1992; Mushrush and Speight, 1995; Storm et al., 1991; Groenzin and Mullins, 2000). Wiehe (1992) obtained a consistent number average molar mass of asphaltene of 3400 by using VPO near the maximum instrument temperature of 130 °C and using one of the best solvents: o-dichlobenzene. He then concluded that either better solvents or the higher temperatures cause asphaltenes to dissociate to a consistent molecular size. Molar mass in other highly polar solvents (such as pyridine) are reported to fall in the range of 2000±500 (Mushrush and Speight, 1995). This value seems to be supported by mass spectrometry (Storm et al., 1990). It is hard at

present to measure the molar mass of isolated asphaltene “monomers”; thus, the molar mass of asphaltene is still debated.

Resins differ from asphaltenes in having a higher affinity for petroleum media; however, the difference is inherently unclear due to the SARA separation method employed. VPO and scattering studies on isolated resin fractions show that they also tend to self-associate in organic solvents (Overfield et al., 1989; Sheu et al., 1995). The resin and asphaltene fractions are probably best viewed as two adjacent portions of a single broad compositional continuum that contains polar, aromatic, and higher molar mass components of petroleum.

The molar masses of asphaltenes and resins are set to ~1000 Amu and ~800 Amu respectively in phase equilibrium models. In some cases, they are treated as adjustable parameters falling in a certain range, such as 1000-1500 for asphaltenes and 500~800 for resins (Pan and Firoozabadi, 1997, 1998 & 1999).

2. Reversibility of asphaltene precipitation

Reversibility of asphaltene precipitation is also debated. Leontaritis et al. (1987) and Mansoori et al. (1988) treated asphaltene precipitation as an irreversible process since the precipitated asphaltenes cannot be dissolved upon further dilution with precipitant. These researchers argue that irreversible chemical polycondensation occurs once asphaltenes precipitate. Other researchers studied the reversibility of asphaltene precipitation due to changes in temperature, pressure and composition respectively. Pressure reversibility at high temperature has been addressed by Hirschberg et al. (1984) and seems to be accepted by others. However, reversibility with respect to composition at low temperature is unresolved. Rassamdana et al. (1996) and Chung et al. (1991) performed

experiments at room temperature to study the reversibility of asphaltene precipitation with respect to composition. They observed that part of the precipitated asphaltene redissolved into the solution and concluded that the asphaltene precipitation is partially reversible. Ramos et al. (1997) verified that the asphaltene precipitation and redissolution process in liquid titration is reversible when ultrasound was used for mixing. Ramos et al. (1997) also observed the redissolution of precipitated asphaltene in a crude/n-heptane mixture by adding toluene. Cimino et al. (1995) and Hirschberg et al. (1984) comment that titration experiments are reversible. At high pressure, Kokal et al. (1992) have observed reversibility of asphaltene precipitation with changes of pressure or composition. Recently Abedi et al. (1998) reported irreversible asphaltene precipitation at high temperatures and pressures (500~720 K and 3~7 MPa). At high temperatures, or with some catalysts, solids may precipitate as a result of chemical reactions which change the composition of asphaltene containing mixtures. “Asphaltenes” may precipitate due to irreversible chemical reactions. Thus the reversibility debate is complicated. Correspondingly, the phase behavior models can also be classified into reversible and irreversible models, as discussed in 2.2.3.

3. The role of resins in asphaltene precipitation

The role of resins in asphaltene precipitation is another debated issue and is related to the reversibility of asphaltene deposition (Hammami, 1998). Those researchers (Mansoori, Park, Leontaritis and others) who argue that asphaltene precipitation is irreversible conclude that resin plays a crucial role in the peptization and stabilization of asphaltene solutions and is physically present at the interface between asphaltene micelles and the crude oil. While other researchers (Cimino, Hirschberg, Pan, and

others), who agree that asphaltene precipitation is reversible, conclude that the presence of resin is not a necessary condition for the stabilization of asphaltene micelles against further aggregation in hydrocarbon media. These latter conclusions are based on experimental results of VPO and light/X-ray scattering studies, which have established that isolated asphaltenes associate spontaneously in hydrocarbons solvents to form micelles comparable in size to those present in crude oil. In addition, they display the same general solution behavior and are thermodynamically stable. The debate of the role of resins in asphaltene precipitation is also reflected in the various phase equilibria models.

4. The state of the precipitated phase

It is generally accepted that the precipitated asphaltenic phase at room temperature is in the solid state. Kokal et al. (1992) observed that the precipitated phase is in the form of dark solid particles when a crude is mixed with propane at room temperature and at elevated pressure. When the same crude was diluted with n-pentane or a heavier normal alkane at room temperature, the precipitated phase was also reported to be crystalline. Chung et al. (1991) found the precipitate to be solid when a crude was mixed with n-pentane. At high temperatures, both Kokal et al. (1992) and Hirschberg et al. (1984) observed the precipitation of a black liquid. Storm et al. (1996) observed a transition temperature from solid to liquid state at about 300 K for the asphaltene phase. However, Abedi (1998) detected a dispersed phase at temperatures above 650 K using X-rays and regarded it as a solid. This debate can also be complicated by chemical reactions at high temperatures or with a catalyst that affects the composition of precipitated phases. So

whether the precipitated phase is in a liquid or in a solid state at high temperature remains unresolved.

Most of the models developed for asphaltene precipitation are based on the assumption that the precipitated phase is in the solid state. This assumption may be true at room temperature but may not be valid at higher temperatures.

5. Effects of temperature and pressure on asphaltene precipitation

Different trends have been reported concerning the effects of temperature and pressure on asphaltene precipitation (Andersen, 1995; Kokal et al., 1992; Hu et al., 2002). For example, in the propane-deasphalting process, the amount of precipitate may rise as temperature increases. However, for normal-alkane diluents with a carbon number above 5, the precipitated amounts fall with increasing temperature (Fuhr et al., 1991; Ali and Al-Ghannam, 1981). Effects of temperature on asphaltene precipitation have been explained qualitatively by the changes of the solubility parameter with temperature (Wu et al., 1998; Pan et al., 1997). An increase in temperature affects the internal energy as well as the molar volume of asphaltene; both of these effects cause a decrease in the solubility parameter of asphaltene. A temperature increase itself leads to a lower tendency to precipitate. However, temperature simultaneously affects the solubility parameter of the solvation medium. The apparent effect of temperature is actually the competing effects of temperature and composition. Wu et al. (1998) give an alternative explanation through the discussion of the effects of temperature on solvent power based on Gibbs mixing energy and liquid density.

Concerning the pressure effect, generally, if the pressure is higher than the bubble-point pressure of the crude oil, rising pressure increases the solubility of asphaltenes in the crude oil; on the other hand, below the bubble-point pressure, a reduction of pressure

enhances the solubility of asphaltenes (Hirschberg et al., 1984; Burke et al., 1990, Kokal et al., 1992). Effects of pressure on asphaltene precipitation have also been explained qualitatively by the changes in solvent power with pressure (Wu et al., 1998; Pan et al., 1997). An increase in pressure affects the liquid density provided that there is no change in oil composition. Thus, at constant temperature and constant oil composition, an increase in pressure raises asphaltene solubility. However, if a vapor phase is present, an increase in pressure also raises the solubility of the light vapor components (such as CH_4 or C_2H_6) in solvent thereby, shifting oil composition towards a reduced solvent power. Therefore, if a vapor phase is present, an increase in pressure is likely to reduce the solubility of asphaltene in oil.

The phase behavior of asphaltenes in oil mixtures is often compared with phase behavior of solid solutes in high pressure gases since both of these two types of mixtures belong to highly asymmetric systems (Figure 2-13). Whether the maxima and minima in Figure 2-13 exist for asphaltene solubility curves is unclear at present since, unlike solids and gas mixtures, there are some middle components, such as aromatics and resins, present between asphaltenes and maltene solvent in asphaltene containing heavy oil mixtures. While these effects can be qualitatively understood, quantitative representation is unsatisfactory at present.

Although experimental and theoretical investigation on asphaltenes and their solution behavior have been conducted for five decades, the physical states of asphaltenes in crude oil and hydrocarbon solvents and their tendency to undergo phase separation remain only partly understood. Many questions are unresolved, such as the reversibility of asphaltene precipitation and the physical state of the precipitate phase at elevated

temperatures. More investigation is needed to settle these disputes and to improve our understanding of asphaltene solution behavior.

2.3.3 Solvent deasphalting process and ROSE process

The petroleum industry is a pioneer in developing novel separation processes, which take advantage of the near-critical and supercritical phase behavior of solvents. Successful applications include solvent deasphalting, and the ROSE process. These are briefly reviewed below.

2.3.3.1 Solvent deasphalting

The solvent deasphalting process was initially devised by Wilson, Keith and Haylett (1936) to selectively separate a lube oil feedstock into paraffin wax, asphalt, heavy ends, naphthenes, color bodies and the desired product which is a purified light oil. It is often called the propane deasphalting process due to the fact that it uses propane as the solvent and makes use of the unique phase behavior of propane in the vicinity of its critical point. The phase behavior associated with this process is illustrated in Figures 2-17 and 2-18.

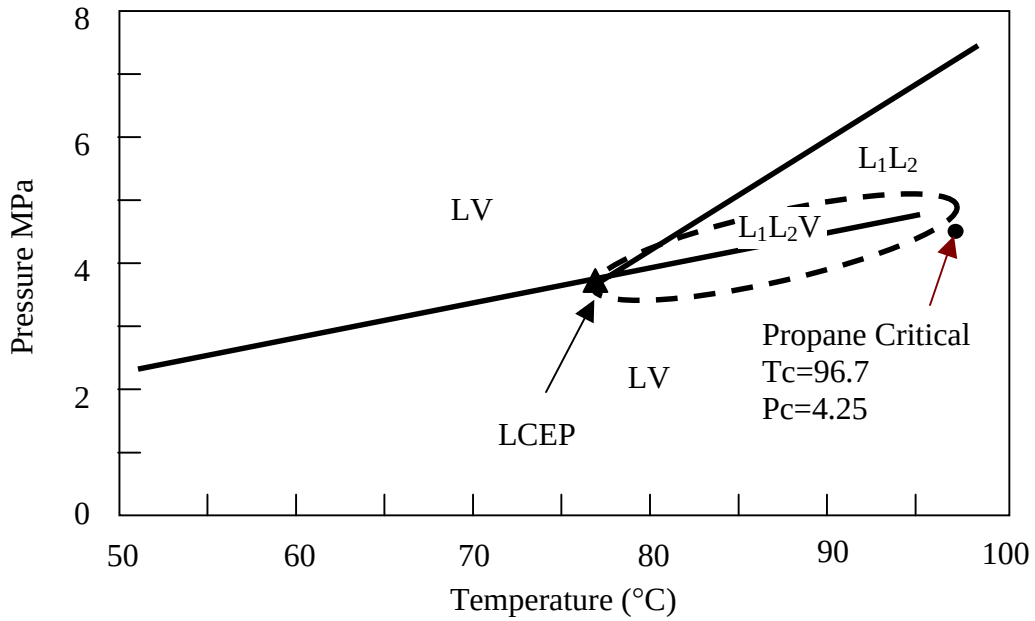

Figure 2-17, PT projection of the phase behavior of the propane-lube oil mixture (Wilson, Keith and Haylett, 1936).

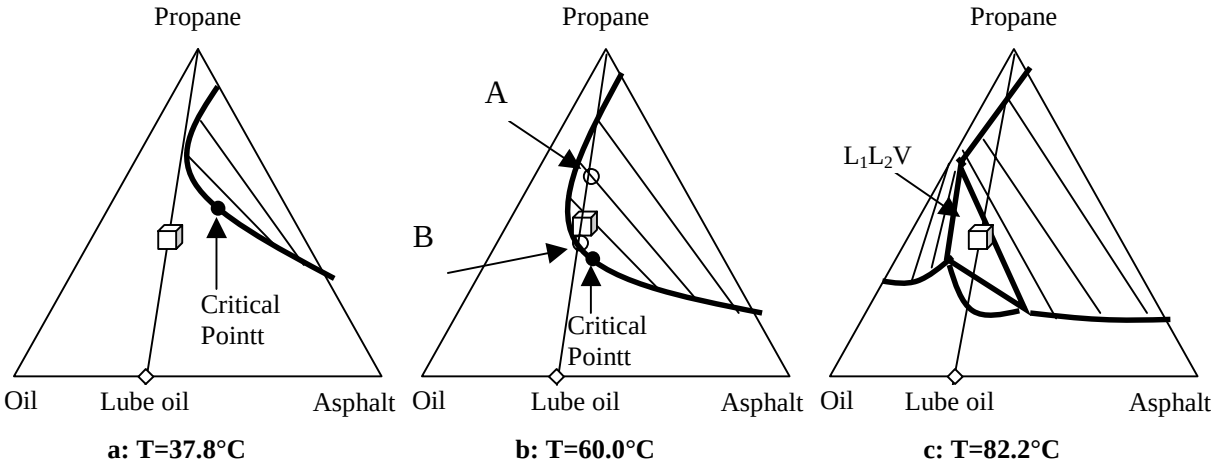

Figure 2-18 Ternary phase behavior of the asphalt-oil-propane mixture at three different temperatures (Wilson, Keith and Haylett,1936).

Wilson et. al. presented a LCEP but no UCEP. Also, the LLV phase behavior should be a region (enclosed by dash curve) instead of a curve, as indicated by the authors, considering lube oil itself is a mixture. In Figure 2-18, the same authors parse the lube oil mixture into two pseudo-components: oil and asphalt, and describe the mixture as a ternary system. The composition point of lube oil should be located on the oil ~ asphalt axis. As the system temperature increases from a to c, the mixture becomes less miscible: larger phase splitting region and one more coexisting phase result. If assuming the composition of lube oil is located at the diamond point on the oil ~ asphalt axis, the line connecting this point and the propane vertex, in fact, represents all composition points of propane and lube oil mixtures at different propane to lube oil ratios. In Figure 2-18a, the line does not intersect with the two-phase region, which means no phase splitting for propane and lube oil mixtures at any solvent to feed ratios. In Figure 2-18b, the line intersects with the two-phase region, which means two-phase splitting for all propane and lube oil mixtures with solvent to feed ratios falling inside the two-phase region but no

phase splitting with solvent to feed ratios falling outside the two-phase region. In Figure 2-18c, the line intersects with both the two-phase and the three-phase regions, which means two-phase splitting for all propane and lube oil mixtures with solvent to feed ratios falling inside the two-phase region, and three-phase splitting with solvent to feed ratios falling inside the three-phase region. For the composition point represented as a cube, the mixture exhibits one-phase, two-phase and three-phase behavior at 37.8, 60.0 and 82.2 °C, respectively. The selectivity of extraction is related to the feed to the solvent ratio, and also the shape of multiphase region that changes with the temperature and pressure of the system. Contrary to the popular belief that high solvent to feed ratio results in high selectivity, Figure 2-18 b shows that, compared with point B, point A has a higher solvent to feed ratio but has a lower selectivity, as deduced by the Lever rule. The above discussion demonstrates what complex phase behavior the propane deasphalting process may encounter and what a crucial role an accurate and complete phase diagram plays in guiding and optimizing process operation.

2.3.3.2 ROSE process

The Residuum Oil Supercritical Extraction (ROSE) process licensed by the Kerr-McGee refining company was developed in 1954 to remove asphaltenes and resins from residuum feed. Since the separation of asphaltenes from residuum feed requires a more powerful solvent than propane, the ROSE process generally uses butane or pentane as solvent and operates at higher temperatures. However, the phase behavior principles behind the ROSE process are quite similar to those of the solvent deasphalting process discussed above. Without repetition, only the process flow diagram (Figure 2-19) of the ROSE process is discussed.

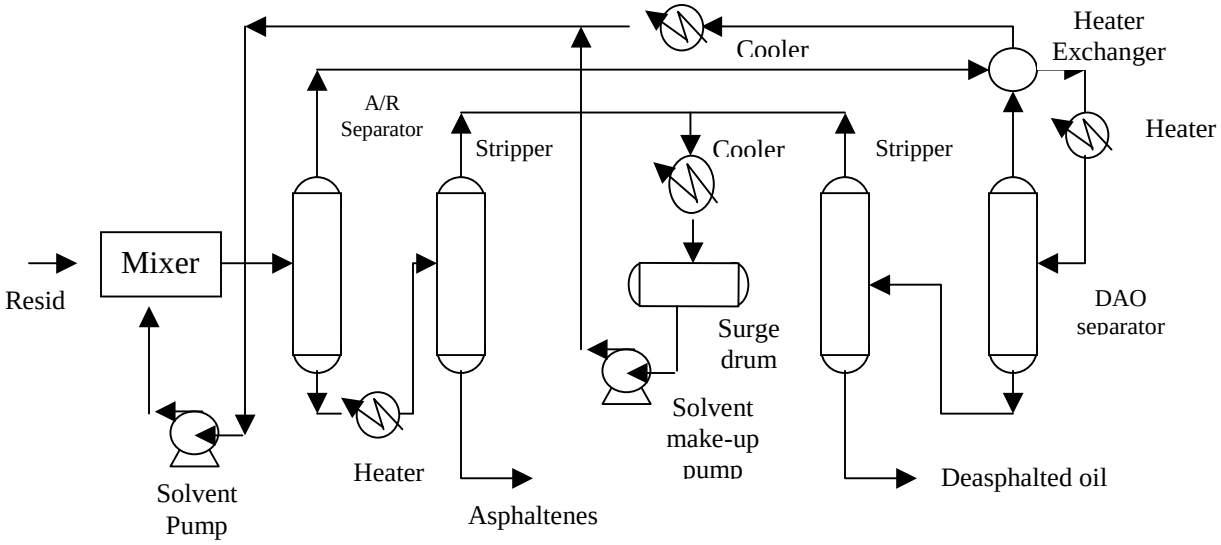

Figure 2- 19 Schematic of the ROSE process (McHugh, 1986).

The residuum feed is mixed with compressed butane or pentane solvent at a pressure above the critical pressure of the solvent but at a temperature just below the critical temperature. At these conditions, asphaltenes precipitate from the bulk solution. The mixture is then sent to a separator where the asphaltenes are removed. If resins are to be removed as a separated product, the overhead from the asphaltene separator is heated and sent to a second separator (not shown in the Figure) where the resins precipitate. The solvent ~ oil mixture is then heated to a temperature just above the critical temperature of the solvent and sent to a third separator where solvent is recycled from the top stream and the remaining deasphalted oil is collected. The solvent is then cooled and sent back to the mixer.

ROSE units are not sufficiently selective for use with heavy oils/bitumen mixtures; up to 50% of the heavy oil/bitumen reports to the “rejected stream” (Shaw, 1999 and Savastano, 1991). As discussed above, thorough understanding of the complex behavior

of the solvent and heavy oils/bitumen mixture is the key step to improve process selectivity.

2.3.4 Distributions of heteroatoms, heavy metals and fine inorganic solids in different fractions of heavy oil/bitumen

Heteroatoms, heavy metals and fine inorganic solids are the main types of problematic species found in heavy oils. Understanding the distribution of these species in different fractions of heavy oils/bitumen is the key step to develop selective removal processes. Much effort has been devoted to heteroatoms and heavy metals, while the research about fine inorganic solids is scarce.

2.3.4.1 Heteroatoms and heavy metal distribution in different fractions of heavy oil/bitumen

Heteroatoms and heavy metal may occur in oil in a variety of forms. The distribution of these species varies markedly among crudes of various origins. However, sulfur, nitrogen, oxygen and heavy metals are prone to concentrate in the heaviest fractions. Figure 2-20 shows the distribution curves for these species in atmospherically topped Athabasca bitumen (Chung et al., 1997). The bitumen are first separated by vacuum distillation and then fractionated by SCFE. In Figure 2-20, C and H are almost evenly distributed; heavy metals are most unevenly distributed; the distributions of S, N and MCR (microcarbon residue) are between those of C, H and heavy metals. The above work also shows that about 80% of heavy metals, 50% of N, and 30% of S can be removed along with 20% of end fractions (asphaltenes). The distribution characteristic of each species is discussed below.

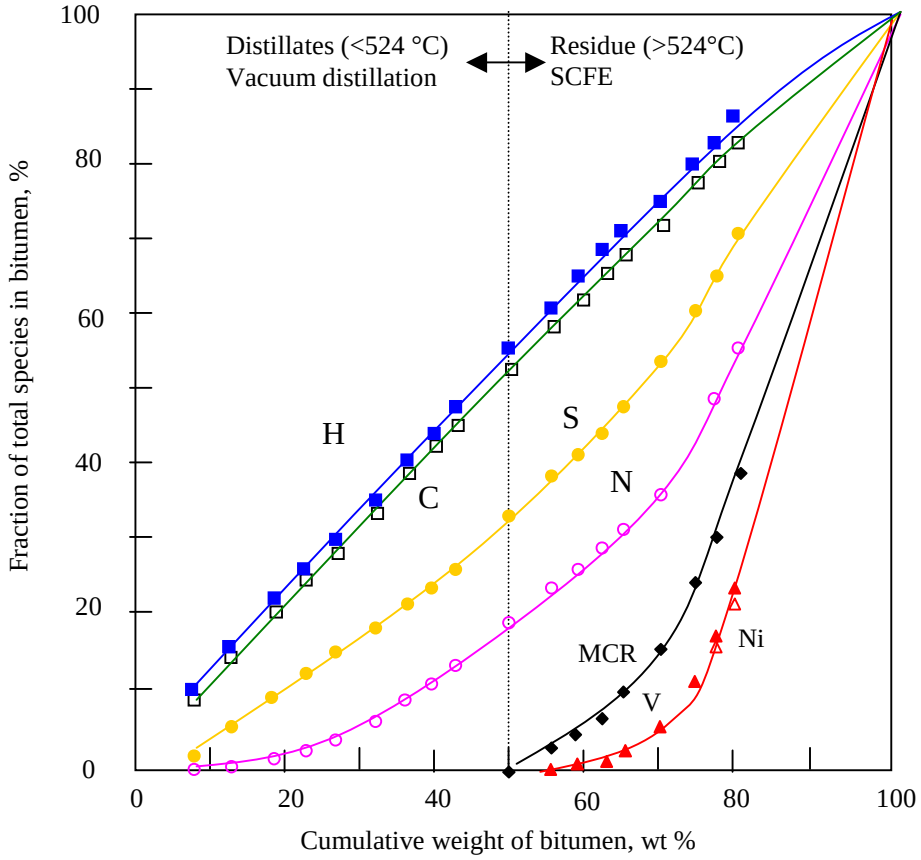

Figure 2-20 Distribution curve for key species in atmospherically topped Athabasca bitumen (Chung et al., 1997).

The heavy metals content of heavy oils falls within the range of 100 ~1000 ppm. Occasionally, the content exceeds 1000 ppm. Most heavy metallic compounds are concentrated in the residues. Although the content of heavy metals in petroleum is quite small, their impact on the upgrading processes is huge. For example, even minute amounts of nickel and vanadium in the feedstock of catalytic cracking units affects the activity of the catalyst, and results in increased gas and coke formation, i.e., reduced yields of valuable products.

The sulfur content of heavy oils falls within the range of 3~7 wt%. Generally, the higher the density of the oil, the higher the sulfur content. The content of sulfur also

increases with the boiling point during distillation; however, middle fractions may actually contain more sulfur than higher boiling fractions due to decomposition of the higher molar mass sulfur-containing compounds during distillation (Reynolds, 1999; Chung et al., 1997 & 1999; Boduszynski, 1987, Gray, 1994; Speight, 1999). Sulfur compounds are among the most problematic constituents of petroleum. The high sulfur content may cause a host of problems in production, such as corrosion, catalyst deactivation and environmental pollution. Consequently, refiners have to remove the sulfur compounds or convert them into less harmful forms.

The nitrogen content of petroleum is low and falls within the range 0.1~0.9 wt %. Nitrogen compounds are concentrated largely in end fractions. Generally, the more asphaltenic the oil, the higher its nitrogen content; the higher the carbon residue, the higher the nitrogen content (Chung et al., 1997 & 1999). The presence of nitrogen in petroleum is of much greater significance in refinery operations than what might be expected from the small amounts present. Nitrogen compounds can be responsible for the poisoning of cracking catalysts and for gum formation in domestic fuel oils.

The oxygen content of petroleum is usually less than 2 wt % although larger amounts have been reported. The oxygen content of petroleum increases with the boiling point of the fractions examined. High oxygen content may result from prolonged exposure of the oil to the atmosphere either during or after production. In fact, nonvolatile residues may have oxygen contents of up to 8.0 wt %. Oxygen is relatively less harmful than other heteroatoms in heavy oils.

2.3.4.2 Fine inorganic solids distributed in different fractions of heavy oil/bitumen

The fine inorganic solids content of heavy oils fall within the range 0.3 to 10 wt % (Kotlyar, et al., 1998 & 1999; Carbognani et al. 1999; Green et al., 1992). The major constituents of fine solids in heavy oil are ultrafine, aluminosilicate, clay crystallites containing small amounts of sulfur and titanium bearing minerals. Table 2-7 and 2-8 list yields and the elemental compositions of bitumen-associated solids (Kotlyar et al., 1999).

Table 2-7 Yield of asphaltenes (n-pentane insolubles) and bitumen-associated solids (BS) (Kotlyar et al., 1999).

	Asphaltenes		BS (wt %)	
Sample	Yield wt % bitumen	MW (GPC)	Concentration in asphaltenes	Concentration in parent bitumen
Bitumen A[a]	16.4	6600	5.2	0.9
Bitumen A[b]	2.3	9000	34.8	0.8
Primary froth bitumen	16.7-17.6	6100-6400	1.8-3.4	0.3-0.6
Rag layer bitumen	21.8-51.8	6700-7003	4.6-6.4	1.4-2.5
End cut	94.0	6606	11.0	10.3

[a] n-pentane insolubles. [b] blend (toluene/n-pentane with molar ratio of 3:5) insolubles.

Table 2-8 Elemental analysis of bitumen-associated solids (BS) from various sources (Kotlyar et al., 1999).

	Nonmetal (wt % of sample)				Metals (wt % of sample)							
Source	C	H	N	S	Fe	Mn	Ca	Ti	V	Ni	Mg	Al
bitumen A	20.2	2.2	0.1	1.2	5.9	0.2	0.6	2.1	0.03	0.02	0.6	n.a.
rag layer	18.3-30.8	2.3-3.3	0.4-0.8	1.3-2.7	3.8-6.0	0.08-0.2	0.5-0.9	2.3-3.0	0.03-0.04	0.02-0.03	0.4-0.5	6.2-9.6
end cut	26.1	2.5	0.3	3.3	5.1	0.2	0.5	1.3	0.03	0.01	0.5	7.2
hydrophilic ultrafines	0.8	0.4	0.0	0.0	1.3	0.1	0.5	0.2	0.005	0.04	0.3	n.a.
primary froth bitumen	19.5-26.0	2.2-2.3	0.4-0.5	2.4-2.6	n.a.	n.a.	n.a.	n.a.	n.a.	n.a.	n.a.	n.a.

n.a.: not available

The surface of fine inorganic solids are rendered asphaltene-like owing to the adsorption of polar, aromatic, toluene insoluble organic compounds, and thus the surface is bi-wettable. Consequently, the solids are often associated with water droplets (often salty) and form clusters of solids and droplets. The clusters disperse in the maltene component of bitumen and thus form a stable colloidal solution. Most of these solids precipitate along with asphaltenes in deasphalting processes and/or deposit within coke in upgrading processes. They also contribute to fouling in the reactor systems and to catalyst deactivation in catalytic hydroprocessing. The solids and salt particles may themselves become entrained in the volatile overhead liquids and cause corrosion and fouling in downstream process units.

In summary, heteroatoms, heavy metals and fine inorganic solids tend to be concentrated in the end fractions—asphaltenes. They are responsible for a host of problems in upgrading processes. The trend in recent years towards cutting deeper into crude to obtain stocks for catalytic cracking has accentuated the harmful effects of the problematic species. In order to accomplish the “cutting deeper” strategy, refiners are in urgent need of more selective removal processes.

2.4 Experimental techniques used to investigate asphaltene precipitation

Experimental data lay the foundation for theoretical models. Accurate detection of complex phase behaviour data is very hard, and particularly challenging for asphaltene-containing mixtures. Many experimental methods have been designed to observe “when”

and “how much” asphaltenes precipitate from solution, with varying degrees of accuracy and difficulty. They are summarized in Table 2-9.

Table 2-9 Methods used to detect asphaltene precipitation.

Method	Principles	Reference
Oliensis spot test	Examination of drops (concentric rings) on filter paper	Sheu, 2002
Electrical conductivity	Electrical conductivity reaches a maximum at the onset point of asphaltene precipitation.	Fotland et al., 1993, MacMillan et al., 1995
Microscopic examination	Based on the utilization of a microscope with light to visually detect the onset of deposition	Hirschberg et al., 1984;
Heat transfer	The solution temperature decreases abruptly (2 ~5 ^{o}C) at the onset point of asphaltene precipitation.	Clark et al., 1996
Viscosity measurement	The onset of asphaltene precipitation is detected by an increase in the viscosity of asphaltene containing solutions when diluted with a precipitant.	Escobedo & Mansoori, 1995&1997; Yang etal., 1998
Light transmission & X-ray scattering	Transmitted light density initially increases with the addition of precipitant, but it decreases dramatically at the onset of asphaltene precipitation..	Reichert et al., 1986; Thomas et al., 1992; Yang and Guo, 1998; Abedi et al., 1999

However, most of the above methods are applicable only in a narrow range of temperature and pressure near ambient conditions. Asphaltene precipitation problems occur over a wide range of temperatures and pressures in industry. This problem was solved by development of a novel technology — polychromatic *X-rays* coupled with a beryllium view cell, developed recently in the research group of Professor Shaw (Abedi et al., 1999). By deconvolution of polychromatic transmitted X-ray images, one can simultaneously obtain the number of phases present, their individual volume, apparent density and elemental compositions of heavy oil mixtures under production temperatures and pressures. The experiments proposed in this study are conducted using this apparatus.

A detailed description of this apparatus is given elsewhere (Abedi et al., 1999). The physical principle behind this technology is described in the next section.

2.5 Principles of phase behavior investigation by deconvolution of polychromatic transmitted X-ray images

The absorption of polychromatic X-rays is similar, in some extent, to colorimetry or photometry with white light. X-ray photons of all wavelengths emitted by the X-ray source, the continuous spectrum as well as the characteristic lines, enter and traverse the sample. The attenuation or absorption of the polychromatic beam or of different energy portions of the beam provides information about the sample regarding its composition, homogeneity, and thickness or density.

2.5.1 Basic physics of X-ray absorption

On passing through a medium, hard X-ray beams lose energy mostly by "true" photoelectric absorption and partly by scattering (Figure 2-21).

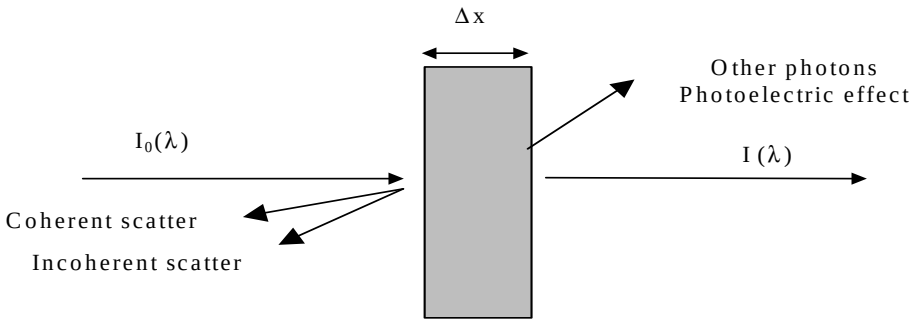

Figure 2-21 Schematic of X-ray absorption (attenuation)

The sum of photoelectric absorption and scattering is often called X-ray absorption or attenuation. The scattering portion of the total absorption becomes significant only for elements lighter than iron, 26, and for X-rays with a wavelength shorter than 0.5 A, or when there are particles dispersed in the sample (Abedi, 1998). For a pure element sample and monochromatic X-ray beam, the absorption is governed by

$$I(\lambda) = I_0(\lambda)e^{-\rho\Delta x\mu(\lambda)} \qquad (1)$$

where $I_0(\lambda)$ is the intensity of the incident beam;

$I(\lambda)$ is the intensity of the transmitted beam;

ρ is the density of the medium, g/cm$^{3;}$

Δx is the thickness of the medium, cm;

$\mu(\lambda)$ is the apparent mass absorption coefficient of the medium at wavelength λ, cm^2/g.

In contrast to ultraviolet, visible, and infrared rays that are absorbed only by the outer electrons that determine the chemical properties of an element, X-rays have high energy and their absorption usually involves only the electrons near the nucleus. Consequently, absorption of X-rays is independent of the chemical or physical state of an element and of whether the element is free, ionized, or combined with others. Thus, absorption of X-rays is dependent only upon the number and kinds of atoms through which they pass. So the mass absorption coefficient of a solution or mixture can be calculated from the mass absorption coefficients of its constituent elements as follows:

$$\mu(\lambda) = \sum_{i=1}^{n} \mu_i(\lambda)W_i \qquad (2)$$

where W_i is the mass fraction of element i in the mixture, and

$\mu_i(\lambda)$ is the mass absorption coefficient of element i at wavelength λ.

In case the incident X-ray beam is polychromatic instead of monochromatic, the intensity of transmitted X-rays is the sum over all wavelengths, λ_j,

$$\sum_j I(\lambda_j) = \sum_j I_0(\lambda_j) \exp\left[-\rho \Delta x \sum_i w_i \mu_{ij} \right] \qquad (3)$$

where $\mu_{ij}(\lambda)$ is the mass absorption coefficient of element i at wavelength λ_j.

The value of $\sum_j I(\lambda_j)$ can be read from the transmitted X-ray image cropped from experiments. The intensity of the incident beam $I_0(\lambda_j)$ is related to a variety of factors, such as the anode material of the X-ray tube, excitation conditions (voltage and current), equipment set-up, etc. It is a constant as long as these factors are fixed, and this is true in a typical phase behaviour experiment. A detailed discussion of these factors is readily available in the literature (D.K.G. de Bore, 1989), and it is beyond the scope of this study.

2.5.2 X-ray mass absorption coefficients

The mass absorption coefficient $\mu(\lambda)$ varies with the atomic number of element (Z) and X-ray wavelength (λ). $\mu(\lambda)$ is an exponential function of Z; a large atom has a much bigger $\mu(\lambda)$ than that of a small atom. For a pure element, $\mu(\lambda) \approx k\lambda^{2.83}$. Experimental data of $\mu(\lambda)$ can be found in literature (D.K.G. de Bore, 1989). The energy of an X-ray photon is related to its wavelength: E (keV) = 1.24 / λ (nm). The mass absorption coefficients of elements most commonly existing in petroleum versus X-ray photon energy are depicted in Figure 2-22. This Figure and Table 2-10 show that mass absorption coefficients of heavy metals, such as Ni and V, are much bigger than those of C and H. As a result,

deconvolution of polychromatic transmitted X-ray images is a well-suited technology to detect the existence of heavy metals and fine solids in petroleum mixtures.

Table 2-10 Comparison of X-ray absorption of different elements at λ=1.24 A (12.4 kev).

Element	H	C	S	V	Ni
μ (cm^2/g)	0.39	0.6310	49	126	313
μ/μ_H	1	1.62	125.64	323	802

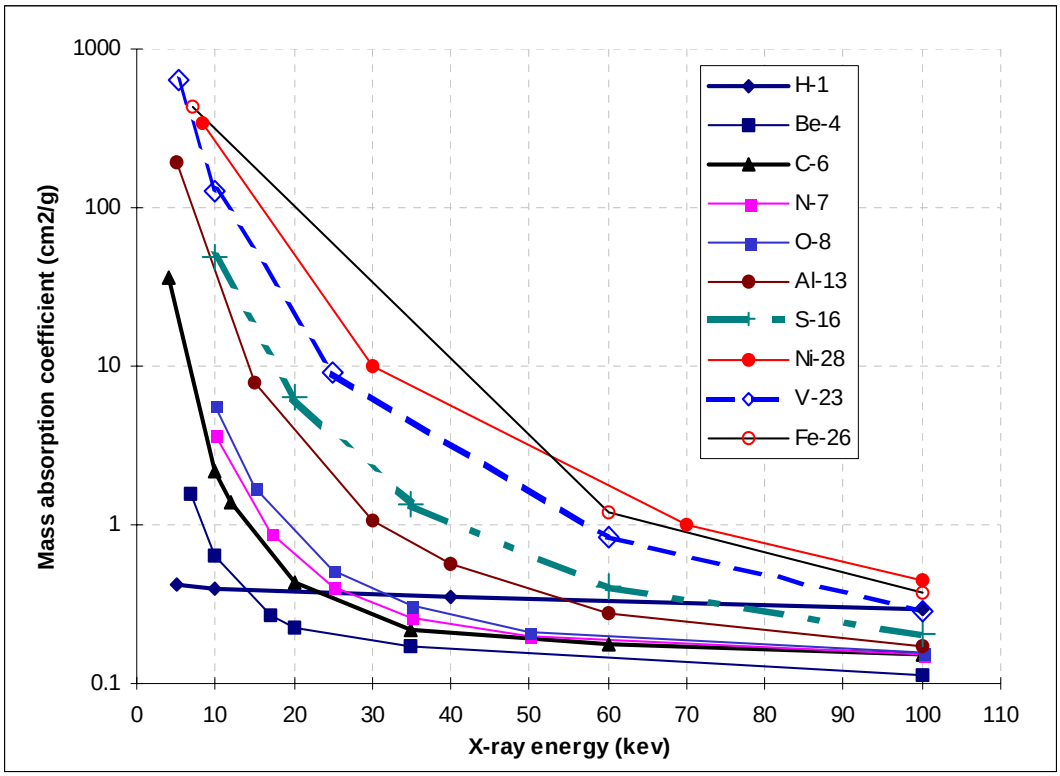

Figure 2-22 X-ray mass absorption coefficients for pure elements versus X-ray energy (data source D.K.G. de Bore, 1989)

2.6 Summary

The design, construction and operation of petroleum recovery and upgrading processes are expensive and demanding. The market is competitive but the profitability is marginal, particularly in the downstream section. Consequently, new technologies are required to meet the challenges with minimum capital investment and operating cost, and thus to ensure flexibility and profitability. At present, the progress in developing new technologies is limited because the thermodynamic and transport properties of heavy oils/bitumen are not fully understood. A major part of investment in petroleum production falls in separation. Development of efficient separation processes depends on the availability of highly accurate thermodynamic and transport property data sets and mathematical models based on these data sets. Unfortunately, relevant data are hard to measure, particularly at high temperature and pressure and as a consequence the models possess a speculative basis. The experimental technique employed in this study and the planned experiments, discussed in Chapter 3, are expected to provide significant insights that will stimulate process development work.

Chapter 3 Experimental

3.1 Introduction

This chapter describes how to use the X-ray and beryllium view cell technology to explore complex phase equilibria of asphaltene-containing heavy oil mixtures. X-ray and beryllium view cell technology gives rich and valuable information about asphaltene-containing heavy oil mixtures, such as phase boundaries, apparent density and volume of each phase, but regrettably not elemental composition by phase in this study due to X-ray scattering by asphaltene particles. Section 3.2 briefly describes the set-up built by Dukhedin-Lalla, 1996 and Abedi, 1998. Subsequent sections focus on new contributions to this technology made in this research. Equipment modifications are introduced in section 3.3. The principle and calibration of an improved apparent density measurement method are covered in section 3.4 and section 3.5, respectively. Phase behavior analysis based on measured apparent densities is described in section 3.6. Due to the huge volume of image data to be analyzed and interference of asphaltene dispersion, experimental data analysis is quite challenging, so automation of data processing is necessary. This addition to the experimental capability is introduced briefly in section 3.7. To investigate partitioning of inorganic solids, heavy metals and sulfur among phases in equilibria, representative samples were withdrawn from the view cell and the procedure of sampling are described in section 3.8. Experimental materials are tabulated in section 3.9. Error analysis is discussed in section 3.10.

3.2 Experimental set-up and view cell specifications

The general experimental set-up and basic components used in this study are the same as those used by Dukhedin-Lalla, 1996 and Abedi, 1998(Figure 3.1) and a detailed description of the set-up is available elsewhere (Dukhedin-Lalla, 1996 and Abedi, 1998).

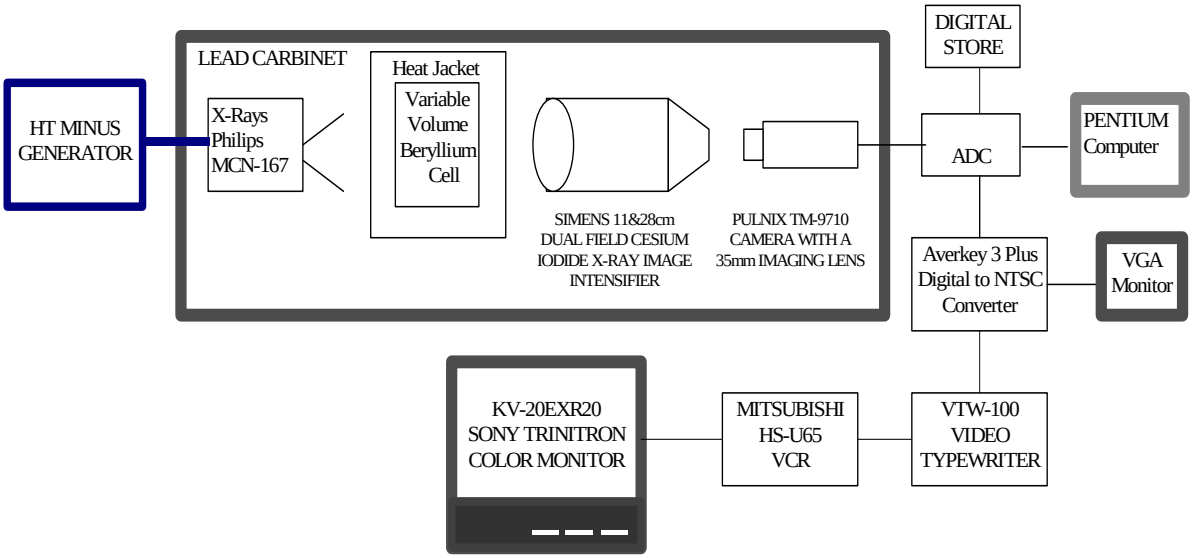

Figure 3-1 Schematic of overall set-up of the x-ray Be view cell apparatus

The core component of the equipment is the beryllium view cell, the key features and specifications of which are listed in Table 3-1 (Abedi et al., 1999). A detailed description of the experimental procedure is included in appendix I.

Table 3-1 The key features and specifications of the view cell.

1. Operating limits	
a. Temperature	Room temperature to ~ 725 K
b. Pressure	0 ~ 28 MPa
c. Volume	10 ~ 175 cm^3
2. Accuracy	
a. Phase boundaries	
Temperature	± 2 K
Pressure	± 0.02 MPa
b. Density	± 12 kg/m^3
c. Elemental composition	
Carbon	± 1 wt %
Hydrogen	± 1 wt %
Sulfur	± 0.2 wt %

3.3 Modifications made in this study to extend equipment capabilities

The following modifications have been made to extend equipment capabilities, to obtain more accurate data, and also to facilitate experiment operation with a focus on dense fluid and solid phases.

(1) New plumbing connections;

(2) Design and installation of a beryllium insert that makes it possible to view small amounts of dense phases;

(3) Adjustment of the X-ray source and view cell position to get better data near the bottom of cell;

(4) New X-ray generator and control unit to improve X-ray source reproducibility.

(5) Multistage speed controller for the mixing system to minimize the time to reach equilibrium.

The last two modifications in the above list are readily understandable, so only the first three modifications are discussed in detail.

3.3.1 New plumbing connections

The flow diagram used in this study is shown in Figure 3-2. The equipment and plumbing connections were designed and built to facilitate leakage tests, protect the bellows, and improve operation safety.

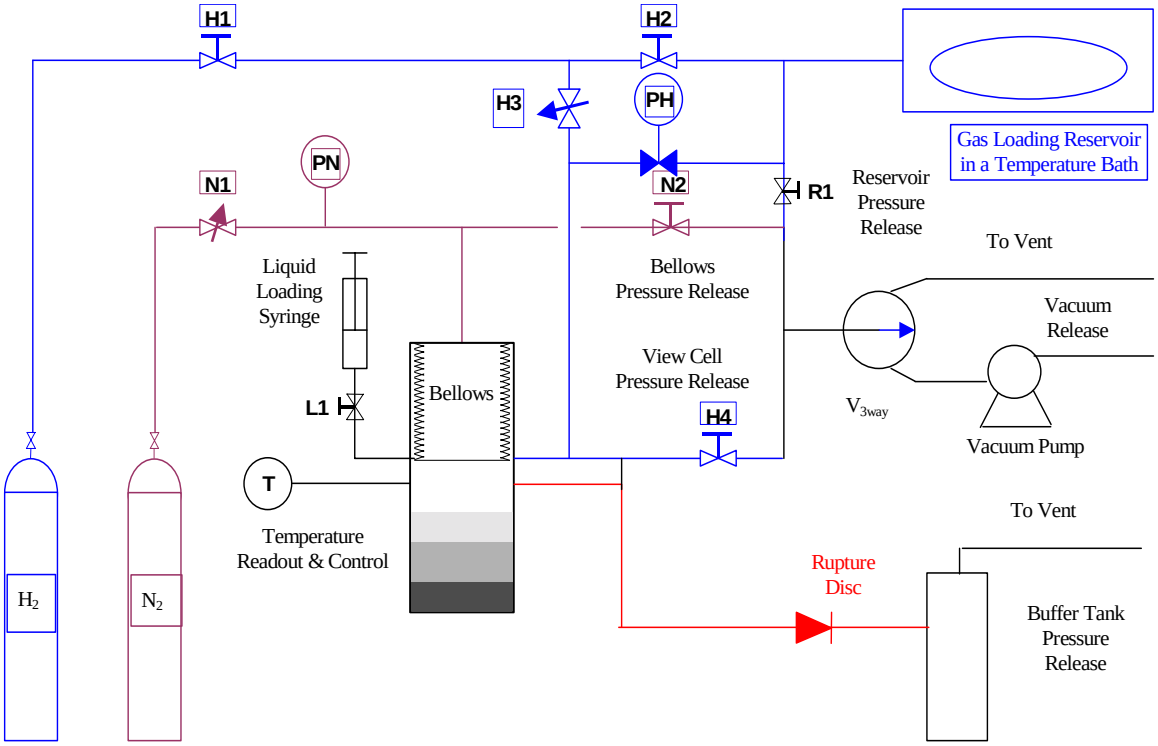

Figure 3-2 New plumbing connections

3.3.2 A beryllium insert to facilitate dense phase detection and sampling

In the previous set-up of the view cell approximately 7 ml volume at the bottom of the view cell could not be observed because of obstruction by the gasket used to seal the view cell and by the magnetic stirrer. Thus, it was difficult to detect the onset and/or to

measure a small volume of a dense phase, a crucial requirements for this study. To solve the problem, a beryllium insert was made and installed in the bottom of view cell (Figure 3-3).

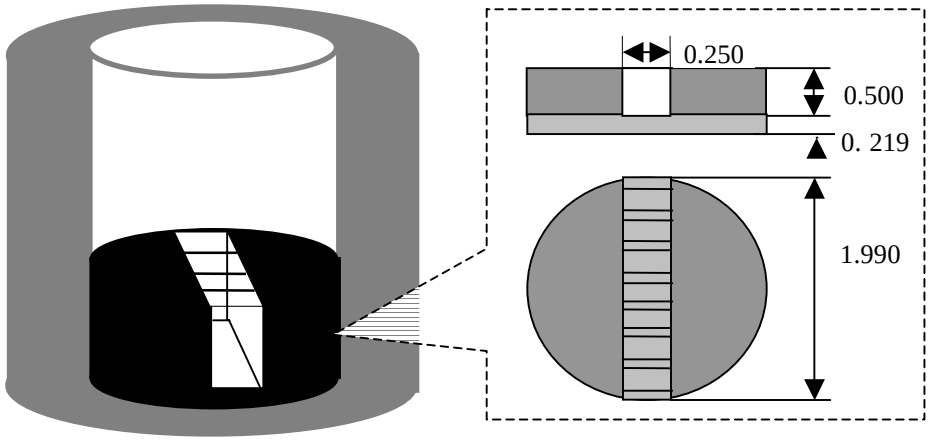

Figure 3-3 A beryllium piece installed inside the view cell to facilitate detection of dense liquid/solid phase.

The beryllium insert is a cylinder with a slightly smaller diameter than the inner diameter of the view cell possessing a square channel cut through the centre. It fills the undetectable volume and raises the level of sample in the view cell. The cross-sectional area of the channel is only 1/6 that of the view cell, so a small amount of dense phase can be detected. Besides, the stirrer spins on top of the insert and no longer obstructs the view. The beryllium insert improves dense phase detection and sampling because it:

(1) Reduces the undetectable volume from ~7 ml to ~1.5 ml

(2) Avoids the obstruction of the dense phase by the stirrer;

(3) Improves greatly the accuracy of dense phase volume measurement;

(4) Facilitates dense phase sampling;

(5) Provides an internal standard for apparent density calibration (see section 3.4.2).

3.3.3 Adjustment of the X-ray gun and view cell positions for optimized dense phase detection

In the previous set-up, the X-ray source position (position A in Figure 3-4) is so high that the gasket blocks the view of a small amount of the dense phase even though the dense phase boundary is above the gasket by a certain height (h). By adjusting the position of the X-ray source (position B in Figure 3-4), all materials above the gasket can be detected.

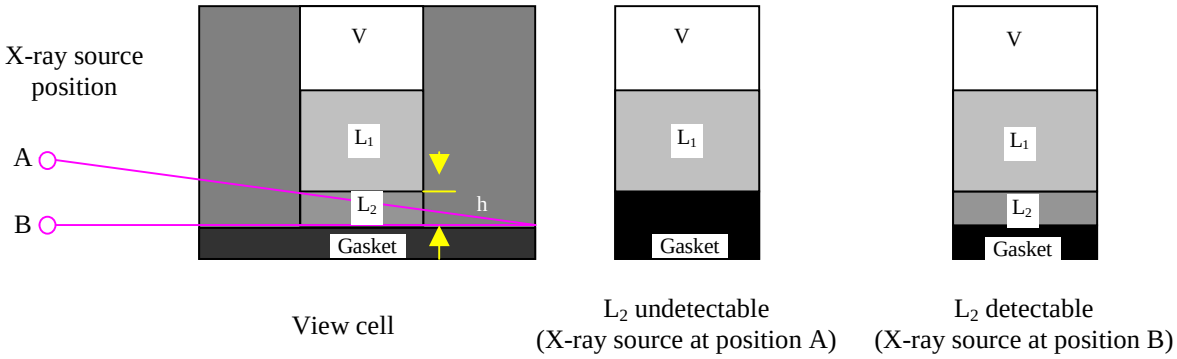

Figure 3-4 X-ray gun and view cell position adjustment for dense phase detection.

3.4 Principles of phase behavior investigation

The absorption of polychromatic X-rays is similar, to some extent, to colorimetry or photometry with white light. X-ray photons of all wavelengths emitted by the X-ray source (the continuous spectrum as well as the characteristic lines) enter and traverse the sample. The attenuation of the polychromatic beam, or of different energy portions of the beam, provides information about the sample regarding its composition, homogeneity, thickness and/or density.

3.4.1 The principle of phase boundary detection

The principle of phase boundary detection can be readily explained on the basis of equation (3) (section 2.5.1). The intensity of a spot in a transmitted X-ray image depends on the elemental compositions w_i, density ρ and thickness Δx of the sample corresponding to that spot. If the sample to be X-rayed is in multiphase equilibrium, composition w_i and density ρ generally vary from one phase to another, as shown in Figure 3-5.

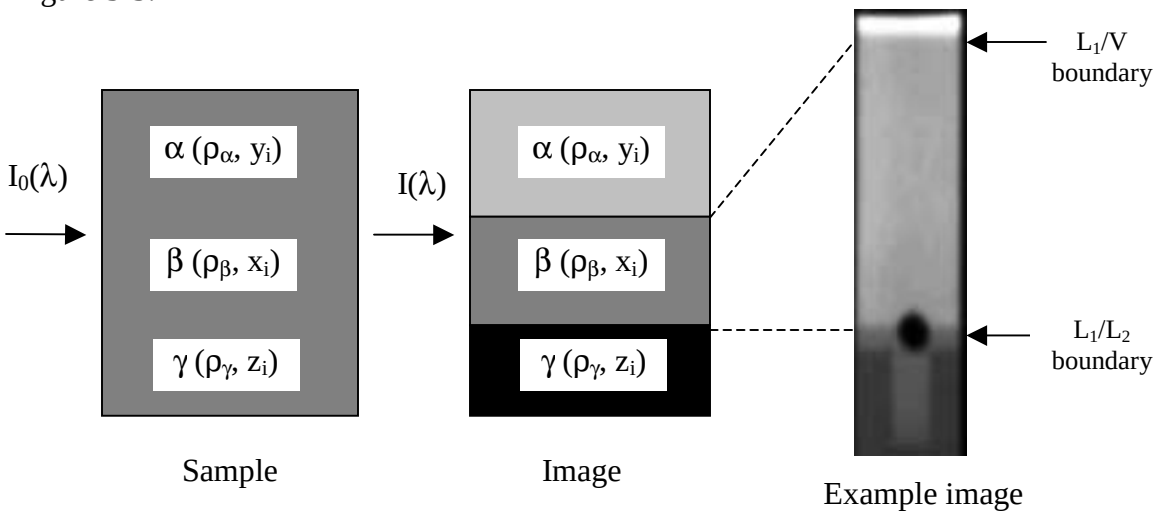

Figure 3-5 Schematic of a transmitted X-ray image of a multiphase heavy oil mixture.

Assuming all phases have the same thickness Δx, equation (3) indicates that the intensities of the transmitted X-ray vary from one phase to another. Consequently, the phase boundaries between phases are easily detected if they sit one on top of the other. A very good analog to phase boundary detection is the chest X-ray image in radiology; bones and meat have different shadow due to their different composition and densities. However, if the sample is multiphase but one of the phases is dispersed, phase boundary detection can be difficult. This issue is discussed in section 3.5.

3.4.2 The principle of apparent density measurements

Figure 3-6 shows the X-ray path when penetrating the Be view cell: the Be cylinder wall → sample inside the view cell → the Be cylinder wall.

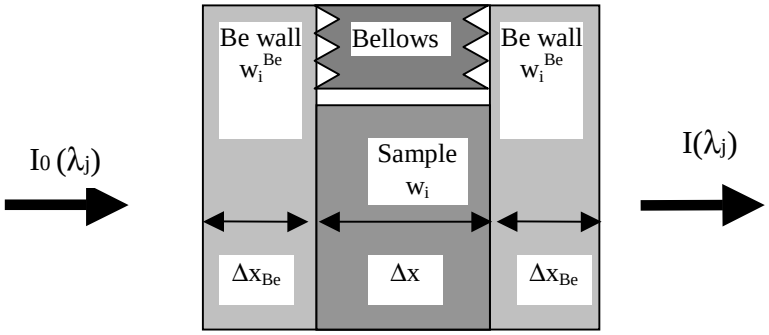

Figure 3-6 Absorption of X-rays passing through Be view cell

Applying equation (3) to this case,

$$\sum_j I(\lambda_j) = \sum_j I_0(\lambda_j) \exp\left[-\rho_{Be}\Delta x_{Be} \sum_i w_i^{Be}\mu_{ij} - \rho\Delta x \sum_i w_i \mu_{ij} - \rho_{Be}\Delta x_{Be} \sum_i w_i^{Be}\mu_{ij} \right] \quad (5)$$

$$\sum_j I(\lambda_j) = \sum_j I_0(\lambda_j) \exp\left[-2\rho_{Be}\Delta x_{Be} \sum_i w_i^{Be}\mu_{ij} - \rho\Delta x \sum_i w_i \mu_{ij} \right] \quad (6)$$

where W_i^{Be} is the mass fraction of element i in the Be wall;

ρ_{Be} is the density of the Be wall;

Δx_{Be} is the thickness of the Be wall.

Expression $\rho_{Be}\Delta x_{Be} \sum_i w_i^{Be}\mu_{ij}$ is a constant since all parameters are properties of the Be view cell. Equation (6) is the basic equation used for deconvoluting sample composition and density provided that X-ray scattering is negligible. At a fixed excitation condition, the spectrum of incident X-rays ($I_0(\lambda_j)$, j=1, 2, …) is available from the literature (Lambert M. C., 1967) and the intensity of transmitted X-rays ($I(\lambda_j)$, j=1, 2, …) can be measured experimentally. The unknown variables in equation (6) are sample composition

and density, which can be obtained by regression of experimental transmitted X-ray intensities at different excitation conditions. As one of the initial objectives for this project was on line density and composition measurement, data at 10 different excitation conditions were obtained at each experimental condition. However, it became clear later that the amount of X-rays scattered by asphaltene particles was not negligible. Consequently, deconvolution of sample density and composition is not realized. Instead Equation (6) is simplified to yield a new concept, apparent density, which is introduced at the end of this section and is used to detect the dispersion of asphaltene particles in equilibrium phases in oil mixtures.

First Equation (6) is simplified by introducing the concept of effective wavelength (λ_e). The effective wavelength of a polychromatic X-ray beam is defined as the wavelength of a monochromatic beam that has equivalent behaviour in an absorption measurement. By introducing λ_e into equation (6),

$$\sum_j I(\lambda_j) = \left[\sum_j I_0(\lambda_j)\right] \exp\left[-2\rho_{Be}\Delta x_{Be}\sum_i w_i^{Be}\mu_i^{\lambda_e} - \rho\Delta x\sum_i w_i\mu_i^{\lambda_e}\right] \tag{7}$$

$$\ln\left[\frac{\sum_j I(\lambda_j)}{\sum_j I_0(\lambda_j)}\right] = -2\rho_{Be}\Delta x_{Be}\sum_i w_i^{Be}\mu_i^{\lambda_e} - \rho\Delta x\sum_i w_i\mu_i^{\lambda_e} \tag{8}$$

where $\mu_i^{\lambda_e}$ is the mass absorption coefficient of element i at wavelength λ_e.

Please note that a polychromatic X-ray beam is never equivalent to a monochromatic beam in all aspects, and it exhibits a particular effective wavelength only for a particular set of conditions, i.e., the value of λ_e varies with conditions, such as X-ray excitation, sample composition, etc. If “s” and “c” are used to represent an experimental sample and a calibrant, respectively, from equation (8), we have for the sample

$$\ln\left[\frac{\sum_j I^s(\lambda_j)}{\sum_j I_0^s(\lambda_j)}\right] = -2\rho_{Be}\Delta x_{Be}\sum_i w_i^{Be}\mu_i^{\lambda_e^s} - \rho_s\Delta x\sum_i w_i^s\mu_i^{\lambda_e^s} \quad (9)$$

where λ_e^s is the equivalent wavelength for X-rays passing through the sample;

w_i^s is the mass fraction of element i in the sample;

$\mu_i^{\lambda_e^s}$ is the mass absorption coefficient of element i at wavelength λ_e^s;

ρ_s is density of the sample;

$I^s(\lambda_j)$ is the intensity of transmitted X-ray at wavelength λ_j (through the sample);

$I_0{}^s(\lambda_j)$ is the intensity of incident X-ray at wavelength λ_j (through the sample).

For the calibrant

$$\ln\left[\frac{\sum_j I^c(\lambda_j)}{\sum_j I_0^c(\lambda_j)}\right] = -2\rho_{Be}\Delta x_{Be}\sum_i w_i^{Be}\mu_i^{\lambda_e^c} - \rho_c\Delta x\sum_i w_i^c\mu_i^{\lambda_e^c} \quad (10)$$

where λ_e^c is the equivalent wavelength for X-rays passing through the calibrant;

w_i^c is the mass fraction of element i in the calibrant;

$\mu_i^{\lambda_e^c}$ is the mass absorption coefficient of element i at wavelength λ_e^c;

ρ_c is density of the calibrant;

$I^c(\lambda_j)$ is the intensity of transmitted X-ray at wavelength λ_j (through the calibrant);

$I_0{}^c(\lambda_j)$ is the intensity of incident X-ray at wavelength λ_j (through the calibrant).

If we subtract (10) from (9),

$$\ln\left[\left[\frac{\sum_j I^s(\lambda_j)}{\sum_j I^c(\lambda_j)}\right]\left[\frac{\sum_j I_0^c(\lambda_j)}{\sum_j I_0^s(\lambda_j)}\right]\right] = -2\rho_{Be}\Delta x_{Be}\sum_i w_i^{Be}\left(\mu_i^{\lambda_e^s} - \mu_i^{\lambda_e^c}\right) - \Delta x\left[\rho_s\sum_i w_i^s\mu_i^{\lambda_e^s} - \rho_c\sum_i w_i^c\mu_i^{\lambda_e^c}\right] \quad (11)$$

To obtain the final calibration equation, a few assumptions must be introduced. The first assumption is

$$\frac{\sum_j I_0^c(\lambda_j)}{\sum_j I_0^s(\lambda_j)} = 1 \tag{12}$$

This assumption means that the X-ray source excitation voltage and current are fixed. Introducing (12) to (11),

$$\ln\left[\frac{\sum_j I^s(\lambda_j)}{\sum_j I^c(\lambda_j)}\right] = -2\rho_{Be}\Delta x_{Be}\sum_i w_i^{Be}\left(\mu_i^{\lambda_e^s} - \mu_i^{\lambda_e^c}\right) - \Delta x\left[\rho_s\sum_i w_i^s\mu_i^{\lambda_e^s} - \rho_c\sum_i w_i^c\mu_i^{\lambda_e^c}\right] \tag{13}$$

The second assumption is that the effective wavelengths are equal.

$$\lambda_e^s = \lambda_e^c = \lambda_e \tag{14}$$

This assumption relies on the similarity of the calibrant and experimental sample, as the Be walls are the same. On substitution equation (13) becomes

$$\ln\left[\frac{\sum_j I^s(\lambda_j)}{\sum_j I^c(\lambda_j)}\right] = -\Delta x\left(\rho_s\sum_i w_i^s\mu_i^{\lambda_e} - \rho_c\sum_i w_i^c\mu_i^{\lambda_e}\right) \tag{15}$$

where Δx is a constant. The values of μ for hydrocarbon mixtures are found to fall in a narrow range (Abedi, 1998). Assuming μ is a constant, i.e., the value of μ for a calibrant equals to that of experimental sample (third assumption),

$$\sum_i w_i^s\mu_i^{\lambda_e} = \sum_i w_i^c\mu_i^{\lambda_e} = m \tag{16}$$

where m is a constant and by substituting (16) into (15),

$$\ln\left[\frac{\sum_j I^s(\lambda_j)}{\sum_j I^c(\lambda_j)}\right] = m\Delta x[\rho_c - \rho_s] = k[\rho_c - \rho_s] \tag{17}$$

where $k=m\Delta x$ so k is a constant.

$$\rho_s = \rho_c - \frac{1}{k}\ln\left[\frac{\sum_j I^s(\lambda_j)}{\sum_j I^c(\lambda_j)}\right] \tag{18}$$

The density ρ_s calculated from equation (18) is not the true density of the sample. In this research, it is referred as the "apparent density". The smaller the errors in the above assumptions, the closer the obtained apparent density ρ_s is to the actual density of the sample. Equation (18) is the basis of apparent density calibration discussed in the next section.

3.5 Calibration

The quality of calibration determines the accuracy of experimental data obtained on the basis of calibration, such as temperature, pressure, volume and apparent density data in this study. Temperature and pressure calibrations are not discussed here because they are quite common and there are standard procedures to follow in the open literature. Volume calibration is included in Appendix II. Only the apparent density calibration method is discussed below.

3.5.1 Calibration without an internal standard

Apparent density calibration without an internal standard is based on equation (18).

$$\rho_s = \rho_c - \frac{1}{k}\ln\left[\frac{\sum_j I^s(\lambda_j)}{\sum_j I^c(\lambda_j)}\right] \qquad (18)$$

In a typical calibration test, a calibrant of known elemental composition and density is X-rayed under fixed excitation conditions, at a fixed temperature and at a fixed pressure. In later experimental runs, an experimental sample is X-rayed under the same excitation conditions as that of the calibration test. Since image intensities can be read from image

files and the density of the calibrant is known, the apparent density of the experimental sample is then calculated from equation (18). As mentioned in the last section when introducing assumptions to derive equation (18), the closer the composition of the calibrant to that of the experimental sample, the closer the apparent density is to the actual density value. Since there are two types of quasi-binary systems investigated in this study, pentane + ABVB and dodecane + ABVB, naturally, the best calibration solution for pentane + ABVB is pentane and for dodecane + ABVB is dodecane. The density calibration curve for pure pentane at different temperatures is shown in Figure 3-7.

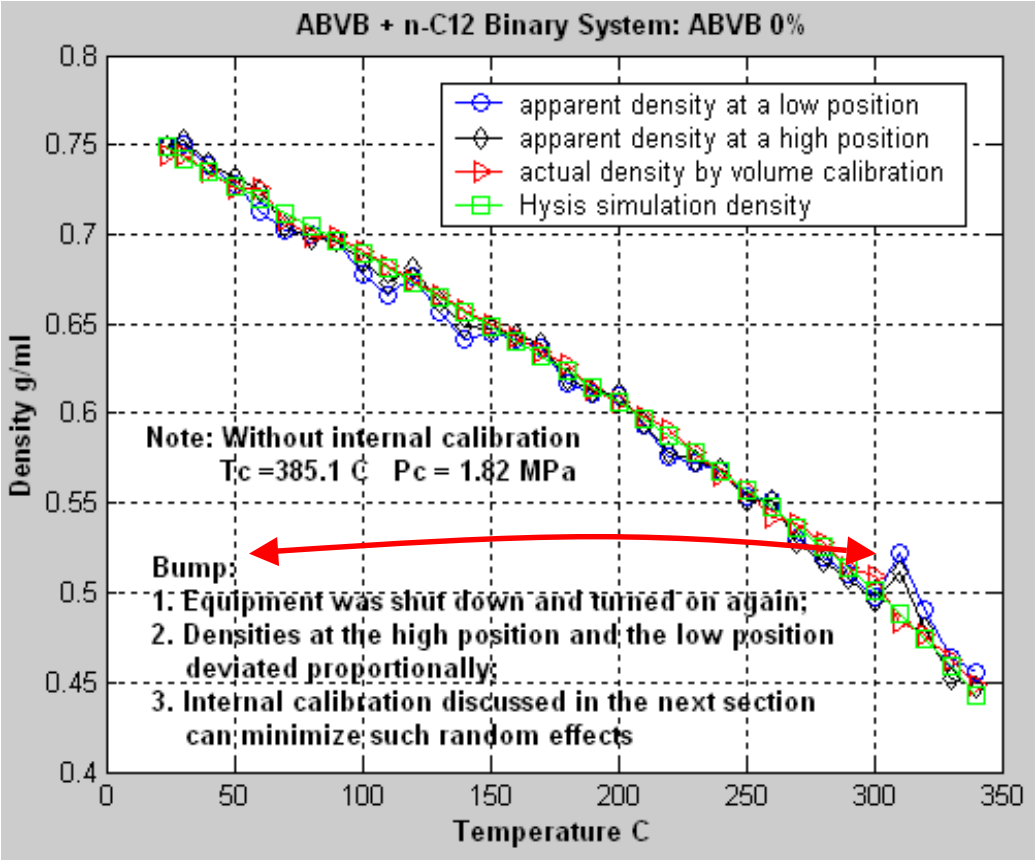

Figure 3-7 Dodecane density calibration without internal standard

The above shows the apparent densities, the actual density obtained by volume calibration, and the HYSIS (PR EOS) simulation result are in good agreement. At T = 310 C, the X-ray source was turned off and then turned on again. This made the apparent densities deviate from the actual density more at 310 °C than at other temperatures and formed a "bump". This kind of bumping due to X-rays source transients can be minimized by calibration using the beryllium piece as an internal standard.

3.5.2 Apparent density calibration using the beryllium insert as an internal standard

The X-ray view cell apparatus is subject to random effects, such as fluctuation of the line voltages and other unpredictable interferences. As a consequence calibration data and experimental data may be collected under different conditions. Therefore, the first assumption (equation (12)) introduces error into the final calibration equation (18). To minimize such effects, an internal calibration is performed. The beryllium insert installed inside the view cell (the dark grey area in Figure 3-8a) acts as an internal standard.

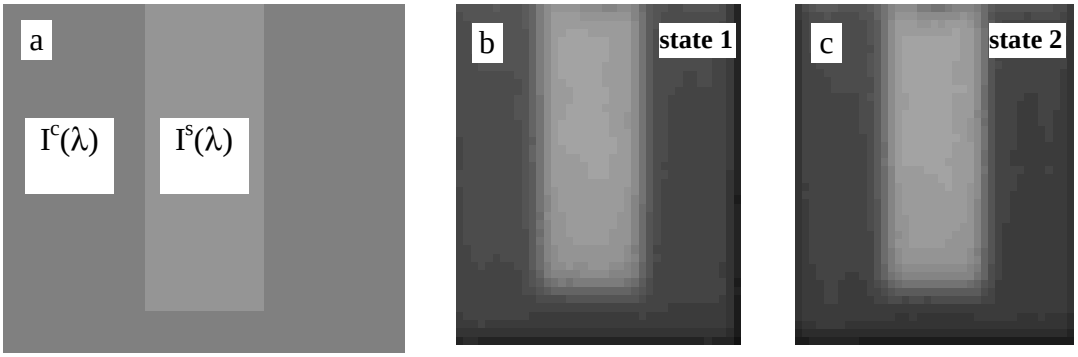

Figure 3-8 Density calibration using the beryllium piece as an internal standard.
a: the internal calibration region; b: calibration test (state 1) ; c: experiment test (state 2).

Since the beryllium insert and beryllium view cell are tightly fitted (negligible space for sample), and care is taken to keep the view cell conditions fixed, for each spot

in the shaded area of the beryllium insert in Figure 3-8, the materials that X-rays passed through during calibration tests and during experimental runs are identical. So,

$$\ln\left[\frac{\sum_j I_{Be}(\lambda_j)}{\sum_j I_0(\lambda_j)}\right] = -\rho_{Be}(2\Delta x_{Be} + \Delta x)\sum_i w_i^{Be}\mu_i^{\lambda_e^{Be}} \qquad (19)$$

The right hand side of equation (19), $-\rho_{Be}(2\Delta x_{Be} + \Delta x)\sum_i w_i^{Be}\mu_i^{\lambda_e^{Be}}$, is a constant at a fixed set of excitation conditions. In case there are random effects that make $I_0(\lambda_j)$ deviate from its normal value and thus result in a small shift in λ_e, $-\rho_{Be}(2\Delta x_{Be} + \Delta x)\sum_i w_i^{Be}\mu_i^{\lambda_e^{Be}}$ can still be treated as a constant. Therefore, the intensity of transmitted X-rays $\sum_j I_{Be}(\lambda_j)$ and the intensity of incident X-rays $\sum_j I_0(\lambda_j)$ fluctuate. For calibration tests and experimental runs conducted under different apparatus states, designated as state 1 (Figure 3-8 b) and state 2 (Figure 3-8 c), respectively:

$$\left[\frac{\sum_j I_{Be}(\lambda_j)}{\sum_j I_0(\lambda_j)}\right]^{state1} = \left[\frac{\sum_j I_{Be}(\lambda_j)}{\sum_j I_0(\lambda_j)}\right]^{state2} \qquad (20)$$

$$\frac{\left(\sum_j I_0(\lambda_j)\right)^{state1}}{\left(\sum_j I_0(\lambda_j)\right)^{state2}} = \frac{\left(\sum_j I_{Be}(\lambda_j)\right)^{state1}}{\left(\sum_j I_{Be}(\lambda_j)\right)^{state2}} \qquad (21)$$

Substitute (21) into (11) and follow the same steps as without using an internal calibration standard,

$$\rho_s^{state1} = \rho_c^{state2} + \frac{1}{k'} \ln \left[\frac{\left(\sum_j I^c(\lambda_j) \right)^{state1}}{\left(\sum_j I^s(\lambda_j) \right)^{state2}} \frac{\left(\sum_j I_{Be}(\lambda_j) \right)^{state2}}{\left(\sum_j I_{Be}(\lambda_j) \right)^{state1}} \right] \quad (22)$$

Equation (22) is the density calibration equation using the beryllium insert as internal standard. This calibration equation is preferred over equation (18) (Figure 3-9) and is used in this study to process the bulk of the experimental data. Equation (18) is only used for experiments conducted before the insert was installed.

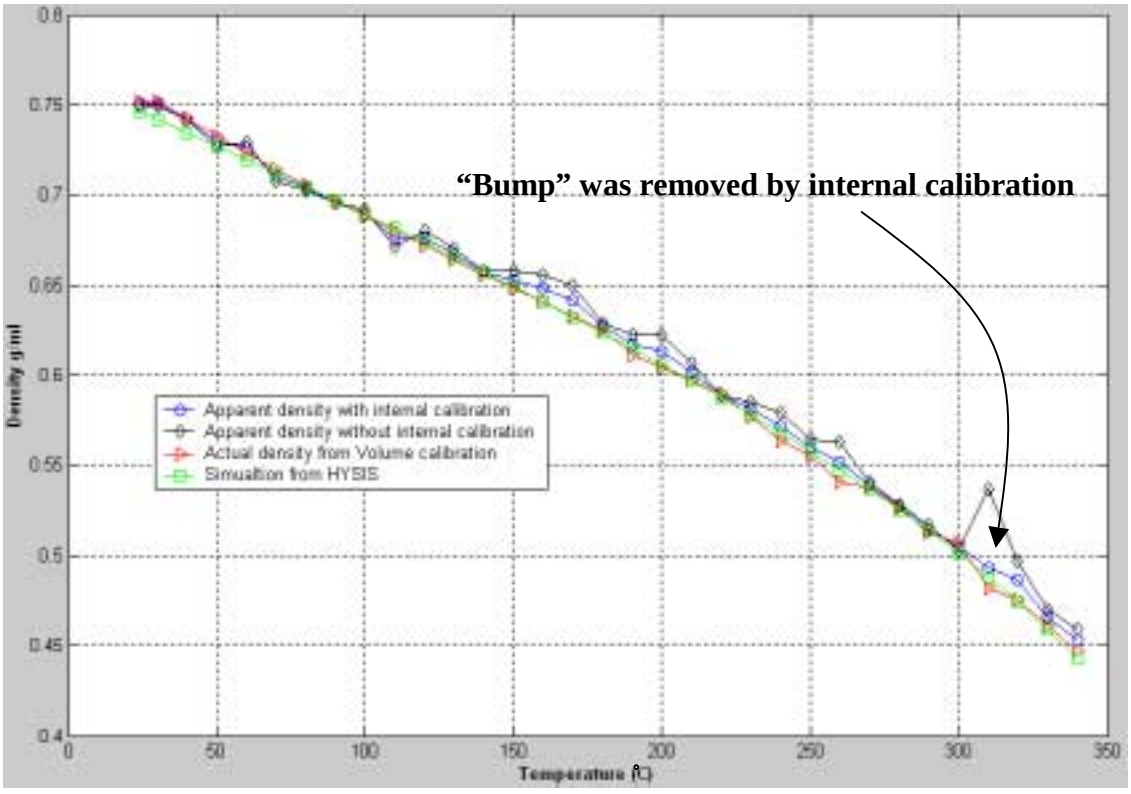

Figure 3-9 Density calibration with and without using the beryllium insert as an internal standard

3.6 Phase behavior investigation based on measured apparent intensities and detected phase boundaries

Phase behavior investigation is based on phase boundary detection and apparent density measurements. For a single X-ray image, if the experimental sample has no dispersed phase, phase boundaries, apparent densities and volumes of phases can be determined from the apparent density. However, if there is one phase dispersed in another phase (or phases), such as asphaltenes dispersed in hydrocarbon solutions, it is often necessary to compare apparent densities obtained from a series of images in order to establish the number and nature of phases present.

3.6.1 Analysis of single images

For a single image, phase behavior investigations focus on the apparent density profiles along the view cell. As shown in Figure 3-10a, b, c and d, there are 4 possible types of apparent density profiles. They correspond to the following phase behaviors:

1. Homogeneous liquids, such as pure pentane (Figure 3-10a). The apparent density profile is flat ($0.48\pm0.01 g/cm^3$), which means that the apparent densities are the same at all pixels. Also, the apparent density is almost the same as the actual density obtained from the volume calibration.
2. Heterogeneous samples with asphaltenes "homogeneously" dispersed, such as dodecane+50 wt% ABVB (Figure 3-10b). The apparent density profile is flat as in case 1, but the apparent density is much higher than its actual density due to X-ray scattering. A LV interface is also shown in this figure.

3. Heterogeneous samples with asphaltene particles partly settled and partly dispersed, such as dodecane + 10 wt% ABVB (Figure 3-10c). The apparent density profile is flat starting from the bottom of view cell, which corresponds to the settled part, but gradually decreases after a certain height, which means asphaltene particles are still settling. A LV interface is also shown but no SL or LL interface is observed.
4. Apparent density profiles for heterogeneous samples such as pentane + 30 wt% ABVB (Figure 3-10d) comprise a series of steps corresponding to L2, L1 and V apparent densities. Additional phases, if present, are dispersed uniformly among another phase (or phases).

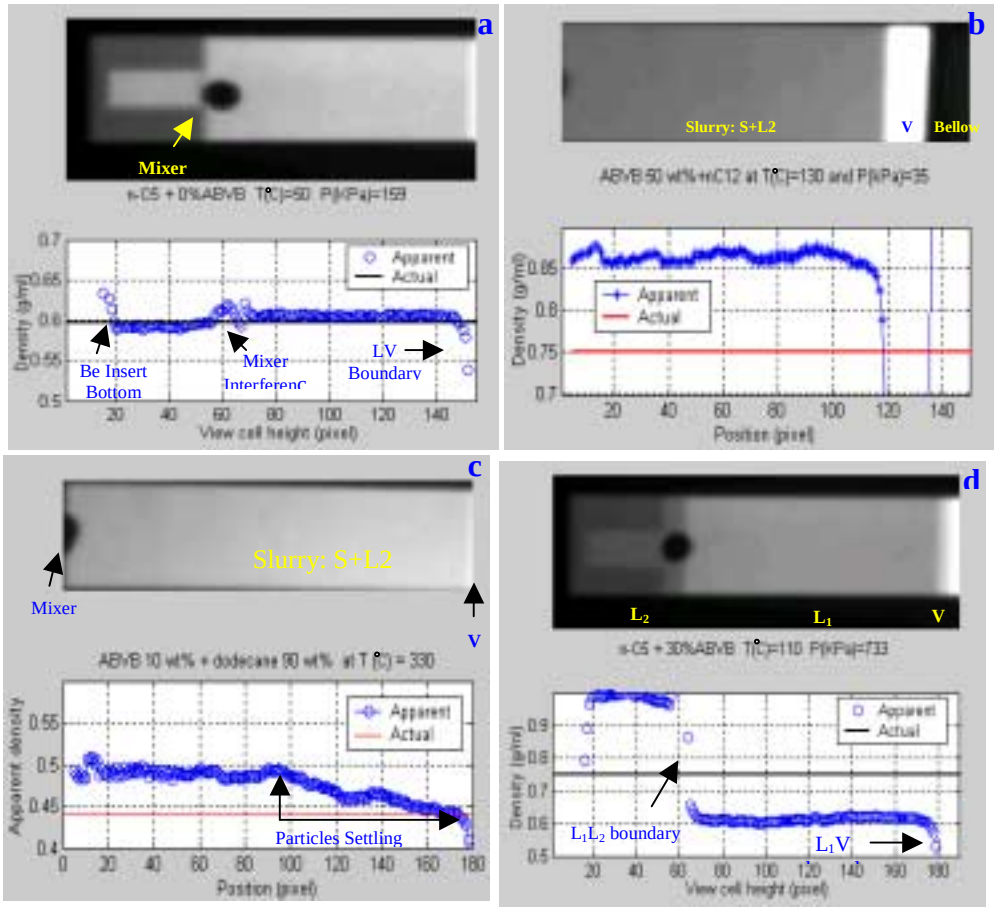

Figure 3-10 Schematic of four types of apparent density profiles across the view cell.
a: homogeneous; b: aspahltenes particles dispersed;
c: asphaltene particles partially settled; d: asphaltene particles settled.

3.6.2 Dispersed phase detection by analyzing a series of images

For a homogeneous sample, the apparent density is uniform (Figure 3-10a). In the vicinity of the onset point of a second dense phase such as a crystalline solid, there would be only small differences between apparent densities with positions even if the new phase has partly settled. Thus, the onset point is hard to detect by observing only the density profile of a single image. In this case, phase transitions may be detected by comparing averaged apparent densities at fixed positions in a series of images, as illustrated in Figure 3-11 for a SLV/LV transition of a 11.9 % anthrancene + 88.1 %pentane mixture. At temperatures above 173 °C, anthrancene melts and dissolves in pentane. The solution was homogeneous, so the apparent densities did not change with elevations. At temperatures below 173 °C, anthrancene solidified and started to settle to the bottom of the view cell, so the apparent densities at the two elevations diverge. By observing the trends of the two curves in Figure 3-11, the SLV/LV transition point can be identified clearly at 173 °C. It would be hard to locate this temperature if only a single image at 173 °C were analyzed.

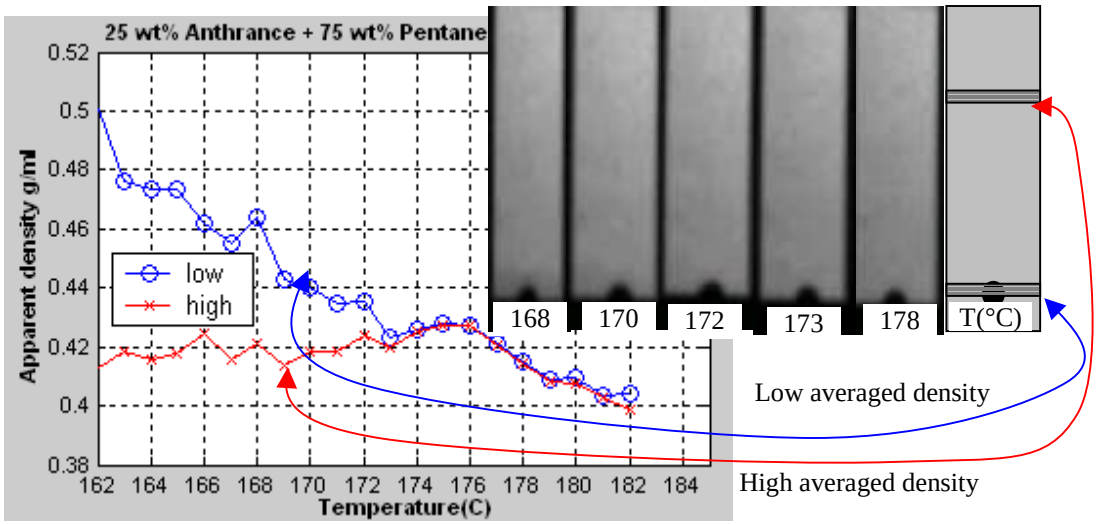

Figure 3-11 Detection of SLV/LV phase transition of anthrancene in pentane by comparing apparent density in a series of images.

3.6.3 An example — SLLV phase behavior detection for pentane + anthrancene mixtures

As discussed in Chapter 2 section 2.2.3, for a binary system, four-phase behavior, such as SLLV, is a point in a PT projection, i.e., it is a very demanding test of the apparatus and operating procedures. In this study, SLV-LV phase transitions of pentane + anthrancene binary systems were investigated using the X-ray view cell equipment and analyzed with the methods outlined above. Its PT projection, Tx melting curve and liquid density at the melting point are given in Figure 3-12 a, b and c, respectively.

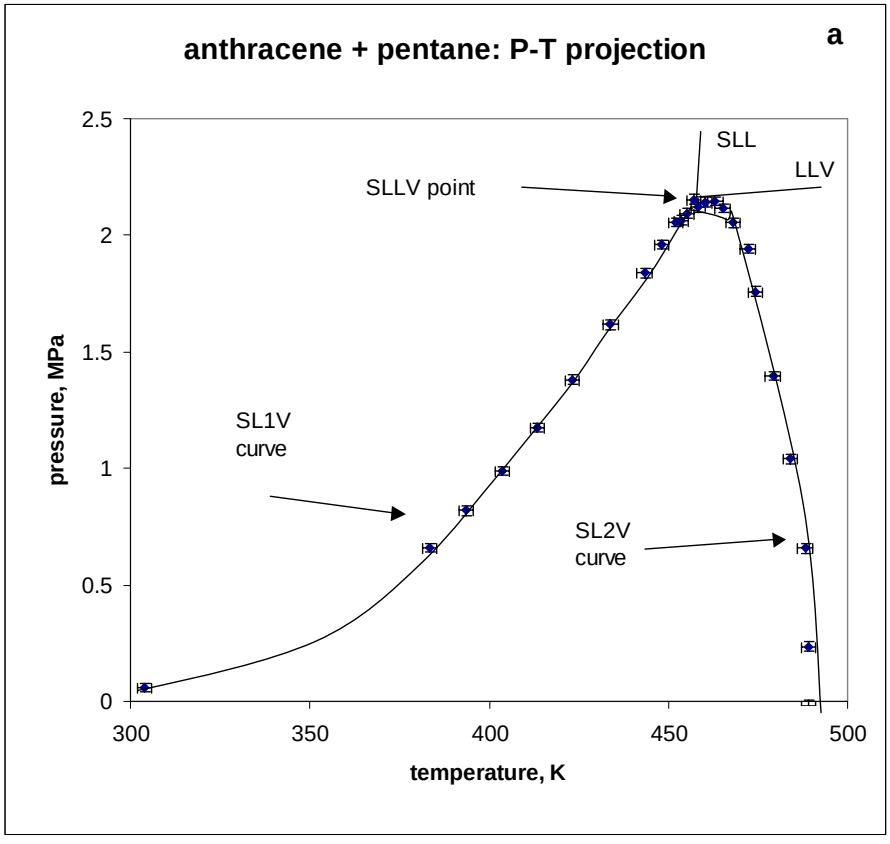

Figure 3-12 SLV –LV phase transitions of pentane + anthrancene systems.
a: PT projection; b: T melting curve; c: liquid density at melting points (Continued)

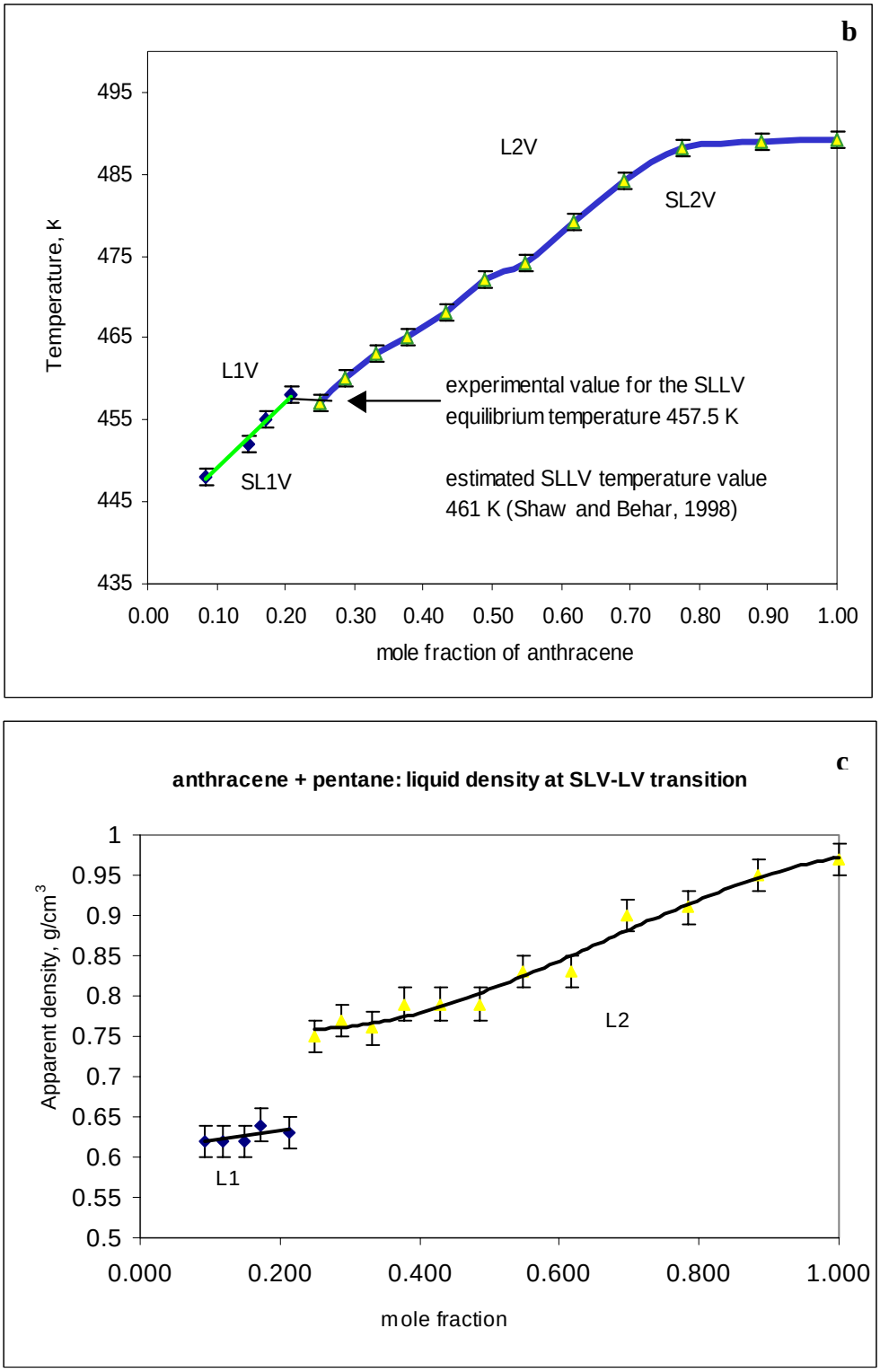

Figure 3-12 SLV –LV phase transitions of pentane + anthrancene systems.
a: PT projection; b: Tx melting curve; c: liquid density at melting points

The apparent density curve jump in Figure 3-12c suggests that the liquids in equilibrium with the solid anthrancene are different: L_1 at low concentrations of anthrancene (the left branch) and L_2 at high concentrations of anthrancene (the right branch). An SLLV Q point is located in PTx space at T=457.5 K (Figure 3-12 b), P=2.18MPa (Figure 3-12 a), and x=0.23 (Figure 3-12 c). The point is in good agreement with the value (T=461 K, P=2.94 MPa) estimated from a SLLV locus prediction model developed by Shaw and Behar, 1998.

The above experimental data demonstrate the capability of the equipment and feasibility of the data analysis method. Part of the SLV-LV phase transition data for anthrancene + pentane have been published (Minicucci, D., Zou, X.-Y. and Shaw, J.M., 2001 and 2002).

3.7 Data analysis software

Automation of image analysis has the following advantages:

1. Voluminous data can easily processed;
2. Different data analysis methods can easily be tested;
3. Error introduced by the analyser is minimized;

In this study much effort was devoted to develop image analysis software. Programs were developed to pre-process data (to eliminate image bouncing, cut regions of interest, filter noise and average images cropped at the same set of conditions) and to detect phase boundaries, and to calculate apparent density and volume of each phase in equilibrium. These programs took ~ 6 months to prepare and comprise Appendix III.

3.8 Sampling procedure for composition analysis

One of the objectives of this project is to examine partitioning of inorganic fine solids, heavy metals and heteroatoms among phases in equilibrium. To attain this objective, we have to know the content of these constituents in all phases in equilibrium. But due to X-ray scattering by particles in experimental samples, on-line composition measurement was not realized in this project. However, representative samples were withdrawn from the view cell, and the procedure of sampling is described here.

Multiphases behaviors of ABVB + pentane mixtures extend unambiguously to room temperature for a range of compositions. During cooling, the mixer was kept on until the mixture reached room temperature. The mixer was then turned off and the mixture was then left undisturbed overnight to attain equilibrium. The vapour phase was virtually pure pentane at the room temperature and its mass was insignificant ($P < 0.65$ bar, $V < 100$ ml, mass < 0.0002 g) compared to the charge mass (>50 g). Consequently, it was not sampled. The light liquid phase was sampled using a syringe as soon as the top cap of the view cell was removed. Considering pentane is highly volatile even at the room temperature, the operation was performed as fast as possible to minimize potential mass transfer among the phases present. The sample of the heaviest phase was collected from the channel of the beryllium insert after the view cell was disassembled. Due to its high volatility, part of pentane evaporated from the samples inevitably, the partitioning of pentane among the phases was not measured. The partitioning of ABVB constituents, particularly the partitioning of inorganic fine solids, heavy metals and heteroatoms was assessed on a pentane free basis based on compositions obtained from Core Labs. These results are reported in section 5.1.2

3.9 Materials

The Athabasca Bitumen Vacuum Bottoms sample was supplied by CANMET and its analysis is list in Table 2-6 (section 2.3.1). The physical properties of other chemicals, their grade, purity and suppliers are given in Table 3-2.

3.10 Error analysis

The physical variables measured in the experiments include temperature, pressure, volume, mass, and apparent density. Measurement of temperature, pressure and mass are quite common practices, and their accuracies as measured in the view cell apparatus are discussed in detail by Abedi (1998) and also listed in Table 3-1. Elemental compositions, Saturates-Aromatics-Resins-Asphaltenes (SARA) analysis are completed by Core Labs (~1%). Measurements of volume and apparent density are based on calibration; their quality depends heavily on the quality of cropped images. For high quality images, the errors in volume measurements are within ± 1 pixel, i.e. ±0.13 ml if the phase boundary falls in the channel of the beryllium insert or ± 0.78 ml if the phase boundary is at a position above the beryllium insert.

Table 3-2 Chemicals used, their formula, molecular weight and purity.

Chemicals	Formula	Molecular Weight	$\rho^{20°C}$ (g/cm^3)	T_b (K)	T_m (K)	T_c (K)	P_c (MPa)	Grade purity	Supplier
Hydrogen	H_2	2.016		20.3	14.0	33.2	1.297	Research	BOC GASES
Nitrogen	N_2	28.013		77.4	63.3	126.2	3.39	Research	BOC GASES
n-Pentane	C_5H_{12}	72.151	0.626	309.2	143.4	469.7	3.37	HPLC	Aldrich
n-Hexane	C_6H_{14}	86.178	0.659	341.9	177.8	507.5	3.01	Research	Sigma
n-Heptane	C_7H_{16}	100.205	0.684	371.6	182.6	540.3	2.74	Research	Sigma
n-Octane	C_8H_{18}	114.232	0.703	398.8	216.4	568.8	2.49	Research	Sigma
n-Nonane	C_9H_{20}	128.259	0.718	424.0	219.7	594.6	2.29	Research	Sigma
n-Decane	$C_{10}H_{22}$	142.286	0.730	447.3	243.5	617.7	2.12	Research	Sigma
n-Dodecane	$C_{12}H_{26}$	170.34	0.749	489.5	263.6	658.2	1.82	Research	Fisher Scientific
Anthracene	$C_{14}H_{10}$	178.234	1.2	613.1	489.7	869.3		HPLC	Sigma
Phenathrene	$C_{14}H_{10}$	178.234	1.2	613.0	373.7	873.0		HPLC	Sigma
Toluene	$C_6H_5CH_3$	92.141	0.867	383.8	178.0	591.8	4.10	Research	Caledon
Tetrahydrofuran	C_4H_8O	72.107	0.889	338.0	164.7	540.1	5.19	Research	Fisher Scientific
Beryllium insert	Material: Brushwellman standard grade S-200 FC (>98.5 wt% Be). Fabricator: Phaedrus Precision								

Note: Toluene and tetrahydrofuran are used for cleaning purpose

Chapter 4 Phase Behavior of ABVB + Alkane Mixtures

From a phase behavior prospective, light alkanes + ABVB mixtures are highly asymmetric since asphaltenes in ABVB are much larger than light alkanes and possess different polarities, structures and physical properties. Phase behavior of these mixtures is comparable to phase behavior of heavy solutes + light gas mixtures in typical supercritical fluid extraction processes. Besides asphaltenes are dark or brown solids at the room temperature, and their melting points are close to or higher than critical point temperatures of light alkanes, so asphaltene solidification interferes with LLV phase behavior at low temperatures. Classical phase behavior of asymmetric mixtures, such as type III, type IV or type V phase behavior, with solid interference, was expected. However since ABVB itself is a mixture containing numerous components, the phase behavior of pentane + ABVB mixtures was found to be more complicated than that of binary mixtures; complex phase transitions with temperature, pressure and composition were observed. Section 4.1 discusses the phase behavior of pentane + ABVB mixtures. The phase behavior of the phase behavior of dodecane + ABVB + hydrogen mixtures is covered in section 4.2. The impact of alkane size on the phase behavior of alkane + ABVB mixtures, and the reversibility of multiphase behavior of asphaltene containing fluids are discussed in section 4.3 and section 4.4, respectively. Key points from this chapter are summarized in section 4.5.

Please also note that the multiphase behaviors observed in this research are interpreted as physical phenomena only. The impact of chemical reactions on multiphase behaviors is assumed to be negligible at temperatures below 340 °C. All experiments in this research were conducted at 10 °C interval ranging from 20 °C to 340 °C.

4.1 Phase Behavior of Pentane + ABVB Mixtures

To facilitate readers' appreciation, the grabbed X-ray images showing phase transitions are presented first, and then phase diagrams describing all these phase transitions are sketched. Finally advanced topics, such as K point location, phase behavior evolution and the state (solid or liquid) of the precipitated asphaltenic materials, are discussed.

4.1.1 X-ray images of pentane + ABVB mixtures

It is helpful to briefly explain the relationship of the height of X-ray image and the position of bellows before introduction of X-ray images. The pressure of Be view cell and the volume occupied by the sample can be reduced/increased by adding/removing some driving gas (nitrogen) to/from the bellows. When the bellows contracts to the top cap of the view cell, the volume occupied by the sample reaches its maximum and the pressure reaches its minimum. With the addition of driving gas to the bellows which makes it expand and move downwards, the volume occupied by the sample is reduced and the pressure is increased. Since the bellows (stainless steel) is not "transparent" to X-rays, the height of the view cell that is "transparent" to X-rays changes with position of bellows. Consequently, the "informative" height of X-ray image cropped depends on the position of bellows (pressure).

The X-ray images for pentane + ABVB mixtures are shown in Figure 4-1a ~ 4-1l. For ABVB + 5~60 wt % mixtures, there were at least two images cropped at different pressures but roughly the same temperature (aligned vertically in Figure 4-1). For an image cropped at the low pressure for T <210 °C, the bellows was at the view cell top

and the sample was under a pressure close to the lowest pressure the view cell could reach. For an image cropped at the high pressure for T <210 °C, the bellows was very close to but not touching the surface of the light liquid phase, in order that the sample was under a pressure as close as possible to its bubble pressure. The numbers listed beneath each image are the temperature and pressure conditions for the image when cropped. Since pressure values change dramatically from room temperature to 340 °C and from 0 % ABVB to 100 % ABVB, there is insufficient space to note pressure values if the same unit for pressure is used and all digits to the right of decimal point are included. Consequently pressure and temperature values are rounded to their nearest integers. However, this may bring some confusion to readers: the same pressure value is noted for different X-ray images, particularly for those with high ABVB content and at low temperatures. For example the pressure values noted in X-ray images in Figure 4-1a for 20 ~ 40 °C are 1 bar. In reality, these values are different. For the low pressure series at 20 °C, 30 °C and 40 °C, the real pressure values are 0.61 bar, 0.89 bar, 1.22 bar respectively; for the high pressure series at 20 °C, 30 °C and 40 °C, the real pressure values are 0.62 bar, 0.90 bar, 1.24 bar respectively. The pressure and temperature values for each image are available in Appendix III.

The X-ray images indicate multiphase behavior over a broad range of temperature and pressure. Sometimes it is hard to observe phase boundaries in an image. For example, two phases are close to a critical point, or the volume of a phase is very small. Using the method discussed in the last chapter, analyzing an X-ray image along with its corresponding averaged density profile, most of phase boundaries could be identified unambiguously.

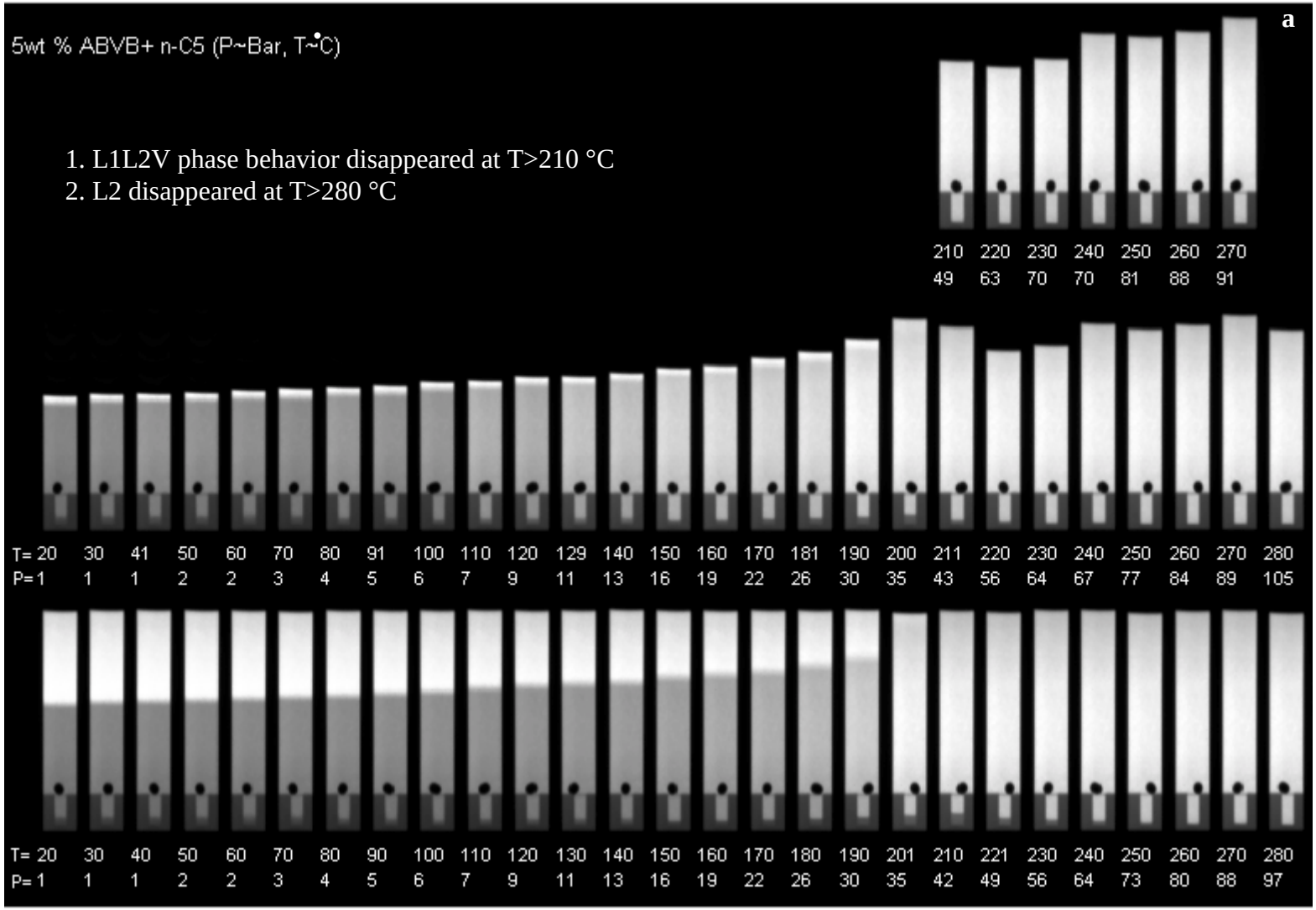

Figure 4-1a X-rays images of pentane + ABVB (5 wt %) mixtures
a. 5; b. 10; c. 20; d. 30; e. 40; f. 45; g. 50; h. 60; i. 70; j. 80; k. 90; l. 100

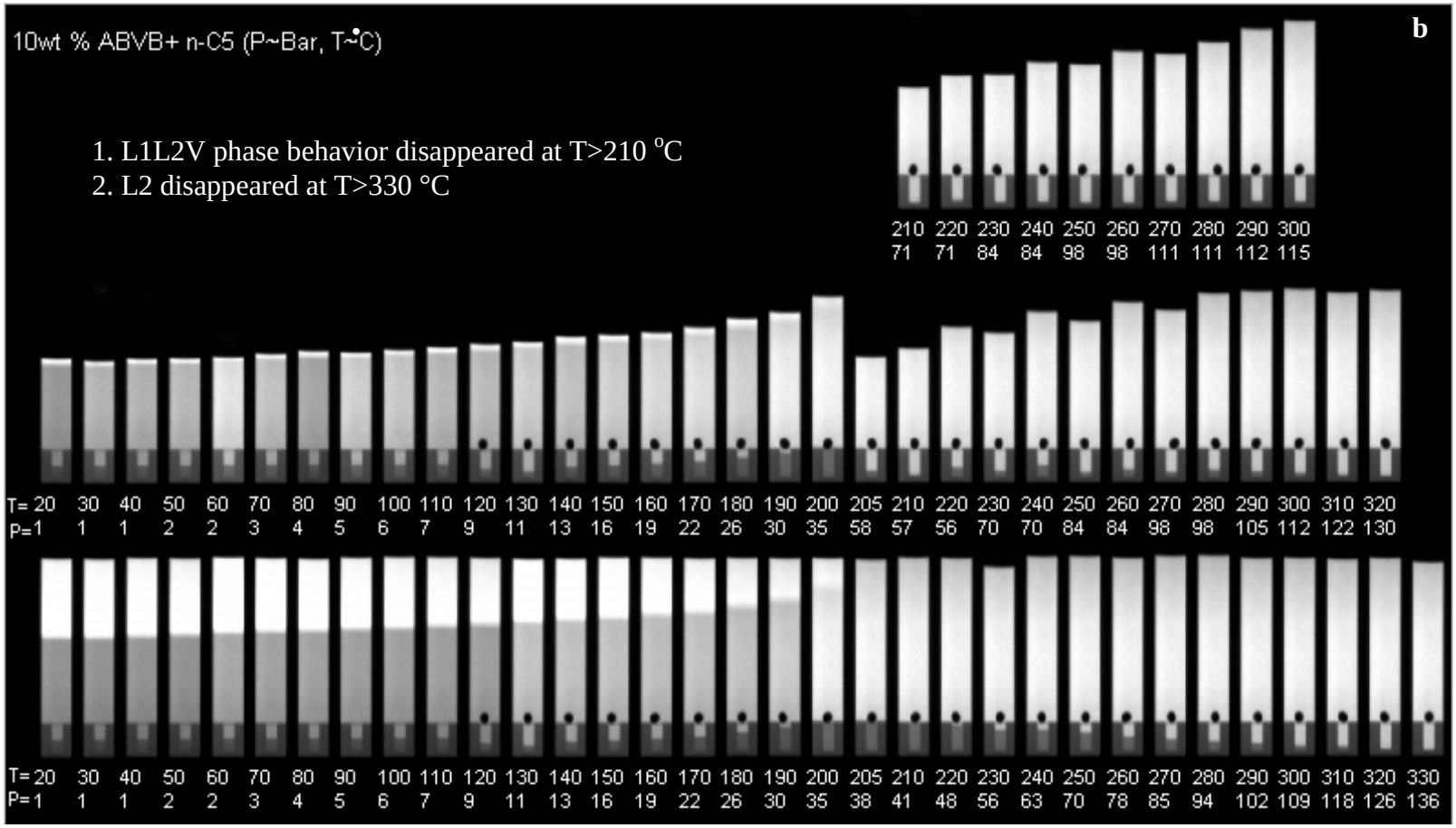

Figure 4-1 b X-rays images of pentane + ABVB (10 wt %) mixtures
a. 5; b. 10; c. 20; d. 30; e. 40; f. 45; g. 50; h. 60; i. 70; j. 80; k. 90; l. 100 (continued)

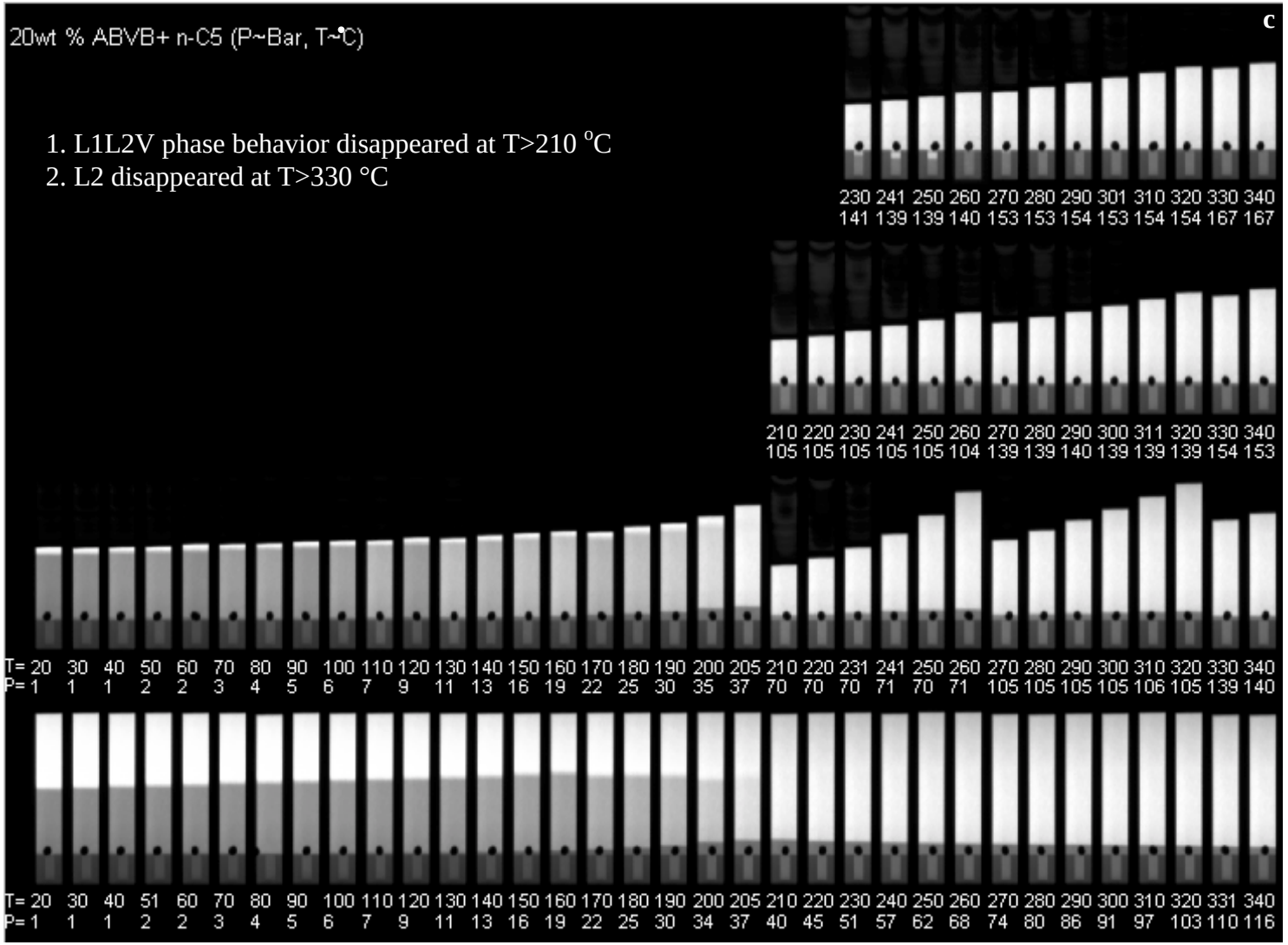

Figure 4-1c X-rays images of pentane + ABVB (20 wt %) mixtures
a. 5; b. 10; c. 20; d. 30; e. 40; f. 45; g. 50; h. 60; i. 70; j. 80; k. 90; l. 100 (continued)

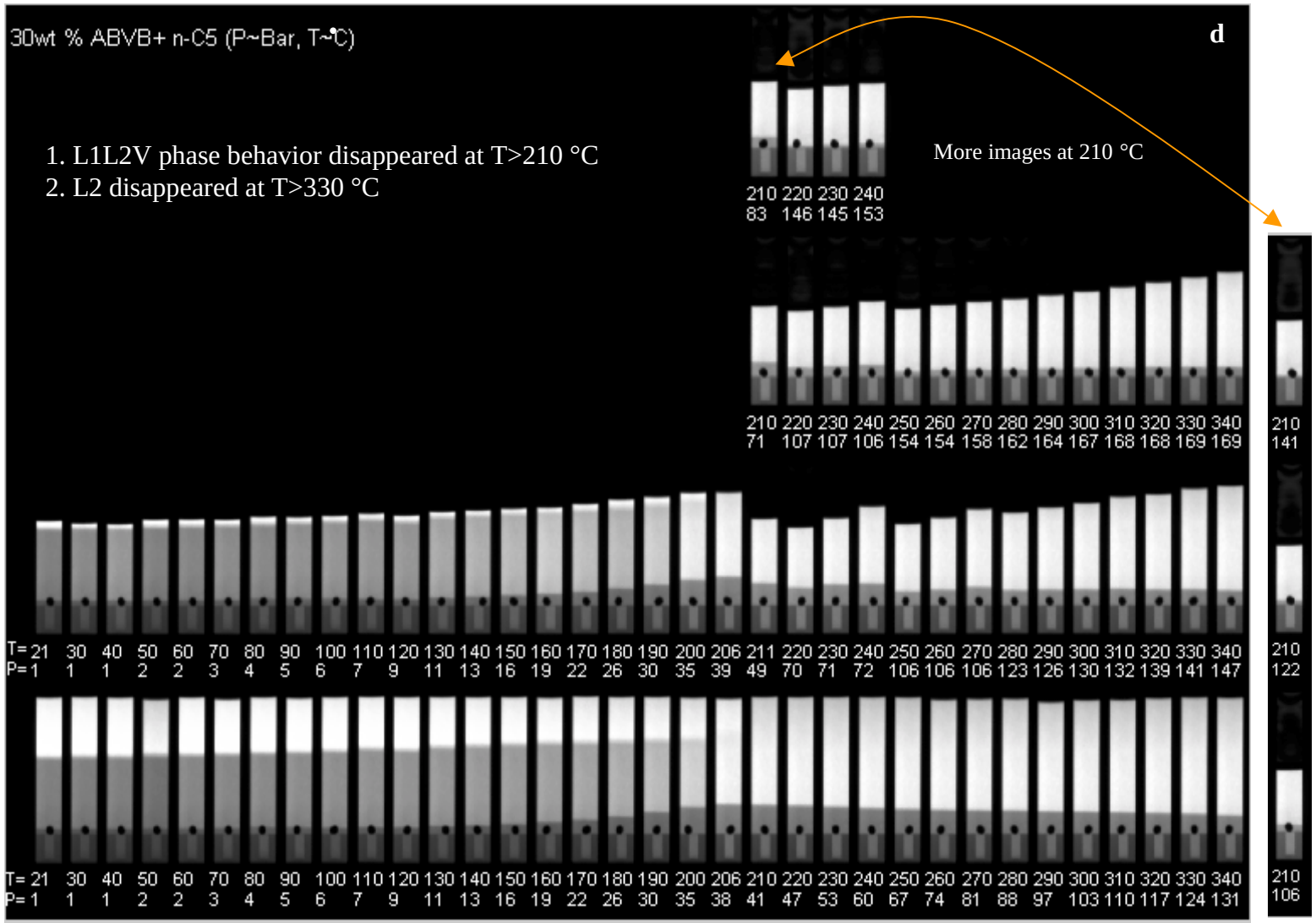

Figure 4-1d X-rays images of pentane + ABVB (30 wt %) mixtures
a. 5; b. 10; c. 20; d. 30; e. 40; f. 45; g. 50; h. 60; i. 70; j. 80; k. 90; l. 100 (continued)

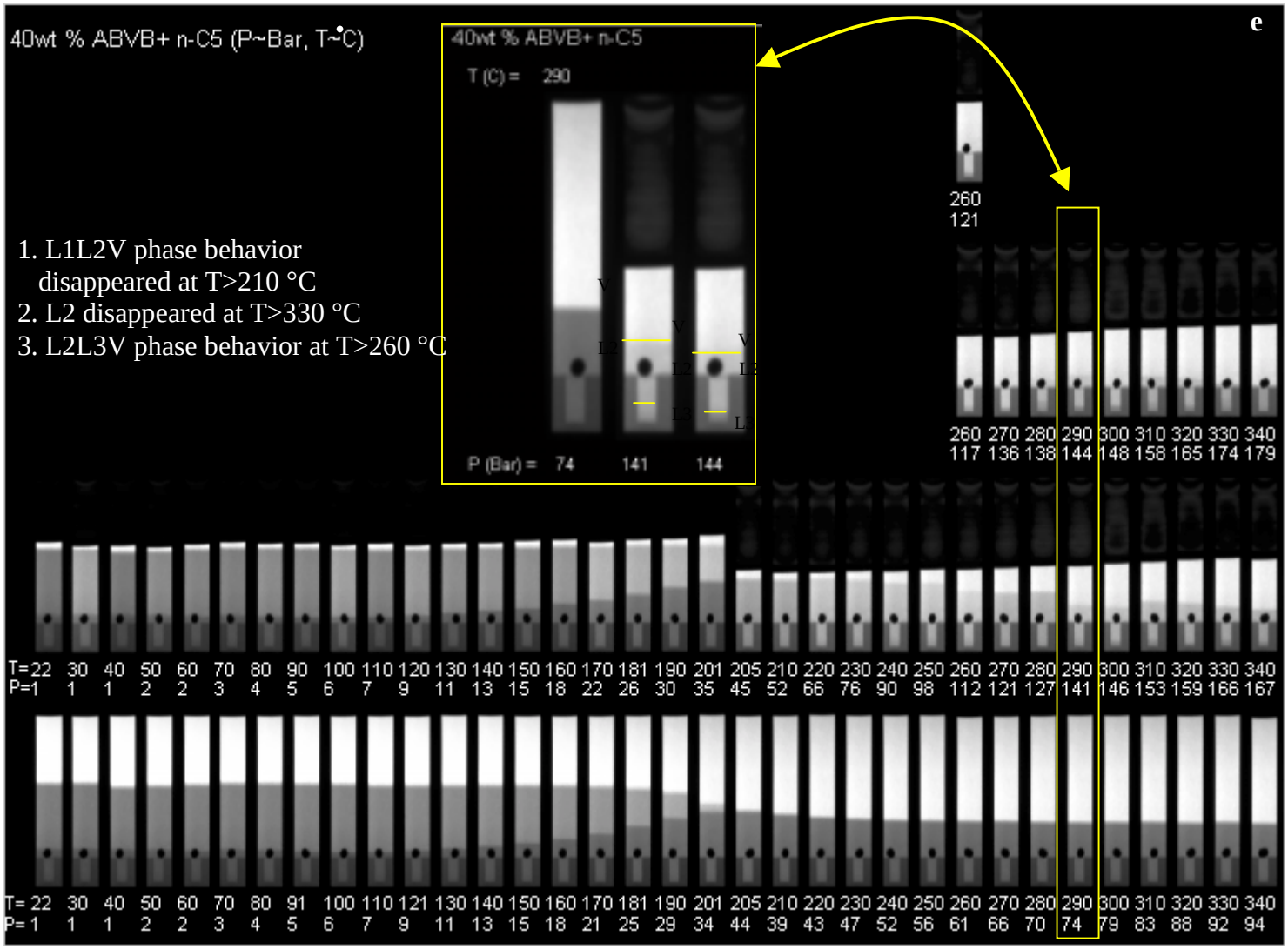

Figure 4-1e X-rays images of pentane + ABVB (40 wt %) mixtures
a. 5; b. 10; c. 20; d. 30; e. 40; f. 45; g. 50; h. 60; i. 70; j. 80; k. 90; l. 100 (continued)

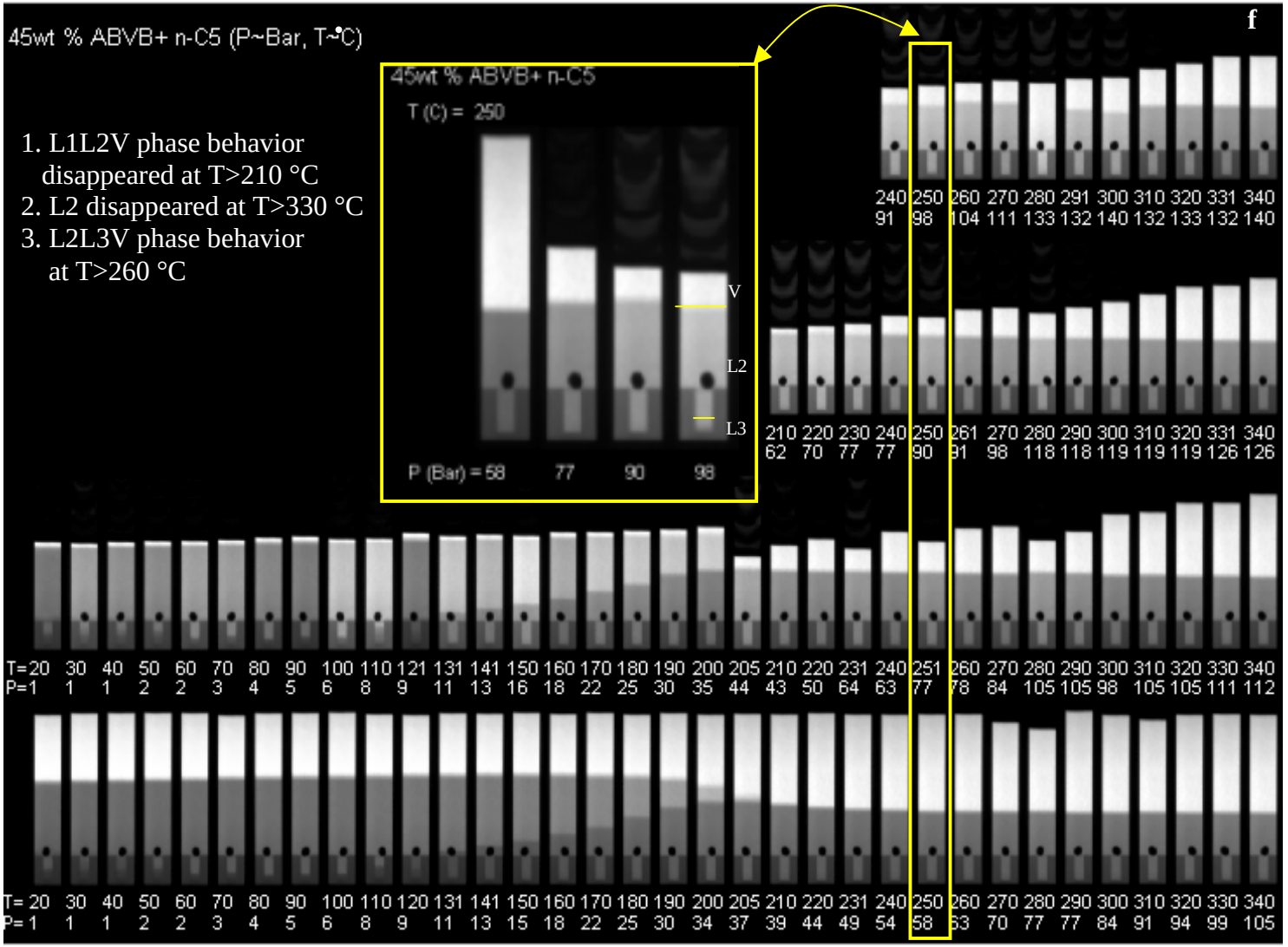

Figure 4-1f X-rays images of pentane + ABVB (45 wt %) mixtures
a. 5; b. 10; c. 20; d. 30; e. 40; f. 45; g. 50; h. 60; i. 70; j. 80; k. 90; l. 100 (continued)

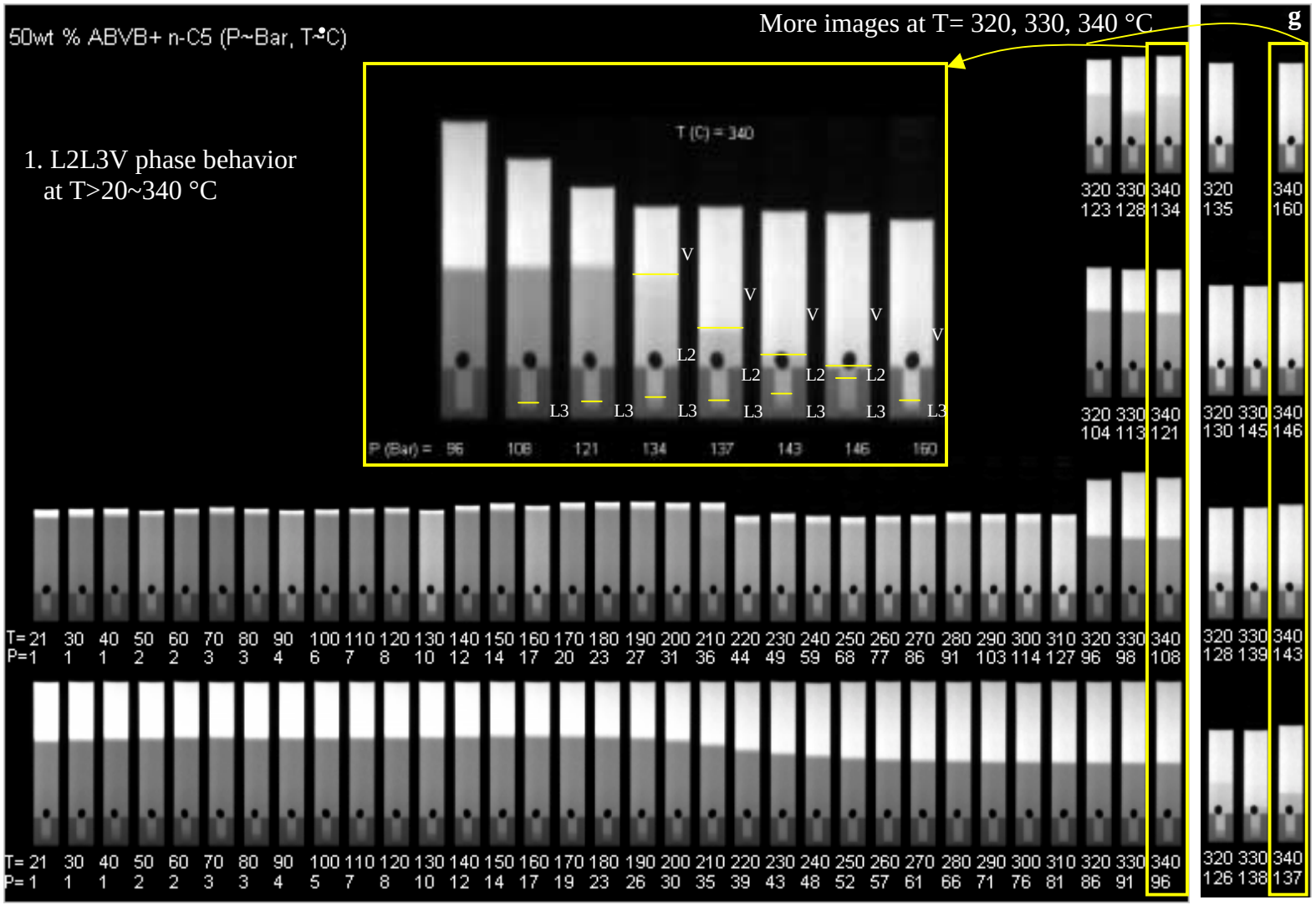

Figure 4-1g X-rays images of pentane + ABVB (50 wt %) mixtures
a. 5; b. 10; c. 20; d. 30; e. 40; f. 45; g. 50; h. 60; i. 70; j. 80; k. 90; l. 100 (continued)

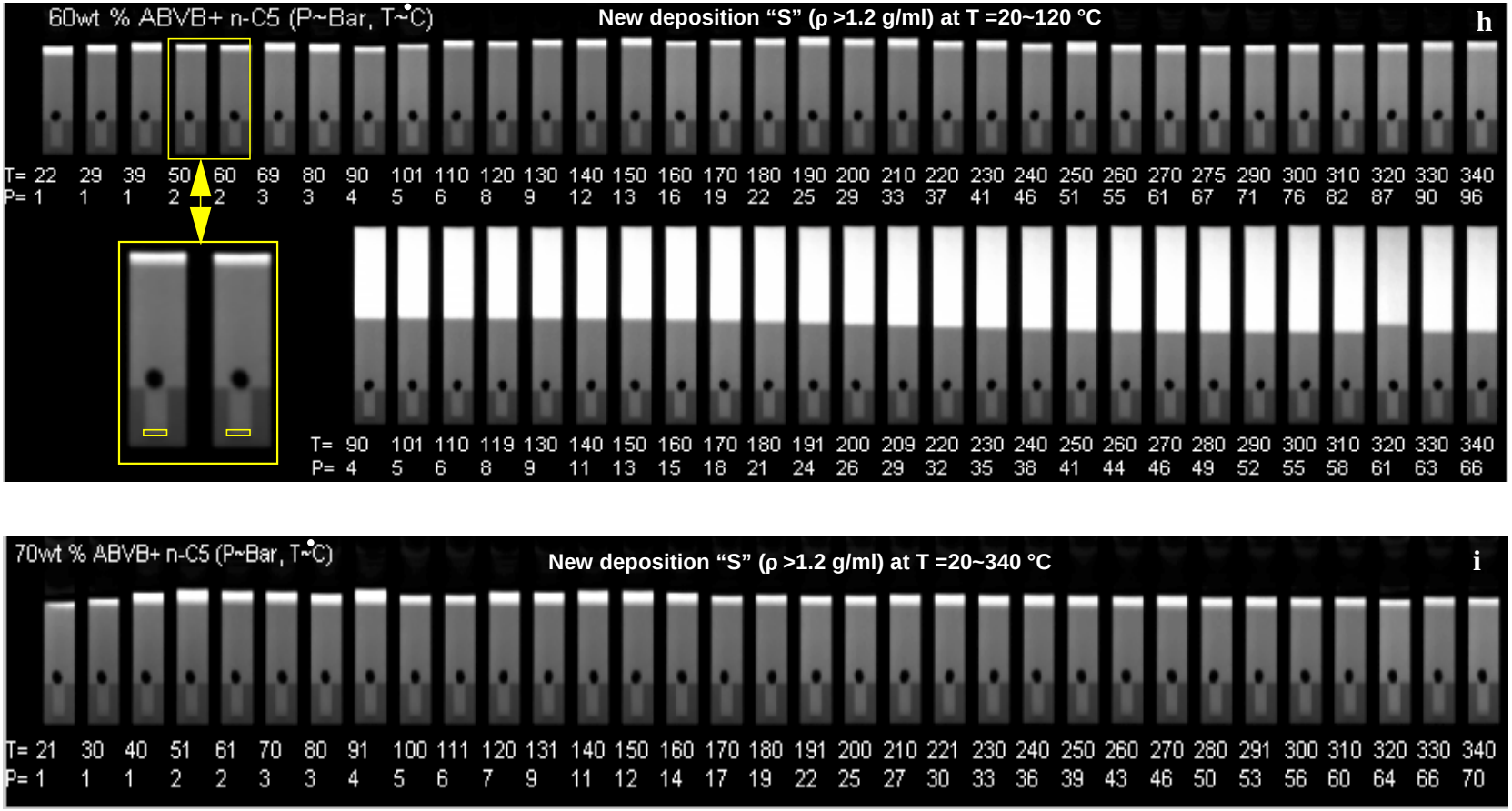

Figure 4-1 h ~ i X-rays images of pentane + ABVB (60 ~ 70wt %) mixtures
a. 5; b. 10; c. 20; d. 30; e. 40; f. 45; g. 50; h. 60; i. 70; j. 80; k. 90; l. 100 (continued)

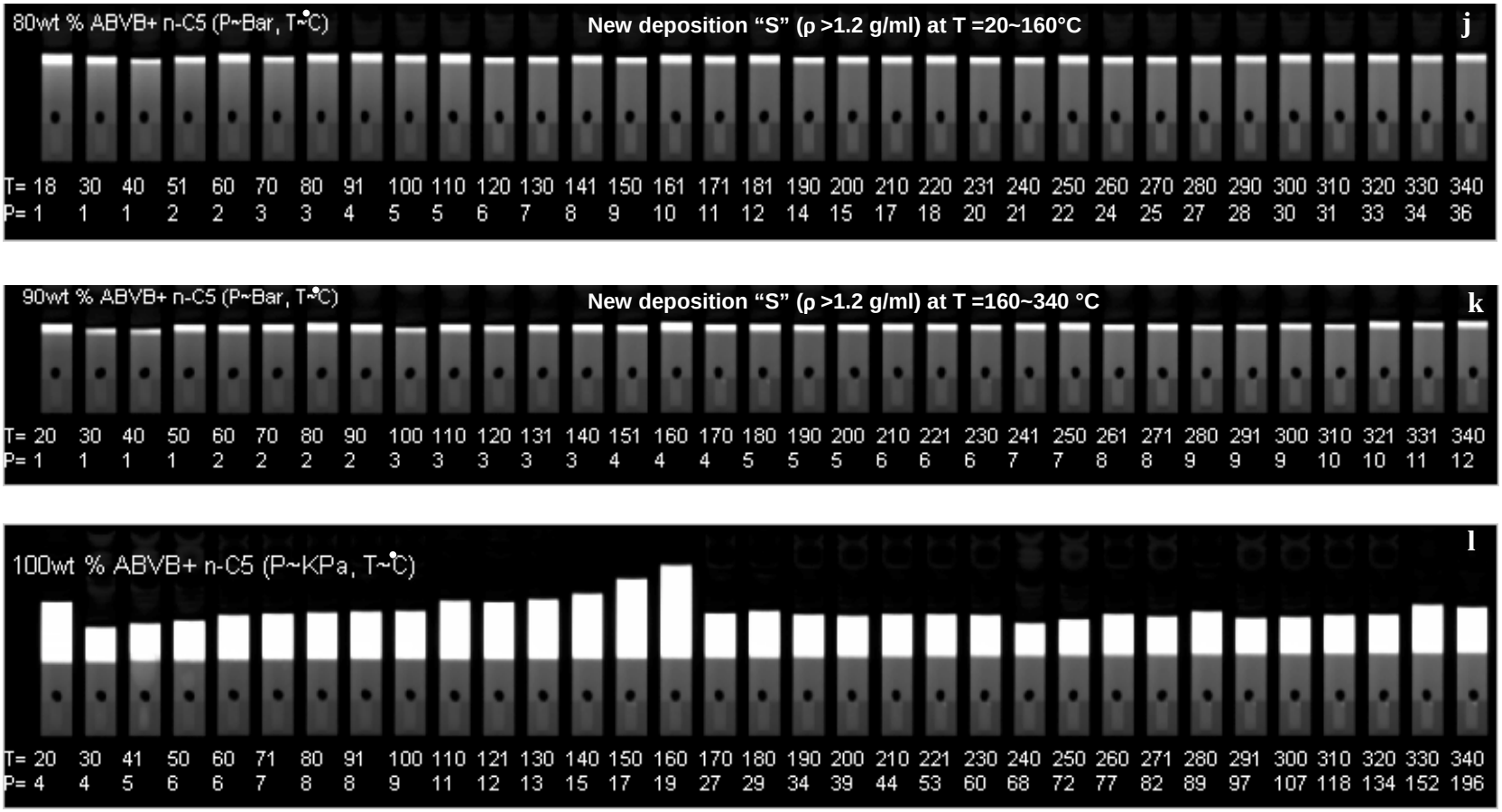

Figure 4-1 j~l X-rays images of pentane + ABVB (80 ~ 100 wt %) mixtures
a. 5; b. 10; c. 20; d. 30; e. 40; f. 45; g. 50; h. 60; i. 70; j. 80; k. 90; l. 100

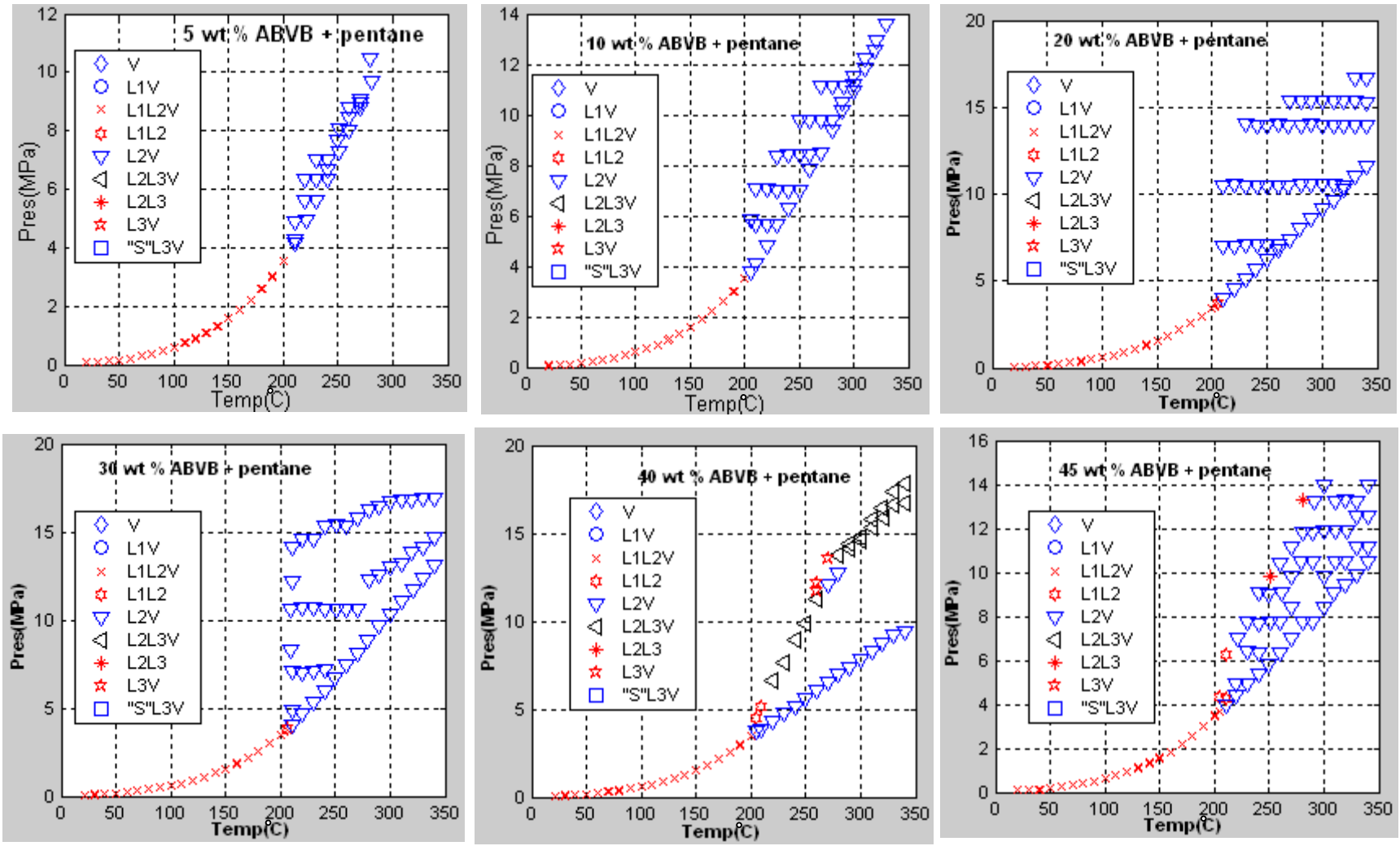

Figure 4-2 Experimental data points in different phase regions (Continued)

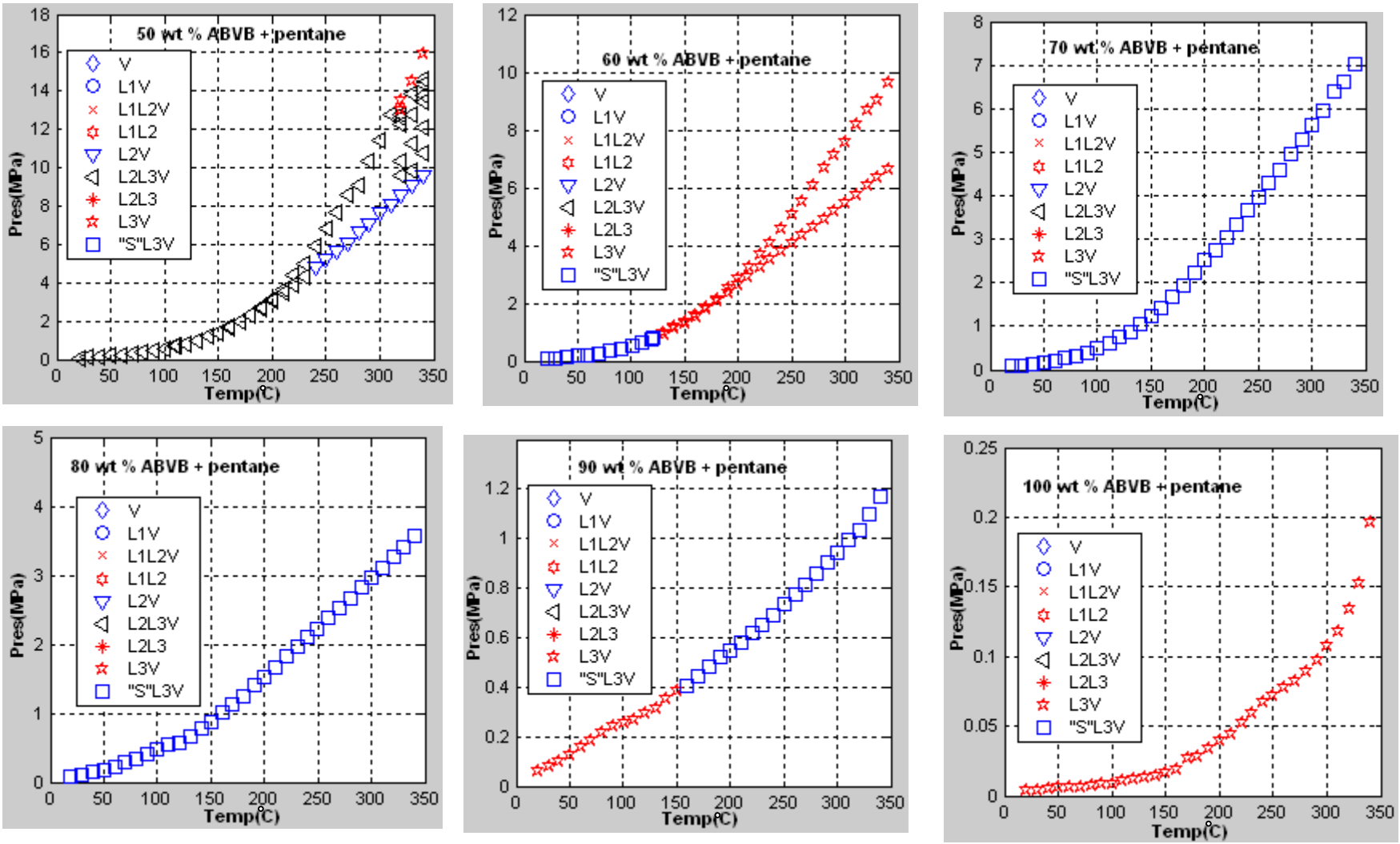

Figure 4-2 Experimental data points in different phase regions.

4.1.2 Preliminary phase diagrams for pentane + ABVB mixtures

Although using X-ray images to present phase behaviors is very intuitive, it is not as efficient as phase diagrams and readers may lose orientation of pressure and temperature. By analyzing each X-ray image using the developed software, the number and natural (volume and apparent density) of phases in equilibria were obtained and summarized in Appendices IV. Consequently the information obtained from the X-ray images was mapped to corresponding preliminary phase diagrams in Figure 4-2. According to the type of phase behavior observed, experimental data points falling in different phase regions were presented in different legends. Also indicated in Figure 4-2 are the phase behavior zones immediately close to the experimental data points, which were determined by the method discussed in the next section.

4.1.3 Determining the location of phase boundary

The phase diagrams in Figure 4-2 are preliminary in nature since the phase transition boundaries, for example L1L2V↔L1L2, are not available. Phase boundaries were determined by extrapolations of volumes and apparent densities of phases in equilibria with pressure, as illustrated by an example in Figure 4-3. Near the phase boundary of L2L3V↔L3V, L2 was diminishing as pressure increases. We extrapolate the curve of the volume of L2 versus pressure to the point at which the volume of L2 equals zero (the x axis). The pressure at this point, 13.1 MPa, was identified as the phase boundary pressure for L2L3V↔L3V. The method works for most cases but has difficulty when the amount of phase diminishing/appearing (L3) is quite small and also a weak function of pressure, such as the L2V↔L2L3V transition in Figure 4-3. In this case, the

phase boundary pressure fell in a range, such as 8.6~9.6 MPa. If accurate boundary pressures are available at neighboring temperatures, the range could be further narrowed; if not, the middle value of this range was used approximately as the phase boundary pressure.

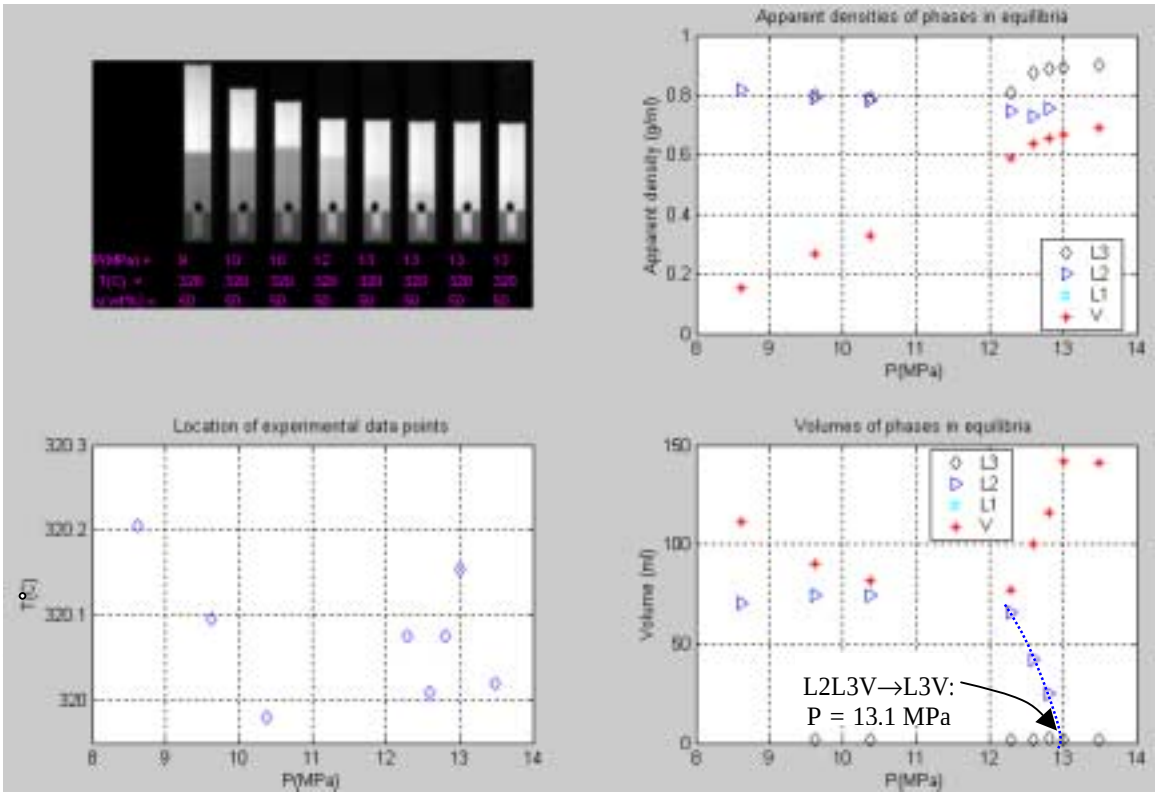

Figure 4-3 Phase boundary pressure determination by extrapolation.

4.1.4 Determining the type of phase behavior of a region immediately neighboring experimental data points

It is almost impossible to obtain experimental data at all conditions because there are numerous data points in PTx space, and because phase behavior experiments are very time-consuming and expensive, and are also limited by current experimental technologies. Quite often practitioners have to identify the type of phase behavior of regions immediately neighboring experimental data points in order to complete a phase

diagram from limited experimental data. In this study, the type of phase behavior of a region immediately neighboring experimental data points was determined using the same method used to determine the phase boundary (Figure 4-4).

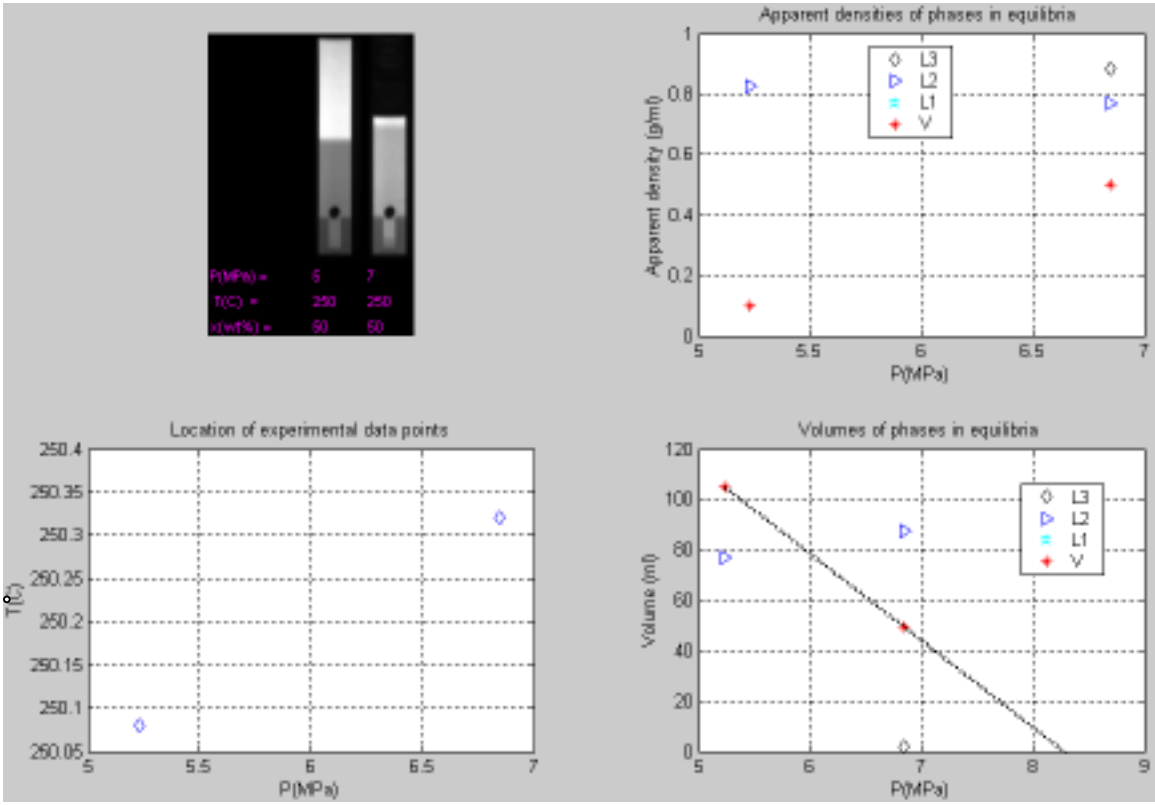

Figure 4-4 Phase behavior type of a neighboring region determined by extrapolation

Clearly, as the pressure increases, the volume of V decreases while the volume of L2 increases, i.e., L1L2V→L1L2. Logically the type of phase behavior of a region immediately above the experimental data (higher pressure) is L2L3, although there is no experimental data in the L2L3 phase region. The phase boundary pressure was estimated to be 8.25 MPa using the method discussed in the last section.

4.1.5 Determining the location of a K point

Locations of K and L points are very useful for identifying the type of phase behavior and determining possible types of multiphase regions around K and L points.

But it is also quite challenging to locate these points since they are only points in PTx space. As reviewed in Table 2-3, at a K point, a light liquid and a vapor phase become critical. It is often difficult to see the critical phenomenon in experiments, so instead what is actually observed is the phenomenon near the K point; the differences between properties (such as density) of the light liquid and the vapor phase are diminishing, but the volume of one phase is increasing while the volume of the other phase is decreasing as illustrated in Figure 4-5.

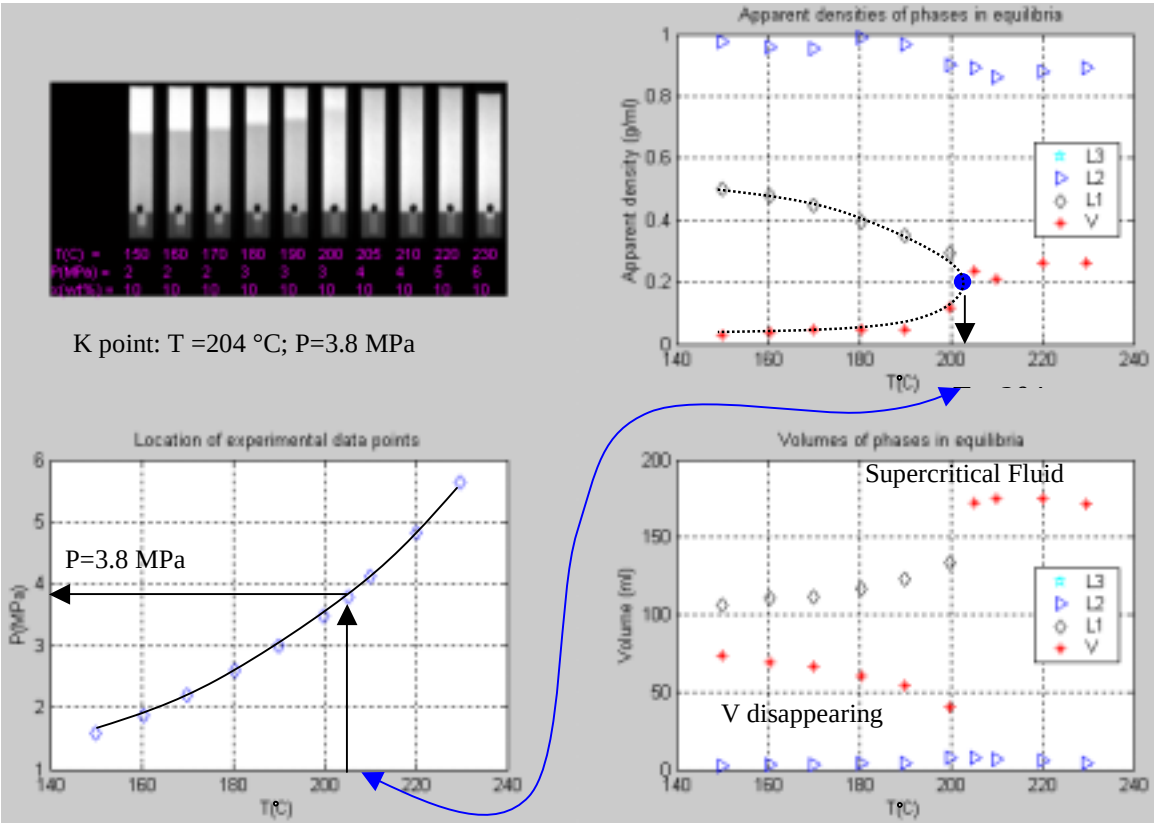

Figure 4-5 Determining the location of a K point by extrapolation

Determination of a K point includes the following steps:

1. Based on the apparent density versus temperature trend of the light liquid phase and vapour phase shown in the upper-left corner of Figure 4-5, locate the K point temperature by extrapolation (T=204 °C).

2. Using the determined K point temperature, interpolate the K point pressure from pressure versus temperature trend shown in the lower-left corner of Figure 4-5 (P=3.8 MPa).
3. Double check the images shown in the upper-left corner of Figure 4-5 and volume versus temperature trend in the lower-right corner to ensure there is a K point around this area.

If experiment data points are not that close to the K point, it is risky to locate the K point by the above method. In this case one has to narrow the location of the K point by checking the observed phase behavior around the K point, as illustrated in Figure 4-6.

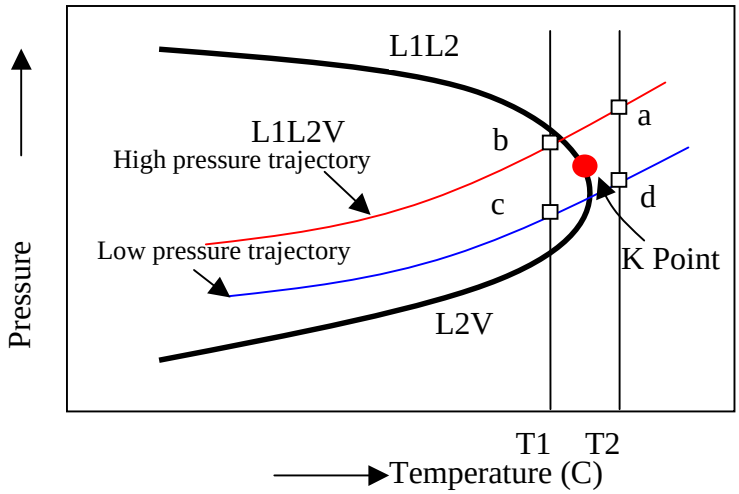

Figure 4-6 Narrow the range of a K point according to the observed phase behavior around the K Point

As a sample exhibiting L1L2V phase behavior is heated up to a temperature above a K point, whether L1L2 or L2V is observed depends on experimental trajectory pressure: L1L2 for the high pressure trajectory and L2V for the low pressure trajectory. By following the observed phase transition, the relative position (pressure range) of the K point to the experimental trajectory could be identified, i.e., the K point was above the pressure trajectory if L2V observed and below the pressure trajectory if L1L2 observed.

It is desirable that the K point falls between the high pressure and the low pressure experimental trajectories. The temperature range of the K point was also bounded by two adjacent experiment temperatures. At one temperature (T1, below the K point), L1L2V behavior was observed while at the other temperature (T2, above the K point) L2V/L1L2 behavior was observed. The above steps bound the K point to the region formed by the points abcd. A good estimate of the K point temperature and pressure can be obtained by interpolation. The estimated locations of K points for 5~45 wt% ABVB + pentane mixtures are listed in Table 4-1 and displayed in Figure 4-7.

Table 4-1 Estimated locations of K points for ABVB + pentane mixture

Wt% ABVB	K point location	
	Temperature (±1°C)	Pressure (±0.1MPa)
5	201	3.6
10	204	3.8
20	207	3.9
30	209	4.0
40	212	4.2
45	213	4.3

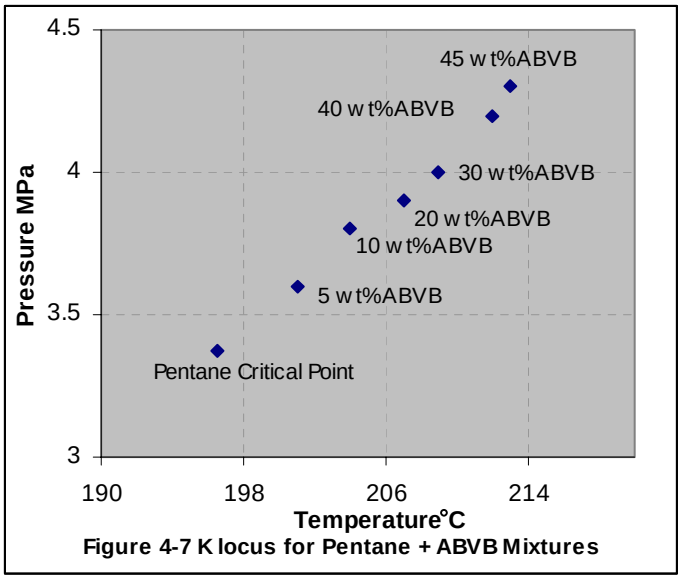

Figure 4-7 K locus for Pentane + ABVB Mixtures

4.1.6 PT at fixed x phase diagrams for pentane + ABVB mixtures

The phase boundaries, the type of phase behavior immediately neighboring the experimental data points, and K point positions were obtained by the method discussed in the above sections. Based on the obtained information obtained, partial phase diagrams of ABVB + pentane mixtures (PT at fixed compositions) were sketched and are shown in Figure 4-8 a-l. In some cases where experimental data are not available, dashed lines indicate the tentative phase boundaries.

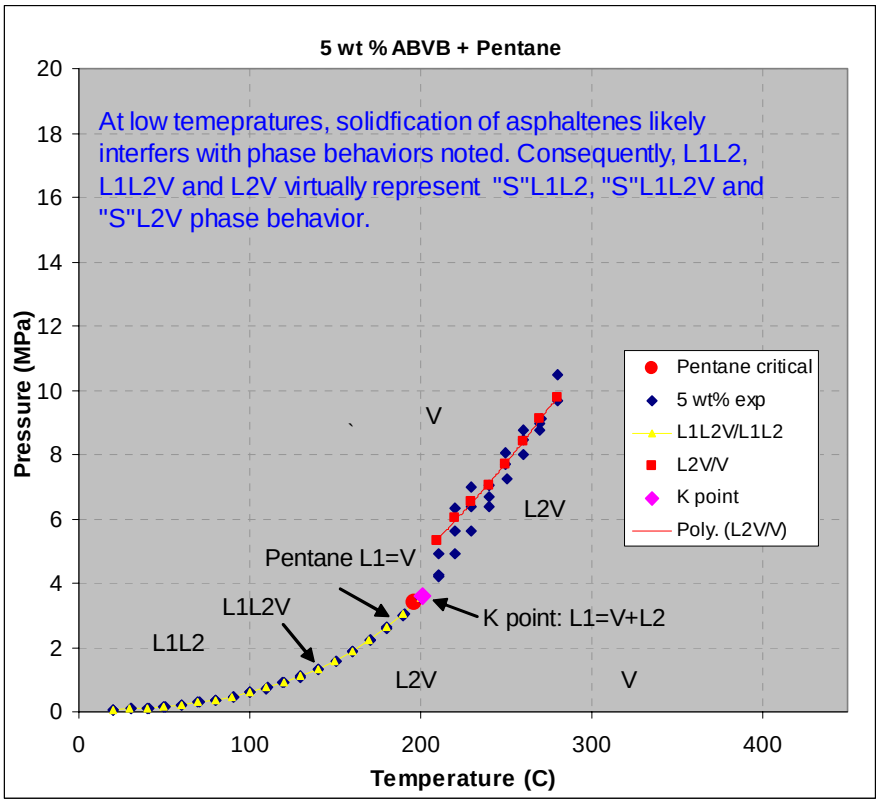

Figure 4-8 PT at constant x phase diagrams for ABVB + pentane mixtures (Continued)

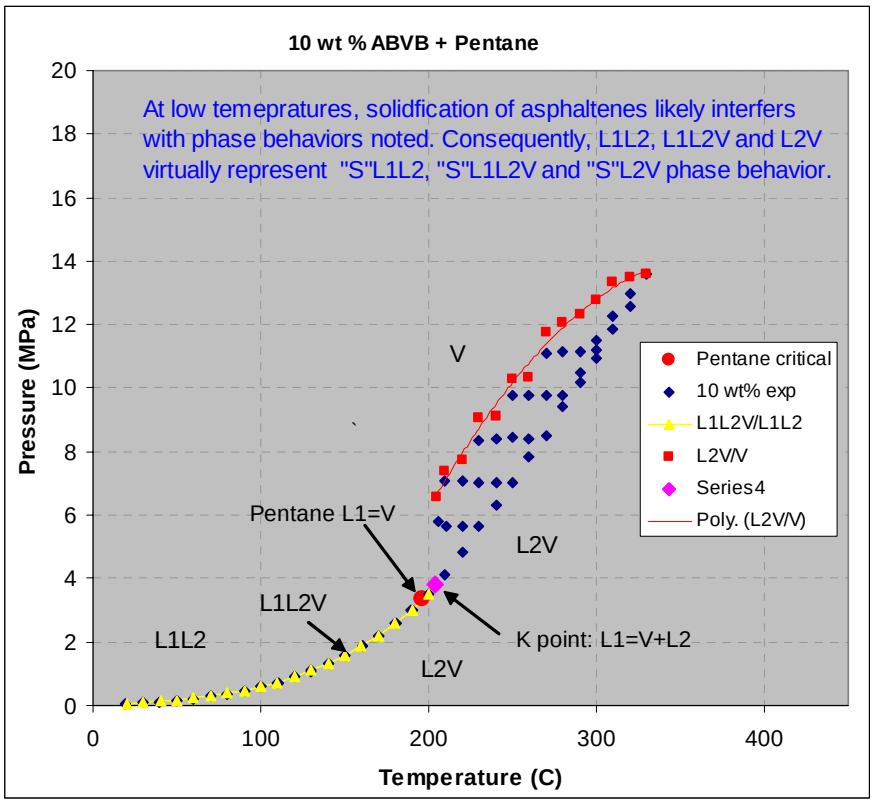

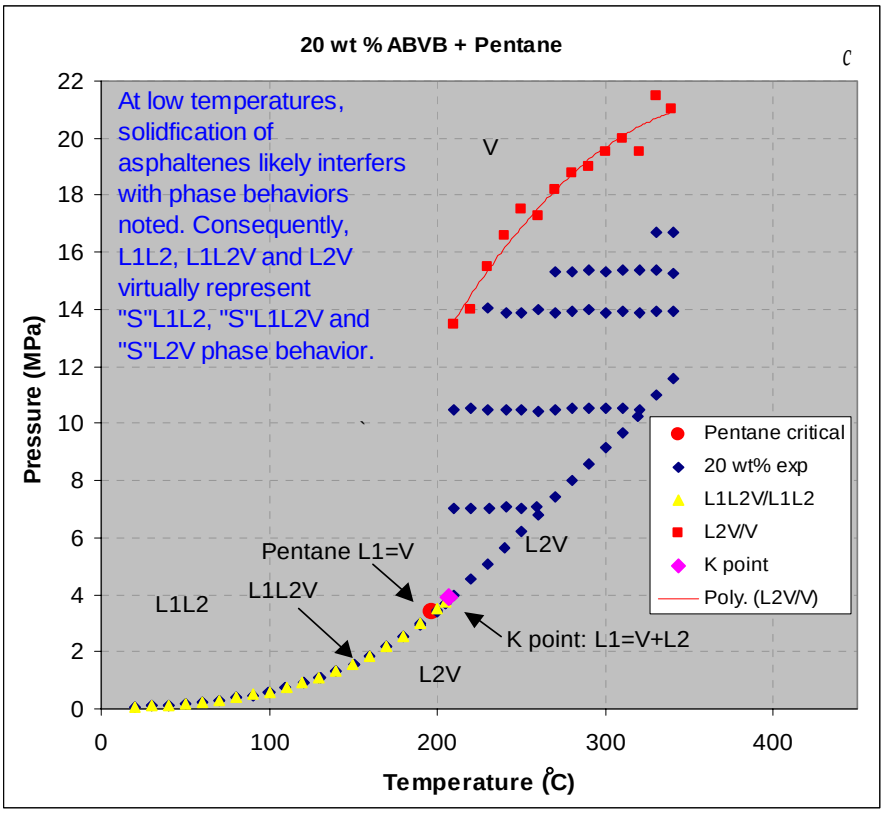

Figure 4-8 PT at constant x phase diagrams for ABVB + pentane mixtures (Continued)

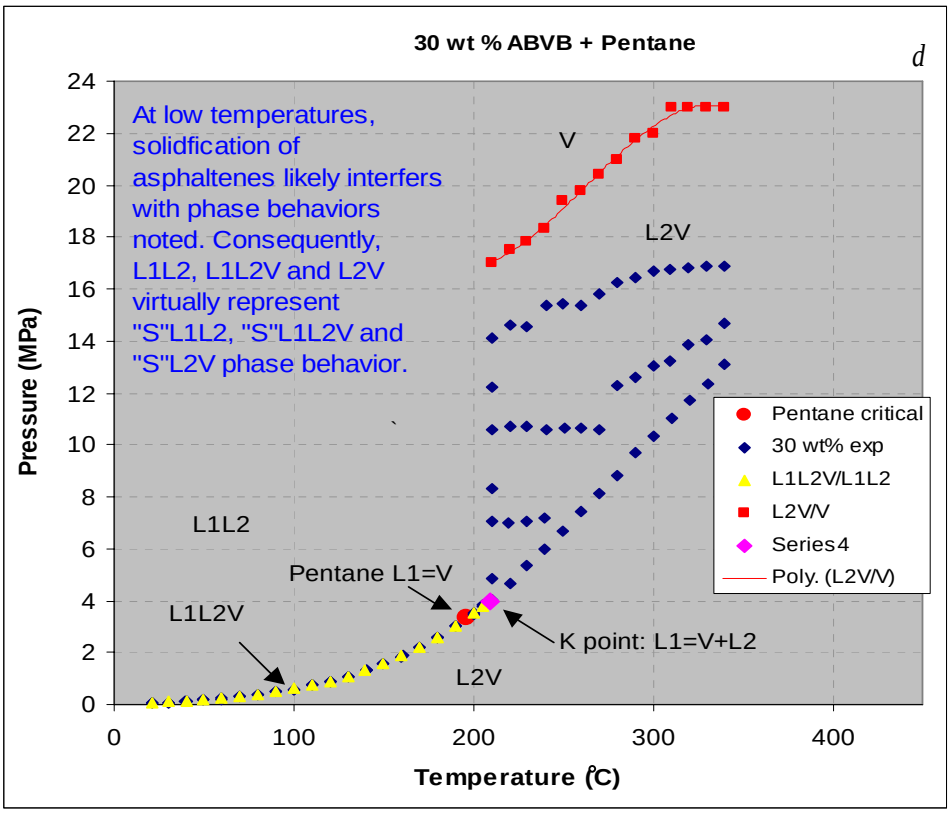

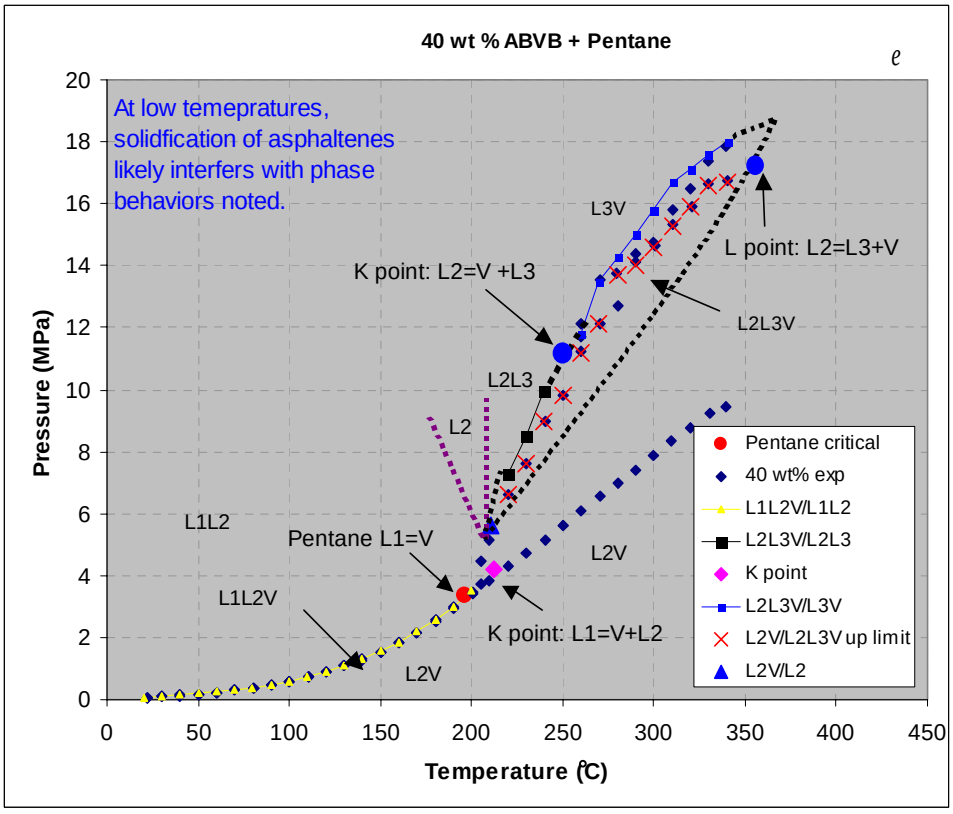

Figure 4-8 PT at constant x phase diagrams for ABVB + pentane mixtures (Continued)

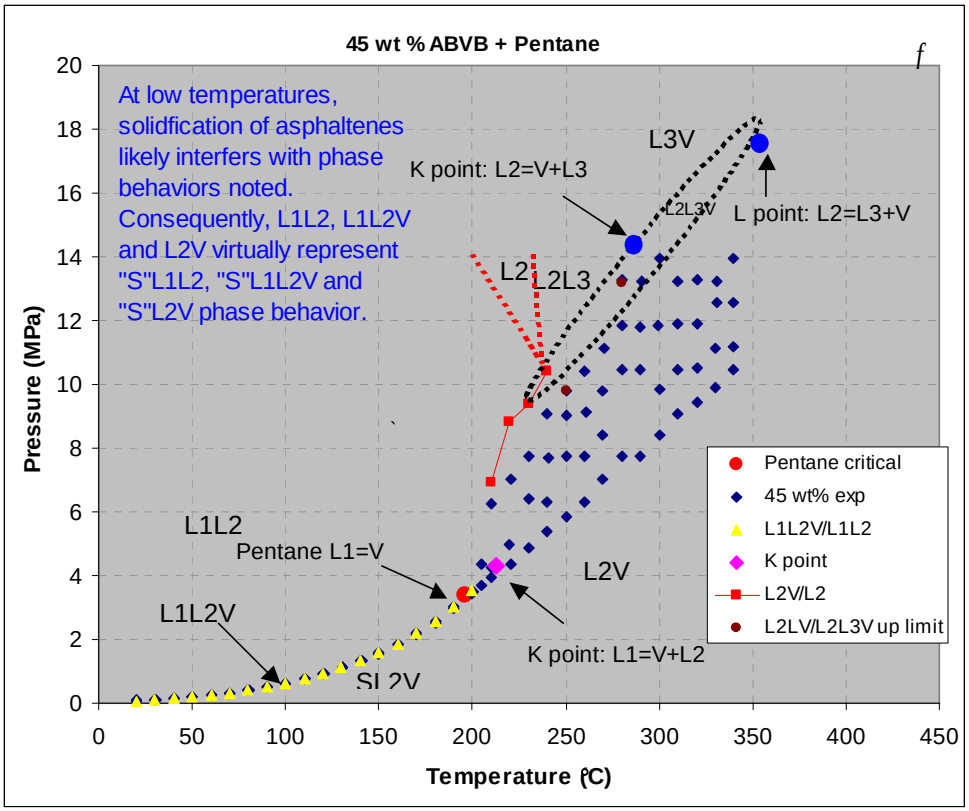

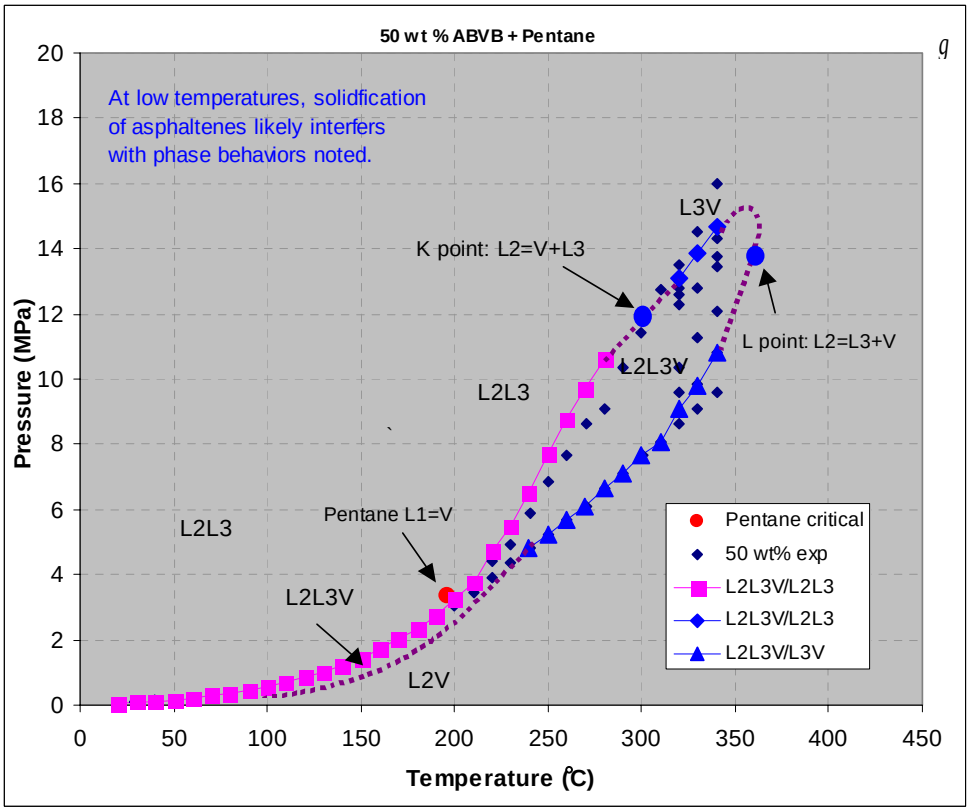

Figure 4-8 PT at constant x phase diagrams for ABVB + pentane mixtures (Continued)

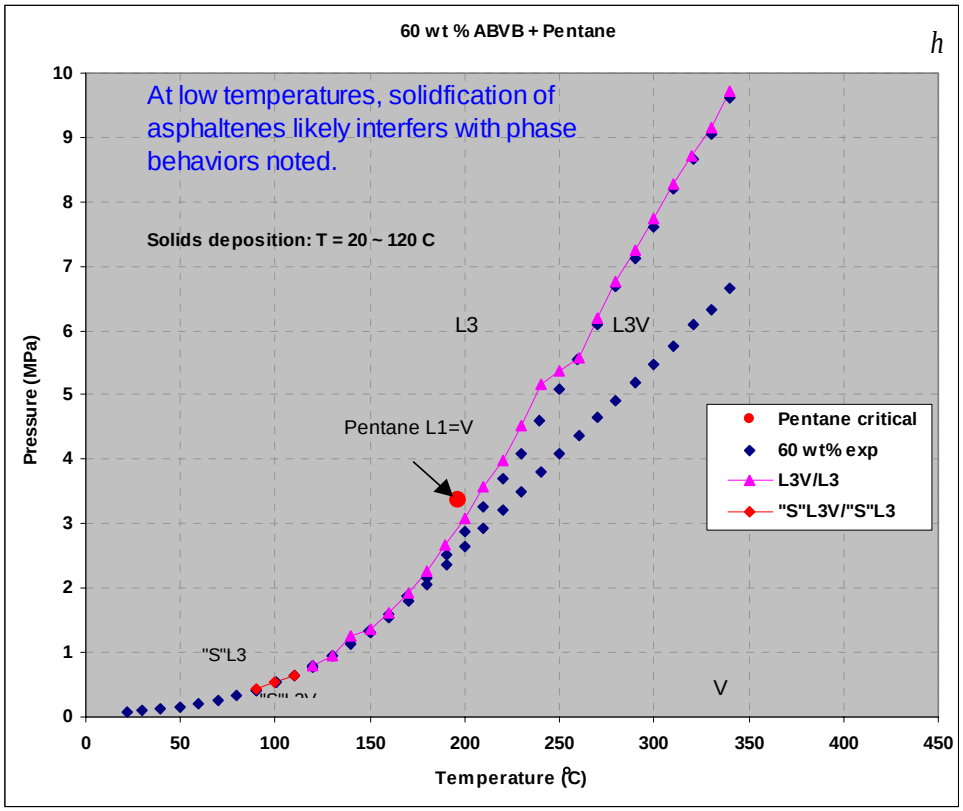

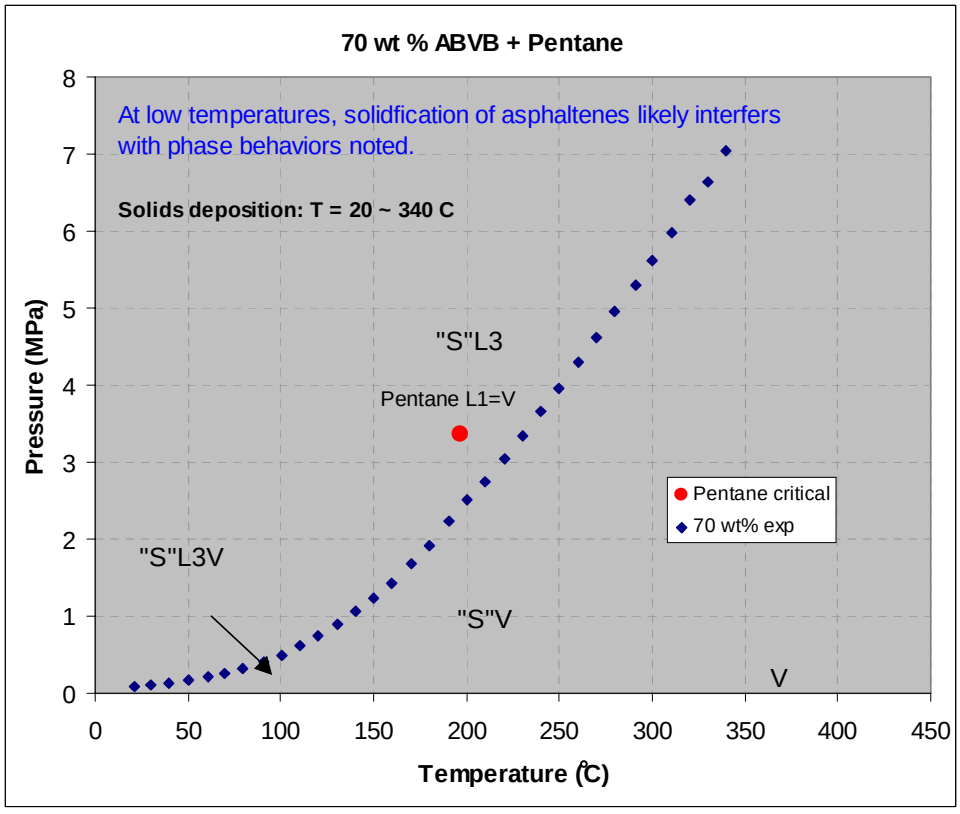

Figure 4-8 PT at constant x phase diagrams for ABVB + pentane mixtures (Continued)

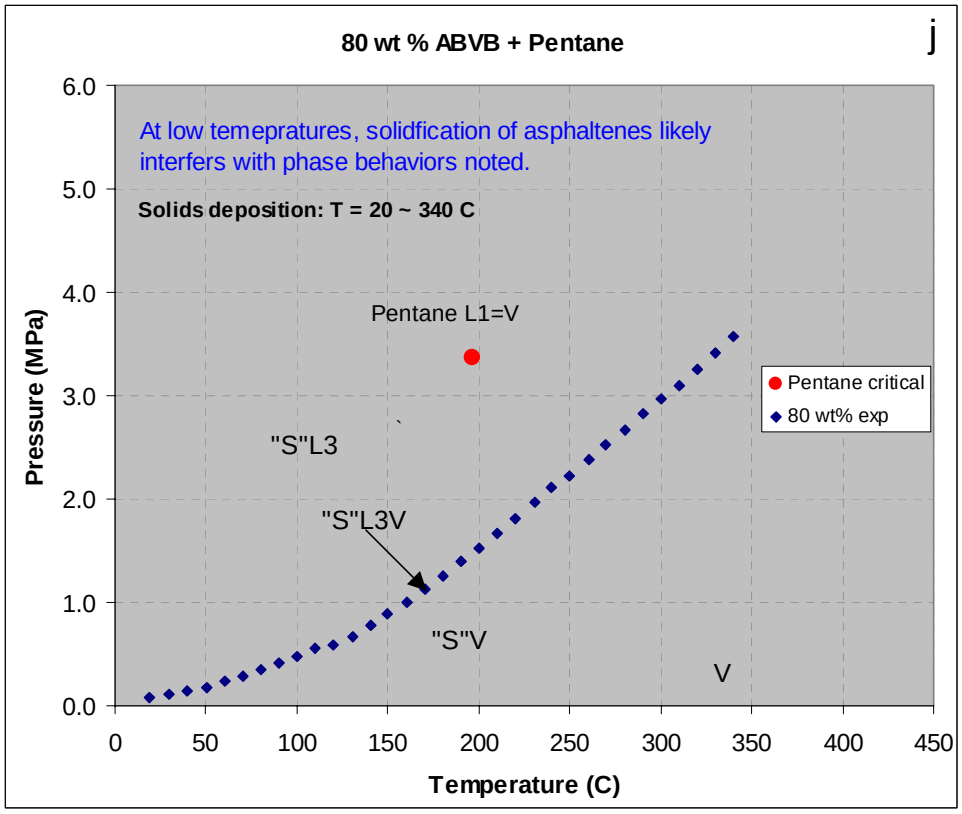

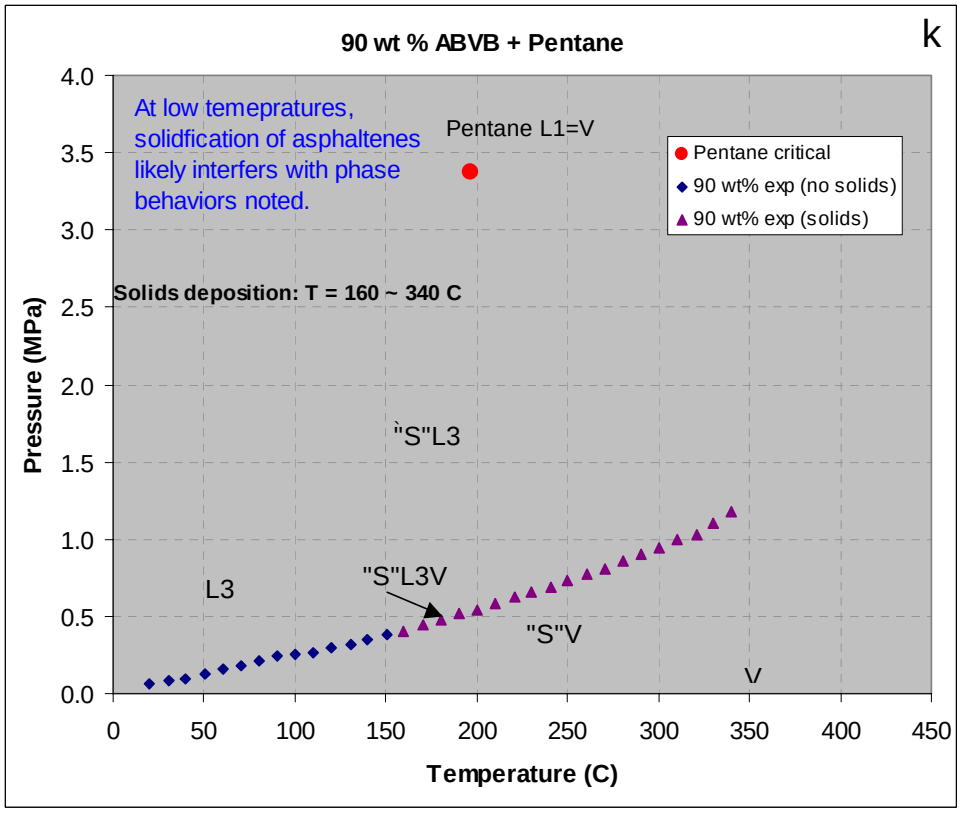

Figure 4-8 PT at constant x phase diagrams for ABVB + pentane mixtures (Continued)

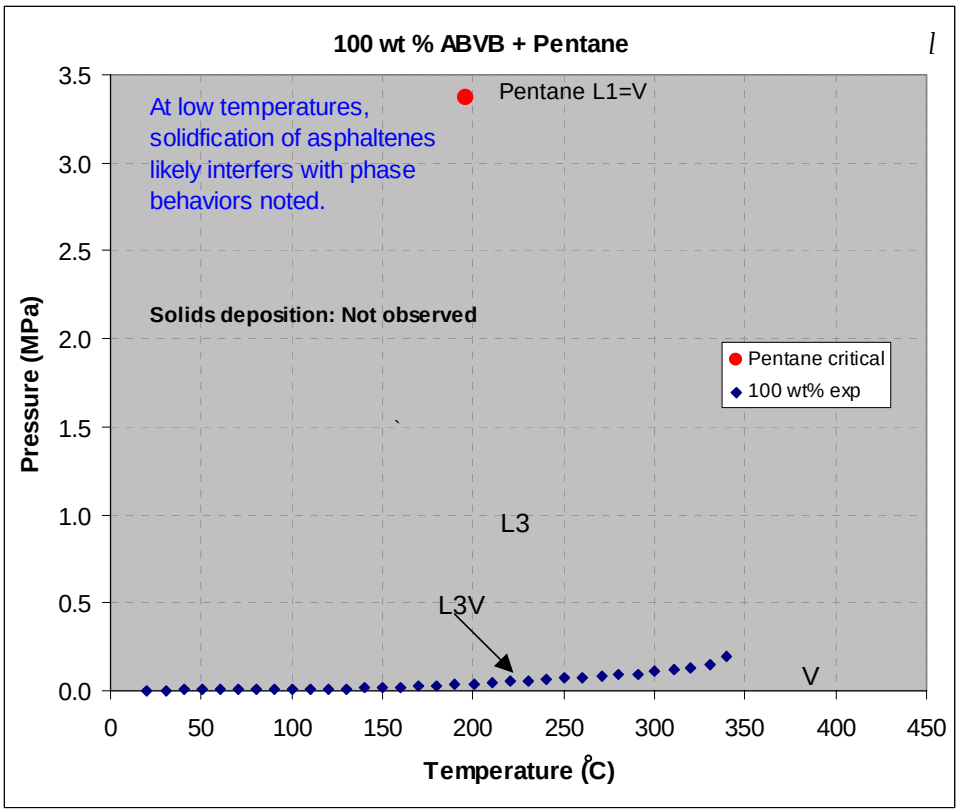

Figure 4-8 PT at constant x phase diagrams for ABVB + pentane mixtures

4.1.7 Px at constant T phase diagrams for pentane + ABVB mixtures

In addition to the PT at constant x phase diagrams, it is always desirable to have other types of phase diagrams, such as P-x at constant T or Tx at constant P. Px at constant T phase diagrams for pentane were constructed. Part of them are quite similar. To avoid repetition, only key diagrams are shown in Figure 4-9. The dashed lines, as well K (L2=V+L3) points and L (L2=L3+V) points, were drawn tentatively to indicate the phase behavior when experimental data are not available or uncertain. Although not observed in experiments, some of zones such as L1V must exist according to phase behavior theory. They were also included for clarity. The evolution of these phase diagrams is discussed in the next section.

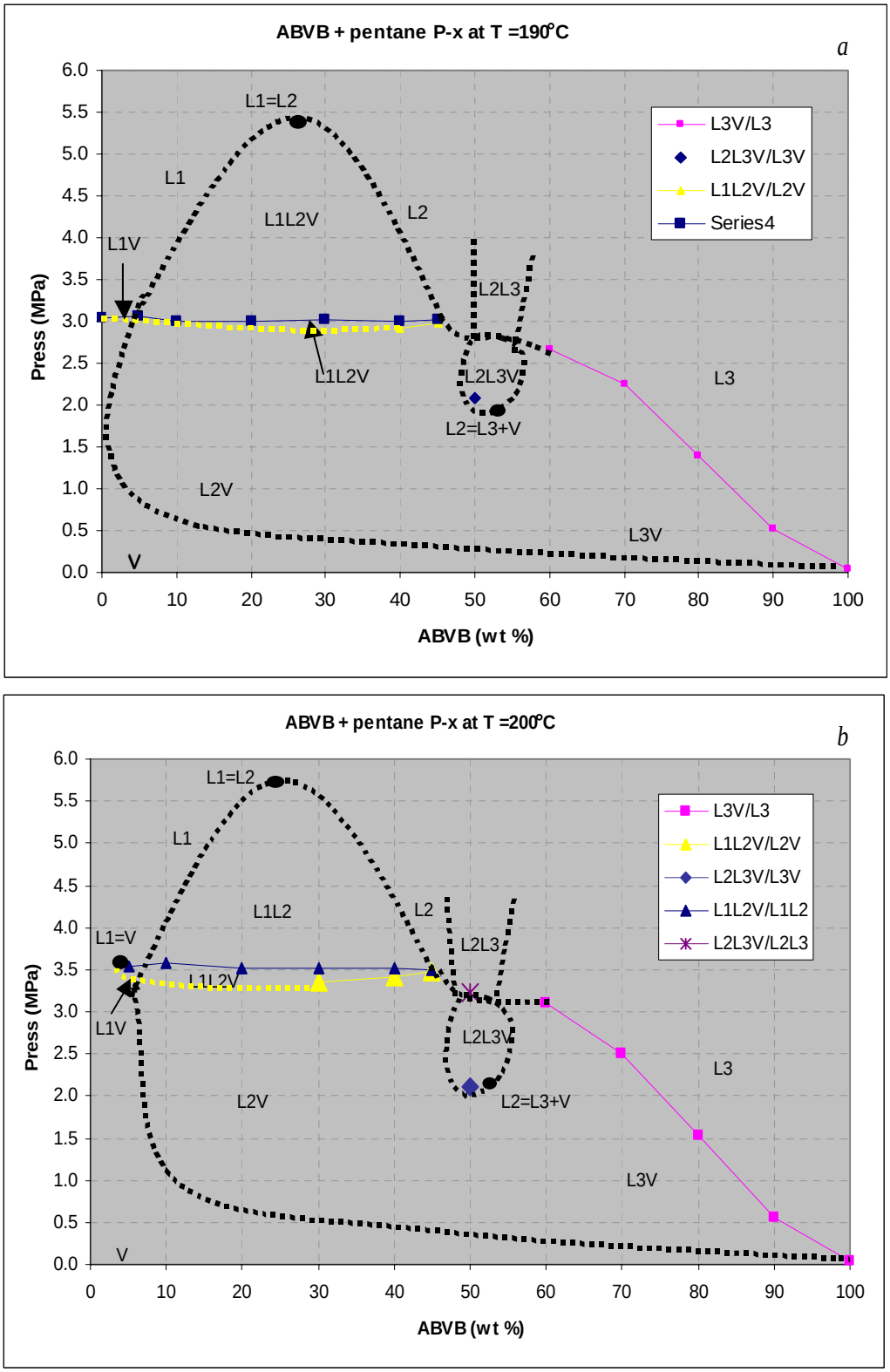

Figure 4-9 Px at constant T phase diagrams for ABVB + pentane mixtures (Continued)

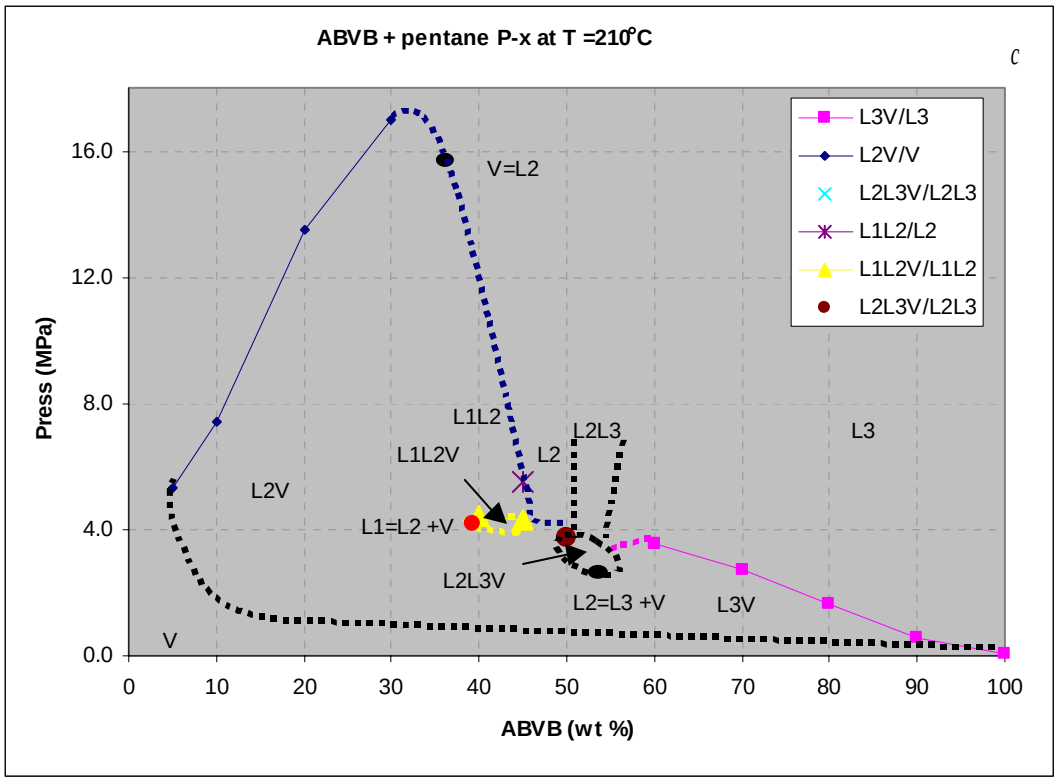

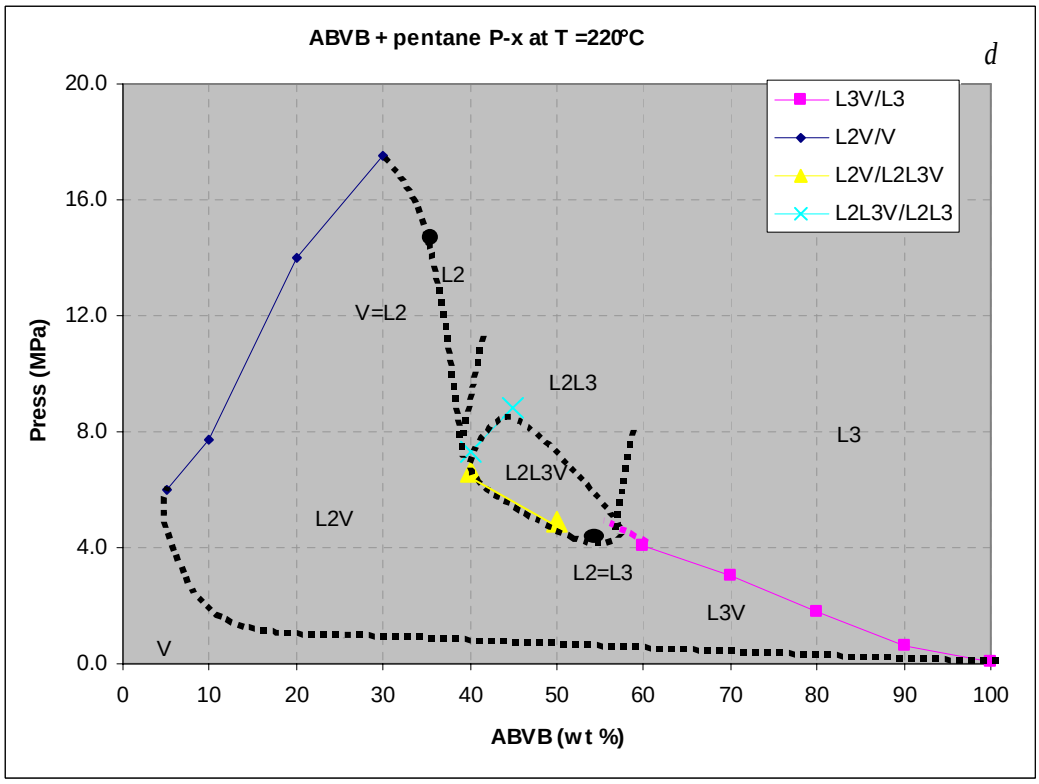

Figure 4-9 Px at constant T phase diagrams for ABVB + pentane mixtures (Continued)

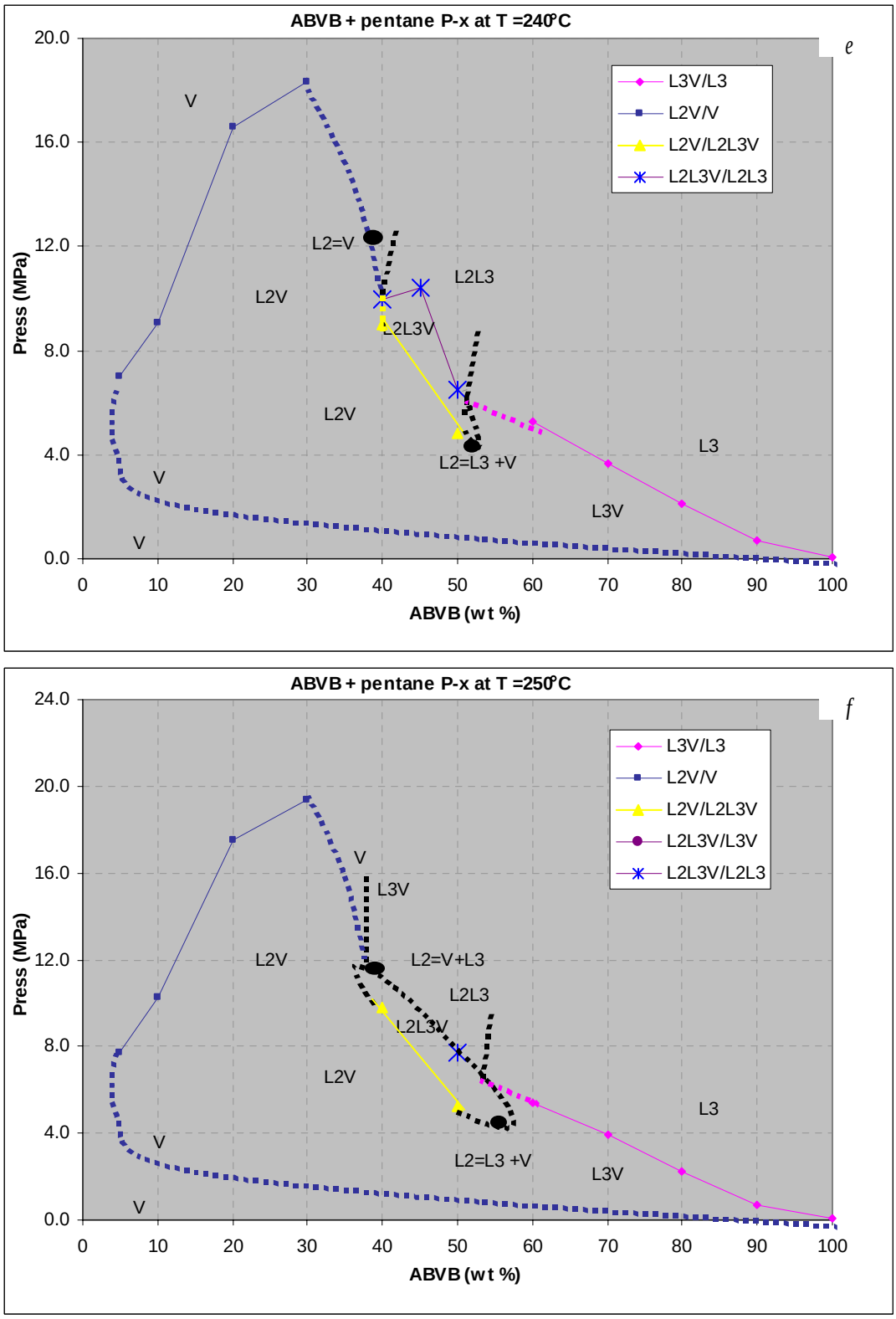

Figure 4-9 Px at constant T phase diagrams for ABVB + pentane mixtures (Continued)

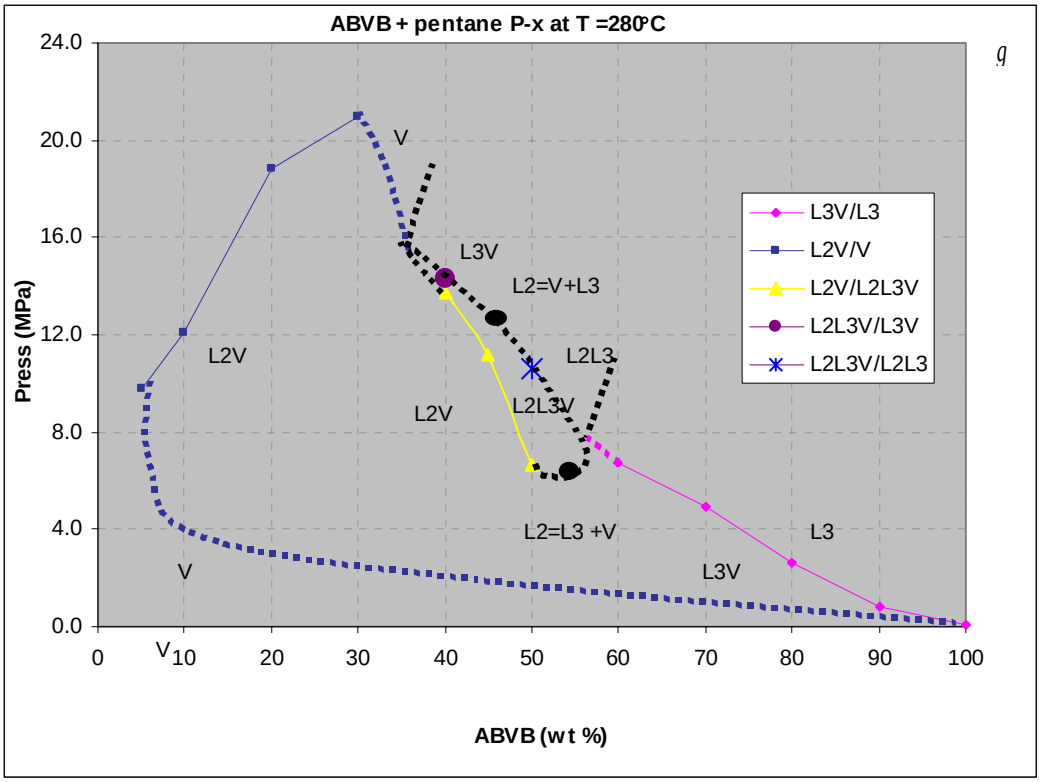

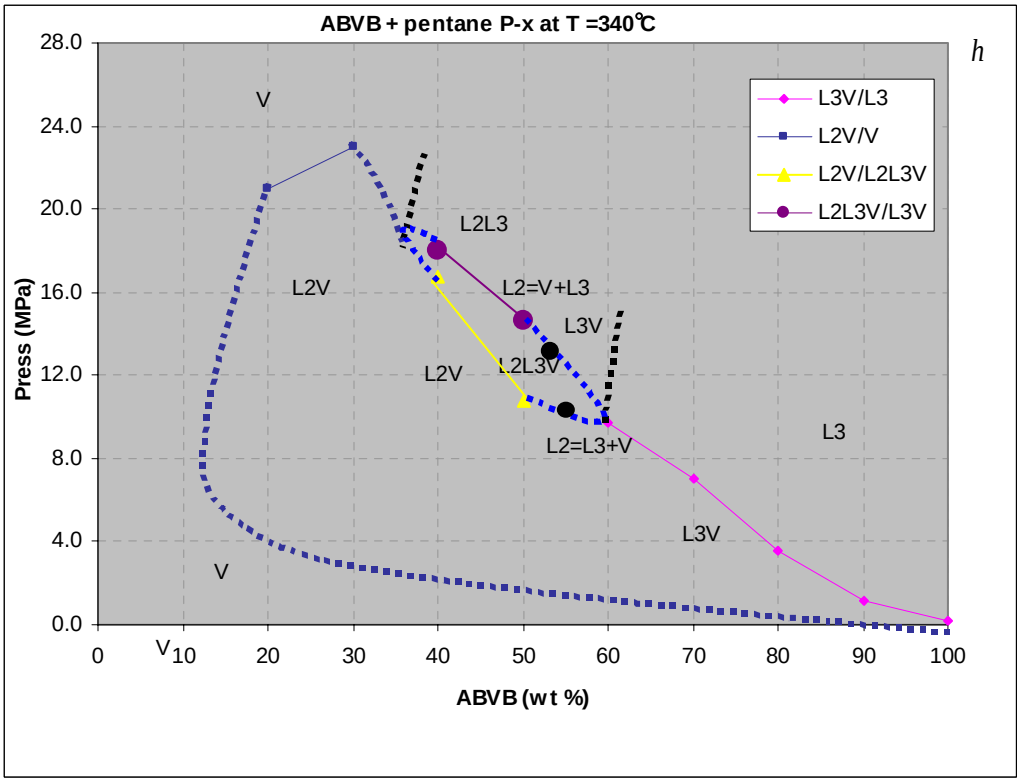

Figure 4-9 Px at constant T phase diagrams for ABVB + pentane mixtures

4.1.8 Evolution of phase behavior for pentane + ABVB mixtures

The phase behavior of pentane + ABVB mixtures still seems somewhat chaotic even after phase diagrams have been constructed. In order to get a clearer picture, this section discusses the evolution of the phase behavior for this type of mixture (Figure 4-10). PT projection in Figure 4-10 indicates that this type of phase behavior has one L locus (L2=L3+V) and two K loci (L1=V+L2 and L2=V+L3). The two loci have no common temperature range. The L1=V+L2 locus corresponds to the K point for an asymmetric binary mixture, and it starts at a temperature slightly higher than the critical temperature of the light component. Evolution of Px at constant T phase diagrams are discussed one by one as follows.

- T<T1 (Figure 4-10 b), both L1L2V and L2L3V phase regions exist and the L1V region starts from the pure component A. There is a L1=L2 critical point at a high pressure for the L1L2V zone and a L2=L3+V L point for the L2L3V phase zone. This corresponds to the phase diagram for ABVB + pentane mixture at T=190 °C (Figure 4-9 a).
- T1<T<T2 (Figure 4-10 c), the phase diagram is similar to Figure 4-10b but the L1V region no longer starts from the pure component A since it is supercritical. This corresponds to the phase diagram for ABVB + pentane mixture at T=200 °C (Figure 4-9 b).
- T2<T<T3 (Figure 4-10 d), L1V disappears. The L1L2V zone shrinks to the right hand side and there is a L1=V+L2 K point for the L1L2V zone. Naturally the L1=L2 critical point becomes a L2=V critical point. This corresponds to the phase diagram for ABVB + pentane mixture at T=210 °C (Figure 4-9 c).

- T3<T<T4 (Figure 4-10 e), the L1L2V phase behavior disappears and no K point exists. The L2=V critical point moves to the right hand side (closer to the L2L3V region). This correspond to the phase diagram for ABVB + pentane mixture at T=220 ~240 °C (Figure 4-9 d & e).
- T4<T<T5 (Figure 4-10 f), the L2=V critical point moves into the L2L3 phase region and becomes a L2=V+L3 K point. The L2L3 phase zone split into L3V and L2L3 phase zones. This corresponds to the phase diagram for ABVB + pentane mixture at T> 250 °C (Figure 4-9 f~h).

As temperature increases further, the L2=V+L3 K point may move to the right hand side (Figure 4-10 f). This explains at T=250 °C, as pressure increases, the L2L3V becomes L3V for the 40 wt% ABVB + pentane mixture but L2L3 for the 50 wt% ABVB + pentane mixture; at T > 320 °C, as pressure increases, the L2L3V becomes L2L3 for both mixtures.

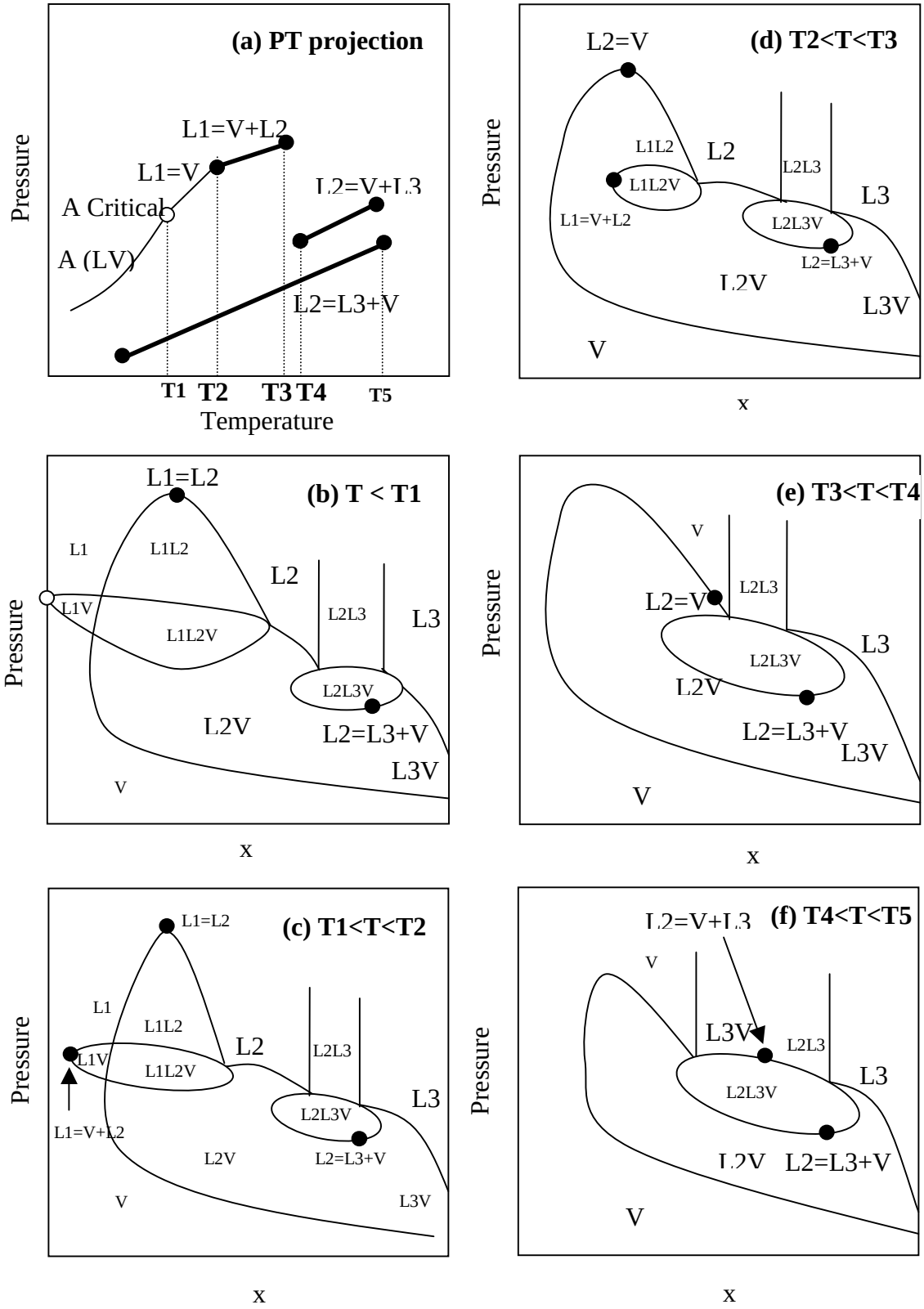

Figure 4-10 Evolution of phase behavior for ABVB + pentane mixtures

4.1.9 Phase behavior type transition with composition and temperature

For ABVB + pentane mixtures, complicated phase transitions with composition and temperature were observed. Figure 4-11 presents an example of phase transitions with composition at 160 °C:

L1V (100% pentane) → "S"L1L2V → L2L3V→ "S"L3V

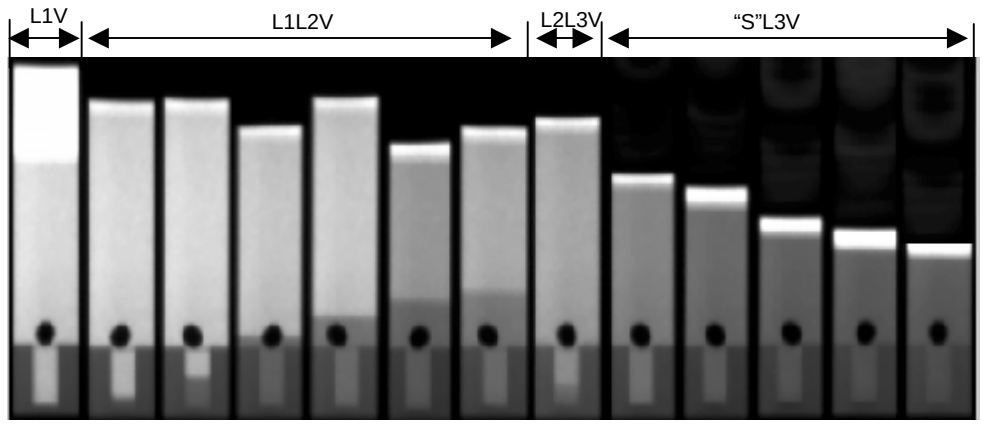

Wt%	0	5	10	20	30	40	45	50	60	70	80	90	100
T (°C)	160.16	159.79	160.16	160.13	160.35	160.31	160.10	160.01	159.71	159.90	160.6	160.04	160.23
P (bar)	18.7	18.7	18.8	18.6	18.6	18.4	18.5	16.8	15.9	14.3	10.0	4.02	0.19

Figure 4-11 Phase behavior transitions of pentane + ABVB mixtures with composition

Considering L2 and L3 were likely a mixture of solids and liquid, these transitions were intriguing and elusive but could still be explained based on the experimental results of Wiehe's (1992) that either better solvents or higher temperatures cause asphaltene aggregates to dissociate to small "monomers". In better solutions or at higher temperatures large asphaltene aggregates broke into small aggregates or monomers, which have stronger interaction with solvents and thus changed the type of phase behavior. For pentane + 5~ 45 wt% ABVB mixtures at T <210 °C, pentane is the dominant component and asphaltenes are large aggregates, so conventional L1L2V phase

behavior of heavy solute + light gas mixtures was observed. As the weight percent of ABVB increases to 50 wt%, the concentration of asphaltenes and maltenes increases proportionally. Since maltenes are good solvent for asphaltenes, a higher content of maltenes means a better solution for asphaltenes. Thus large asphaltene aggregate broke into smaller aggregates, which in turn have stronger interaction with solvent media, and finally induced the L1L2V→L2L3V phase behavior transitions. As the weight percent of ABVB increased further to 60~90 wt%, the solution became even more friendly to asphaltenes. Most of aphaltenes remained in solution except that only a small amount of inorganic solids precipitated, along with other adsorbed asphaltenic materials, from solution due to its high density (L2L3V→"S"L3V). Similarly the 40~45 wt% ABVB + pentane mixture exhibited L1L2V phase behavior at low temperatures but L2L3V phase behavior at high temperatures. Large asphaltene aggregates at low temperatures broke up into smaller "monomers" at high temperatures, and thus induced the L1L2V→L2L3V phase behavior transitions. ABVB itself was a stable solution and only L3V phase behavior was observed.

4.1.10 Characteristics of phase behavior for pentane + ABVB mixtures

As depicted in the phase diagrams in Figure 4-8, the ABVB + pentane demonstrated very complicated phase behaviors, including both expected and unexpected. The key characteristics are discussed below.

A. L1L2V phase behavior region

The L1L2V phase behaviors were observed in the following conditions:

- Composition: 5~45 wt % ABVB;

- Temperature: 20 ~ 220 °C;
- Pressure: a narrow range around the vapor pressure curve of pure pentane.

The L1L2V phase region was expected. In pentane + 5 ~ 45 wt % ABVB mixtures, pentane is the dominant component and the mixtures are expected to demonstrate phase behavior similar to heavy solids + light gas in supercritical extraction process, in which the mixtures are highly asymmetric and demonstrate type III, IV or V phase behavior. For pentane + 5 ~ 45 wt % ABVB mixtures, the L1L2V phase behaviors started from the room temperature and ended at K points, the temperatures (200~215 °C) of which are slightly higher than the critical temperature of pure pentane (196 °C). This is the characteristic of type III phase behavior.

B. L2L3V phase behavior

The L2L3V phase behaviors were observed under the following conditions:

- T>230 °C for 40 wt % ABVB+ pentane mixture;
- T>250 °C for 45 wt % ABVB+ pentane mixture;
- All temperatures for 50 wt % ABVB + pentane mixture;
- Pressure ranges varied with composition and temperature.

The L2L3V phase region was unexpected at the outset. Please note that "L2L3V" was used to denote the new three-phase behavior here to differentiate it from the three-phase behavior (L1L2V) at low temperatures. L3 was a new and denser liquid phase separated from the bulk liquid phase L2, which obviously was the same L2 phase at low temperatures (see X-ray images in Figure 4-1e~f). At higher temperatures both L2V→L2L3V→L2L3 and L2V→L2L3V→L3V phase transition with pressure were observed. This suggests a second set of K point at high temperatures. The pressure range

of the L2L3V region sometimes was very narrow and ideal for industrial application, which is discussed in the next Chapter.

C. Solids deposition

The solids deposition was observed under the following conditions:

Table 4-2 Conditions for solids depositions

wt% ABVB	60	70	80	90	100
T (°C)	20~120	20~340	20~340	160~340	Not observed

The deposition was labeled as “S” and treated as “solids” because it has only a tiny amount but with a high apparent density $\rho > 1.2$ g/ml (Figure 4-12), which is larger than the density of asphaltenes and other organic materials.

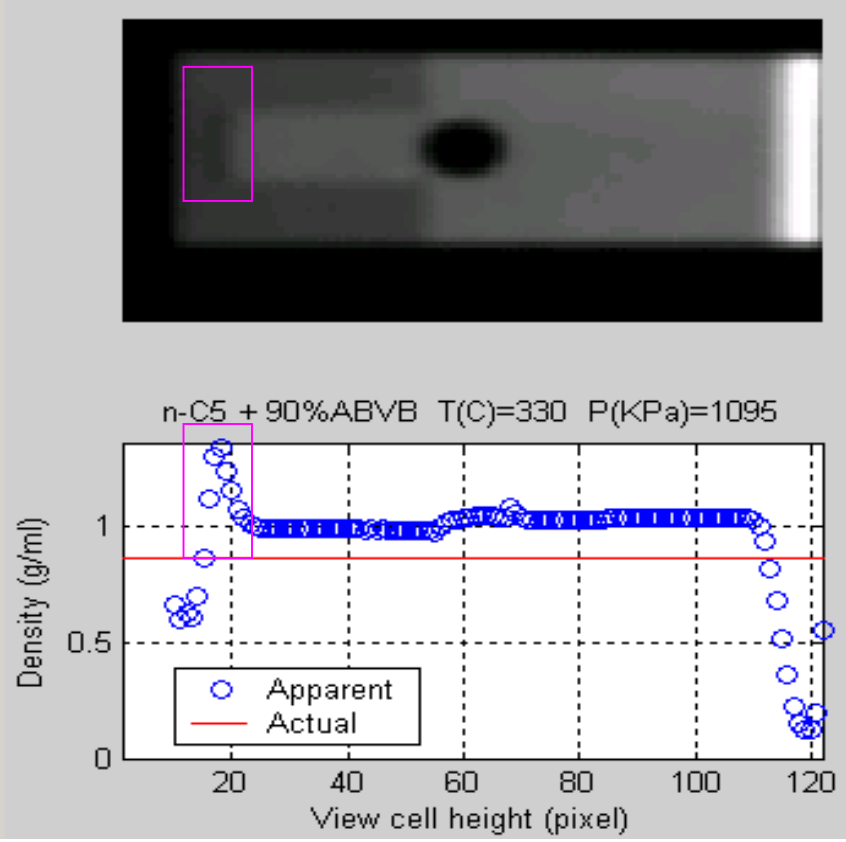

Figure 4-12 an example of “solids” deposition

The solids deposition was suspected to be a mixture of inorganic solids and some highly asphaltenic materials adsorbed on the surface of these solids because:

1. According to SARA analysis in this study (Table 5-1), ABVB contains 32 wt% pentane asphaltenes, which contains 5.2 wt% bitumen-associated solids (Kotlyar et al., 1999). So there is about 1.7 wt% Bitumen-associated Solids in ABVB, which is consistent with the tiny amount of deposition observed.
2. Sample analysis in this study found that the deposited phase contains high concentration of inorganic fine solids (Table 5-1).

D. The state of the precipitated phase in L1L2V and L2L3V phase regions

As reviewed in section 2.3.2, the state of the precipitated asphaltenic materials (solids or a liquid) is stilled unresolved. In this study, the precipitated asphaltenic materials are treated as a mixture of solids and liquid at low temperatures because:

1. Asphaltenes are dark or brown solid powders at room temperature. ABVB sample is also “a solid chunk” at room temperature. Microscopy diagrams of pentane asphaltenes and ABVB samples at room temperature are shown in Figure 4-13. Besides, the SLLV Q point temperature for anthracene + pentane mixture is 173 °C and asphaltenes are bigger than anthracene, so the melting point of asphaltenes in pentane should be higher than 173 °C.Obviously at least part of asphaltenes and ABVB are solids at room temperature.
2. Complementary phase transition study of ABVB, asphaltenes, asphaltenes-free oil using calorimetry in this research group (Elham Mahmoodaghdam, 2002) detected asphaltenes phase transitions around 0 °C and 100~200 °C. At least parts of asphaltenes or ABVB are liquid.

3. Sample analysis (Section 5.2) in this study also showed that some solvent molecules (pentane or light oil in ABVB) are trapped in the precipitated phase.
4. SAXS by R. Tanaka et al., 2002 shows that large asphaltene aggregates broke up around 190 ~240 °C. Before being broken up, these large asphaltene aggregates are likely solids.
5. The stirrer was unable to rotate at low temperatures and suggested that the asphaltenic phase is very viscous and probably in semi-solid at low temperatures (section 5.3).
6. The amount of the precipitated phase (L2 in Figure 4-1) increased with temperature from 110~210 °C.The melting of semi-solid asphaltenic material is likely responsible for this phenomenon. The interactions between pentane molecules and large solid asphaltene aggregates are much weaker than those between pentane molecules and small liquid asphaltene “monomers”. At low temperatures, large asphaltene aggregates are solids, and the amount of the precipitated phase remained the same because of weak interaction. As temperature was increased, large asphaltene aggregates broke into small “monomers” and mixed with solvent molecules. The stronger interaction of asphaltene monomers and solvent molecules lead to increasing amount of L2.

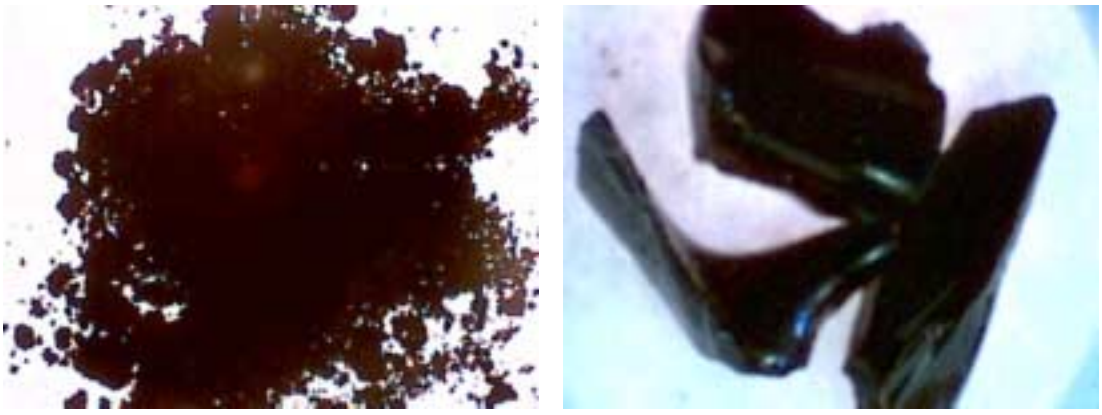

a. “solid” pentane asphaltenes (x10) b. “solid” ABVB (x10)

Figure 4-13. Photomicrographs of pentane asphaltenes and ABVB samples at T=20 °C.

Considering interference of asphaltene solidification, the L1L2V phase behavior for pentane + 5 ~45 wt % ABVB mixtures below 210 °C is virtually “S”L1L2V, which resembled but was more complicated than a type III binary system with solid interference. Naturally one may ask at what temperature asphaltene solidification interferes with the L1L2V phase, i.e., where is the Q (SLLV) point? This question is still unresolved here since asphaltenes are a mixture containing numerous components the melting temperatures of which are expected to span a wide range of temperatures. so both types of solid interference in Figure 2-6 were likely. There is a Q point line instead of a single Q point for a binary mixture.

4.2 Phase behavior of dodecane + ABVB + hydrogen mixtures

Hydrogenation is a technology used in many oil upgrading processes, particularly in those heavy oil upgrading processes. The impact of multiphase behavior on chemical reactions and the impact of hydrogen on multiphase behavior in these processes are of great theoretical and practical significance. Therefore the phase behavior for the 24.6 wt % ABVB + 73.8 wt% dodecane + 1.6 wt % H2 was set as one of the starting point of this research. But it was abandoned because hydrogen addition is not a promising option in industrial application based on its impact on the phase behavior of 25 wt % ABVB + 75 wt % dodecane. ABVB + pentane mixtures are a much better choice since they are mixtures in Residuum Oil Supercritical Extraction (ROSE) processes, which are of great industrial significance but suffer low selectivity problems due to insufficient understanding of phase behavior of pentane + heavy oil mixtures. The phase behavior of dodecane + ABVB + hydrogen mixtures was not the focus of this study, but it is briefly discussed in this section.

4.2.1 Phase behavior of 25 wt % ABVB + 75 wt % dodecane mixture

The phase behavior for the 25 wt% ABVB + 75 wt% dodecane mixture was a bridge to connect the work finished by Abedi (1998) and Dukhedin Lalla (1996) and the work covered in this study. It is a key experiment to identify the impact of hydrogen addition on the phase behavior of ABVB + alkanes and the best operating conditions for selective removal of fine inorganic solids, heavy metals and sulfur from heavy oils. The X-ray images for 25 wt % ABVB + 75 wt % dodecane mixture are shown in Figure 4 -

14. The mixture exhibited L1V phase behavior at T < 240 °C but L1L2V at T ≥240 °C (Figure 4-15). The LLV/LV boundary is sketched tentatively. An example of X-ray image (T=280 °C) was also shown on the left side of Figure 4-15. The amount of L2 was only ~1 ml and apparent densities of L1 and L2 were 1.15 g/ml and 0.67 g/ml, respectively.

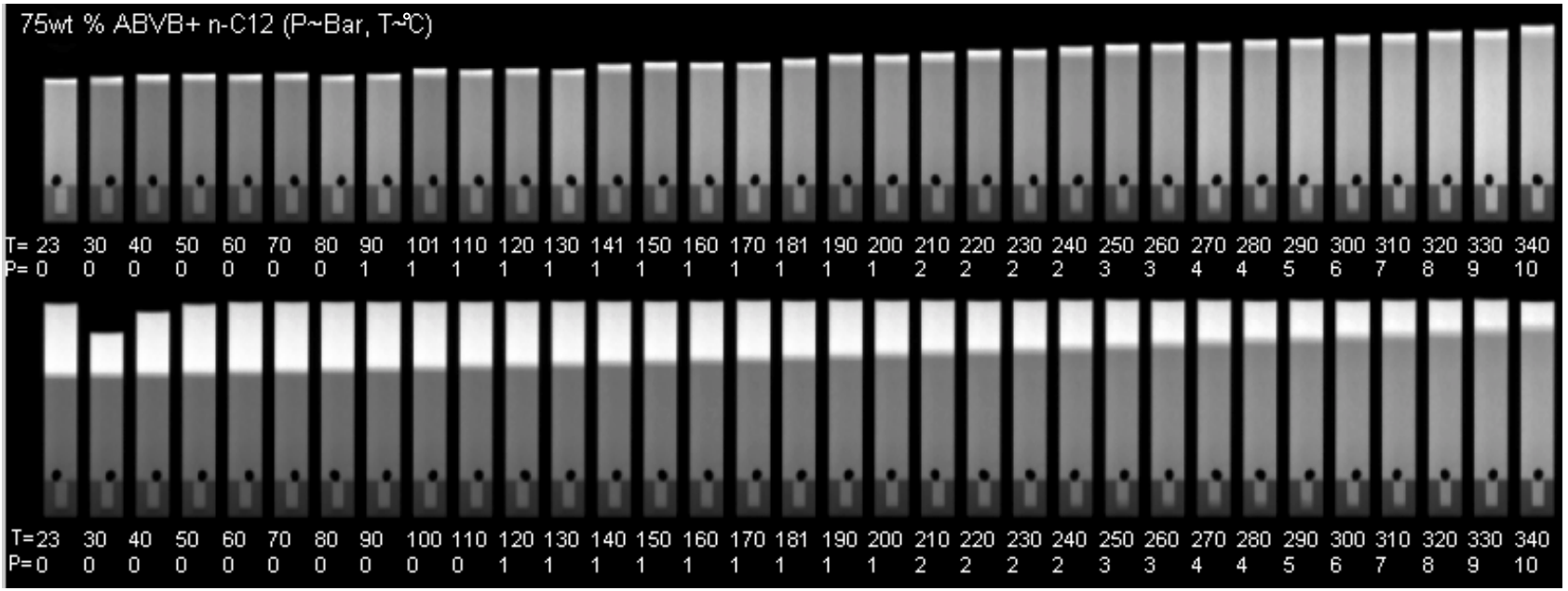

Figure 4-14 X-rays images of 25 wt % ABVB + 75 wt % dodecane mixture

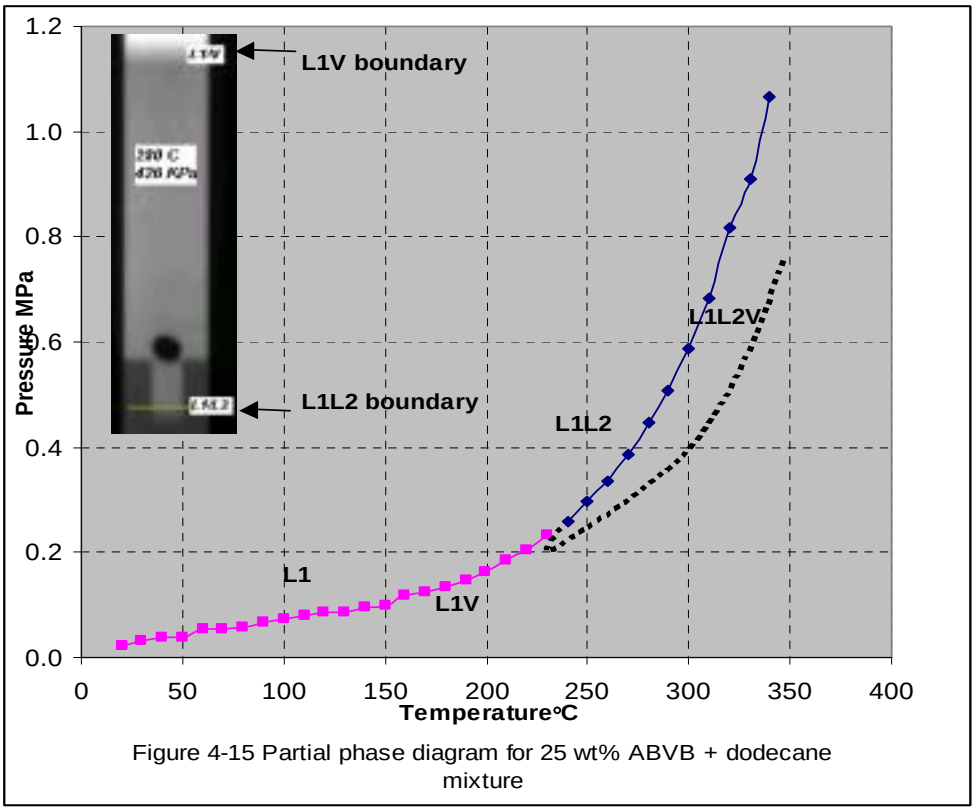

Figure 4-15 Partial phase diagram for 25 wt% ABVB + dodecane mixture

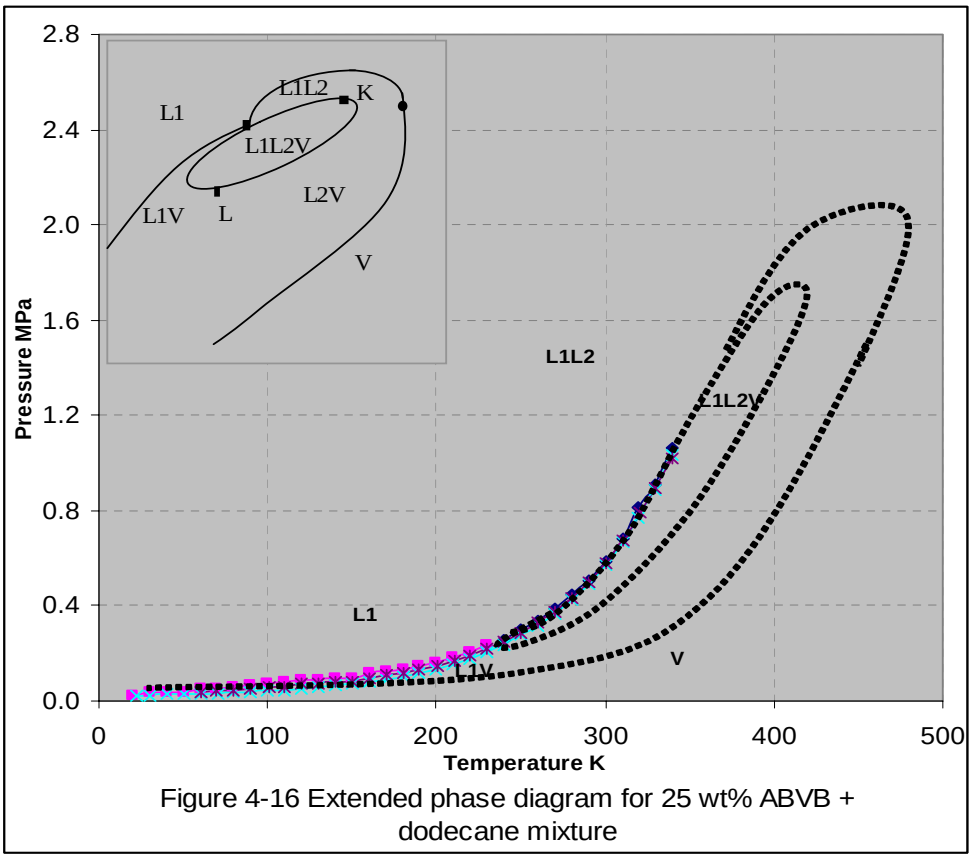

Figure 4-16 Extended phase diagram for 25 wt% ABVB + dodecane mixture

4.2.2 Possible type of phase behavior for ABVB + dodecane mixtures

The 25 wt% ABVB + 75 wt% dodecane mixture was found to be miscible below 240 °C and immiscible above 240 °C.Therefore a possible type of phase behavior for this mixture is type IV, V or VI. Type VI is unlikely since type VI phase behaviors have thus far been discovered only in aqueous mixtures. Type V has a much higher possibility than type IV since the maximum experimental temperature (340 °C) is close to the critical temperature of dodecane (385 °C) and only one LLV region was encountered in experiments (20 °C ~ 340 °C). Abedi (1998) interpreted the phase behavior of 24.6 wt% ABVB + 73.8 wt% dodecane + 1.6 wt% H2 mixture as that of type V binary + an immiscible third component – top-left insert in Figure 4-16. Considering ABVB is a heavy oil sample which contains numerous components, 25 wt% ABVB + 75 wt% dodecane mixture should exhibit the same type of phase behavior as that of 24.6 wt% ABVB + 73.8 wt% dodecane + 1.6 wt% H2 mixture but at lower pressures. The dashed lines in Figure 4-16 denoted tentatively the relevant phase boundaries.

4.2.3 Effects of hydrogen addition on the LLV phase behavior of ABVB + dodecane (25 wt % : 75 wt %) mixture

To facilitate comparison, the LLV phase behavior of ABVB + dodecane (25 wt% : 75 wt %) mixture and the LLV phase behavior of ABVB + dodecane (25 wt% : 75 wt %) + 1.6 wt% H_2 mixture are shown in Figure 4-17. The figure clearly indicated that the addition of hydrogen shifted the L1L2V region vertically to high pressures and expanded its temperature range and pressure range. Since hydrogen is the lightest component and immiscible with both dodecane and ABVB, the shift and expansion to high pressures and low temperatures were expected (Figure 2-8). Dan Minicucci (MASc Thesis, 2001)

showed similar results for anthracene + n-alkane mixtures. This result led us to abandon hydrogen addition, as it does not contribute materially to selective separation of heavy metals etc. from heavy feedstocks. Hydrogen addition is also of low industrial interest because of high pressure required effecting the LLV phase split and of extra hydrogen consumption.

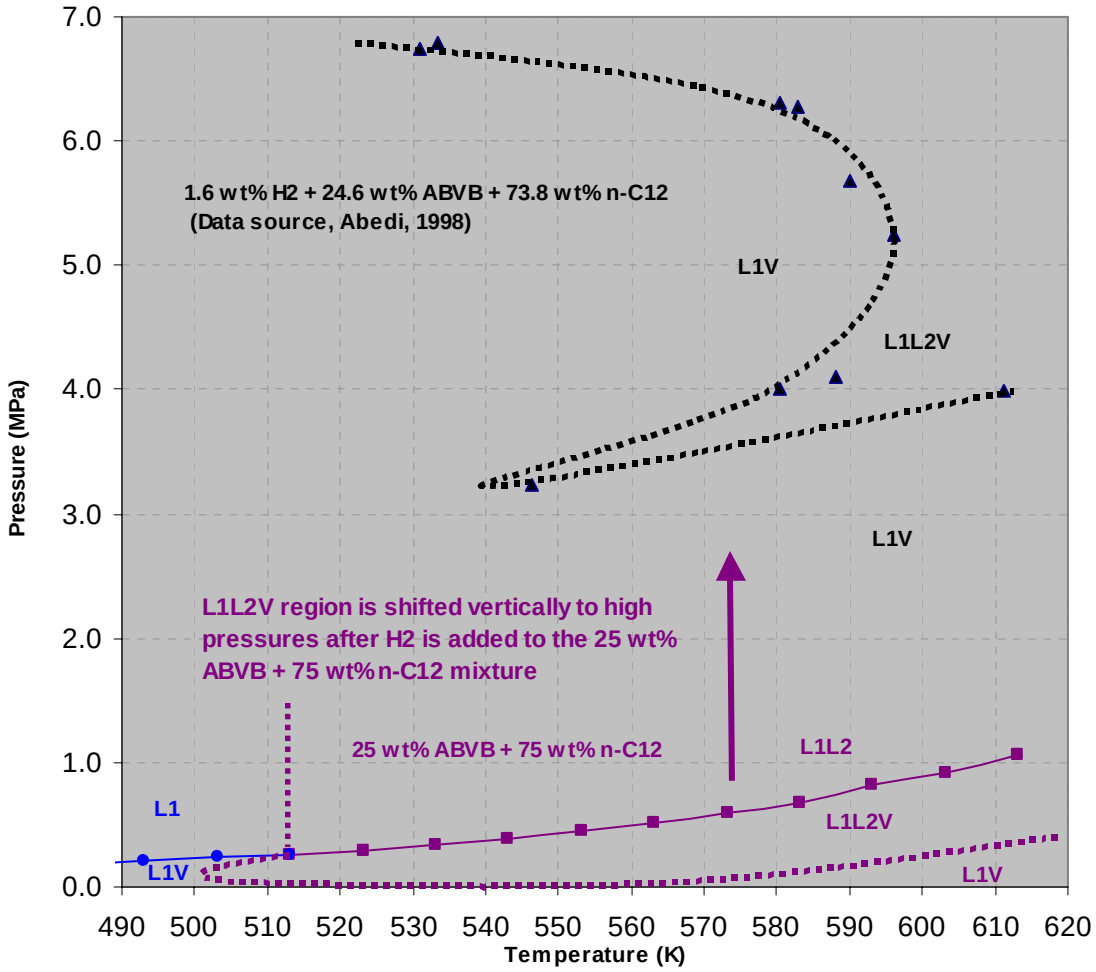

Figure 4-17 Impact of H2 on the LLV phase behavior of ABV 25 wt. % + dodecane75 wt.% mixture

4.3 The Impact of Alkane Size on the Phase Behavior type of ABVB + Alkanes Mixtures

The ABVB + alkanes mixtures exhibited very complicated phase behavior, such as L1L2V, L2L3V and "S"L3V for pentane + ABVB mixtures. Clearly from a phase behavior perspective, the mixtures cannot be simplified as a binary system. However when light alkane is the dominant component, ABVB + alkane mixtures demonstrated phase behaviors which similar to but more complicated than those exhibited by asymmetric binary systems (type III, IV and V). The ABVB + alkane mixtures exhibited different types of phase behavior depending on the size of alkanes and were summarized in table 4-3.

Table 4-3. The impact of alkane size on the type of phase behavior exhibited by ABVB + alkane mixtures

Mixture	Type of phase behavior exhibited
Pentane + ABVB	III
Heptane + ABVB	III
Dodecane + ABVB	V
ABVB itself	I (miscible in experimental range)

The above impact of alkane size linked well with the simulation work of anthracene + alkanes (Minicucci et al., 2001) as shown in Figure 4-18. As the size of alkane increases, the anthracene + alkane mixtures experienced type III→ type IV→ type V → type I phase behavior transition. Also, solidification of anthracene converts what would otherwise be type IV phase behavior to type V and suppresses type II phase behavior

entirely. As the alkane size increases, the ABVB + alkane mixtures demonstrated the exactly the same sequence of phase transitions. The consistency of phase behavior transitions between these two types of mixtures is very interesting but not surprising. Anthrancene is a widely used model component for asphaltenes due to their similar structure. However for ABVB + alkanes mixtures, both solute (asphaltenes) and solvent (alkanes + maltenes in ABVB) themselves are mixtures, which means ABVB + alkane mixtures may exhibit even more complicated phase behavior type transitions.

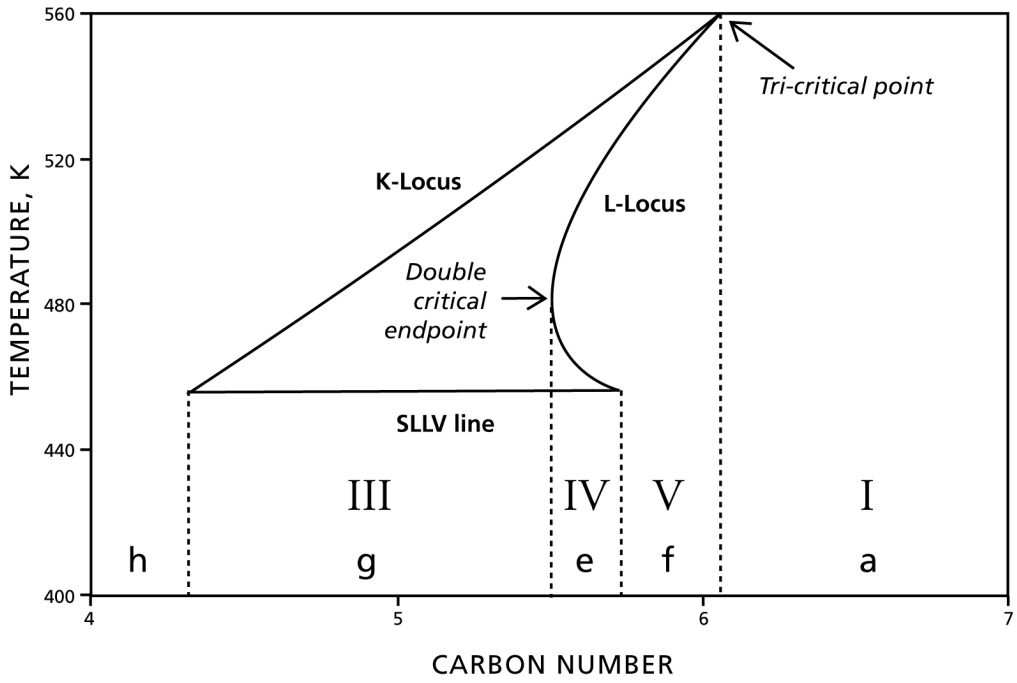

Figure 4-18: Phase behavior type transitions for anthrancene + alkane mixtures

4.4 Reversibility of observed multiphase behavior

As reviewed in Chapter 2, the reversibility of asphaltene precipitation is still hotly debated. This study focuses on the multiphase behavior of asphaltene containing oil mixtures instead of the precipitation of "pure" asphaltenes. Are the multiphase behaviors of asphaltene containing oil mixtures observed reversible? To answer this question, the experiment for 25 wt% ABVB + heptane mixture was repeated and the repeat experiment (Trial 2) was conducted ~80 days later after the completion of the first experiment (Trial 1). Representative images from these two trials are shown in Figure 4-19 and Table 4-4. Differences between corresponding images from these two trials are too small to be detected by naked eyes. Table 4-4 indicates that at the same temperature and pressure condition, the differences in phase volumes and densities between the two trials, obtained by calibration, are less than 0.78 ml and 0.01 g/ml, respectively, i.e., they are within experimental errors. Therefore the results from two separate trials are repeatable.

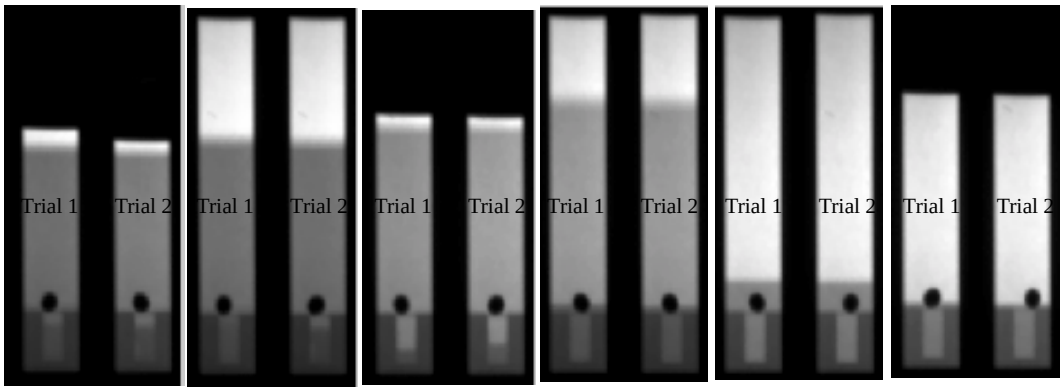

Figure 4-19. Repeatability of multiphase behavior in two separate trials for 25 wt% ABVB + heptane mixture

Table 4-4 Repeatability of multiphase behavior for 25 wt% ABVB in heptane

Repeated Points		T (°C)	P (Bar)	Vapor (V)		Light Liquid (L1)		Dense Liquid (L2)	
				Volume (ml)	Density (g/ml)	Volume (ml)	Density (g/ml)	Volume (ml)	Density (g/ml)
No. 1	Trial 1	21.05	0.16	45.95	Too low to be accurately measured using this method.	93.41	0.79	3.72	1.08
	Trial 2	20.46	0.19	43.90		92.63	0.78	3.72	1.09
No.2	Trial 1	69.86	0.58	80.43		97.85	0.73	3.97	1.04
	Trial 2	70.33	0.61	80.43		98.53	0.73	3.72	1.05
No. 3	Trial 1	150.26	3.61	38.75		109.46	0.70	1.73	1.02
	Trial 2	150.39	3.75	38.17		108.68	0.69	2.23	1.02
No. 4	Trial 1	250.41	20.3	57.83		116.60	0.52	8.33	0.96
	Trial 2	250.17	20.0	58.78		117.38	0.53	6.77	0.96
No. 5	Trial 1	340.12	61.0	159.50	0.32	Heptane Supercritical		22.27	0.82
	Trial 2	339.70	59.9	159.66	0.32			23.05	0.80
No. 6	Trial 1	340.33	91.2	147.29	0.47			6.65	0.94
	Trial 2	340.13	91.4	147.00	0.46			5.99	0.94

The L2V→V phase boundary conditions determined from these two separate trials are also within experimental errors, as shown in Figure 4-20 for 25 wt % ABVB + heptane mixture at 310°C (not displayed in table 4-4). The L2V→V phase transition pressures obtained from the two trials are roughly the same, ~11 MPa. The repeatability of experiments suggests that the bulk phase behaviors of asphaltene containing oil mixtures observed in this study are reversible from a thermodynamics point of view, if the mixture is given enough time to attain equilibria. The above result also suggests that the mixture of 25 wt% ABVB + heptane is quite stable — at least under the ambient conditions (no detectable changes over ~80 days).

The phase behavior experiments for a mixture at the same temperature in pressurization and de-pressurization procedures are also within experimental errors. An

example is given in Appendix III. The result suggests that the multiphase behaviors observed are reversible with respect to pressure.

The author is aware of the debate over the reversibility of multiphase behavior in industrial processes. The debate often convolutes with the process kinetics, i.e., how long a phase transition takes to reverse. Typically in this research, the mixture was well mixed and then left undisturbed for about 10~15 minutes to attain equilibrium. Section 5.3.1 briefly discusses the separation kinetics, which is not a focus in this study.

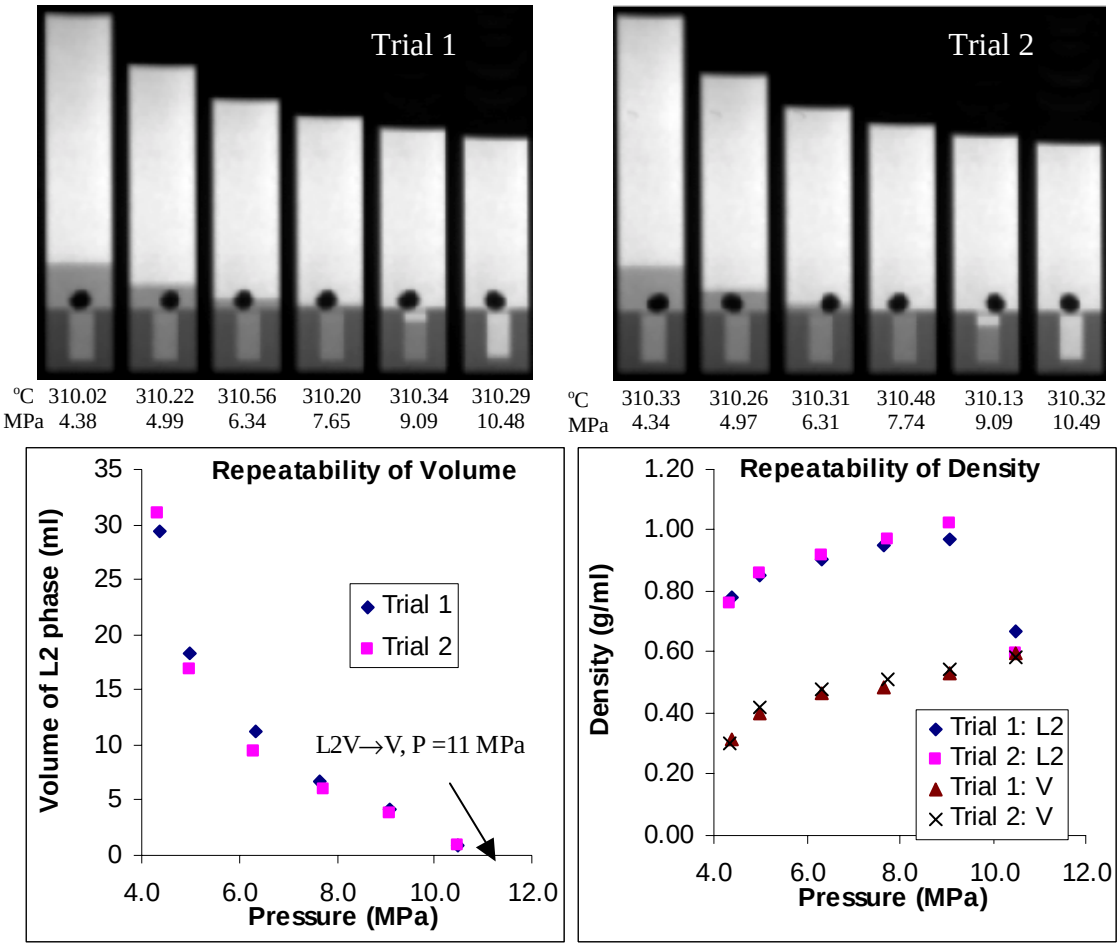

Figure 4-20. Example of repeatability in determining L2V→V phase boundary

4.5 Summary

Phase behavior results of ABVB + alkane mixtures were described in detail in this chapter. Key findings and their implications for the development of selective separation processes were noted. These mixtures demonstrated very complicated phase behaviors including both expected (L1L2V) and unexpected (L2L3V) phase behavior. Asphaltene solidification happened at low temperatures. The observed bulk phase behaviors were reversible. Methods used to detect K points and phase transition boundaries were discussed. Preliminary PT at constant x phase diagrams and Px at constant T phase diagrams were presented. The evolution of phase behavior of ABVB + pentane mixtures was tentatively illustrated. As the alkane size increases, the ABVB + alkane mixtures experienced type III→ type IV→ type V → type I phase behavior transitions. The addition of hydrogen shifted the multiphase region vertically to high pressures and expanded its temperature range and pressure range. Hydrogen addition is not a promising option for developing selective separation processes.

For ABVB + pentane mixtures, both L1L2V and L2L3V could be exploited for ABVB extraction, but which is better? The L1L2V (5~45 wt% ABVB at T<230 °C) region has been exploited as the operating region for ROSE like processes. The L2L3V (40~50 wt % ABVB at T > 230 °C) phase region seems more promising because the amount of precipitated (rejected) phase varies dramatically over a very narrow range of pressure, suggesting high selectivity and easy operation. However this only provides a gross indication of selective separation, and more important information such as partition of the problematic constituents, such as inorganic fine solids, heavy metals and sulfur, among the precipitated phase and the bulk phase is unknown. These topics, along with other topics that have impact on phase separation, such as settling time, viscosity and solids re-dispersion, are the topics of the next Chapter.

Chapter 5 Selective Removal of Inorganic Fine Solids, Heavy Metals and Sulfur from Heavy Oils/Bitumen

This Chapter assesses the potential for developing selective separation schemes for bitumen/heavy oil based on LLV and SLLV phase behaviour arising in the phase diagrams of bitumen/heavy oil + alkane mixtures. Section 5.1 first presents the experimental data for selective rejection of ABVB constituents, and then discusses how to improve the selectivity of current industrial processes (ROSE). Section 5.2 discusses the solid dispersion and apparent density. Section 5.3 discusses phase separation kinetics. Adherent nature and re-dispersion of precipitated phases are discussed in sections 5.4.

5.1 Selective Rejection of ABVB constituents

5.1.1 Fraction of ABVB rejected using pentane as solvent

During phase equilibrium experiments for the mixtures pentane + ABVB, the volumes and apparent densities of phases present were obtained. These data were combined to compute the mass of the reject phase (the L2 phase in the case of L1L2V and L2V phase behavior, the L3 phase in the case of L2L3V and L3V phase behavior, and the "S" phase in the case of "S"L3V phase behavior). To facilitate the following discussion, a new concept "reject ratio" is introduced as follows:

$$\text{reject ratio} = \frac{\text{The mass of the reject phase}}{\text{The mass of ABVB in the mixture}}$$

Normally reject ratio is less than 1.0 since part of oils in ABVB partitioned to the light phase/phases. A reject ratio larger than 1.0 means part of solvent is rejected along

with the ABVB constituents. The pentane reject ratios of ABVB are shown in Figure 5-1a ~ h.

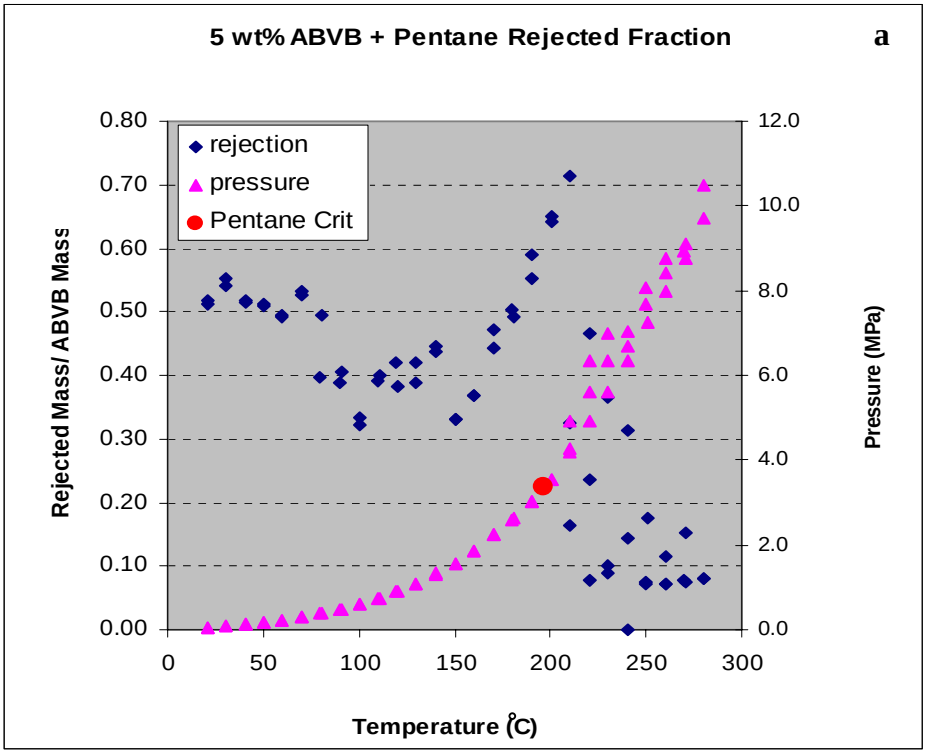

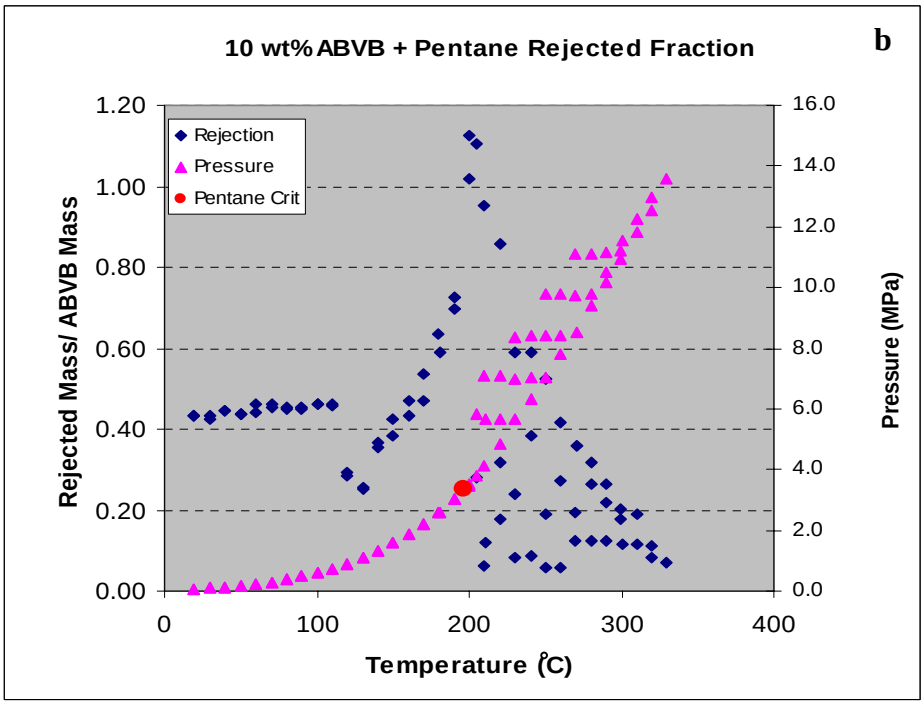

Figure 5-1. Pentane reject ratio of ABVB as a separation indicator (continued)

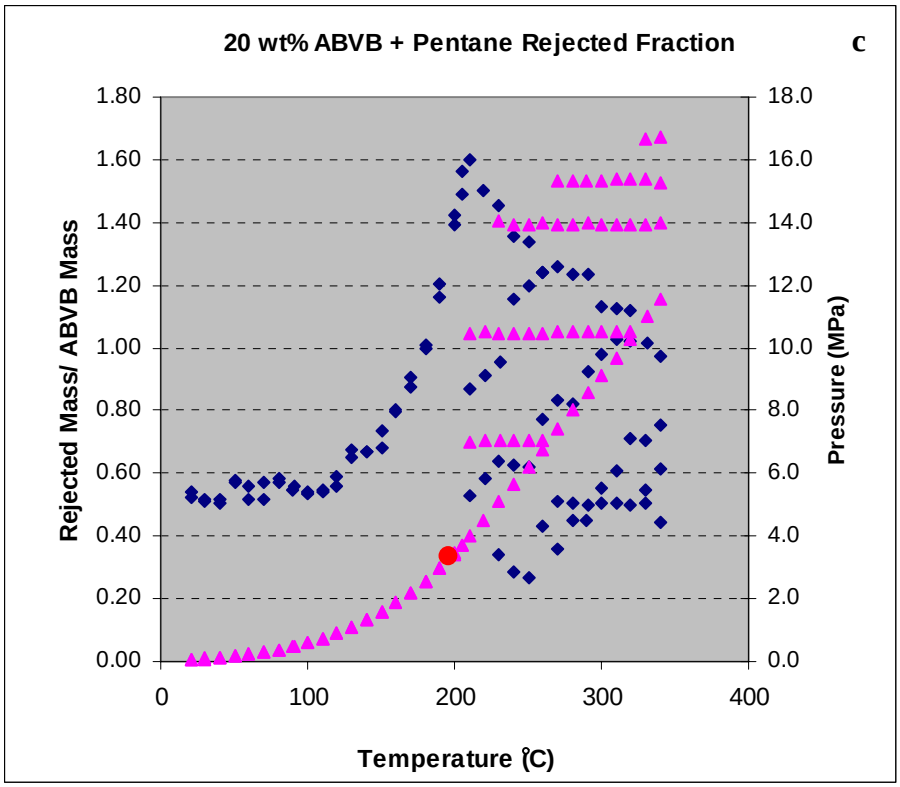

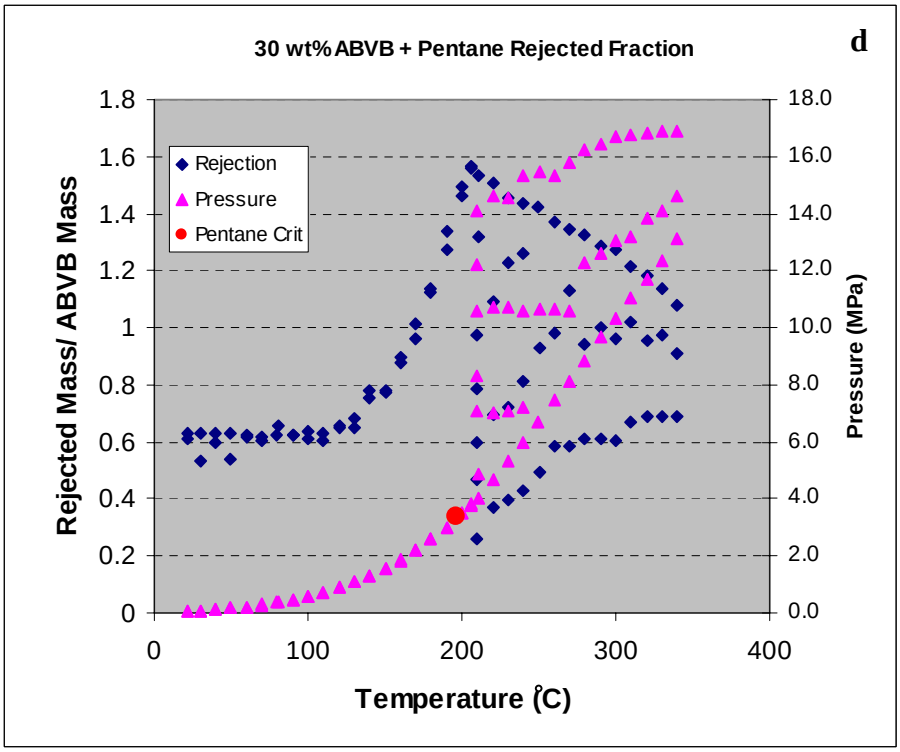

Figure 5-1. Pentane reject ratio of ABVB as a separation indicator (continued)

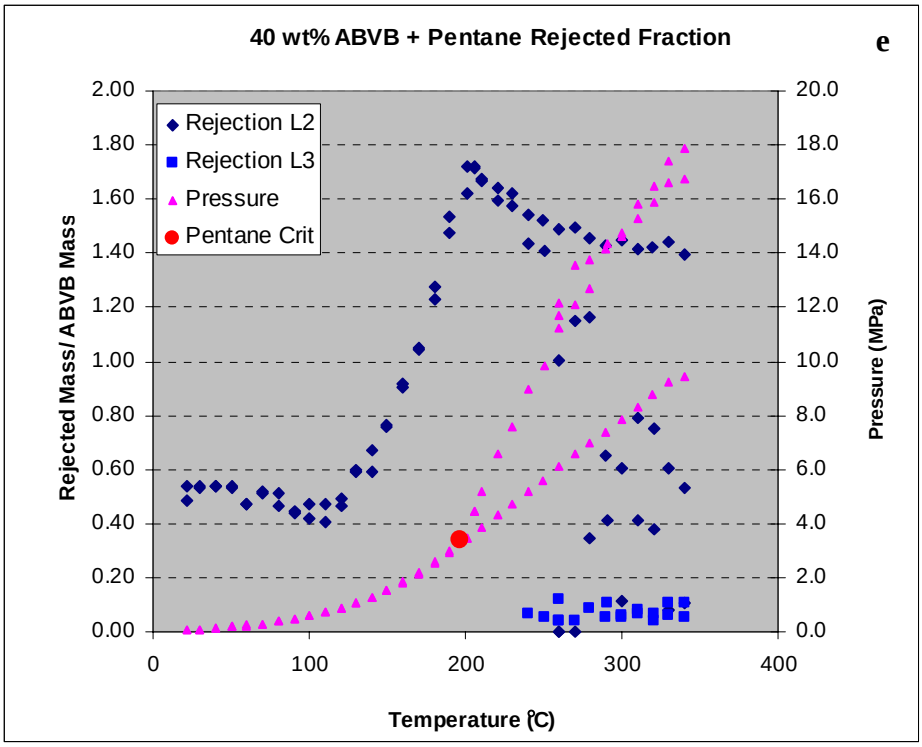

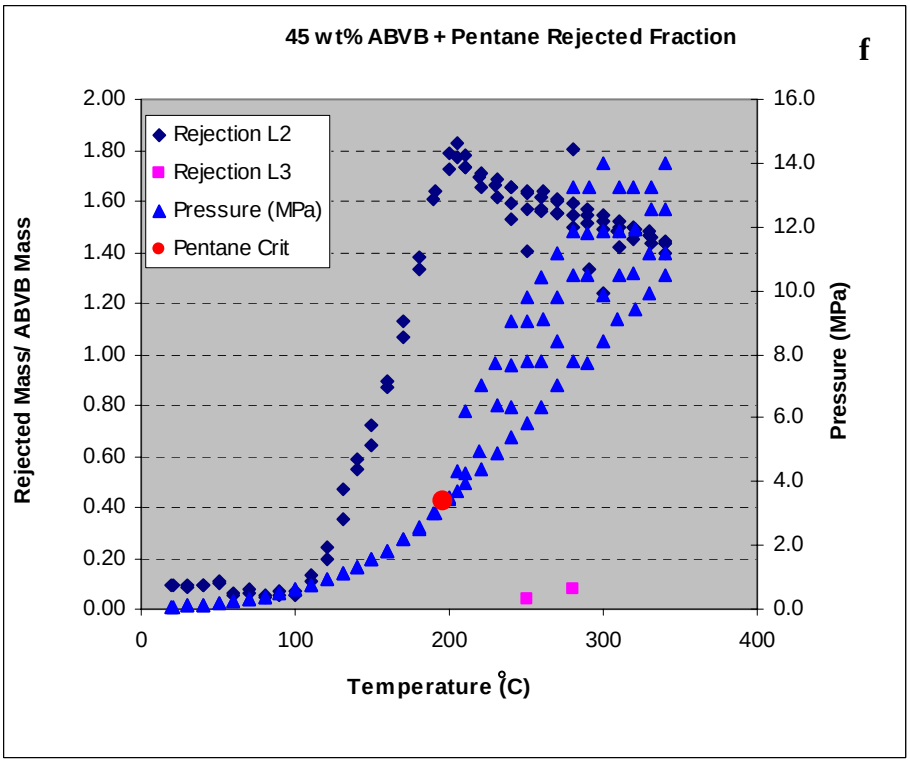

Figure 5-1. Pentane reject ratio of ABVB as a separation indicator (continued)

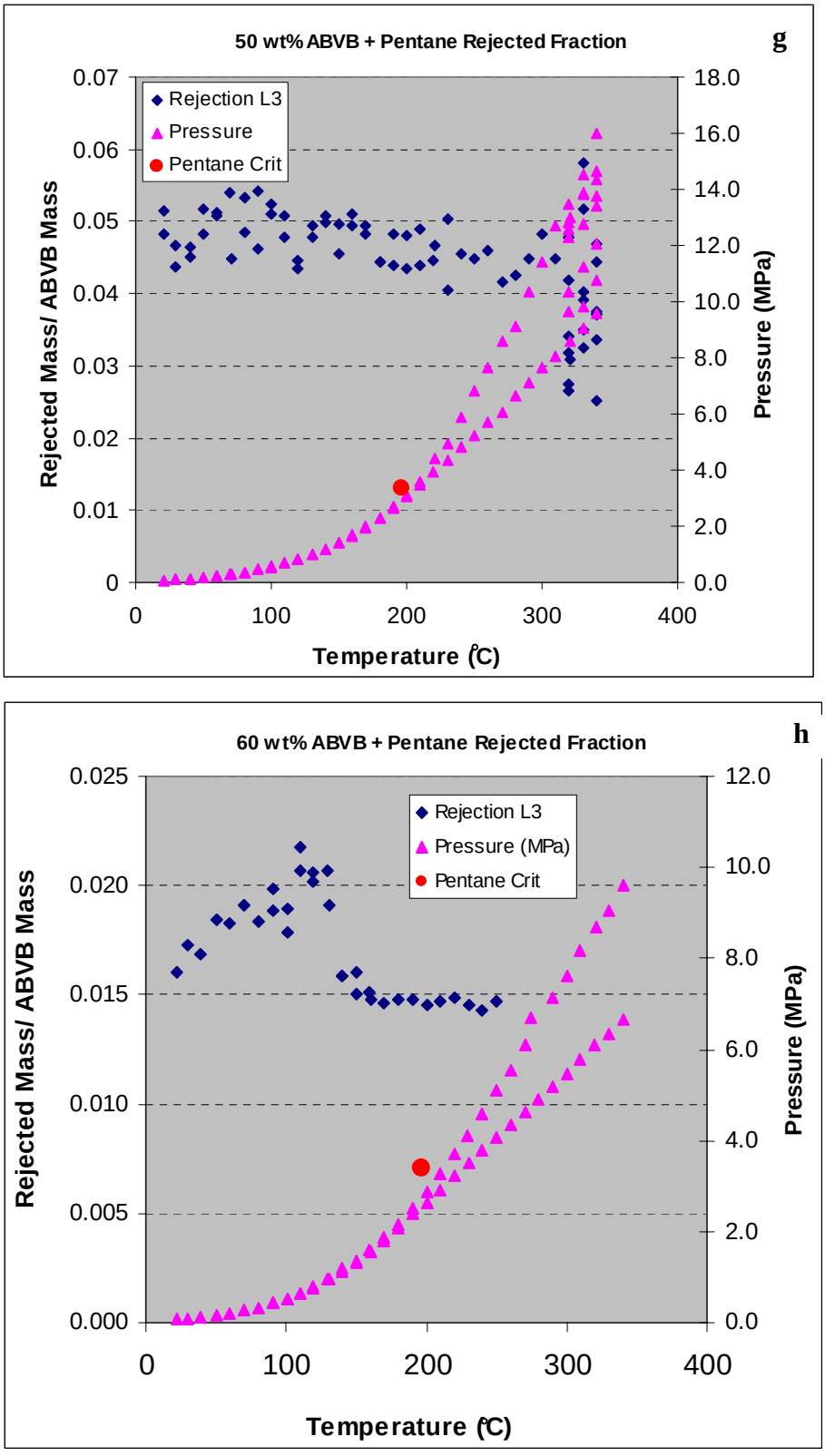

Figure 5-1. Pentane reject ratio of ABVB as a separation indicator

The diagrams for the 70~90 wt % ABVB mixtures are not shown in Figure 5-1 since they basically show the same scenario as the 60 wt% ABVB + pentane mixture. By comparing reject ratios one obtains a clear indication of the partitioning of the constituents present in the ABVB.

1. For the pentane + 5~40 wt% ABVB mixtures, the reject ratios below 110 °C (L2 from L1L2V) fall in a range of 0.4~0.6. Between T = 110 ~210 °C, the reject ratios increase sharply and reach maxima (0.7 for 5 wt%, 1.1 for 10 wt%, and 1.6~1.8 for 20~40 wt%) around 200~210 °C. At T > 210 °C, the reject ratios (L2 from L2V) decrease depending on the mixture composition and operating pressure. Increasing pressure could also reduce the reject ratio.
2. For the pentane + 45 wt% ABVB mixture, the reject ratio below 110 °C (L2 from L1L2V) is ~ 0.1. At T > 110 °C, the reject ratio increases sharply and reaches a maximum (~1.8) around 200~210 °C. At T > 210 °C, the reject ratio (L2 from L2V) decreases but is still larger than 1.4; the reject ratio for L3 from L2L3V at high pressure is about 0.05.
3. For the pentane + 50 wt% ABVB mixture, the reject ratio (L3 from L2L3V or L3V) is ~0.05 and decreases gradually with temperature. At high temperatures, the reject ratio approximates zero as pressure increases.
4. For the pentane + 60 ~ 90 wt% ABVB mixtures (“S” from “S”L3V), the reject ratios are ~0.015. As discussed in chapter 4, “S” is a mixture of inorganic solids and the most asphaltenic materials adsorbed on the surface of these inorganic solids. Understandably, the mass of “S” remains more or less the same and so does the reject ratio.

In summary, the following phase zones are preferred if the low reject ratio is the only concern:

1. L3L2V, L3V;
2. “S”L3V;
3. L1L2V for 45 wt % ABVB + pentane mixture at T<100 °C;
4. L1L2V and L2V for the dilute ABVB (<10 wt%) + pentane mixtures at high temperatures (> 210 °C) and pressures (>5.0 MPa).

5.1.2 Rejection of ABVB constituents using pentane as solvent

The above section only discussed the rejection of all ABVB constituents as a phase, and the information about partition of each species between the reject phase and the bulk phase/phases is unknown. As discussed in Chapter 1 and Chapter 2, only the problematic species such as inorganic fine solids, heavy metals and sulfur should be selectively removed, so the partition of these problematic species is the key information for developing selective separation schemes. In this study, samples were extracted from phases extending unambiguously to the room temperature. The detailed analysis of these samples was performed by Core Labs and is summarized in Table 5-1 and Figure 5-2.

Table 5-1 Summary of sample analyses for reject phases

Samples	100%	50 wt% ABVB		40 wt% ABVB		30 wt% ABVB		20 wt% ABVB	
	ABVB	L3	L2	L2	L1	L2	L1	L2	L1
SARA Analysis	wt.%								
Saturates	6.80	4.80	9.42	2.09	7.62	1.69	9.90	1.58	9.84
Aromatics	41.99	28.90	43.11	19.18	51.16	18.97	60.35	14.74	57.39
Resins	19.04	11.84	19.75	7.32	18.75	7.97	24.28	5.37	27.61
Asphaltenes	32.18	54.47	27.72	71.41	22.48	71.37	5.47	78.31	5.16
Elemental Analysis	wt.%								
Carbon	81.66	80.31	83.01	78.11	83.29	81.15	83.20	80.95	83.08
Hydrogen	9.54	8.87	9.84	8.07	9.92	8.51	10.89	8.55	10.19
Nitrogen	0.65	0.91	0.68	0.99	0.69	1.06	0.55	1.03	0.60
Sulfur	6.87	4.68	5.87	6.60	5.31	6.95	5.29	7.41	5.19
	ppm								
Tin (Sn)	0.7	0.7	0.6	1	0.5	0.3	<0.1	0.8	0.2
Lead (Pb)	1	4	8	9	0.7	2	0.5	3	0.3
Copper (Cu)	1	17	0.2	7	0.3	8	0.1	9	0.2
Aluminum (Al)	734	2820	12	1608	11	1472	2	1528	1
Silicon (Si)	898	3489	26	2099	26	2037	28	2106	20
Iron (Fe)	322	1387	11	730	10	695	2	737	1
Chromium (Cr)	3	7	1	5	0.7	5	0.1	6	0.2
Silver (Ag)	<0.1	<0.1	<0.1	<0.1	<0.1	<0.1	<0.1	<0.1	<0.1
Zinc (Zn)	5	22	3	9	2	20	2	12	1
Magnesium (Mg)	44	157	2	99	0.4	90	0.4	94	<0.1
Nickel (Ni)	137	281	113	224	105	257	48	281	52
Barium (Ba)	4	15	4	11	<0.1	10	<0.1	7	<0.1
Sodium (Na)	48	167	4	118	5	97	4	100	4
Calcium (Ca)	65	264	16	143	8	125	5	142	4
Vanadium (V)	344	549	281	494	259	590	107	611	132
Phosphorus (P)	8	18	3	16	3	15	3	15	4
Molybdenum (Mo)	17	56	6	38	5	36	0.4	39	0.2
Boron (B)	3	8	0.9	5	<0.1	5	2	7	1
Maganese (Mn)	11	35	0.5	23	0.9	19	0.4	19	0.4
Titanium (Ti)	70	231	7	157	4	133	2	139	0.5

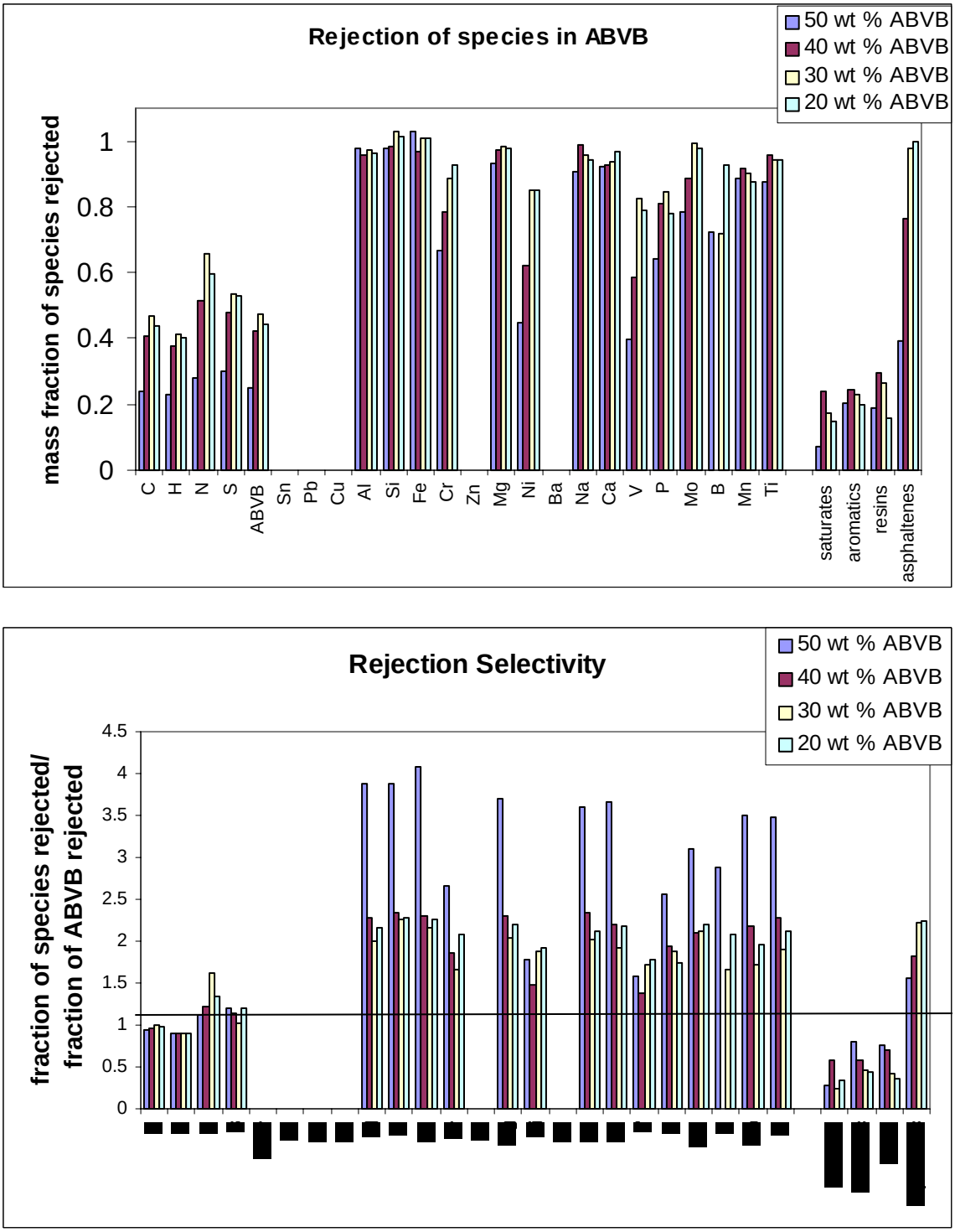

Figure 5-2. Rejection and rejection selectivity of species in ABVB

Table 5-1 and Figure 5-2 clearly indicate:

1. Metals present in mineral matters (aluminum, silicon, iron, calcium, titanium, sodium, magnesium, etc.) are readily and quantitatively separated from the bulk through the creation of a reject phase. For example, more than 95 wt% of the aluminum, silicon, and iron are rejected in all cases. This suggests that fine inorganic solids can be selectively rejected.
2. Heavy metals are not rejected as selectively as inorganic solids. Ni and V are particularly problematic. 80 + wt% rejection rates are only achieved if more than 40 % of the vacuum bottoms is rejected.
3. Nitrogen and sulfur rejection are even poorer than heavy metals. With 40 % of ABVB rejected, only 53% N and 44% S were removed.
4. SARA analysis indicated that the rejected phases still contained some saturates, aromatics and resins while the extracted phases also contained some asphaltenes. This suggests that:
    a. The popular assumption that precipitated phase only consisted of “pure” asphaltenes underestimates the impact of asphaltenes precipitation in industrial production, such as line plugging.
    b. Some valuable constituents are trapped in and precipitated along with asphaltenes. In some case, the reject ratio was larger than 1.0. This accounts for the high product loss in some ROSE processes.
    c. As dilution ratios increase, the asphaltene content in the light liquid phase decreases while content in the denser liquid phase increases. The

difference of SARA distribution between phases in equilibrium increases with the dilution ratio of the alkane.

d. The existence of all SARA pseudo-components in all dense phases suggested that all constituents in the mixtures interacted with each other and took part in the phase splitting. This is consistent with the notion that aromatics, resins and asphaltenes constituted a compositional continuum with respect to both molar mass and polarity.

e. This also explains why only limited success was achieved in developing models for predicting asphaltene precipitation. Up to now, most experimental and modeling research works focus on the asphaltenes precipitation (not including the co-precipitated materials such as resin, etc.) when diluted with light hydrocarbon solvents at ambient temperature and pressure. On the other hand, the scenarios in most of industrial processes are different, for example high temperature and pressure operating conditions.

f. To break the above bottleneck, accurate and complete phase behavior data of “real” asphaltenes-containing oil mixtures at “real” operating temperatures and pressures are needed.

5.1.4 Fraction of ABVB rejected using dodecane as solvent

The rejection of ABVB for the 25 wt% ABVB + dodecane mixture is shown in Figure 5-3. The reject ratio gradually increases with temperature but in most case falls in a range of 0.05~0.07, which is much less than 0.40 ~ 0.6 for 20~30 wt% ABVB + pentane mixtures (Figure 5-1 c & d). The amount of precipitate phase decreases with the

molecule size of alkane solvent. This is consistent with experiments shown in Figure 2-15 (Speight et al., 1999). Unfortunately, no sample was extracted and analyzed in this set of experiments. Comparison of the rejections of individual ABVB constituents using pentane as solvent and using dodecane as solvent is unavailable.

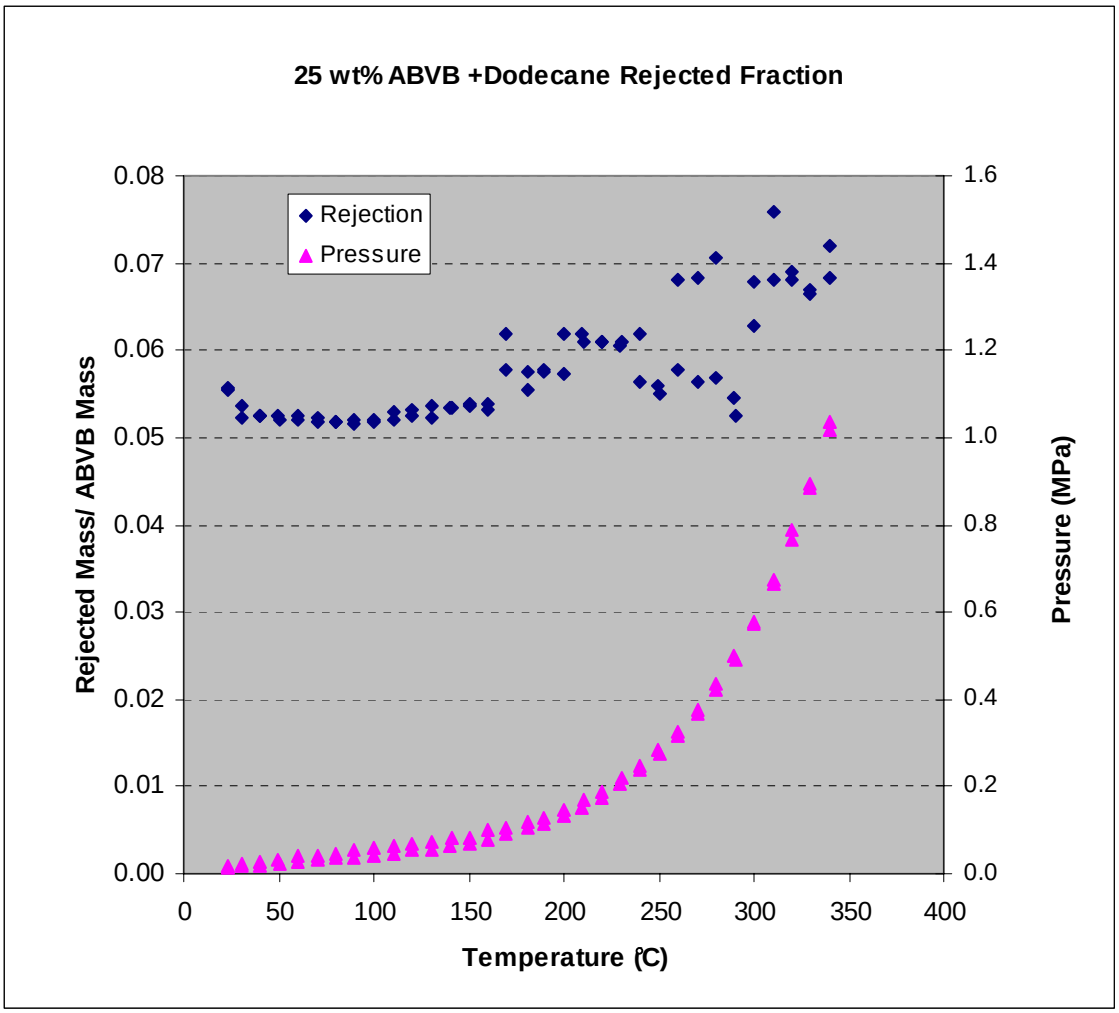

Figure 5-3. Dodecane reject ratio of ABVB as a separation indicator

5.1.5 Industrial Implications

In general terms, as long as a reject phase is created through the addition of an alkane solvent to ABVB, inorganic matter reports to it quantitatively. As more solvent is added,

a greater fraction of the asphaltenes is rejected while saturates, aromatics and resins are largely retained. Nickel and vanadium rejection appears linked with asphaltene rejection but nitrogen and sulfur are well distributed among all ABVB fractions and are not separated to a significant degree. In the absence of chemical reaction in the reject phase leading to deposition of solid material, the selectivity for vanadium and nickel removal is poor. Traditional ROSE processes used a 3~6 mass ratio for light hydrocarbon to heavy oils and operate at a region around the critical point of light hydrocarbon, which correspond to the 10 ~ 30 wt% ABVB + pentane at temperatures T =180~220 °C. The reject ratios reach maximums under these conditions. Obviously, the operating region is not a good choice. Considering the objective of achieving a selective separation with minimum amounts of solvent, the best operating conditions for separating fine inorganic solids, heavy metals, and sulfur from ABVB using pentane as solvent are:

- Composition: 40~50 wt% ABVB;
- Temperature: ~ 250 °C;
- Pressure: ~10 MPa.

Under the above conditions, reject ratio is a strong function of pressure, and the precipitated phase is mostly liquid with low viscosity, which means easy to handle. It provides the best compromise between selectivity and fluidity.

Based on the experimental results of pentane + ABVB mixture, there is no highly selective zone that can concentrate above 90 wt% of all nasty materials (inorganic fine solids, heavy metals and sulfur) in only 10 wt% of precipitated phase. This suggests that in order to achieve a highly selective separation; one has to introduce chemical reactions or/and change the solvent.

5.2 Apparent density and solid dispersion

As discussed in Chapter 3, when a phase has solids dispersed, its apparent density is greater than its actual density at the same temperature. Since it is impossible to obtain actual densities of all phases in equilibria, the averaged actual density for all dense phases (not including vapour) are used as a reference to check whether there is any solids dispersion. The averaged actual density was obtained by dividing the mass of dense phase by the volume of dense phase (from volume calibration). The mass of dense phase was obtained by subtracting, from the total mass, the mass in vapour phase, which could be approximated using EOS and pure pentane data. This method works fine at low temperatures when the vapour phase is virtually pure pentane, but naturally not as well at high temperatures. An example is illustrated in Figure 5-4 for ABVB + pentane mixtures at 100 °C. Figure 5-4 indicates when there is a phase splitting, the precipitated phases have much higher apparent densities than the averaged actual densities and the apparent densities of the bulk phases, suggesting that most asphaltenes were dispersed in the precipitated phase. Although the L1 phase for 5~40 wt% ABVB + pentane mixtures have apparent densities slightly lower than their actual densities, sample analysis (Table 5-1) indicated that there are asphaltenes dispersed in L1 phase. This is because the actual density is an averaged value of all dense phases not the actual density of L1 phase. Therefore, asphaltenes are dispersed in all dense phases at low temperatures. Consequently, the ratio of apparent total mass, obtained by summarizing the products of volume and apparent density of phases in equilibria, to the actual total mass falls in the range of 1.0~1.25. The apparent density for the gas phase at low temperature and pressure is often too low to be measured accurately.

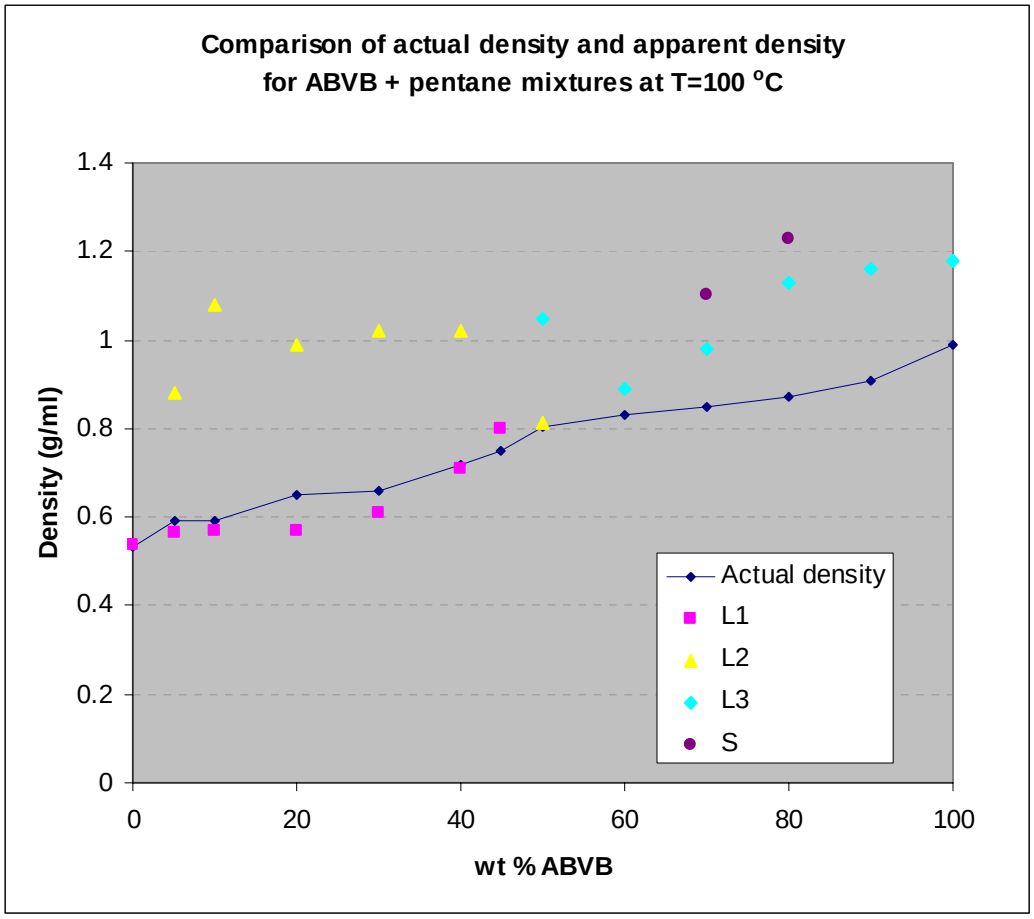

Figure 5-4. Comparison of apparent density and averaged actual density of dense phases

5.3 Settling time

As discussed in Chapter 2, phase equilibrium is an ideal state which practical mixtures can infinitely approximate but very hard to reach. Practical mixtures are often treated as equilibrium systems depending on specific error tolerance. Phase behavior is a very time-consuming and expensive practice. It is challenging to obtain high quality data with limited experimental resource. The key issue is how fast the system approximates its equilibrium state. For the phase behavior experiments in this study, the equipment has very good mixing and delicate temperature and pressure control system, so the major

concern remains how long equilibrium phases (including solids if present) need to settle from each other after temperature and pressure reached their set points. The time needed for phases to settle down depends on the mixture composition, temperature, pressure, and also changes whether the mixture has emulsion, solids dispersion, etc. Only phase settling time and qualitative viscosity are discussed below.

5.3.1 Phase settling time

Generally the higher the concentration of ABVB, and the lower the temperature, the longer the phases in the mixture need to settle. Long settling time is also needed for mixtures close to a critical point. For experiments in this study, we set 30~ 60 minutes settling time for the high ABVB wt% mixtures at low temperatures, and 10~15 minutes for the other situations, which was proven enough as shown in Figure 5-4 for pentane + ABVB 45 wt% mixture at 140 °C. At t = 0 min, the densities at four different positions along the view cell height are almost the same and there is a big vortex in the X-ray image, which are indications for good mixing. At t = 0 ~ 3 min, the denser liquid is settling down and densities in different phases are no longer the same. At t = 3 ~ 5 min, the mixture approximately settled: clear phase boundary and identical apparent densities at different positions but within the same phase. This was further confirmed by the data at t=180 min. Therefore in this case, 5 minutes is barely enough but 10~15 minutes is sufficient for the equilibrium phases to settle.

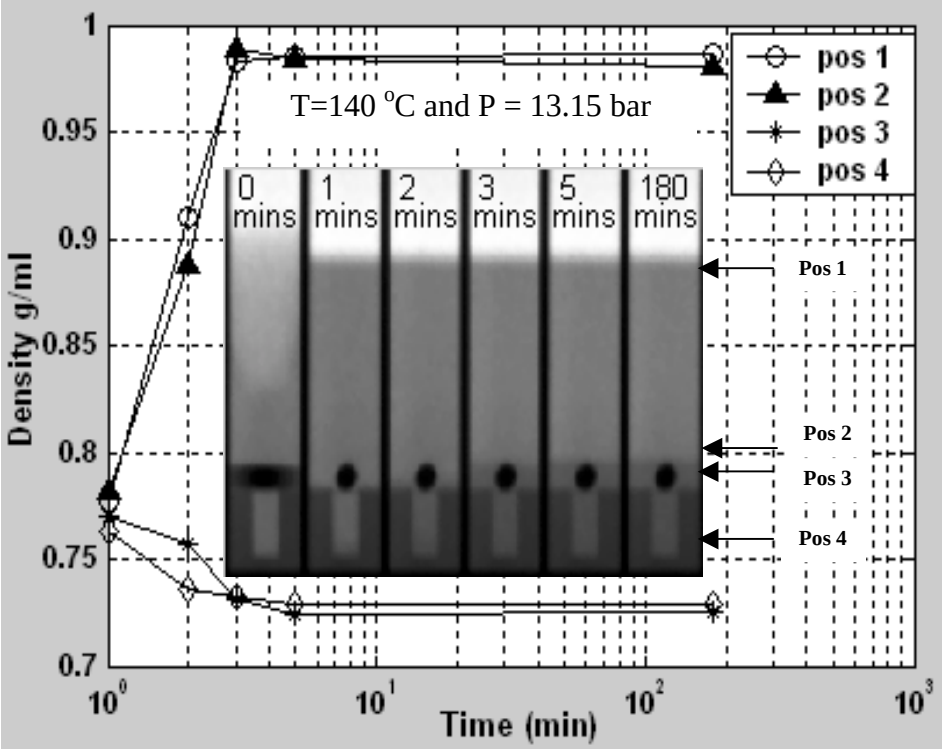

Figure 5-5. Settling kinetics for equilibrium phases.

5.3.2 Solids partially settled regions

There are four types of apparent density profiles along the view cell as discussed in Chapter 3. The type 3 apparent density profile (Figure 3-10 c) suggests a case where solid particles have only partially settled. The scopes where type 3 profiles were encountered were summarized in table 5-2. Experiments from this study found that such density profile keep the shape for weeks, suggesting that part of asphaltene particles have not yet fully settled from the solution. Whether the dispersion is stable or metastable is unknown at the moment. The time needed for solid particles to settle relates to the viscosity of the solution, density differences between solid particles and surrounding media, and the size, concentration and shape of solid particles. A detailed discussion of this topic is beyond the scope of this research.

Table 5-2. Solids partially settled and partially dispersed regions

Composition		Temperature (°C)
Alkane	Wt% ABVB	
Pentane	80	20~110
Pentane	90	20~100
Dodecane	2	20~340
Dodecane	10	80~340

5.4 Adherent nature and re-dispersion of precipitated phases

The properties of the deposited phase could also have huge impact on industrial application. For example, the more viscous or adherent the precipitated phase is, the more problematic the precipitated phase tends to be. The view-cell is not currently equipped to measure the viscosity of phases directly. However, above a threshold viscosity or apparent viscosity or when the deposit is very adherent, the stirrer on the base of the view-cell does not turn at maximum torque. “Sticky” phases, adherent solids, are examples of materials that can inhibit stirrer operation. The “V” curve in Figure 5-4 a shows the temperature below which the stirrer “sticks” to the base plate (if turned on). ABVB itself is semi-solid at the room temperature and naturally one would not expect to mix the sample until it is more fluid above ~ 130 °C. Also as ABVB is diluted with pentane, the sample become less viscous, which results in a decrease in the agitation temperature increase dilution (the left branch of “V” curve). As the sample is further diluted, an asphaltenic phase deposits on the bottom base of the view cell and the agitation temperature depends principally on the properties of deposited phase, which often becomes more and more viscous and adherent as the oils and solvent in the deposits

are stripped to the bulk phase with dilution. Consequently, the agitation temperature increases with the dilution at the low ABVB wt% side (the right branch of the "V" curve). The connection between the ease of mixing and phase behavior is clear. Mixtures comprising 40 to 50 wt. % ABVB are readily agitated at room temperature, while mixtures comprising as little as 5 wt. % ABVB (1.5 wt % asphaltenes) generate adherent deposits at temperatures greater than 150 °C. Chodakowski (2002) observed a similar phenomenon at 190 °C during the course of a SAXS experiment with a mixture comprising 1 wt % ABVB. Clearly, dilution of maltene + asphaltene mixtures with low molar mass paraffinic fluids does not solve and can exacerbate deposition problems.

Equilibrium is not readily achieved in the absence of agitation. Re-dispersion of the settled phase can be difficult and Figure 5-4 provides two excellent if qualitative illustrations. Viscous liquid phases also do not re-disperse even at high shear as illustrated in Figure 5-4b where a vortex is clearly visible above the stirrer.

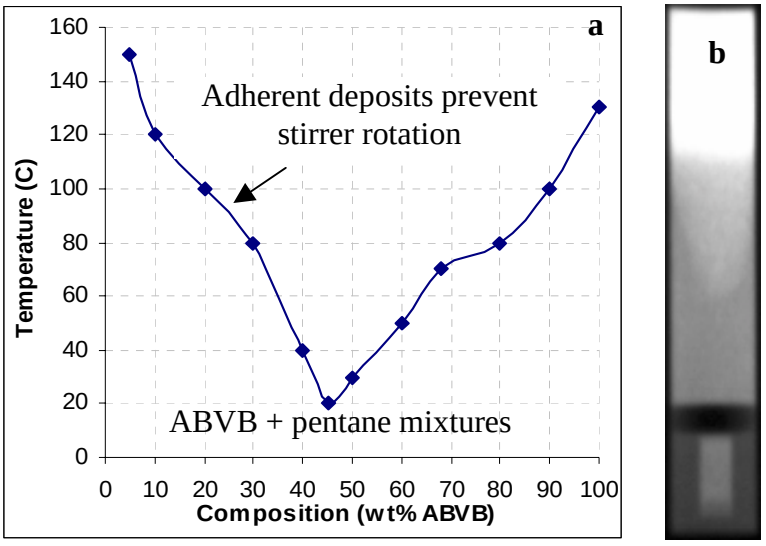

Figure 5-6: Adherent and viscous nature of the precipitated phase and its re-dispersion

CHAPTER 6 CONCLUSIONS

6.1 Phase behavior for ABVB + alkane mixtures

1. The ABVB + pentane mixtures demonstrate complicated multiphase behaviors. The L1L2V phase region was expected while the L2L3V is unexpected at the outset of the project.
2. The L1L2V phase behavior for 5~45 wt % ABVB + pentane mixtures at temperature T <220 °C is an expansion of type III binary phase behavior which is a typical phase behavior for heavy solutes + pressured gases in supercritical extraction processes. This zone was observed from the room temperature to a temperature slightly higher than the critical temperature of pentane.
3. The L2L3V phase behavior is observed for the pentane + 40 ~ 45 wt % ABVB mixtures at temperatures above T>230 °C, for the pentane + 50 wt% mixture from the room temperature to 340 °C. The L2L3V phase region can be very narrow in pressure and it is of great potential for developing selective separation process.
4. L1L2V and L2L3V phase behavior are likely interfered by asphaltene solidification at low temperatures. The L1L2V and L2L3V can virtually represents SL1L2V and SL2L3V phase behavior.
5. Small amount of solids depositions are found for 60~90 wt% ABVB + pentane mixtures.
6. The phase behavior demonstrated by the 25 wt% ABVB + dodecane mixture is consistent with the expansion of type V binary phase behavior.

7. As the size of alkane solvent increases, ABVB + alkane mixtures exhibit type III, type IV, type V and type I phase behavior, which has the same sequence as that of anthrancene + alkane mixtures.
8. Hydrogen shifts the multiphase regions for the ABVB + alkane mixtures to higher pressure and may expand the size of the multiphase region. It only unnecessarily increases prospective operating pressures for selective separation processes.
9. Saturates, aromatics, resins and asphaltenes distribute in all dense phases in equilibrium (bulk phase and precipitated phase). This contradicts the assumption that the precipitate phase is "solid" and pure asphaltenes. It also suggests to solve the asphaltene related problems, one should obtain more accurate multiphase behavior data of asphaltene containing heavy oil mixtures at the same temperature and pressure conditions as production process. Currently many researchers are still focusing on very dilute asphaltene containing heavy oil + alkanes mixture at ambient temperatures and pressures.
10. Multiphase behaviors of asphaltene containing heavy oil mixtures observed in this project are reversible, from a thermodynamics point of view.

6.2 Selective removal of fine inorganic solids, heavy metals and heteroatoms from heavy oils/bitumen

1. Mineral matter is easily and quantitatively separated from ABVB by adding sufficient amounts of an alkane solvent to create a second liquid phase.

2. Selective removal of nickel and vanadium from ABVB + pentane mixtures is not realized in the L1L2V or L2L3V multiphase regions without coincident rejection of asphaltenes.
3. Selective removal of sulfur and nitrogen from ABVB is not readily achieved using this separation approach.
4. There is no highly selective zone that can concentrate above 90 wt% of all nasty materials (inorganic fine solids, heavy metals and sulfur) in only 10 wt% of precipitated phase. This suggests that in order to achieve a highly selective separation; one has to introduce chemical reactions or/and change the solvent.
5. Considering the objective of achieving a selective separation with minimum amounts of solvent, the best operating conditions for separating fine inorganic solids, heavy metals, and sulfur from ABVB using pentane as solvent is 40~50 wt% ABVB + pentane at T ~ 250 °C and P ~10 MPa. It is in the L2L3V phase zone but the conventional operating conditions for ROSE processes fall in the L1L2V phase zone. This accounts for the high product loss in some ROSE processes.
6. Asphaltene-related solid drop out problems can cause a larger amount of “solid” precipitation than the total amount of asphaltenes in solution by co-precipitating maltenes and solvent.
7. Parts of readily upgradeable constituents (saturates, aromatics, resins) precipitate with asphaltenes, and this explains the low selectivity and high product loss in ROSE processes.

8. As the dilute ratio increases, the asphaltene content in the light liquid phase decreases while content in the precipitated phase increases. The difference of SARA distribution between phases in equilibrium increases with the dilute.
9. However, it is the multiphase zones arising at low asphaltene concentration that pose the greatest solid and liquid deposition problems. Zones such as the SL1, SL1V, L1L2V, and L1L2 are particularly prone to the production of adherent deposits. The deposits once formed are not readily dislodged even at temperatures approaching 200 °C.

6.3 Experimental technique

1. The beryllium insert improves the capability of the equipment in detecting the onset of the deposited phase and in obtaining more accurate volume of the deposited phase.
2. This study develops a new calibration method using the beryllium insert as an internal calibration standard to remove the random effects in apparent density measurement.
3. In this research, solids dispersion, precipitation and settling are detected successfully by comparing the apparent density and actual density, by observing apparent density profile of a single image and by comparing the apparent densities from a series of X-ray images.
4. The software developed in this study automates data processing process and will greatly extend the capability of the application of the X-ray view cell technology in phase behavior study.

CHAPTER 7 RECOMMENDATIONS

This study raises as many questions as it answers. Issues meriting further exploration arising directly from this study include both high and low temperature investigations. Some relate to the properties of asphaltenes and heavy fractions more generally rather than to selective separation more specifically:

1. The properties of asphaltenes and the changes in their properties with composition (i.e., the nature or mass fraction of solvent) appear of great interest. Examples include:
    - how does the shape/structure/size of asphaltenes vary with composition/temperature?
    - what are the energies associated with these transitions?
    - how can these transitions be controlled or modelled?
    - how do these transitions affect selective separation?
    - How do the contents of heavy metals in pentane and dodecane asphaltenes differ?
    - In what phases do asphaltenes precipitate or remain dispersed?
    - Is there any difference between asphaltenes precipitated and dissolved, such as heavy metals, sulfur and inorganic solids content?
2. While adequate selective separation was found in the L2L3V region at elevated temperatures, in order to develop a industrial process, we need complete and accurate phase behavior data, and partition of fine inorganic solids, heavy metals and heteraoatoms among the phases in equilibria inside the L2L3V zone.

3. Development of live sampling techniques merits further exploration.
4. Due to the complexity of the phase diagrams, the sub-atmospheric phase behavior and the phase behavior of ABVB + diluent mixtures at low ABVB mass fractions, merit detailed investigation. Such a study would link results obtained in reservoir fluids phase behavior studies with those obtained here.
5. The possiblity of using a solvent other than alkanes and exploiting chemical reactions to achieve a more selective separation merits further investigation.
6. Impact of multiphase behavior on chemical reactions such as coking merits further exploration.
7. X-rays are scattered by solids in a sample. The relationship between the amount and properties of solid in a sample and the amount of x-ray scattering (the difference between apparent density and actual density) is unknown. Progress in this area will lay the technical basis for on line composition and density detection for asphaltenes containing heavy oil mixtures.
8. Collimation of incident and transmitted X-rays can reduce X-ray scattering, and thus may improve contrast of the transmitted X-ray images. Whether collimation can improve density measurement merits further investigation.

References

Abedi, S. J.; Cai, H.-Y.; Seyfaie, S.; Shaw, J. M.; Simultaneous Phase Behavior, Elemental composition and Density Measurement Using X-Rays Imaging; Fluid Phase Equilibria 158-160 (1999) 775-781.

Abedi, S. J., PhD Thesis, University of Toronto, 1998; Unusual Retrograde Condensation and Asphaltene Precipitation in Model Oil System Using X-Ray Imaging.

Abedi, S. J.; Seyfaie, S.; Shaw, J. M.; Unusual Retrograde Condensation and Asphaltene Precipitation in a Model Heavy Oil System; Petroleum Science and Technology 16 (3&4), 209-226 (1998).

Al-Atar,E. and A.P. Watkinson (1999); Effect of Resins/Asphaltenes Ratio on Heat Exchanger Fouling of Mixtures Containing Heavy Oil. Proc. Eng. Foundation Conf., Heat Exchanger Fouling and its Mitigation, Banff, Alberta, July 1999, T.R. Bott (Ed.), Begell House, New York (2001), pp359-366.

Ali, L.H. and K.A. Al-Ghannam, Investigations into asphaltenes in heavy crude oils. I. Effect of temperature on precipitation by alkane solvents. Fuel, 1981.

American Society for Testing and Materials. 1970. Test No. ASTM D2006. American Society for Testing and Materials, Philadelphia, PA.

American Society for Testing and Materials. 1980. Test No. ASTM D2007.American Society for Testing and Materials, Philadelphia, PA.

American Society for Testing and Materials. 1984. Test No. ASTM D4124. American Society for Testing and Materials, Philadelphia, PA.

Andersen, S. I.; Lindeloff, N. and Stenby, E.; Investigation of Asphaltene Precipitation at Elevated Temperature; Petroleum Science and Technology 16 (3&4), 323-334 (1998).

Anderson, S. I.; Speight, J. G. Thermodynamic models for asphaltene solubility and precipitation. Journal of Petroleum Science and Engineering. **1999**, 22, 53-66.

Andersen, S. I.; Effect of Precipitation Temperature on the Composition of n-Heptane Asphaltenes Part 2; Fuel Science and Technology Int'l., 8 (6),579-604 (1995).

Andersen, S. I. and Birdi, K. S.; Influence of Temperature and Solvent on The Precipitation of Asphaltenes; Fuel Science and Technology Int'l., 8 (6),593-615 (1990).

Asomaning, S. and A. P. Watkinson (1999). Deposit Formation by Asphaltene-Rich Heavy Oil Mixtures on Heat Transfer Surfaces. Understanding Heat Exchanger Fouling and its Mitigation, T. R. Bott (Editor) Begell House, New York pp283-290.

Boduszynski, Mieczyslaw M. Composition of heavy petroleum, 1. Molecular weight, hydrogen deficiency, and heteroatom concentration as a function of atmospheric equivalent boiling point up to 1400 ^{o}F (760 ^{o}C), Energy & Fuel, Vol. 1, No. 1, 1987.

Burke, N. E., Hobbs, R. E. and Kashou, S. F. Measurement and Modeling of Asphaltene Precipitation. JPT, 1990, 1440-1446.

de Bore, D.K.G., Fundamental Parameters for X-ray Fluorescence Analysis, Spectrochimica Acta 44B (11) (1989) 1171-1190.

Carbongnani, L.; Garcia, C.; Izquierdo, A.; DiMarco; M.P., Perez, C.; Rengel, A., Sanchez, V.; Correlation between physical properties and hydroprocessing of Venuzeulan Heavy ends; ACS Pet. Div. Prepr. 32, 406-412.

Cartlidge, C. R.; Dukhedin-Lalla, L.; Rahimi, P. and Shaw, J. M; Preliminary phase diagrams for ABVB+n-dodecan+hydrogen; Fluid Phase Equilibria 117 (1996) 257-264.

Cartlidge, C. R.; Dukhedin-Lalla, L.; Rahimi, P. and Shaw, J. M.; Preliminary phase diagrams for bitumen/heavy oils and related mixtures; Fuel Science and Technology Int'l., 14 (1&2), 163-178 (1996).

Chodakowski, M.; PhD thesis, University of Alberta, (in progress) 2003.

Cimino, R.; Correra, S.; Del Bianco, A.; and Lockhart, T.P.: "Solubility and Phase Behavior of Asphaltenes in Hydrocarbon Media," Asphaltenes: Fundamentals and Applications, E.Y. Sheu and O. C. Mullins (eds.), NY: Plenum Press (1995) 97-130.

Clarke, P. F. and Pruden, B. B.; Asphaltene Precipitation From Cold Lake and Athabasca Bitumens; Petroleum Science and Technology 16 (3&4), 287-305 (1998).

Chung, F.T-H.; Sarathi, P., and Jones, R.: "Modeling of Asphaltene and Wax Precipitation," Topical Report, Cooperative Agreement No. DE-FC22-83FE60149, NIPER-498 (Jan. 1991).

Chung, K. H.; Xu, C.; Hu, Y.; Wang, R.; Supercritical Fluid Extraction Reveals Resid Properties; Oil and Gas J. Jan 20, 1997.

Chung, K. H.; Xu, C.; Narrow -cut Characterization Reveals Resid Process Chemistry *Fuel, Volume 80, Issue 8, June 2001, Pages 1165-1177*

de Loos, Th. W. Understanding Phase Diagrams, Supercritical Fluids, 65~69, E. Kiran and J. M. H. Levelt Sengers (eds), Kluwer Academic Publishers, 1994.

Dukhedin Lalla, L.; A Study of Complex Phase Behavior Arising in Heavy Oil/Bitumen Mixtures Using X-Ray Imaging, PhD thesis; University of Toronto, 1996.

Dukhedin Lalla, L.; Yushun, S.; Rahimi, P. and Shaw, J.M.; Phase Splitting of Complex Hydrocarbon Mixtures; Fluid Phase Equilibriua, Vol. 53, P.415-422, 1989.

Escobedo, J. and Mansoori, G. A., SPE, U. of Illinois; Viscometric Determination of the Onset of Asphaltene Flocculation : A Novel Method; SPE Production & Facilities, May 1995, 115-118.

Escobedo, J. and Mansoori, G. A., SPE, U. of Illinois; Viscometric Principles of the Onset of Colloidal Asphaltene Flocculation in Paraffinic Oils and Asphaltene Micellization in Aromatics; SPE Production & Facilities, May 1998, 116-122.

Estrera, S.S. and Luks, K.D., Liquid-Liquid-Vapour Equilibria Behavior of Certain Ethane + n-Paraffin Mixtures. J. Chem. Eng. Data, 1987, 32, 201-204.

Fall, J. and Luks, K.D., Effects of Additive Gases on the Liquid-Liquid-Vapour Immiscibility of the Carbon Dioxide + n-Nonadecane Mixture. J. Chem. Eng. Data, 1986, 31, 332-336.

Floter, E.; de Loos, Th., W., de Swaan Arons, J., Solid-Fluid and Vapor-Liquid Equilibria of Binary Reservoir Model Fluids. Fluid Phase Equilibria, 1996, Vol. 117, 153-159.

Fotland, P.; Anfidsen, H.; and Fadnes, F.H. "Detection of Asphaltene Precipitation and Amounts Precipitated by Measurement of Electrical Conductivity," Fluid Phase Equil. (1993) 82, 157.

Fuhr, B.J.; C. Cathrea; L Coates; H. Kalra, and A.I. Majeed, Properties of asphaltenes from a waxy crude. Fuel, 1991. 70: p. 1293-1297.

Gray, M. R.; Jokuty, P.; Yeniova, H.; Nazarewycz, L., and Wanke, S. E.; Achia, U., Krrzywicki; A., Sanford, E.C.; Sy, O.K.Y.; The relationship between chemical structure and reactivity of Alberta bitumens and heavy oils; Can J. Chem. Eng. 69, 833-843.

Gray, M. R.; Upgrading petroleum Residues and Heavy oils; Marcel Dekker, Inc, Press, New York, 1994.

Green, J.B.; Shay, J.Y.; Reynolds, J.W.; Green, J.A.; Young, L.L. and White, M. E.; Microcarbon Residue Yield and Heteroatom Partitioning Between Volatiles and Solids for Whole Vacuum Resid and their Liquid Chromatographic Fractions; Energy &Fuel, 1992,6,836-844.

Gregorowicz, J.; de Loos, Th.W. and de Swaan Arons, J.; Unusual retrograde condensation in ternary hydrocarbon systems; Fluid Phase Equilibria, 73, 109-115 (1992).

Gregororwicz J.; de Loos Th. and de Swaan Arons J.; Liquid-Liquid-Vapour Phase Equilibriua in the System Ethane+propane+eicosane: Retrograde Behavior of the Heavy Liquid Phase; Fluid Phase Equilibriua. 84: 225-250, 1993.

Groenzin, H. and Mullins, O. C. Molecular Size and Structure of Asphaltenes from Various Sources," Energy and Fuels (2000) 14, 677-684.

Hammami, A.; Chang-Yen, D.; Nighswander, J. A. and Stange, E.; An Explanation Study of the Effect of Paraffinic Solvents on the Onset and Bulk Precipitation of Asphaltenes; Fuel Science and Technology Int'l., 13 (9), 1167-1184 (1995).

Hammami, A.; Ferworn ,K. A. and Nightswander,J. A.; Asphaltenic Crude Oil Characterization: An Experimental Investigation of the Effects of Resins on the Stability of Asphaltenes; Petroleum Science and Technology 16 (3&4), 227-249 (1998).

Hischberg, A.; de Jong, L.N.J.; Schipper, B.A. and Meijers, J.G.; Influence of temperature and pressure on asphaltene precipitation; SPE J (Jun., 1984) 283.

Hu, Y.-F. and Guo, T.-M., Effects of temperature and molecular weight of n-alkane precipitants on asphaltene precipitation. Fluid Phase Equilibria, 2001, Vol. 192, 13-25.

Jangkamolkulchai, A.; Arbuckle, M., and Luks, K.D. Liquid—liquid—vapor phase equilibria behavior of certain binary ethane + n-alkylbenzene mixtures. *Fluid Phase Equilibria, Volume 40, Issue 3, December 1988, Pages 235-245*

Kamath, V.A.; Kakade, M.G. and Sharma, G.D.; An Improved Molecular Thermodynamics Model of Asphaltene Equilibria; Asphaltene Particles in Fossil Fuel Exploration, Recovery, Refining, and Production Processes; Sharma, M. K. and Yen, T. F. (eds), Plenum Press, New York, 1994.

Kawanaka, S. SPE; Park, S. J. and Mansoori, G. A., SPE, U. of Illinois; Organic Deposition From Reservoir Fluids: A Thermodynamic Predictive Technique; SPE Reservoir Engineering, May 1991, 185-192.

Kokal, S. L.; Najman, J.; Sayegh, S. G.; and George, A. E.; Measurement and Correlation of Asphaltene Precipitation from Heavy Oils by Gas Injection; J. Can. Petrolem Technology, 31 (4): 24 (1992).

Kotlyar, L.S.; Sparks, B.D.; Woods, J.R.; Raymond, S.; Le Page, Y. and Shelfantook, W.; Distribution and Types of Solids Associated with Bitumen; Petroleum Science and Technology, 16 (1&2), 1-19 (1998).

Kotlyar, L.S.; Sparks, B.D.; Woods, J.R.; Solids Associated with Asphaltenes Fraction of Oil Sands Bitumen; Energy & Fuel, 1999, 13, 346-350.

Kurnick, R. T.; and Reid R. C. Solubility Extrema in Solid-Fluid Equilibria. AIChE J., 27, 861(1981).

Lambert, M. C.; Handbook of X-rays for Diffraction, Adsorption and Microscopy, McGraw-Hill, 1967.

Larson, L. L.; Silva, M. K.; Taylor, M. A.; and Orr, F. M., Temperature Dependence if LLV Behavior in Carbon Dioxide / Hydrocarbon System, SPE Reservoir Engineering, 1989, 105-114.

Lemke, H.K.; Stephenson, W.K.; Deposit Formation in Industrial Delayed Coker/Visbreaker Heaters; Petroleum Science and Technology, 16 (3&4), 335-360 (1998).

Leontaritis, K.J.; SPE, Amaefule, J.O., SPE; and Charles, R.E., SPE, Core Laboratories. A Systemic Approach for the prevention and treatment of Formation Damage Caused by Asphaltene Deposition; SPE Production and Facilities August 1994. 157-164.

Leontaritis, K.J. and Mansoori, G. A., "Asphaltene Deposition During Oil Production and Processing: A Thermodynamic Colloidal Model," SPE Paper No. 16258, SPE International Symposium on Oilfield Chemistry, February 4-6, 1987, San Antonio, TX.

Lindeloff, N.; Heidmann, R. A.; Adersen, S. I. and Stenby, E.; A Thermodynamic Mixed-Solid Asphaltene Precipitation Model; Petroleum Science and Technology 16 (3&4), 307-321 (1998).

Long, R. B. and Speight, J. G.; The composition of petroleum; Petroleum Chemistry and Refining; Speight, J. G. (eds), Taylor& Francis Press, Washington DC, 1999.

Mansoori, G.A. Modeling of asphaltene and other heavy organic depositions, Journal of Petroleum Science & Engineering, Vol. 17, pp.101-111, 1997.

McHugh, Mark A.; Krukonis, Val J. Supercritical Fluid Extraction: Principles and Practice. Butterworth Publishers, 1986.

Minicucci, D.; Zou, X.-Y.; Shaw, J.M. The impact of liquid-liquid-vapour phase behavior on coke formation from model precursors, Fluid Phase Equilibria, 2002, Vol. 194-197, 353-360.

Mullins, O. C.; Sulfur and Nitrogen Molecular Structures in Asphaltenes and Related Materials Quantified by XANES Spectroscopy; Asphaltenes, Fundamentals and Applications; Sheu, E. Y. and Mullins, O. C. (eds), Plenum Press, New York, 1995.

Mushrush, G. W. and Speight, J. G.; Instability and incompatibility of petroleum products; Petroleum Chemistry and Refining; Speight, J. G. (eds), Taylor& Francis Press, Washington DC, 1999.

Northrup, A.H.; Sloan, H.D.; Annual Meeting. National Petroleum Refiners Association. San Antonio, Texas. Paper AM-96-55.

Onukwuli, O.D.; Onyia, I.M.; Ekumankama, E.O. and Okeke, S. I.; Solvent Demetalization of Atmospheric and Vacuum Residues; Petroleum Science and Technology, 17 (1&2), 37-49 (1999).

Overfield, R.E.; Sheu, E.Y.; Sinha, S.K.; Liang, K.S.; SANS Study of Asphaltene Aggregation; Fuel Science & Technology International, 7 (5-6), 611-624 (1989).

Pacheco-Sanchez, J. H. and Mansoori,G A.; Prediction of The Phase Behavior of Asphaltene Micelle/Aromatic Hydrocarbon Systems; Petroleum Science and Technology 16 (3&4), 377-394 (1998).

Pan, H., SPE, and Firoozabadi, A., SPE, reservoir Engineering Inst.; Thermodynamic Micellization Model for Asphaltene Aggregation and Precipitation in Petroleum Fluids SPE Production and Facilities; May 1998.

Pan, H., SPE, and Firoozabadi, A., SPE; Thermodynamic Micellization Model for Asphaltene Precipitation Inhibitation; AICHE National Spring Meeting, March 14-17,Houston, 1999.

Pan, H., SPE, and Firoozabadi, A., SPE, reservoir Engineering Inst.; Thermodynamic Micellization Model for Asphaltene Precipitation from Reservoir Crudes at High Pressures and Temperatures; SPE 1997 Annual Technical Conference and Exhibition held in San Antonio, Texas,5-8 October 1997.

Pan, H., SPE, and Firoozabadi, A., SPE, reservoir Engineering Inst.; Pressure and Composition Effect on Wax Precipitation: Experimental Data and Model Results; SPE Production & Facilities; November 1997.

Park, S. J.; Escobedo, J. and Mansoori, G. A.; Asphaltene and other heavy organic depositions; Asphaltenes and Asphalts, Chapter 8; Edited by Yen, T.F. and Chiligarian, G.V., 179-205.

Park, S. J. and Mansoori, G. A.; Aggregation and deposition of Heavy Organics in Petroleum Crudes; Energy Source, Volume 10. Pp.109-125.

Peters, C. J.; Rijkers, M. P. W. M.; de Roo, J. L., de Swaan Arons, Phase equilibria in binary mixtures of near-critical propane and poly-aromatic hydrocarbons. J. Fluid Phase Equilibria, 1989, Vol. 52, 373-387.

Peters, C. J. Multiphase Equilibria in Near-Critical Solvents, Supercritical Fluids, 117-145, E. Kiran and J. M. H. Levelt Sengers (eds), Kluwer Academic Publishers, 1994.

Prausnitz, J. M.; Lichtenthaler, R.N.; Azevedo, E. G. De; Molecular Thermodynamics of Fluid-Phase Behavior; Second edition, Prentice-Hall Inc., Englewood Cliffs, N.J. 07632, 1986.

Raeissi; S., K; Gauter, C. J. Peters. Fluid Multiphase Behavior in Quasi-Binary Mixtures of Carbon Dioxide and Certain l-Alkanols. Fluid Phase Equilibria 147,1998, 239-249.

Ramos, A.C.S.; Delgado, C.C.; Mohamed, R.S.; Almeida, V.R.; and Loh, W.: Reversibility and Inhibition of Asphaltene Precipitation in Brazilian Crude Oils," Petrol. Sci. Tech. (1999) 17, 877-896.

Rassamdana, H.; Dabir, B.; Nematy, M.; Farhani, M. and Sahimi, M.; Asphalt flocculation and Deposition: I. The onset of precipitation; AIChE J. (1996) 42, 10.

Reichert, C.; Fuhr, B.j. and Klein, L.L.; Measurement of Asphaltene Flocculation in Bitumen Solutions; J. Can. Petrolem Technology, 25 (5): 33 (1986).

Reynolds, J. G; Metals and heteroatoms in heavy oils; Petroleum Chemistry and Refining; Speight, J. G. (eds), Taylor& Francis Press, Washington DC, 1999.

Reynolds, J. G.; Effects of asphaltene precipitation on the size of Vanadium-, Nickel- and Sulfur-containing compounds in heavy crude oils and residua; Asphaltenes and asphalts, 1; Yen, T. F. and Chilingarian, G.V. (eds), Elsevier Science Press, New York, 1994.

Robinson, D.B.; The Interface Between Theory and Experiment; Fluid Phase Equilibrium 52: 1-14, 1989.

Robinson, D. B.; Ng, H.-J. and Chen, C.-J., The effect of nitrogen on the phase behaviour of an aromatic condensate. AIChE Annual Meeting, 1990, Chicago, IL, November 11-16, paper 31 a.

Sanaie, N.; Watkinson, A.P.; Bowen, B. D.; Smith, K. J.; Effects of Minerals on Coke Formation; Canada Chem. Eng. Meeting, 1999.

Savastano,C. A.; The Solvent Extraction Approach to Petroleum Demetallation Fuel Science and Technology Int'l., 9 (7), 855-871 (1991).

Shaw,J. M.; Selective removal of sulfur, heavy metals and solids from heavy oils/bitumen Re.: a proposal for research on upgrading of bitumen and heavy oil (CONRAD), 1998.

Shaw, J. M.; de Loos, Th. W. and de Swaan Arons, J.; Prediction of unusual retrograde condensation in model reservoir fluids; Fluid Phase Equilibria 84 (1993) 251-266.

Shaw, J.M.; de Loos, Th. W. and de Swaan Arons, J.; An explanation for solid-liquid-liquid-vapor phase behavior in reservoir fluids; J. Petroleum Science and Technology 15(5&6) 503-521 (1997).

Shaw, J. M.; de Loos, Th. W. and de Swaan Arons, J.; An explanation for solid-liquid-liquid phase behaviour in reservoir fluids; Petroleum Science and Technology 16 (3&4), 209-226 (1998).

Shaw, J. M., 2002; Toward Common Generalized Phase Diagrams for Asphaltene Containing Hydrocarbon Fluids II – implications for the correlation and prediction of condensed phase deposition, HOD 2002, Mexico.

Shaw, J. M., Towards Common Generalized Phase Diagrams for Asphaltene Containing Hydrocarbon Fluids. ACS, Petroleum Division Preprints, vol. 47 (4), 338-342 (2002).

Shaw, J. M.; Behar, E., IFP, 1999, Report 94952.

Shelton, J. L.; and Yarborough, L., Multiple Phase Behavior in Porous Media During CO2 or Rich-Gas Flooding, SPE-AIME Conf. Tulsa Oklahoma, 1976, March 22-24, paper # SPE 5827.

Sheu, E. Y.; Asphaltene precipitation and liesegang ring. HOD 2002, Mexico.

Sheu, E. Y.; De Tar, M. M.; Storm, D. A. and DeCanio, S. J.; Aggregation and kinetics of Asphaltenes in Organic Solvents; Fuel, 71, 299 (1992).

Sheu, E. Y.; De Tar, M. M.; Storm, D. A.; Structure, Interaction and Phase Transition of Vacuum Residue in Apolar Solvents; Fuel Science and Technology Int'l., 10 (4-6), 607-647 (1992).

Sheu, E. Y., and Storm, D.A.: Colloidal Properties of Asphaltenes in Organic Solvents, in Asphaltenes Fundamentals and Applications, Sheu, E. Y. and O.C Mullins, eds, NY, Plenum Press (1995) 1-52.

Speight, J.G.; Petroleum analysis and evaluation; Petroleum Chemistry and Refining; Speight, J. G. (eds), Taylor& Francis Press, Washington DC, 1999.

Speight, J.G.; Asphaltenes and Structure of petroleum; Petroleum Chemistry and Refining; Speight, J.G. (eds), Taylor& Francis Press, Washington DC, 1999.

Stegeman, J.R.; Kyle, A.L.; Burr, B. L.; Jemison, H.B.; Davison, R.R.; Glover, C.J. and Bullin, J.A. Compositional and Physical Properties of Asphalt Fractions Obtained by Supercritical and Solvent Extraction; Fuel Science and Technology Int'l., 10 (4-6), 767-794 (1992).

Storm, D.A. and Sheu,E.Y.; Colloidal nature of petroleum asphaltenes; Asphaltenes and asphalts, 1; T. F. Yen and G.V. Chilingarian (eds), Elsevier Science Press, New York, 1994.

Storm, D.A.; DeCanio, S. J.; De Tar, M. M.; Nero, V. P.; Upper bound on number average molecular weight of asphaltenes; Fuel, 1990, Vol 69.

Strausz, O. P.; Mojelsky, T. W. and Lown, E. M.; The Molecular Structure of Asphaltene: an unfolding story; Fuel, 1992, Vol 71.

Streett, W.B.; Phase equilibria in Fluid and Solid Mixtures at High Pressure; Paulaitis, M.E., J.M.L., Penninger, R. D. Gray, and P. Daridson (eds), "Chemical Engineering at Supercritical Fluid Conditions," Ann Arbor Science, Ann Arbor, Michigan, 1983.

Szewczyk, V.; Behar, E., Compositional model for predicting asphaltenes flocculation, Fluid Phase Equilibria, 1999, Vol. 158-160, 459-469.

Takatsuka, T.; Wada, R., Hirohama, S. and Fukui,Y.; A Prediction Model for Dry Sludge Formation in Residue Hydroconversion; Journal of chemical engineering of Japan, Vol.22 No 3 1989, 298-303.

Taylor, L. T. Supercritical Fluid Extraction, John Wiley & Sons, Inc. New York, New York, 1996

Thawer, R., SPE; Nicoll, D. C. A.; Dick, G.; Asphaltene Deposition in Production Facilities; SPE Production Engineering, 1990.

Thomas, D.C. and Becker, H.L.; Del Real Soria, R.A.; Controlling Asphaltene Deposition in Oil Wells; SPE Production & Facilities. May 1995.

Turek, E. A.; Metcalfe, R. E.; Fishback, R. E., Phase behaviour of Several CO2 /West Texas Reservoir Oil Systems, SPERE, May 1988, 505-516.

van Konynenburg, P. H.; Scott, R. L., Critical Lines and Phase Equilibria in Binary van der Waals Mixtures. Phil. Trans. Roy. Soc., 1980, Vol. 298, 495-540.

Watkinson, P. A.; Advance in Fouling of Petroleum Systems; Canada Chem. Eng. Meeting, 1999.

Werner, A.; Behar, F.; de Hemptinne, J. C.; Behar, E.; Thermodynamic properties of petroleum fluids during expulsion and migration from source rock. Org. Geochem, 1996, Vol. 24, no. 10/11, 1079-1095.

Wiehe, I. A.; A Phase-Separation Kinetic Model for Coke Formation; Ind. Eng. Chem. Res. 1993,32,2447-2454.

Wiehe, I. A.; A Solvent-Resid Phase Diagram For Tracking Resid Conversion; Ind. Eng. Chem. Res. 1992,Vol. 31,No. 2, 531-536.

Wiehe, I. A.; Polygon Mapping With Two-Dimensional Solubility Parameters; Ind. Eng. Chem. Res. 1995,34, 661-673.

Wiehe, I. A.; The Pendant-Core Building Block Model of Petroleum Residua; Energy & Fuels 1994, 8, 536-544.

Wiehe, I. A. and Liang, K.S.; Asphaltene, Resin, and Other Petroleum Macromolecules; Fluid Phase Equilibrium 117 (1996) 201-210.

Wilson, R. E.; P. C. Keith; and R. E. Haylett. 1936. Liquid Propane —Use in dewaxing, deasphalting, and refining heavy oils. Ind. Eng. Chem. 28:1065.

Wu, J. and Prausnitz, J., FirooZabadi,A.; Molecular-Thermodynamic Framework for Asphaltene-oil Equilibria; AIChE Journal, May 1998 Vol.44, No5 1188-1199.

Yang, Z.; Ma, C.-F.; Lin, X.-S.; Yang, J.-T.; Guo, T.-M.; Experimental and Modeling Studies on the Asphaltene Precipitation in Degased and Gas-Injected Reservoir Oils;Fluid Phase Equilibrium 8th Holland international Meeting.

Yarranton, H.W.; Masliyah, J. H., Molar Mass Distribution and Solubility Modeling of Asphaltenes, AIChE Journal, 1996, Vol. 42, 3533-3543.

Yen, T. F.; The role of trace metals in petroleum, ann arbor science pulishers inc., Michigan, 1975.

Yen, T. F.; The Colloidal Aspect of a Macrostructure of Petroleum Asphalt;Fuel Science and Technology Int'l, 723-733 (1992).

Yen, T. F.; Wu, W. H. and Chilingar, G. V.; A Study of the Structure of Petroleum Asphaltenes and Related Substances by Proton Nuclear Magnetic Resonance; Energy Source, Volume 7, Number 3, 275-304 (1984).

Yen, T. F.; Wu, W. H. and Chilingar, G. V.; A Study of the Structure of Petroleum Asphaltenes and Related Substances by Infrared Spectroscopy; Energy Source, Volume 7, Number 3, 203-235 (1984).

Yudin, I. K.; Nikolaenko, G.L.; Gorodetskii, E.E.; Markhasov, E.L.; Frot, D.; Briolant, Y.; Agayan, V. A.; Anisimov,M.A.; Universal Behavior of Asphaltene Aggregation in Hydrocarbon Solutions; Petroleum Science and Technology 16 (3&4), 395-414 (1998)

Zou, X.Y. and Shaw, J. M.; The Phase Behavior of Athabasca Bitumen Vacuum Bottoms + Alkane Solvent Systems, HOD 2002, Mexico.

Appendix I: Sample Preparation and Insertion for Phase Behavior Experiments

Sample preparation is the key step for any phase behavior experiment. Ideally, sample preparation should ensure not only a correct sample composition but also a suitable amount of sample mass. The following sample preparation procedure should be followed for phase behavior experiments to be conducted on the x-ray view cell apparatus:

1. Determine the sample composition and experimental condition;
2. Calculate the sample mass;
3. Load the solid components;
4. Vacuum test;
5. Pressure test;
6. Load the liquid components;
7. Load the gas components;
8. Check the sample composition;
9. Preheat the sample to the highest experimental temperature.
10. Remove the trapped gases.

1. Determine the sample composition and experimental condition

The sample composition and experimental condition are generally determined by your research objectives. This should be figured out at the very beginning.

2. Calculate the sample mass

The view cell unit has the following limited operating ranges:

- Pressure ≤ 27.5 MPa,
- Temperature ≤ 450 C
- Volume ≤ 240 ml

Calculate the upper limit for the sample mass, Mmax, through simulation calculations at the most extreme experimental condition you plan to explore. The actual sample mass should be less than Mmax for safety reasons.

Caution: The volume and/or pressure of the sample may increase very rapidly at high temperatures; therefore, the most extreme experimental condition generally means at the highest temperature.

On the other hand, the more sample in the view cell, the lager the amount of each phase in equilibrium, so the more accurate the data. Such as the volume and properties of each phase you measure from experiment. The actual sample mass should be larger than a certain value. Therefore, the sample mass is determined on the basis of a trade-off between safety and accuracy.

The mass of each component can be easily determined from the sample composition and sample mass.

3. Load the solid components

1. Make sure the view cell and all tubing is clean and satisfies the phase behavior experimental standards.
2. First prepare the correct amount of each solid component on a proper balance.
3. Following the installation instructions for the view cell assembly from the D.B. Robinson Company, install the view cell bottom cap, gaskets, and the Beryllium cylinder.
4. Load all solid components and the magnetic stirrer into the view cell.
5. Following the installation instructions for the view cell assembly from the D.B. Robinson Company, install the view cell top cap and seal it.

Caution: Don't forget to load the magnetic stirrer.

4. Vacuum test

1. Close all valves in Figure 1, and connect each of the view cell ports with proper tubing.
2. Open valve H4 and N2 and switch V3 to the vacuum position. Evacuate the view cell for 20 minutes and close valve V3. Record the temperature and pressure of the view cell.
3. Record the temperature and pressure of the view cell 24 hours later; do necessary calculations to find any vacuum leakage.
4. Find the leak and correct for it.

Caution: Keep valve H4 and N2 open during the vacuum test to protect the bellows.

5. Pressure test

1. **Slowly** open H1, H3 and load the gas into the view cell until the pressure of view cell reaches the maximum experimental pressure. Close H1 and H3.
2. Record the temperature and pressure of the view cell.

3. Record the temperature and pressure of the view cell 24 hours later; do necessary calculations to find any pressure leakage.
4. Find the leak and correct for it.
5. **Slowly** switch V3 to the vent position and release the pressure of gas inside the view cell to atmospheric pressure.

Caution:

1. For safety reasons, use nitrogen gas first. If no leakage detected, repeat the test with hydrogen.
2. Keep valve H4 and N2 open during the pressure test to protect the bellows.

6. Load the liquid components

1. Switch V3 to the vacuum position and evacuate the view cell for 20 minutes.
2. Close V3, N2 and H4.
3. Use a clean syringe and weigh the desired amount of a liquid component; connect the syringe to valve 1.
4. Slowly open the valve L1 and allow the liquid sample to be sucked into the view cell.
5. Repeat the step 3 and 4 immediately above to load other liquid components if necessary.
6. Open H4 and switch V3 to the vacuum position and degas the liquid and solid components if necessary.

Caution: Close N2 and N4 after the vacuum.

7. Load the gas components

1. Start up the temperature controller for the gas-loading reservoir and initialize the set point of the controller to a proper value (generally 30C).
2. Open R1 and H2. Switch V3 to the vacuum position and evacuate the gas-loading reservoir and connecting tubing for 20 minutes.
3. Close V3 and open H1. Flush the gas-loading reservoir and connecting tube with the gas sample. Vent the gas by switching V3 to the vent position.
4. Repeat the step 3 and 4 (Vacuum and Flush) immediately above if necessary.
5. Close R1 and open H1 and H2; load a gas component into the gas-loading reservoir. Close H1, let the reservoir attain thermal equilibrium (at least 1 hours) and record its temperature T1 and pressure P1.

6. According to the mass of this gas component, T1, P1 and the volume of the gas loading reservoir, calculate the final pressure of the gas-loading reservoir according to the desired amount of this gas component to be loaded from the gas-loading reservoir.
7. Start up the X-ray machine and the image system following their established procedures respectively. Make sure you can see a clear image on the TV and find the position of the bellows.
8. Very slowly open the valve H3 slightly. In the meantime, observe the position of the bellows. Close H3 before the bellows reach the top limit mark of the TV screen.
9. Very slowly open the valve N1 slightly and load the nitrogen gas into the bellows. In the meantime, observe the position of the bellows. Close N1 before the bellows reach the vapor and liquid/solid boundary.
10. Repeat the two steps immediately above to load more liquid components until the desired final pressure is reached. Close H3 and N1.
11. Let the reservoir attain thermal equilibrium (at least 30 minutes) and record its final temperature T2 and final pressure P2. Calculate the amount of the gas added to the view cell.
12. Repeat steps 1-11 to load other components if necessary.

Caution: Operate the valves very carefully to ensure the pressure difference between the view cell and the bellows is less than 50 psi when loading the gas components.

8. Check the sample composition

Recalculate the sample composition according the mass of each component added to the view cell. If the difference between this composition and the your desired composition determined at the beginning (step1) is within an acceptable error, you can start up the experiment. Otherwise, disassemble, clean the view cell, and repeat from step 3.

9. Preheat the sample to the highest experimental temperature

Preheating is a key step to ensure consistent experimental data for the asphaltene-containing heavy oil samples. Heavy oil sample, such as ABVB, are often solid or semi-solid, which make it very hard to completely mix with light hydrocarbon solvents at room temperatures. Besides Asphaltenes are prone to form aggregates in solution, and these aggregates need to be broken so that asphaltene “monomer” have sufficient opportunities to interact with solvent molecules. These problems are solved by preheating the asphaltene-containing heavy oil samples to the highest experimental temperature. Preheating also help remove gases trapped in heavy oils and solvents and thus guarantees more consistent experimental data. In this

project, the maximum experimental temperature is 340 °C above which chemical reactions are not negligible.

Typically in experiment, the heavy oil + light hydrocarbon solvent mixtures are heated to 340 °C and the mixer is switched to high speed and kept running for 30 minutes at this temperature. Turn off the heating system but keep the mixer on, and let the mixture cool down to room temperature. **Caution:** Don't over heat the sample!

10. Remove the trapped gas

Turn on the vacuum system and evacuate the view cell to remove the trapped gases driven into the vapour phase by the above preheating procedure.

Caution: Some light hydrocarbon solutions could be very volatile and poisonous. Safety precautions are mandatory. Also do not evacuate the view cell too long since it may result in imnegligible change to the sample composition due to the loss of volatile solvent.

Let the sample settle for at least 12 hours and then you can start your formal experiment.

Appendix II: Volume Calibration

Both the view cell and beryllium piece are of regular shape so the volume below a certain height from the bottom of the view cell increases linearly with the height, as expected (Figure A-1). However, the slope may change with height intervals as shown in Figure A-1b and corresponding values are listed in Table A-1. This relationship can be used to calculate the volume of each dense phase, provided that the phase boundaries can be detected. The volume for the vapor phase equals the whole volume of the view cell subtracted by the total volume of the dense phases and the volume occupied by the bellow. The volume of the bellows varies linearly with the lower end position of the bellows. Relevant parameter values are also listed in Table A-1.

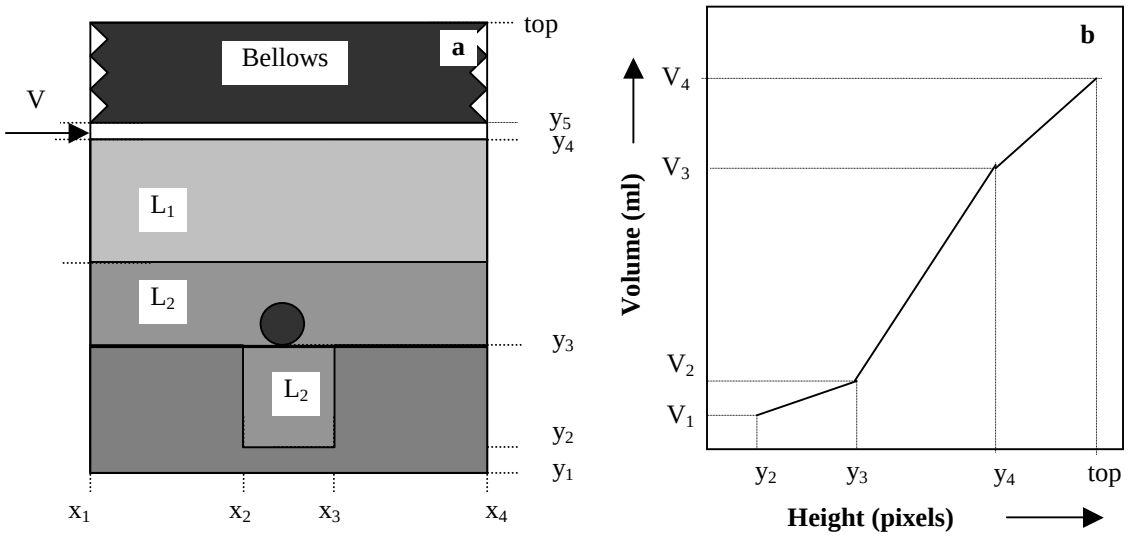

Figure A-1View Cell Volume Calibration.

Table A-1 Volume Calibration Parameters

Dense phase volume calibration (ml)		
Height range (pixels)	Intercept	Slope
$y_2<y<y_3$	0.61	0.1243
$y_{4<}y$	0.61	0.7811
Bellows volume calibration		
	Intercept	Slope
y_5	60.99	0.4718
Vapor phase calibration		
$V^v = V^{total} - V^{dense} - V^{Bellows}$		

Appendix III: Reversibility of multiphase behavior with respect to pressure

Reversibility of multiphase behavior for asphaltene containing heavy oil mixtures is a key topic which is still in debate. The reversibility with respect to pressure was explored by conducting the phase experiment at the same temperature but in a pressurization procedure and de-pressurization procedure, respectively. In the pressurization procedure, the experiment started from the lowest possible pressure. At each pressure, the mixture was given 10~15 minutes to attain equilibria. The image was cropped and the pressure was increased to a higher value. The procedure was repeated until the mixture attained the highest possible pressure. In the de-pressurization procedure, the experiment followed the opposite procedure. It started from the highest possible pressure and ended in the lowest possible pressure. One example for 50 wt% ABVB + pentane mixture at 330 ^{o}C is displayed in Figure A-2. The volumes and apparent densities of L2 from the pressurization and de-pressurization procedures are within experiment errors. This result suggests that the multiphase behaviors of asphaltene containing heavy oil mixture are reversible with respect to pressure change.

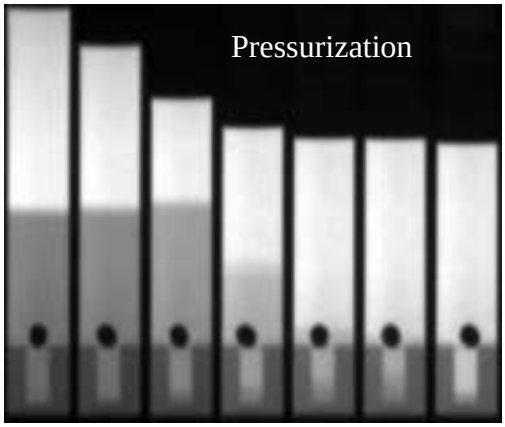

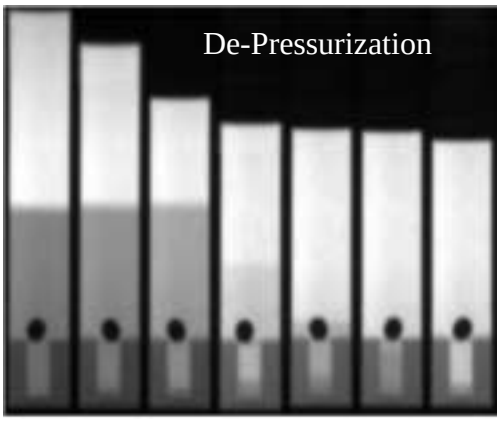

°C	330.13	330.11	330.00	330.03	330.02	330.20	330.11	330.19	330.28	330.41	330.36	330.26	330.13	33.03
MPa	9.06	9.83	11.26	12.77	13.82	13.86	14.51	9.05	9.80	11.23	12.75	13.81	13.85	14.53

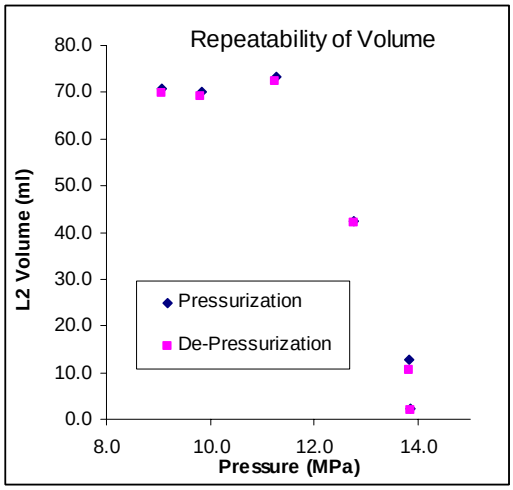

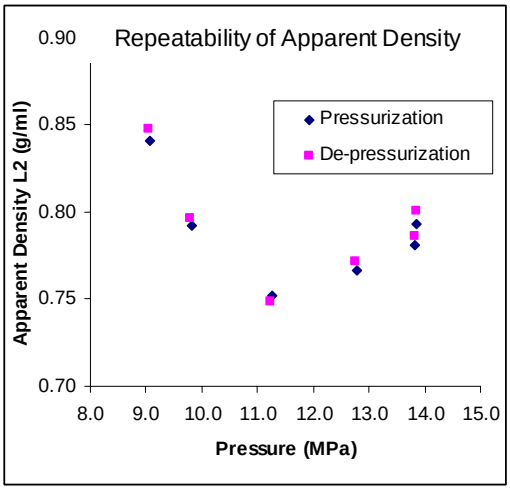

Figure A-2 Repeatability of multiphase behavior of ABVB 50 wt% + pentane mixture at 330 °C in pressurization and de-pressurization procedures